AGSO JOURNAL
OF AUSTRALIAN GEOLOGY & GEOPHYSICS

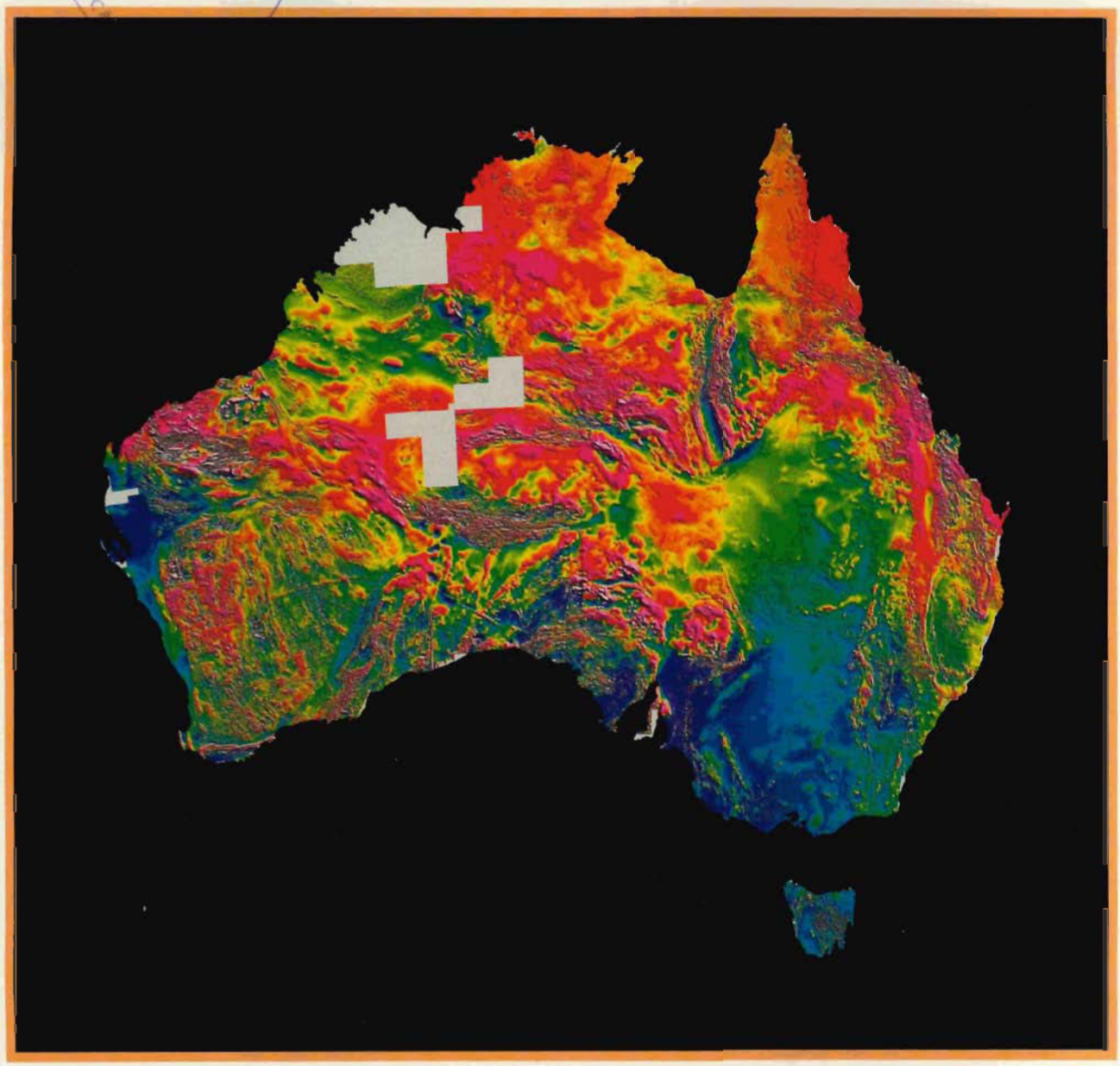

VOLUME 14 NUMBER 1
1993

AGSO JOURNAL

OF AUSTRALIAN GEOLOGY & GEOPHYSICS

VOLUME 14 NUMBER 1, 1993

CONTENTS

Editor, AGSO Journal: Dr Karl H. Wolf
Cover design by Saimonne Bissett
Figures prepared by AGSO Cartographic Services Unit unless otherwise indicated
Prepared for publication by Lin Kay

AUSTRALIAN GOVERNMENT PUBLISHING SERVICE CANBERRA 1993

ISSN 1320–1271

Subscriptions to the AGSO Journal are available through the Australian Geological Survey Organisation (GPO Box 378, Canberra ACT 2601; tel. 06 249 9642, fax 06 249 9982) or through the Australian Government Publishing Service (Mail Order Sales, GPO Box 84, Canberra ACT 2601; tel. 06 295 4485).

Other matters concerning the Journal should be sent to the Editor, AGSO Journal

Printed in Australia by
National Capital Printing, Fyshwick, A.C.T. 2609

***Front-cover illustration*: Magnetic anomaly map of Australia (1993): gradient-enhanced residuals of total intensity.**

AGSO Journal of Australian Geology & Geophysics, 14, 1–19

Miocene to Pleistocene foraminiferal biostratigraphy of dredge samples from the Marion Plateau, offshore Queensland, Australia

George C.H. Chaproniere[1] & Christopher J. Pigram[1]

Planktic and larger benthic foraminiferids have been studied in thin section from a suite of dredge samples of two sites on the Marion Plateau, offshore Queensland. The two sites gave different results. (1) The northern site sampled an Early to Middle Miocene carbonate platform, with shallow-water foraminiferal assemblages. This limestone has solution cavities (developed during periods of subaerial exposure) infilled with Late Miocene shallow-water planktic foraminiferid-bearing sediments. The rock is cross-cut by several generations of mud-filled borings. Some of the fill in these borings could be biostratigraphically dated, with ages ranging from Pliocene to Pleistocene. (2) At the southern site, a Late Miocene carbonate platform was sampled; the only sample recovered was a limestone slab consisting of a late Miocene rhodolith-bearing floatstone with a marine hardground overlain by a condensed section of phosphatic wackestone of Pliocene age. A series of mounds is present down the slope from the Late Miocene platform sampling site; these also were sampled and were found to be of probable Pliocene and probable Pleistocene age (Zones N.18 and N.22).

Water depths for the deposition of the platform phase were shallow, probably less than 50 m, as testified by the presence at the northern site of large benthic foraminiferids, *Halimeda*, hermatypic corals, and nodular coralline algae. The cavity-fill sediments, probably typical of the overlying sediments, have good planktic foraminiferal faunas, but also include some shallow-water faunal components (*Amphistegina*) and reworked older faunas (*Lepidocyclina*). The infilled borings tend to be almost totally composed of planktic foraminiferids, as do some discrete samples. This faunal evidence indicates that for the northern platform no deposition took place during much of the Middle Miocene and early Late Miocene, probably due to a long period of subaerial exposure. During the Late Miocene, the northern platform slope was flooded and subsided to its present depth by the Pleistocene. The southern platform was built during the Late Miocene and subsided to its present depth in the Pliocene. Samples from the mounds contain shallow-water assemblages of two ages: one may be of similar Pliocene age as found on the platform sites, and another of probable Pleistocene age.

The presence of hermatypic corals, *Halimeda*, and larger benthic foraminiferids suggest warm surface water temperatures since the Early Miocene.

Introduction

The Marion Plateau is the southern of two major carbonate platforms off the east coast of northern Australia (Figs 1, 2) (Davies & others, 1989). It is roughly triangular in shape, bounded to the west by the southern end of the Great Barrier Reef; to the north separated from the Queensland Plateau by the Townsville Trough; and to the east bounded by the Cato Trough. At its southern end is the Capricorn Basin. Modern reef development is confined to the Marion Reef in its northeastern corner and Saumarez Reef in the south.

Two Neogene phases of carbonate platform development have taken place on the Marion Plateau (Davies & others, 1989; Pigram & others, in press) (Fig. 3). The first was the construction of a late Early to early Middle Miocene (Zones N.7 to N.9) platform (the northern, M1), which was subsequently exposed during the Middle and early Late Miocene (Pigram & others, 1992; Pigram & others, in press). A second platform (the southern, M2) originated during the Late Miocene. Evidence for these developments comes from the faunal assemblages within the various sediments of the Marion Plateau sequence. These faunas have been documented below.

This study is based on a number of samples from two dredge sites (Figs 1, 2). The first site is at the northern end of the Marion Plateau and was sampled by dredges 75DR02, 75DR03, 76DR02 to 76DR05; the target was the oldest known phase of platform building (M1) (Figs 2, A; 4). The second site (Figs 2, B; 5), at the southeastern end of the Marion Plateau, north of Saumarez Reef, was sampled by dredge 76DR09; the target was the younger phase of platform development (M2) as well as some low-relief mounds (dredge 76DR07) developed north of a scarp. Good and very good assemblages were obtained from only three dredges, namely 75DR03, 76DR07 and 76DR09; the samples from them are well-cemented carbonates which can be studied only by thin-section techniques.

Quilty (in press) studied faunal assemblages from seamount samples in the Tasman Sea and Lord Howe Rise areas. Comparisons between the Marion Plateau study and that of the Tasmantid and Lord Howe seamounts are impossible, because Quilty's is based on only few samples from each seamount, making it difficult to assemble a concept of the stratigraphic succession overlying the igneous core of the seamounts. However, most of the faunal assemblages from the seamounts are very similar to those recorded from the Marion Plateau.

Though planktic foraminiferids are difficult to identify in thin section, most species can be identified with confidence if sufficient numbers are present; those taxa with distinct morphologies can be even more readily recognised. The illustrations given by Postuma (1971) and Sartorio & Venturini (1988) have greatly aided these identifications. Only those samples with good populations of planktic species have been assigned to zones. Faunal distributions within samples are illustrated in Tables 1 to 3.

The biostratigraphic zonal scheme of Blow (1969), as modified by Kennett & Srinivasan (1983), has been adopted for the planktic foraminiferids, and the East Indian Letter Stage scheme as modified by Adams (1984) and Chaproniere (1981, 1984a) has been used for the larger benthic foraminiferids (Fig. 6). The chronology of Berggren & others (1985) has also been used. All figured specimens are registered and housed in the Commonwealth Palaeontological Collection (CPC), Australian Geological Survey Organisation (AGSO), Canberra.

The sample nomenclature used is based on the number of the cruise and the dredge from which it originated; for

[1] Marine Geoscience and Petroleum Geology Program, Australian Geological Survey Organisation, Canberra ACT 2601

example, 75DR03. The roman numerals, which were not always used, refer to the lithological group to which the samples were assigned during shipboard sorting. In some cases, these groupings were further subdivided, based on shore-based studies, as indicated by alpha-numeric symbols (for example -A2-). The next digits refer to the individual rock sample from which the thin sections were taken. The lower case letters (a, b, etc.) ending the sequence

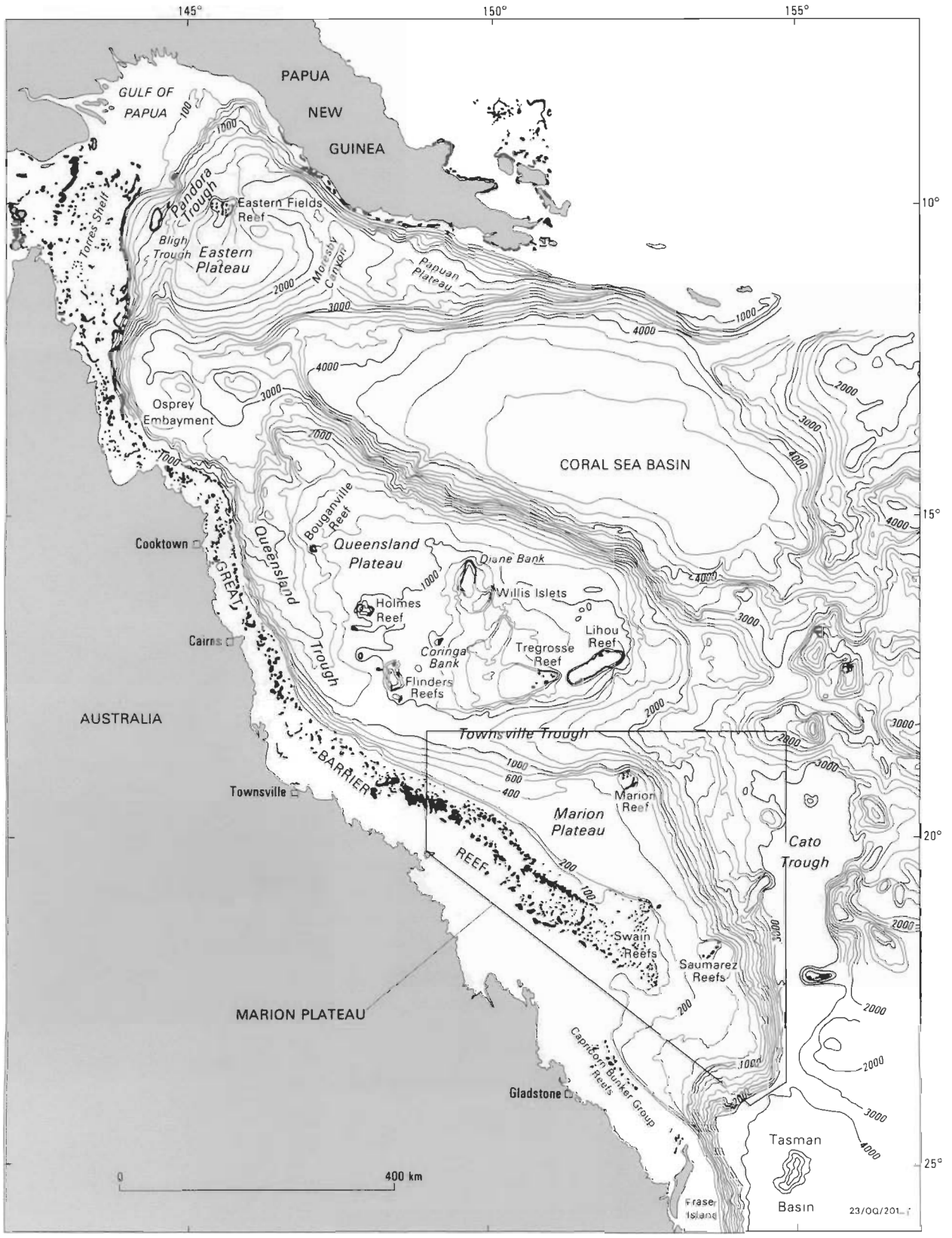

Figure 1. Map showing the geographical relationships of the various plateaus and troughs along the margin of northeast Australia.

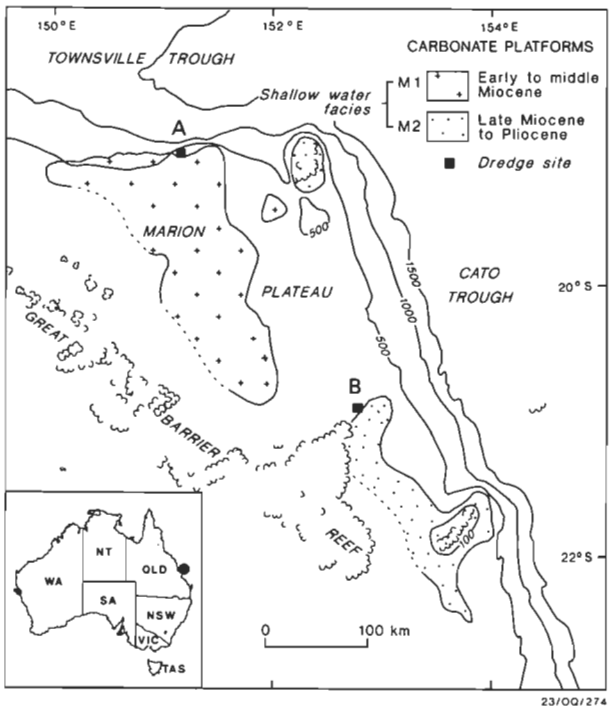

Figure 2. Locality map of dredge sites on the Marion Plateau from which the samples used in this study were collected.

refer to different lithologies identified in the thin section: a– represents the main rock body; b– a different lithology cross-cutting the main lithology; and c– or d–, etc., to various generations of borings or other cross-cutting features.

Lithologic descriptions of the studied samples are summarised below. Detailed descriptions and the diagenetic histories are presented elsewhere (Pigram & others, in press).

Lithology of samples

The primary rock in many of the samples from the northern site (M1) consists of bioclastic rudstone (Fig. 8, A, C) and floatstone (both dolomitised) with shallow-water bioclasts (fragments of calcareous algae, *Halimeda*, hermatypic corals, benthic foraminiferids, bryozoans, echinoids, gastropods, and bivalves) of late Early and early Middle Miocene age. Some of these samples have solution cavities (Fig. 8, A, C, E, G), with many having several generations of borings. In general, the cavities and borings are filled with internal sediments (Fig. 8, C), finer-grained than those of the primary rock. The bioclasts within these internal sediments are of a deeper-water origin and of a different age. The sediment fill of the solution cavities are bioclastic wackestones with deeper-water bioclasts (planktic and benthic foraminiferids), although some shallow-water fauna may be present (Fig. 8, E); they are of Late Miocene age. The borings are usually filled with fine-grained mud, with or without planktic foraminiferids, and, where age diagnostic forms are present, range in age from Pliocene to Pleistocene.

The major lithology recovered from the M2 phase is of partially dolomitised rhodolith-bearing floatstone with a marine hardground and a thin, condensed section of phosphatic wackestone along one face of the sample (Figs 7; 8, B, H). This wackestone comprises lenses with Late Miocene planktic foraminiferids in mud, bound by anastomosing laminae of apatite that merge and split apparently at random (Fig. 8, D, F). The surface on which the wackestone rests has been eroded, bored and impregnated with manganese and iron oxides.

A series of mounds in deeper waters adjacent to the M2 site yielded coarse (undolomitised) bioclastic packstones with shallow-water bioclasts (coralline algae, hermatypic corals, bryozoans, and shallow-water benthic foraminiferids) together with planktic foraminiferids providing ages of probable Pliocene and probable Pleistocene.

In general, the earlier Miocene lithologies contain larger foraminiferids with very rare planktic forms, whereas the younger Miocene and Pliocene lithologies have moderate to good planktic faunas, with or without contemporary or reworked, earlier Miocene, larger and smaller benthic forms (Fig. 8, D, F).

Faunal assemblages

Some genera of larger benthic foraminiferids were studied biometrically. Normally, this requires oriented sections of individuals previously removed from their host rock.

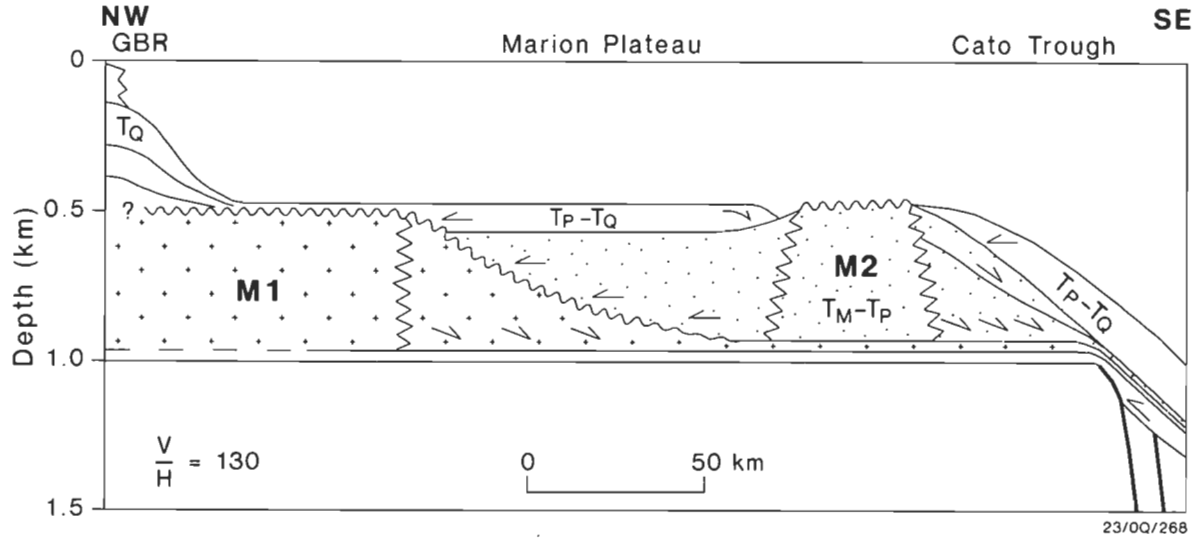

Figure 3. Cartoon showing the stratigraphic relationships within the Marion Plateau, as interpreted from seismic data.

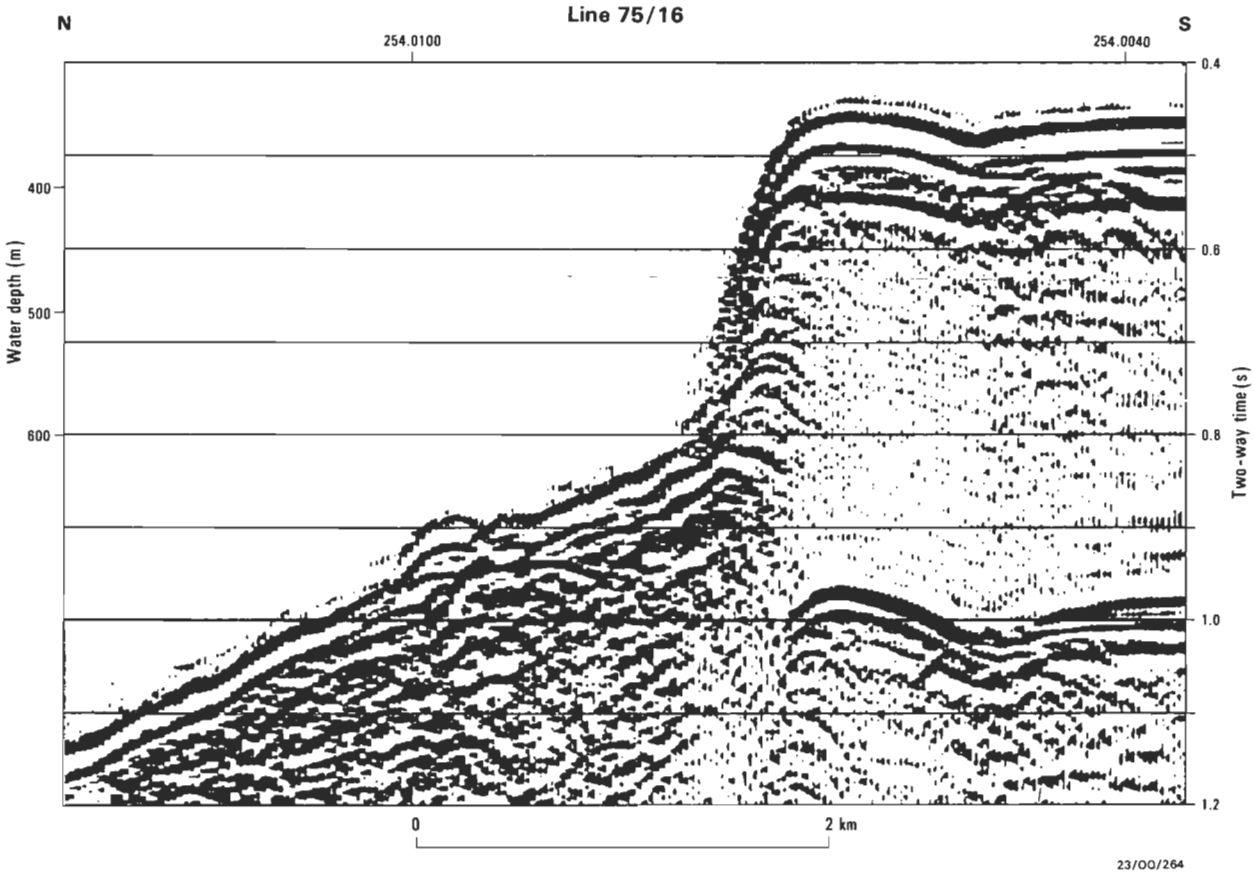

Figure 4. Seismic line 75/16 showing the scarp developed on the older, M1 Platform, sampled by dredges 75DR02, 75DR03, 76DR02 and 76DR05.

Because of the high degree of cementation, only random thin sections were possible, thus limiting the detail of biometric studies. However, it was possible to employ a parameter F for *Lepidocyclina (Nephrolepidina)* in random thin sections (Chaproniere, 1980, 1983, 1984b) — this same approach has been used here. In some cases, sections show the initial neanic whorl of *Cycloclypeus* (parameter pc), permitting a more accurate specific and biostratigraphic designation. In general, the taxonomic designations for the larger foraminiferids of Chaproniere (1983, 1984b) is used here, although some generic assignments previously adopted (Chaproniere, 1983, 1984b) have been modified following Loeblich & Tappan (1988).

Older platform — M1

Primary rock body. The majority of samples contain only larger benthic foraminiferids, although rare planktic forms are also present.

The most common larger foraminiferids found in these samples are *Cycloclypeus (Cycloclypeus) carpenteri* (Fig. 9, M, N), *Lepidocyclina (Nephrolepidina) howchini* (Fig. 9, A, B, E, F, I), and *Operculina complanata* (Fig. 9, G); present also may be rare *Borelis pygmaeus*, *Cy. (Katacycloclypeus) annulatus* (Fig. 9, J), *Discogypsina howchini*, *Ladoronia vermicularis* (Fig. 10, A, B) (which is present within some of the rhodoliths), *Operculinella venosa* (Fig. 9, K), and *Sphaerogypsina globulus* (Fig. 9, La). The smaller benthic foraminiferid *Amphistegina radiata* (Fig. 9, Ca, D) dominates many samples; other smaller benthic forms identified are *Biarritzina carpenteriaeformis* (Fig. 9, Lb), *Carpenteria balaniformis*, *Cymballoporetta ?squamosa* (Fig. 9, H), *Planorbulinella larvata*, and *Rotalia sp.* Planktic species, often unidentifiable globigerines, are rare. However, *Dentoglobigerina altispira* (Fig. 10, H), *Praeorbulina glomerosa* (Fig. 10, C to E), *Orbulina suturalis* (Fig. 10, F), and *O. universa* (Figs 9, Cb; 10, G) have been identified.

Mean values for Parameter F for populations of *L. (Ne.) howchini* range from 3.00 to 3.33. One sample (75DR02II-07a), with *Orbulina* (indicating Zone N.9), has a value of 3.33 (based on 12 specimens), and three others (75DR03I-06a, 75DR03I-07, 75DR03I-08a), with *Praeorbulina* (indicating Zone N.8), have values of 3.17, 3.25 and 3.29 (based on 12, 56 and 44 specimens, respectively). These values fall within the range obtained by Chaproniere (1980, 1983, 1984b) for levels within the upper part of Zone N.7 and N.8 within the Australian region. Here, the only samples known to have come from a level within Zone N.9 (from the Stark Bay Formation in the Perth Basin, Chaproniere, 1980, 1984b) gave mean values for Parameter F of 3.78 and 4.10 (based on 34 and 9 specimens, respectively); these values are higher than those obtained in this study. Even so, the value of 3.33 from the one sample with *Orbulina* is the highest recorded here, but is based on only 12 specimens. From the evidence of these three samples, they have been assigned to Zone N.8 (on the basis of *Praeorbulina* without *Orbulina*) and one to Zone N.9 (on the presence of *Orbulina*). Fifteen samples (e.g. 75DR03I-06a, 75DR03-05B2a, 75DR03II-04a, 76DR02-07a) have been referred to the zonal interval upper N.7 to N.8 [on the basis of mean values for Parameter F of *L. (Ne.) howchini*]. Two samples (75DR02III-04a, 75DR03III-03a) have too few specimens of *L. (Ne.) howchini* for parameter F to be measured, but

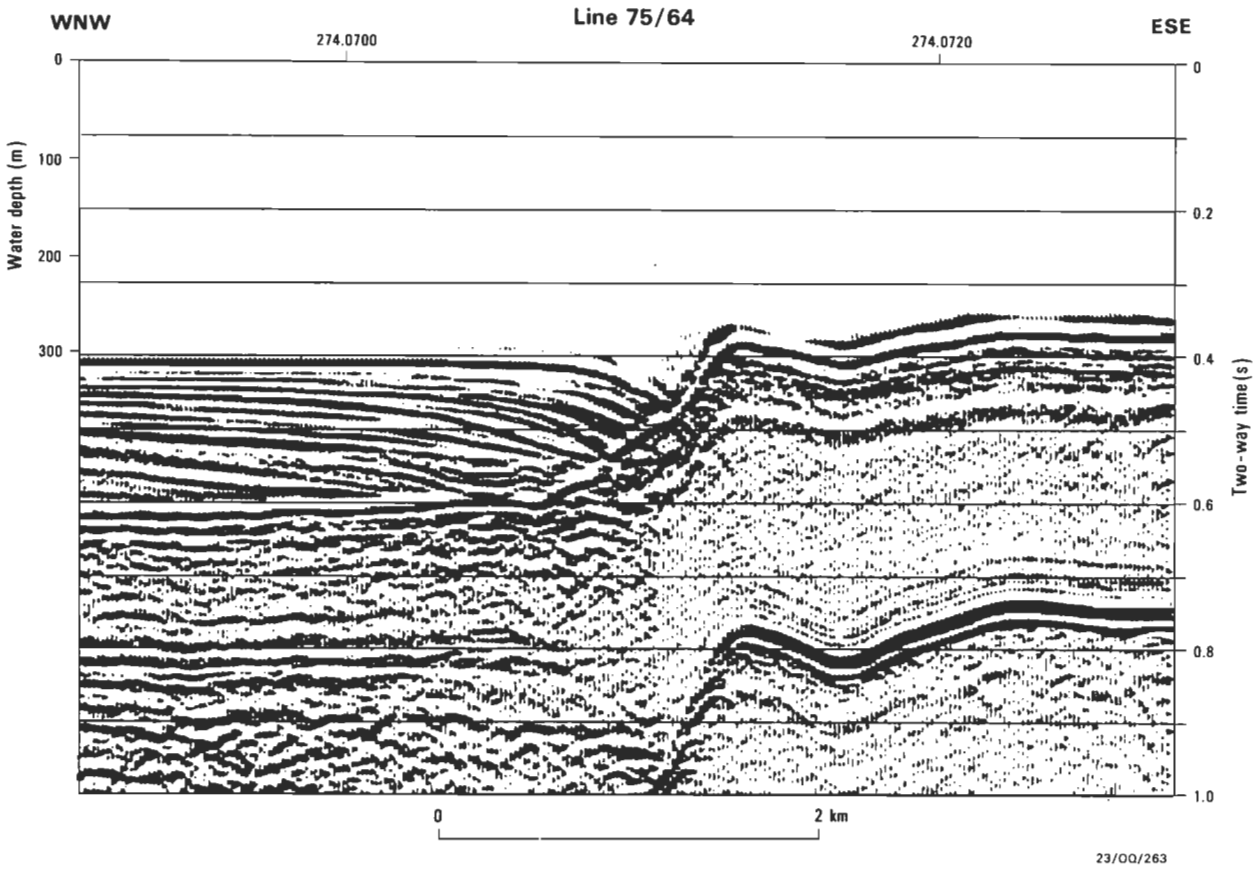

Figure 5. Seismic line 75/64 showing the scarp developed on the younger, M2 Platform, sampled by dredge 76DR09, and the low mounds sampled by dredge 76DR07.

the presence of *Orbulina* indicates they can be from no older than Zone N.9. As the only other sample with *Orbulina,* from which Parameter F values have been measured, is probably from Zone N.9, these other two are referred to this zone as well. One part of another sample (75DR03-06Bb) has only *Cycloclypeus (Cy.) ?carpenteri* and *Amphistegina radiata* with nodular coralline algae and lacks younger planktic foraminiferids, but another part of the same sample has a cavity with a younger Zone N.17B planktic fauna. As other samples show a similar relationship between the lithology and the larger and planktic foraminiferal faunas, it is probable that the larger foraminiferal assemblage in this sample was sedimentologically reworked from the Zone N.7 to N.9 interval. A further sample (76DR02-09) contains only *Borelis* and *Ladoronia*; this too is referred to the same zonal interval because *Ladoronia* seems confined to the late Early and early Middle Miocene.

Cavity fill. A number of planktic foraminiferid-rich samples of Late Miocene and Pliocene age were studied from cavity-fill sediments. Two faunal assemblages were recognised: one associated with reworked Early Miocene larger foraminiferids, and another lacking them. The shallow-water bioclasts almost certainly had two sources: reworked from an older carbonate sequence, and transported in from a contemporaneous shallow-water environment. A number of the larger foraminiferal species [*L. (Ne.) howchini* (Fig. 10, K), *Cy. (Cy.) ?carpenteri*, and *Cy. (K.) annulatus*] must have been derived from the underlying earlier Miocene carbonate sequence. Others, such as *Marginopora vertebralis*, *Operculina complanata, Sphaerogypsina globulus* (Fig. 10, L), and the smaller benthic, *Amphistegina radiata* (Fig. 10, M), as well biotic debris of hermatypic corals, bryozoa, and nodular calcareous algae, may also have been reworked from the older sequence; or more probably, may be contemporaneous with the younger planktic fauna, but displaced from shallow to deeper waters. Evidence that some of this shallow-water debris is contemporaneous with the planktic fauna is the presence of *Gypsina plana* in algal nodules, and *Homotrema rubra.* Neither species has been recorded prior to the Late Miocene elsewhere. Instead, *Ladoronia vermicularis* is found within the algal nodules in the older sequence. Thus, it is probable that specimens of *Amphistegina radiata, Operculina complanata,* and *Operculinella venosa* (Fig. 10, P) of both ages are present; in addition, it is possible that some specimens of *Cy. (Cy.) carpenteri* (found in Recent sediments) may also be from the two sources. The planktic-rich nature of the assemblages implies bathyal water depths, suggesting that the shallow-water components have been reworked and displaced.

Good planktic faunas are present in cavity-fill sediments, and diagnostic zonal assemblages occur in some. However, a number of samples contain planktic faunas in which diagnostic species could not be identified, and thus cannot be accurately referred to any zones. One sample (76DR02-16) has *Dentoglobigerina altispira altispira* (Fig. 11, I), *Globigerinoides quadrilobatus, Globorotalia (Gr.) tumida plesiotumida* (Fig. 11, G, K, M), and *Sphaeroidinellopsis seminulina* (Fig. 11, A), without *Pulleniatina primalis*; this assemblage is referred to Zone N.17A. Five samples (75DR03-05B2b, 75DR03-06Bb, 75DR03III-03b, 75PDR03II-05, 76DR02-06a) have *De. altispira altispira,*

Table 1. Distribution of larger and planktic foraminiferids in dredge samples from the older M1 Platform of the Marion Plateau.

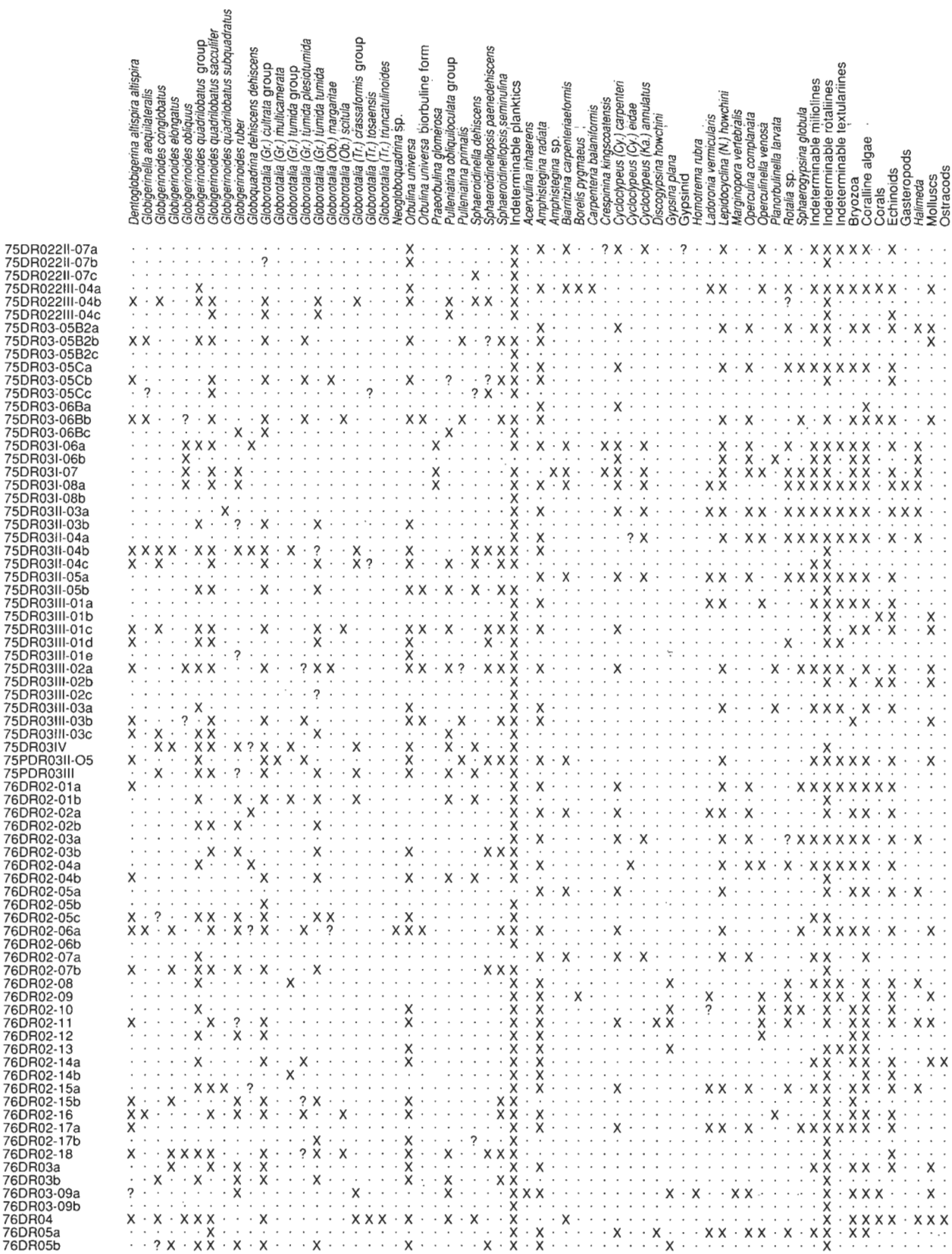

23/OQ/286

Gds. quadrilobatus, *Gr. (Gr.) tumida plesiotumida*, *Pu. primalis* (Fig. 11, L), and *Sphaeroidinellopsis ?paenedehiscens* (Fig. 11, C); whereas *Gr. (Obandyella) margaritae* (Fig. 11, J) is present in one sample (76DR02-06a). The absence of *Gr. (Gr.) tumida tumida* and *Sphaeroidinella dehiscens* indicates that this assemblage is typical of Zone N.17B. *Amphistegina radiata* is also present in both Zone N.17 assemblages. Seven samples (75DR03III-01c, 75DR03III-02a, 75DR03III-03b, 75PDR03II-05, 76DR02-05c, 76DR02-07b, 76DR02-18) have the same assemblages noted above, but with *Gr. (Gr.) tumida tumida* (Fig. 11, P) — *Gds. conglobatus* (Fig. 11, H, N) may be present in some. This assemblage is referred to Zone N.18. Four samples (75DR02III-04b, 75DR03II-04b, 75DR03IV, 75PDR03III) have *De. altispira altispira*, *Gds. conglobatus*, *Gr. (Gr.) tumida tumida*, *Gr. (Truncorotalia) crassaformis* (Fig. 11, R), *Pu. obliquiloculata*, and *Sphaeroidinella dehiscens* indicating a Zone N.19-20 assignment. No samples were found to have *S. dehiscens* without *Gr. (Tr.) crassaformis*, and so none can be referred with confidence to Zone N.19.

Borings. Although most borings contain very limited populations of planktic species and the assemblages cannot be referred to zones with confidence, their cross-cutting relationship indicates that they must be younger. Some diagnostic forms are present permitting some zonal assessment, as described below.

Sample 75DR03II-05b has infilled borings with *Gr. (Gr.) tumida tumida* and *Sphaeroidinella dehiscens*, indicating a minimum age of Zone N.19; this boring cross-cuts a Zone N.7 to N.8 assemblage.

A boring which cross-cuts a Zone N.17B assemblage in sample 75DR03II-03 has both *Gr. (Gr.) tumida tumida* and *De. altispira altispira*, limiting the age to within the N.18 to N.19-20 zonal interval.

Samples 75DR03-05Cc and 75DR03II-04c each have single specimens of *Gr. (Truncorotalia)*, which appears to be very close to *Gr. (Tr.) tosaensis*, but due to the angle of the section cannot be identified with certainty; thus, the samples have been questionably referred to Zone N.21.

Borings cross-cutting a late Early Miocene assemblage in sample 76DR02-01 contain a specimen of *Gr. (Tr.) crassaformis* (Fig. 11, T) giving a minimum age of Zone N.19-20, and within samples 76DR02-02 and 76DR02-17 borings with *Gr. (Gr.) tumida tumida* indicate a minimum age of Zone N.18.

Sphaeroidinellopsis sp. and *Gr. (Gr.) tumida tumida* (Fig. 11, W) are present in samples 76DR02-03 and 76DR03b denoting an age with the zonal interval N.18 to N.19-20.

Other samples. Dredge 76DR04 recovered samples, presumably derived from the top of the Marion Plateau. These samples have mainly shallow-water bioclasts (coralline algae, corals, *Halimeda*, molluscs, and echinoids), mixed with rare planktic and benthic foraminiferids.

The planktic fauna comprises *Dentoglobigerina altispira*, *Globorotalia (Truncorotalia) truncatulinoides* (Fig. 11, Y, BB), *Gr. (Tr.) ?tosaensis* (Fig. 11, Z), *Gr. (Tr.) crassaformis* (Fig. 11, AA), *Gr. (Globorotalia) tumida tumida*, and *Pulleniatina obliquiloculata* (Fig. 11, X). The presence of these species is indicative of the lower part of Zone N.22 (*Globigerinoides quadrilobatus fistulosus* or *Globorotalia (Truncorotalia) crassaformis viola* Subzones).

Younger platform — M2

All samples studied from the M2 platform are from a single large limestone slab of rhodolith-bearing, orange-brown floatstone, with a condensed interval represented by a phosphatic wackestone along one face of the slab. Both the floatstone and wackestone have been bored, and the borings filled with younger wackestone. The studied samples are from the floatstone, the condensed section/phosphatic wackestone, and the cross-cutting borings, separately described below.

Floatstone. Though larger benthic foraminiferids are present within many samples, planktic forms are more common than for similar samples from the M1 platform. It is clear that some of the larger foraminiferids are reworked from the Early Miocene.

Large rhodoliths make up the main component of the primary rock, containing the encrusting foraminiferid *Gypsina plana* (Fig. 13, D to G). This species appears to range from the Late Miocene; *Ladoronia vermicularis* occupies the same environmental niche for the earlier Miocene algal nodules. The matrix surrounding the rhodoliths has coralline algal, bryozoan, coral, echinoid, and molluscan bioclasts as well as numerous larger and smaller benthic foraminiferids. At least some of the benthics are reworked, as testified by *Lepidocyclina (Ne.) howchini* (Fig. 12, D); present also are specimens of *Amphistegina radiata* (Fig. 12, H), *Cycloclypeus (Cy.) ?carpenteri* (Fig. 12, I), *Operculina complanata* (Fig. 12, G), *Operculinella venosa*, and *Sphaerogypsina globulus*. As noted above, these last five species range to the Recent and some, at least, may be contemporaneous with the planktic species. The latter fauna is of low diversity, but the presence of *Globorotalia (Gr.) tumida plesiotumida* (Fig. 12, A, B, E) and *Sphaeroidinellopsis paenedehiscens* (Fig. 12, C) without *Globigerinoides conglobatus*, *Gr. (Obandyella) margaritae*, *Pulleniatina primalis*, and *Gr. (Gr.) tumida tumida* in a number of samples (e.g. 76DR09-1a, 76DR9-2a, 76DR09I-A1- 1a, 76DR09-A2-1a) indicates that the rhodoliths were deposited during Zone N.17A.

Condensed section/phosphatic wackestone. The wackestone differs from the floatstone in lacking rhodoliths, having fewer shallow-water components (such as rare bryozoans and molluscs), and a greater diversity of planktic species. Specimens of *L. (Ne.) howchini* (Fig. 12, O), present in some samples (e.g. 76DR09-01b, 76DR09-02b, 76DR09-03b), indicate some reworking from the Early Miocene. As with the primary rock, other benthic forms — such as *Cy. (Cy.) carpenteri* and *Amphistegina radiata* — may also have been reworked, but rare specimens of *Acervulina inhaerens* (Fig. 12, M) (in sample 76DR09I-A1-02b) and *Homotrema rubra* (in sample 76DR09I-A2-02b) suggest that some parts of the benthic assemblage are probably contemporaneous with the planktic assemblage.

The presence of *Dentoglobigerina altispira* (Fig. 12, L), *Gds. conglobatus* (Fig. 12, K), *Gr. (Gr.) tumida plesiotumida*, *Gr. (Gr.) tumida tumida* (Fig. 12, J), *Pulleniatina obliquiloculata*, and *Sphaeroidinellopsis* spp. (Fig. 12, N), without *Sphaeroidinella dehiscens*, indicates Zone N.18. However, as it is difficult from thin-section studies to be certain that *S. dehiscens* is absent, it is uncertain whether

Table 2. Distribution of larger and planktic foraminiferids in dredge samples from the younger M2 Platform of the Marion Plateau.

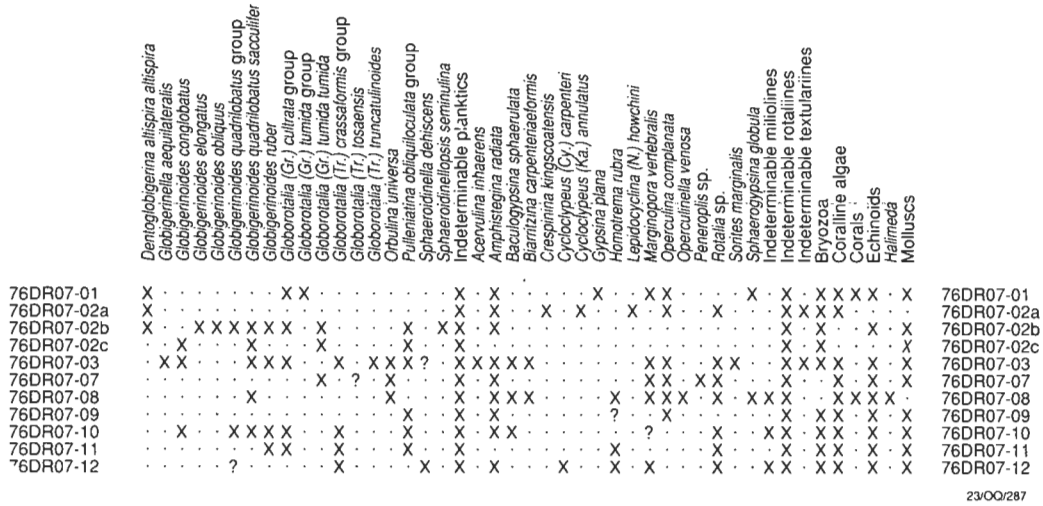

Table 3. Distribution of larger and planktic foraminiferids in dredge samples from mounds developed north of the scarp on the M2 Platform of the Marion Plateau.

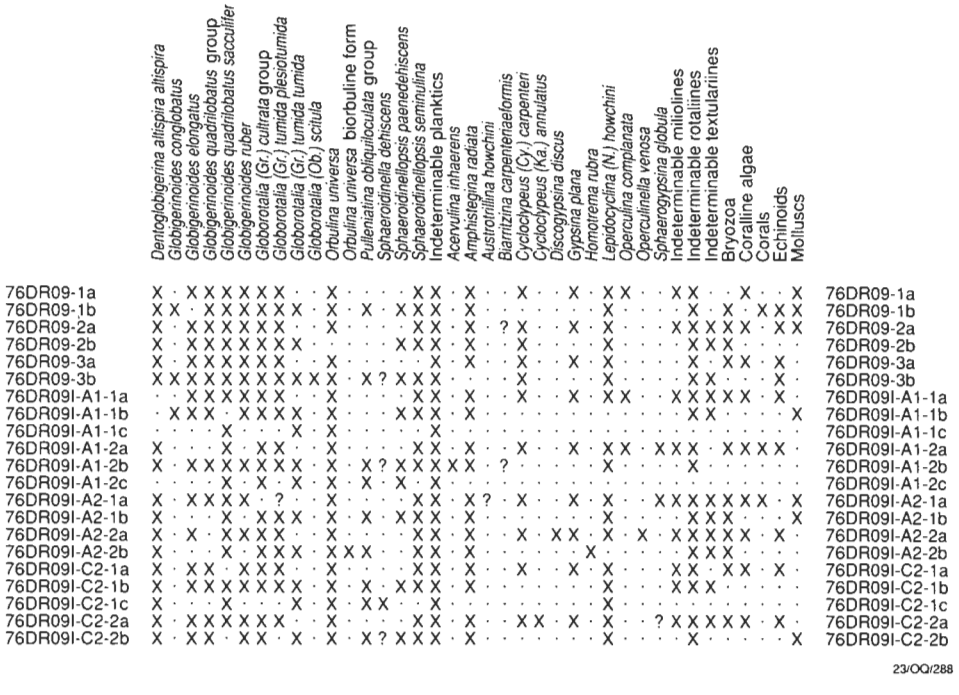

Zone N.19 is present. The large number of sphaeroidinellines suggests that the fauna is probably from Zone N.18.

Borings. Only three borings cross-cutting the floatstone and wackestone lithologies (76DR09I-A1-1c, 76DR09I-A1-2c, 76DR09I-C2-1c) have identifiable faunal assemblages, and as with those discussed above, they were of low diversity. *Gr. (Gr.) tumida tumida* was identified in all three, with *Sphaeroidinellopsis paenedehiscens* in one and *Sphaeroidinella dehiscens* in another. On the basis of these

species, the borings range in age from Zone N.18 to within the lower part of Zone N.21. As the borings are rare, it seems probable that they are of the same age, and the overlap of *Sis. paenedehiscens* and *S. dehiscens* indicates a level within the zonal interval from N.19 to the lower part of N.21.

Mounds

Eight samples were examined from the mounds. All contained shallow-water bioclasts (coralline algae, hermatypic corals, *Halimeda*) as well as larger benthic foraminiferids (of shallow-water origin) and rare planktic species. The larger foraminiferids include *Amphistegina radiata*, *Baculogypsina sphaerulata* (Fig. 13, A), *Cycloclypeus (Cy.) carpenteri*, *Gypsina plana* (within algal nodules), *Homotrema rubra* (Fig. 12, V), *Marginopora vertebralis* (Fig. 12, Z), *Operculina complanata*, *Operculinella venosa* (Fig. 12, W), *Peneroplis* sp. (Fig. 13, C), *Sorites marginalis*, and *Sphaerogypsina globulus* (Fig. 12, Y). *Baculogypsina sphaerulata* (in samples 76DR07-03, 76DR07-08, 76DR07-10) appears to be Pleistocene or younger (Adams, 1984). *Homotrema rubra*, also in samples 76DR07-08, 76DR07-11, 76DR07-12, with a questionable occurrence in 76DR07-09, has not been recorded from below the Late Miocene. *Gypsina plana*, another form not recorded below the Late Miocene, occurs in sample 76DR07-01. Sample 76DR07-07 has only long-ranging larger benthic species, including *Marginopora vertebralis*. Based on these assemblages, all samples are probably no older than Pliocene, with at least three of likely Pleistocene age.

Planktic species occur in all samples, but most have very low diversity faunas. Sample 76DR07-01 contains only *Gr. (Gr.) tumida* and *Dentoglobigerina altispira altispira*, indicating a Zone N.17 to N.21 age range. Only *Pulleniatina obliquiloculata* (Fig. 12, S) was identified in sample 76DR07-09 giving a maximum age of Zone N.19. *Gr. (Truncorotalia) crassaformis* (Fig. 12, Q) with *S. dehiscens* (Fig. 12, T) in samples 76DR07-10 to 76DR07-12 gives a maximum age of Zone N.19-20. A questionable specimen of *Gr. (Tr.) tosaensis* (Fig. 12, U) with *Gr. (Gr.) tumida tumida* (Fig. 12, X) suggests that this sample is no older than from Zone N.18, but possibly as young as Zone N.21 to the lower part of Zone N.22 (the *Globorotalia (Truncorotalia) crassaformis viola* Subzone of Chaproniere, (1991). *Gr. (Tr.) truncatulinoides* occurs in 76DR07-03,

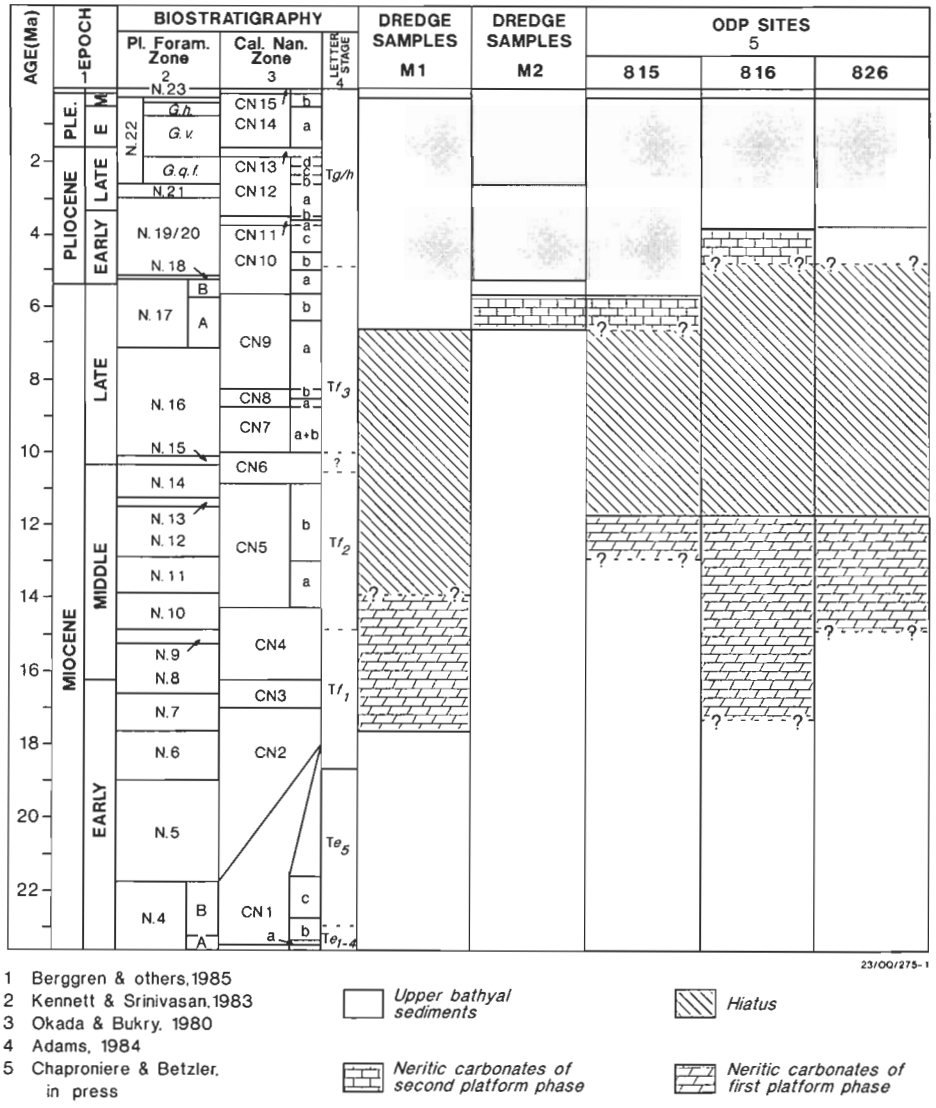

Figure 6. Biostratigraphic summary for the Marion Plateau, showing results from this study as well as from the ODP drilling.

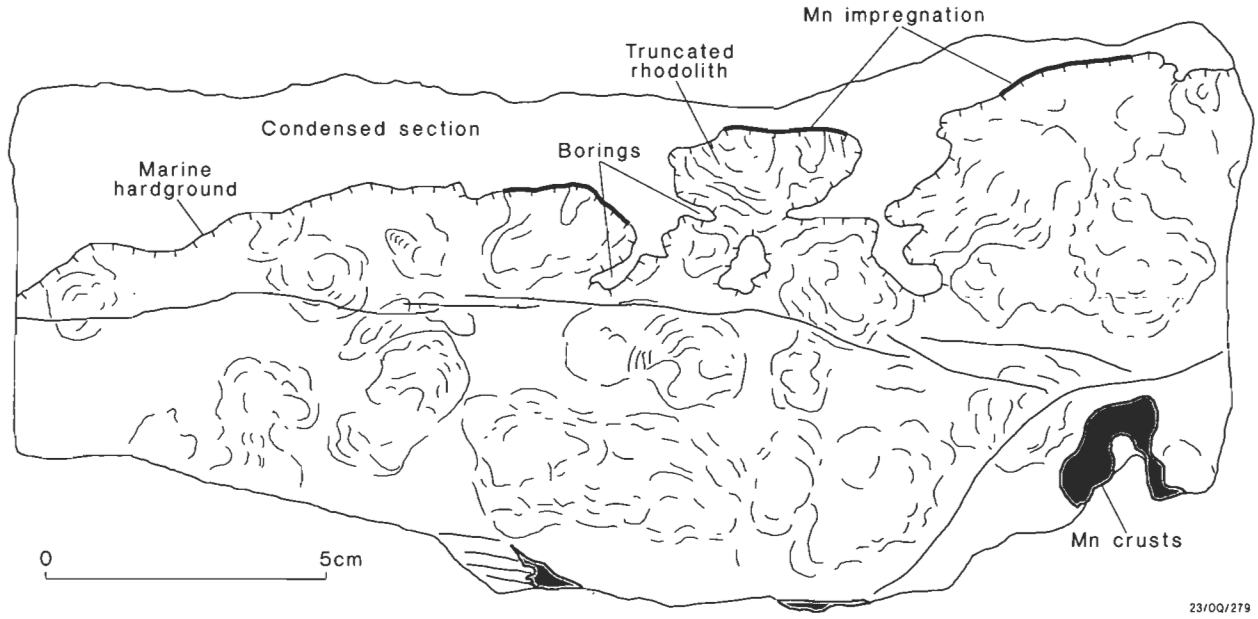

Figure 7. Drawing showing the relationships between the various lithologies studied from the sample from DR09, dredged from the M2 platform phase.

denoting Zone N.22 or younger. The only identifiable planktic species in sample 76DR07-08 is *Orbulina universa*, indicating Zone N.9 or younger, but as noted above, *Baculogypsina sphaerulata* is also present suggesting a Pleistocene age. *Baculogypsina* with *Gr. (Tr.) ?truncatulinoides* in sample 76R07-10 indicates that this is almost certainly Pleistocene. These data prove that there is no conflict between the results from both planktic and larger foraminiferids, but it is possible that all samples except for 76DR07-01 (which can be no younger than Zone N.21) may all be from the Pleistocene.

Biostratigraphic synthesis

Older platform, M1 phase

The oldest rock samples from the oldest known phase of platform development contain larger benthic foraminiferids of shallow-water origin and very rare planktic species. The present biostratigraphic results are based on the mean values for Parameter F for populations of *Lepidocyclina (Nephrolepidina) howchini*. These values are typical of Zones N.7 to N.8 within the Australian region. However, *Orbulina* in some samples, particularly those with the highest mean values for Parameter F, indicates that at least some are from Zone N.9.

The above late Early to early Middle Miocene samples also have a second fauna within infilled cavities. These internal sediments have both derived older larger benthic foraminiferal species and specimens contemporary with the low diversity planktic faunas. *Gypsina plana* and *Homotrema rubra* suggest ages of Late Miocene or younger. Three planktic assemblages occur within the cavity-fill sediments: these are typical of Zones N.17A, N.18 and N.19-20; Zones N.17B or N.19 were not recorded.

Borings cross-cut both the Early and early Middle Miocene lithologies as well as the younger solution cavity infill-sediment phases. These borings are filled with fine mud and have a limited, but sometimes diagnostic, faunal assemblage. They indicate that the borings were infilled within the interval of Zone N.19-20 to possibly N.21.

Shallow-water derived early Pleistocene to Recent sediments cap the plateau.

Younger platform, M2 phase

The oldest sediments at the southern site have both reworked larger benthic foraminiferids and those contemporaneous with a low diversity planktic fauna. The presence of *Gypsina plana* within rhodoliths suggests that these are no older than Late Miocene. The associated planktic fauna is typical of Zone N.17A. The rock with these assemblages is overlain by a complex condensed section with a second assemblage of larger benthic foraminiferids *Acervulina inhaerens* and *Homotrema rubra* (Late Miocene or younger) with a typical Zone N.18 planktic association. No definite Zone N.19 assemblages

Figure 8. Typical lithologies used in this study. A, C, E, G from the M1 phase and B, D, F, H are from the M2 phase of platform development.

A, A middle Miocene (Zone N.8 to N.9) rudstone (left side) with abundant larger foraminiferids, showing part of a large dissolution cavity filled with upper Miocene (Zone N.17) hemipelagic sediment (right side) containing mainly planktic foraminiferids. Field of view 17 mm. Sample 75DR03-5-B2-1. **B**, Late Miocene (Zone N.17A) algal floatstone, in contact with a phosphatic wackestone (probably Zone N.18). Field of view 14 mm. Sample 76DR09I-C2-1. **C**, Extensively bored rudstone with abundant larger foraminiferids, with at least three phases of boring, often cross-cutting one another. The borings are mainly infilled with hemipelagic sediment, often with planktic foraminiferids. Field of view 18 mm. Sample 76DR02/5. **D**, Pliocene phosphatic wackestone with reworked middle Miocene *Lepidocyclina (Nephrolepidina) howchini* showing the complex development of phosphatic deposition. Field of view 8 mm. Sample 76DR09I-A1-2. **E**, Late Miocene hemipelagic sediment with a specimen of a reworked middle Miocene larger foraminiferid, *Lepidocyclina (Nephrolepidina) howchini*, and an early Miocene lithoclast (lower left) containing fragments of other larger foraminiferids (probably *Cycloclypeus*). Field of view 18 mm. Sample 75DR03-7A-1. **F**, Same sample as D, but showing additional specimens of reworked middle Miocene benthic foraminiferids (*Lepidocyclina (Nephrolepidina) howchini* and *Amphistegina radiata*). Field of view 8 mm. Sample 76DR09I-A1-2. **G**, Middle Miocene lithoclasts of dolomitised rudstone in a matrix of early Pliocene hemipelagic sediment. A fracture, infilled with younger, late Pliocene hemipelagic sediment and apatite crusts, extends from the lower left to upper right of the photomicrograph. Field of view 16 mm. Sample 75DR02III-4. **H**, View of the contact between the Late Miocene floatstone and the Pliocene phosphatic wackestone with boring infilled with hemipelagic sediment. Field of view 8 mm. Sample 76DR09-3.

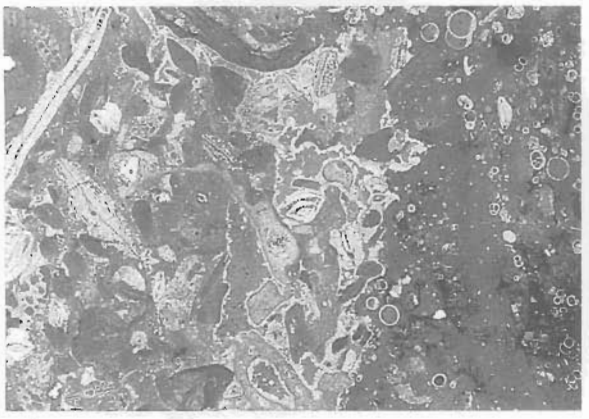

A

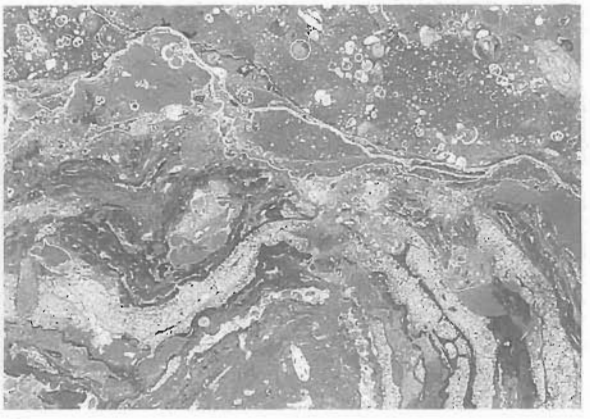

B

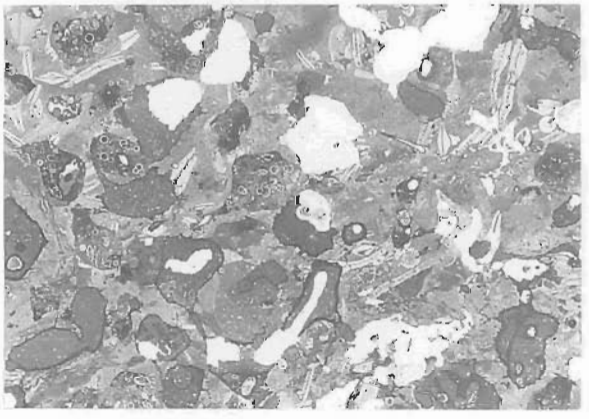

C

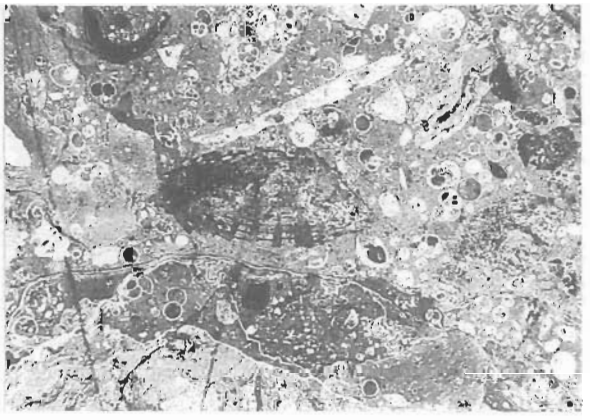

D

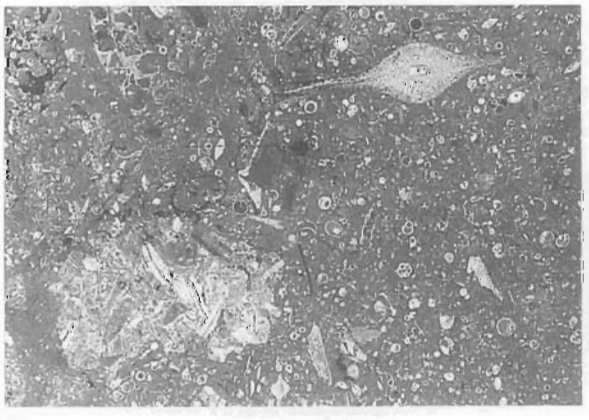

E

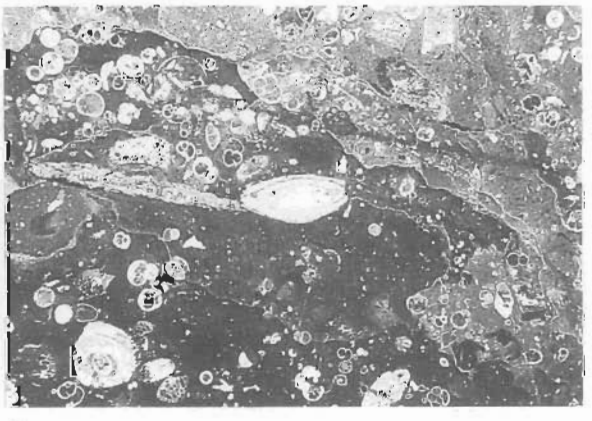

F

G

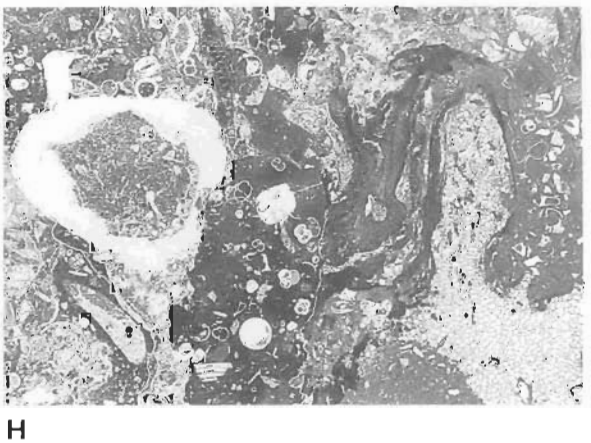

H

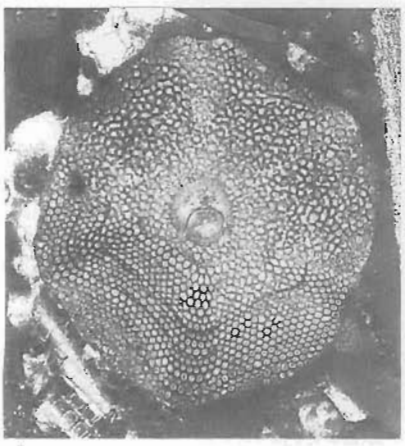

A

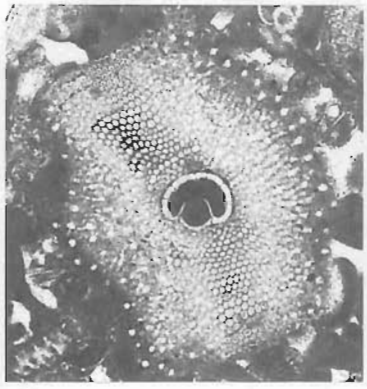

B

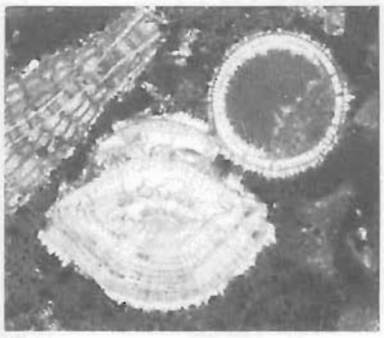

C

D

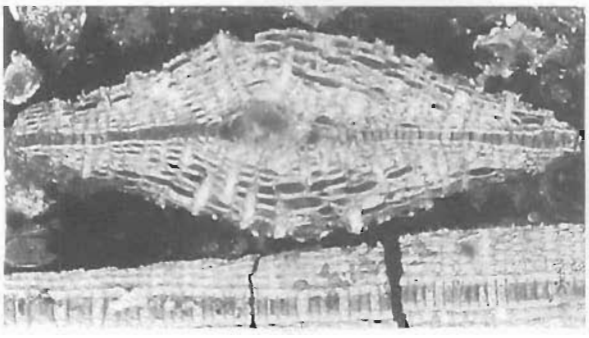

E

G

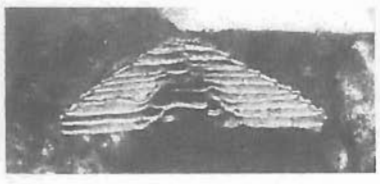

H

K

F

I

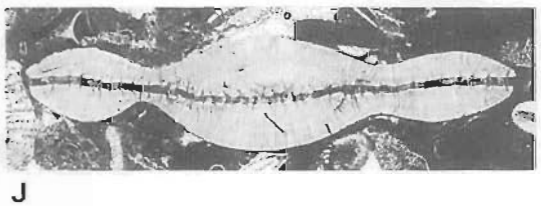

J

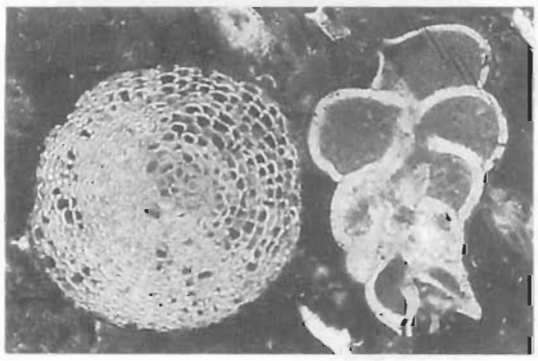

L

M

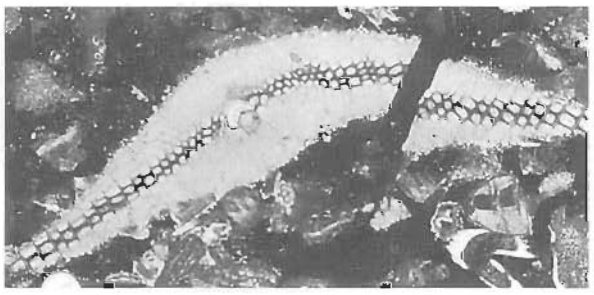

N

were found. Borings cross-cut these lithologies and have taxa that range from Zone N.18 to Zone N.21.

The assemblages of both the floatstone and the wackestone of the condensed section contain reworked larger foraminiferids derived from the older M1 platform phase. However, the low diversity planktic faunas indicate that the M2 platform phase was developed during Zone N.17A, with the condensed section being formed, at least in part, during Zone N.18. No definite Zone N.19 or Zone N.19-20 assemblages were found. Borings that cross-cut these sediments have faunas no older than Zone N.18, may be as young as Zone N.21.

Mounds

Faunas from the mounds are dominated by shallow-water larger benthic forms with some rare planktic species. There appear to be two distinct assemblages, one with the Late Miocene or younger *Gypsina plana* and *Homotrema rubra*, and the other with these species as well as the Pleistocene *Baculogypsina sphaerulata*. *Dentoglobigerina altispira altispira* in one sample limits this to a minimum age of Zone N.21. *Gr. (Truncorotalia) crassaformis* in some of the samples indicates that they are no older than Zone N.19–20, but with the absence of diagnostic younger species, no upper limit can be placed on them. However, as noted above, *Baculogypsina* suggests that most are probably no older than Pleistocene.

Summary

The first phase of platform development (M1) took place within the Early Miocene and ended during the early Middle Miocene. Dissolution cavities were developed on these limestones, probably as a result of exposure (Pigram & others, in press). Deposits of this age have also been recorded by Quilty (in press) from the Britannia Seamount in the Tasman Sea southeast of Brisbane, and from Argo Bank on the Lord Howe Rise; the former exhibit evidence of subaerial exposure. During the Late Miocene (Zone N.17A), the slope of the M1 platform was flooded and the cavities filled both by fauna derived from the underlying carbonates as well as contemporaneous species. At this time, the second phase of platform development (M2) was already underway, probably being developed on the late Early Miocene as suggested by reworked specimens of *Lepidocyclina*, indicative of exposure of the M1 phase (Davies, McKenzie, Palmer-Julson & others, 1992). Zone N.17B and N.19–20 assemblages have been found in cavity-fill sediments only associated with the M1 phase and are absent from the other sites, although some borings may be from these zones at the M2 site; Zone N.18 faunas are present at both platform sites. At both sites, the borings appear to have been infilled over the period of Zones N.19–20 to N.21. One sample from the mounds is probably representative of this same zonal interval, with all other samples likely from within Zone N.22 (Pleistocene).

Palaeoenvironments

The M1-phase sediments are dominated by larger benthic foraminiferids, with rare planktics. The larger benthics, together with bioclasts of hermatypic corals, nodular coralline algae, and *Halimeda*, suggests water depths well within the photic zone, and probably less than 50 m (Chaproniere, 1975), and the planktics and rarity of miliolines normal oceanic salinities, whereas the chlorozoan assemblage indicates warm surface waters (Lees, 1975; Lees & Buller, 1972).

The M2-phase sediments likewise contain shallow-water larger benthic forms and large rhodoliths, which indicates water depths within the photic zone. The absence of *Halimeda*, the higher proportion of planktics, and the rhodoliths, suggest greater water depths than those prevailing at the time of the M1 phase. The hermatypic corals and planktics of the *Gr. (Gr.) tumida* group denotes warm surface water temperatures and normal oceanic salinities.

At the M1 site during Zone N.17A, the diverse planktic faunas are suggestive of water depths greater than at the M2 site. Larger benthic foraminiferids at both sites suggest that there may not have been large differences in depth, although these benthic forms may have been carried in from shallower depths, or were reworked. Certainly, the Early Miocene larger benthics indicate that these were eroded from shallow-water rocks exposed elsewhere.

During Zone N.18 at both sites, Early Miocene larger benthics indicate erosion of older rocks. The rarity of larger foraminiferids contemporary with the diverse and plentiful planktic faunas denotes water depths typical of outer neritic or upper bathyal depths.

The internal sediments of the borings at both sites are dominated by planktic species suggesting they were infilled at depths beyond the range of shallow-water taxa, although, as the sediments are fine-grained and often have small specimens of planktics, it is possible the larger bioclasts were not able to enter the borings.

The diverse planktic assemblages with warm-water forms, such as *Gr. (Gr.) tumida*, suggests a tropical surface water mass throughout the Late Miocene and Pliocene.

The samples from the mounds are dominated by shallow-water bioclasts, including hermatypic corals, coralline algae, *Halimeda*, as well as shallow-water larger benthic foraminiferids (*Marginopora vertebralis*, *Peneroplis* sp., and *Sorites marginalis*). Planktics, though present, are rare. Water depths were within the photic zone. Water temperatures were distinctly tropical. Salinities were probably normal oceanic, judged by the presence of planktic species, although the presence of the miliolines suggests that some of the bioclasts may have been derived from lagoonal environments.

Figure 9. Benthic foraminiferids from the middle Miocene rudstone from the older platform M1 phase.
A, *Lepidocyclina (Nephrolepidina) howchini*. Equatorial section of a stellate specimen. CPC30922, sample 75DR03I-6, x 20. **B**, *Lepidocyclina (Nephrolepidina) howchini*. Equatorial section of a polygonal concentric specimen. CPC30923, sample 75DR03I-8, x 20. **Ca**, *Amphistegina radiata* (CPC30924) with **Cb**, *Orbulina universa* (CPC30925). Off-centre vertical sections, sample 75DR02II-7; x 35. **D**, *Amphistegina radiata*. Off-centre vertical section. CPC30926, sample 75DR03I-6, x 20. **E**, *Lepidocyclina (Nephrolepidina) howchini*. Median section. CPC30927, sample 75DR02II-7, x 25. **F**, *Lepidocyclina (Nephrolepidina) howchini*. Off-centre vertical section of a stellate specimen. CPC30928, sample 75DR03I-6, x 20. **G**, *Operculina complanata*, off-centre vertical section. CPC30929, sample 75DR03I-6, x 25. **H**, *Cymbaloporetta ?squamosa*. Vertical section. CPC30930, sample 75DR03I-6, x 40. **I**, *Lepidocyclina (Nephrolepidina) howchini*. Off-centre vertical section of a polygonal concentric specimen. CPC30931, sample 75DR02II-7, x 20. **J**, *Cycloclypeus (Katacycloclypeus) annulatus*. Off-centre vertical section. CPC30932, sample 75DR03I-6, x 15. **K**, *Operculinella venosa*. Off-centre vertical section. CPC30933, sample 75DR03I-6, x 20. **La**, *Sphaerogypsina globulus* (CPC30934) and **Lb**, *Biarritzina carpenteriaeformis* (CPC30935). Off-centre vertical sections, sample 75DR03I-8, x 20. **M**, *Cycloclypeus (Cycloclypeus) ?carpenteri*. Off-centre vertical section. CPC30936, sample 75DR03I-6, x 15. **N**, *Cycloclypeus (Cycloclypeus) ?carpenteri*. Equatorial section. CPC30937, sample 75DR02II-7, x 15.

Conclusions

(1)The older M1 carbonate platform was built up in a warm shallow-water environment during the late Early to early Middle Miocene (Zones N.7 to N.9).

(2)Sedimentation on the M1 platform ceased within or shortly after Zone N.9, owing to its emergence and was subject to subaerial erosion.

(3)Sedimentation resumed on the M1 platform in the Late Miocene (Zone N.17A), at the same time as the M2 platform was being built in a warm, shallow-water environment.

(4)By the Early Pliocene (Zone N.18), sedimentation had resumed on both platforms, with water depths greater than those during Zone N.17.

(5)Mounds were developed in shallow-water during the Pleistocene adjacent to the M2 platform. Some material from the mounds may be of similar age to sediments found on the platform (Pliocene, Zones N.18 or N.19–20).

(6)No samples were obtained from Zone N.19, possibly suggesting either a period of non-deposition, or sediments of this age were not sampled.

(7)Water salinities were probably oceanic for most of the time at all sites, and surface water temperatures remained warm.

Acknowledgements

We thank Samir Shafik (AGSO) for his comments on the manuscript, the two reviewers Patrick J. Coleman and Patrick G. Quilty for their helpful comments, and Lindell Emerton for drafting the tables.

References

Adams, C.G., 1984 — Neogene larger foraminifera, evolutionary and geological events in the context of datum planes. *In* Ikebe, N. & Tsuchi, R. (editors), Pacific Neogene datum Planes. Contributions to Biostratigraphy and Chronology. *University of Tokyo Press.* 47–67.

Berggren, W.A., Kent, D.V. & van Couvering, J.A., 1985 — The Neogene: Part 2. Neogene geochronology and chronostratigraphy. *In* Snelling, N.J. (editor), The Chronology of the Geological Record. *The Geological Society of London, Memoir* 10, 211–250.

Blow, W.H., 1969 — Late Middle Eocene to Recent planktonic foraminiferal biostratigraphy. *In* Brönnimann, P. & Renz, H.H. (editors), *Proceedings of the First International Conference on Planktonic Microfossils*, I, 199–421.

Chaproniere, G.C.H., 1975 — Palaeoecology of Oligo-Miocene larger Foraminiferida, Australia. *Alcheringa*, 1, 37–58.

Chaproniere, G.C.H., 1980 — Biometrical studies of Early Neogene larger Foraminiferida from Australia and New Zealand. *Alcheringa*, 4, 153–181.

Chaproniere, G.C.H., 1981 — Australian mid-Tertiary larger foraminiferal associations and their bearing on the East Indian Letter Classification. *BMR Journal of Australian Geology and Geophysics*, 6, 145–151.

Chaproniere, G.C.H., 1983 — Tertiary larger foraminiferids from the northwestern margin of the Queensland Plateau, Australia. *Bureau of Mineral Resources, Australia, Bulletin* 217, 31–57.

Chaproniere, G.C.H., 1984a — The Neogene larger foraminiferal sequence in the Australian and New Zealand regions, and its relevance to the East Indian Letter Stage classification. *Palaeogeography, Palaeoclimatology, Palaeoecology*, 46, 25–35.

Chaproniere, G.C.H., 1984b — Oligocene and Miocene larger Foraminiferida from Australia and New Zealand. *Bureau of Mineral Resources, Australia, Bulletin* 188, 1–98.

Chaproniere, G.C.H., 1991 — Pleistocene to Holocene planktic foraminiferal biostratigraphy of the Coral Sea, offshore Queensland, Australia. *BMR Journal of Australian Geology and Geophysics*, 12, 195–221.

Chaproniere, G.C.H. & Betzler, C., in press — Larger foraminiferal biostratigraphy of Sites 815, 816, and 826, Leg 133, northeastern Australia. *In* Davies, P.J., McKenzie, J., Palmer-Julson, A.A., & others, Proceedings of the Ocean Drilling Program, Scientific Results, 133. *College Station, TX (Ocean Drilling Program).*

Davies, P.J., McKenzie, J., Palmer-Julson, A.A., & others, 1992 — Leg 133. Proceedings of the Ocean Drilling Program, Initial Reports, 133, 59–69. *College Station, TX (Ocean Drilling Program).*

Davies, P.J., Symonds, P.A., Feary, D.A. and Pigram, C.J., 1989 — The evolution of the carbonate platforms of northeast Australia. *In* Crevello, P.D., & others (edirors), Controls on carbonate platform and basin development. *Society of Economic Paleontologist and Mineralogists Special Publication*, 44, 31–36.

Kennett, J.P. & Srinivasan, M.S., 1983 — Neogene Planktonic Foraminifera. A Phylogenetic Atlas. *Hutchinson Ross, Stroudsburg, Pennsylvania.*

Lees, A., 1975 — Possible influence of salinity and temperature on modern shelf carbonate sedimentation. *Marine Geology*, 19, 159–198.

Lees, A. & Buller, A.T., 1972 — Modern temperate-water and warm-water shelf carbonate sediments contrasted. *Marine Geology*, 13, M67–M73.

Loeblich, A.R. & Tappan, H., 1988 — Foraminiferal

Figure 10. A to J, Benthic and planktic foraminiferids from the middle Miocene rudstone from the older platform M1 phase. **A, B,** *Ladoronia vermicularis*. Vertical section through a coralline algal nodule, x 10. 2, detail of 1 showing shape and arrangement of chambers. CPC30938, sample 75DR03I-8, x 65. **C to E,** *Praeorbulina glomerosa*. Cross-sections through juvenile stage, showing no areal apertures. **C,** CPC30939, sample 75DR03I-7, **D,** CPC30940, **E,** CPC30941, both from sample 75DR03I-6, x 60. **F,** *Orbulina suturalis*. Cross-section through juvenile stage, showing areal apertures. Restricted to the lower part of the final chamber. CPC30942, sample 75DR03I-6, x 70. **G,** *Orbulina universa*. Cross-section through juvenile stage, showing areal apertures covering most of the final chamber. CPC30943, sample 75DR03I-8, x 60. **H,** *Dentoglobigerina altispira*. Axial section. CPC30944, sample 75DR03I-6, x 50. **I,** *Globigerinoides quadrilobatus*. Axial section. CPC30945, sample 75DR03I-6, x 60. **Ja,** *Globigerinoides quadrilobatus*. (CPC30946); **Jb,** *Dentoglobigerina altispira* (CPC30947). Oblique sections; both from sample 75DR03I-6, x 50. **K to S,** Benthic and planktic foraminiferids from the late Miocene hemipelagic sediment filling solution cavities in rudstones from the older platform M1 phase. **K,** *Lepidocyclina (Nephrolepidina) howchini*. Median section. CPC30948, sample 75DR03III-2, x 30. **L,** *Sphaerogypsina globulus*. Oblique section. CPC30949, sample 75DR03III-2, x 30. **M,** *Amphistegina radiata*. Median section. CPC30950, sample 75DR03III-1, x 50. **N,** *?Globigerinoides obliquus*. Oblique section. CPC30951, sample 75DR03III-2, x 50. **O,** *Orbulina universa*. Axial section. CPC30952, sample 75DR03III-1, x 50. **P,** *Operculinella venosa*. Median section. CPC30953, sample 75DR03III-1, x 10. **Q,** *Sphaeroidinellopsis seminulina kochi*. Oblique section. CPC30954, sample 75DR03III-1, x 50. **R,** *Globorotalia (Obandyella) scitula*. Axial section. CPC30955, sample 75DR03III-1, x 135. **S,** *Globorotalia (Globorotalia) cultrata menardii*. Axial section. CPC30956, sample 75DR03III-2, x 50.


A

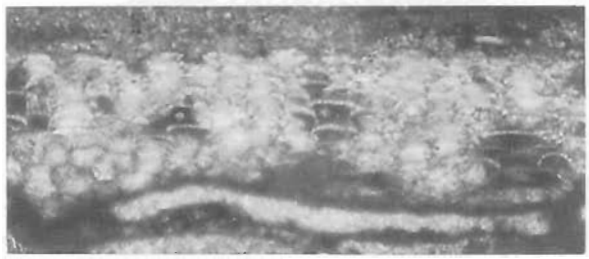
B


C


D

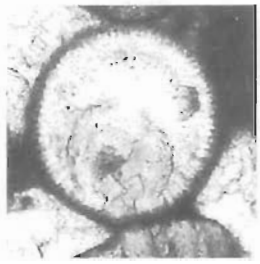
E


F


G


H


I


J

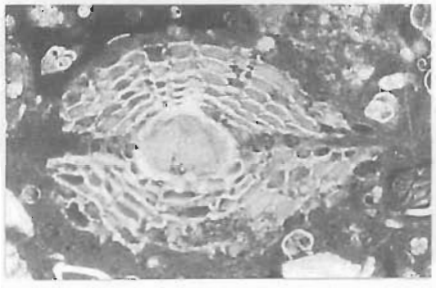
K

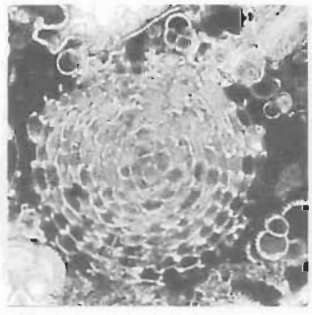
L


M

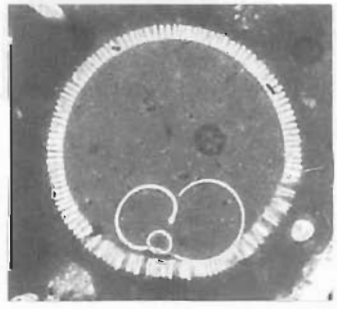
O


P

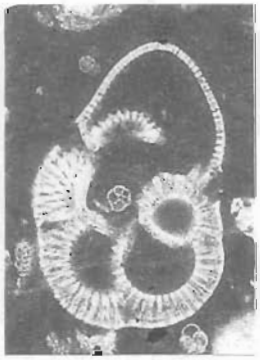
Q


N


R


S

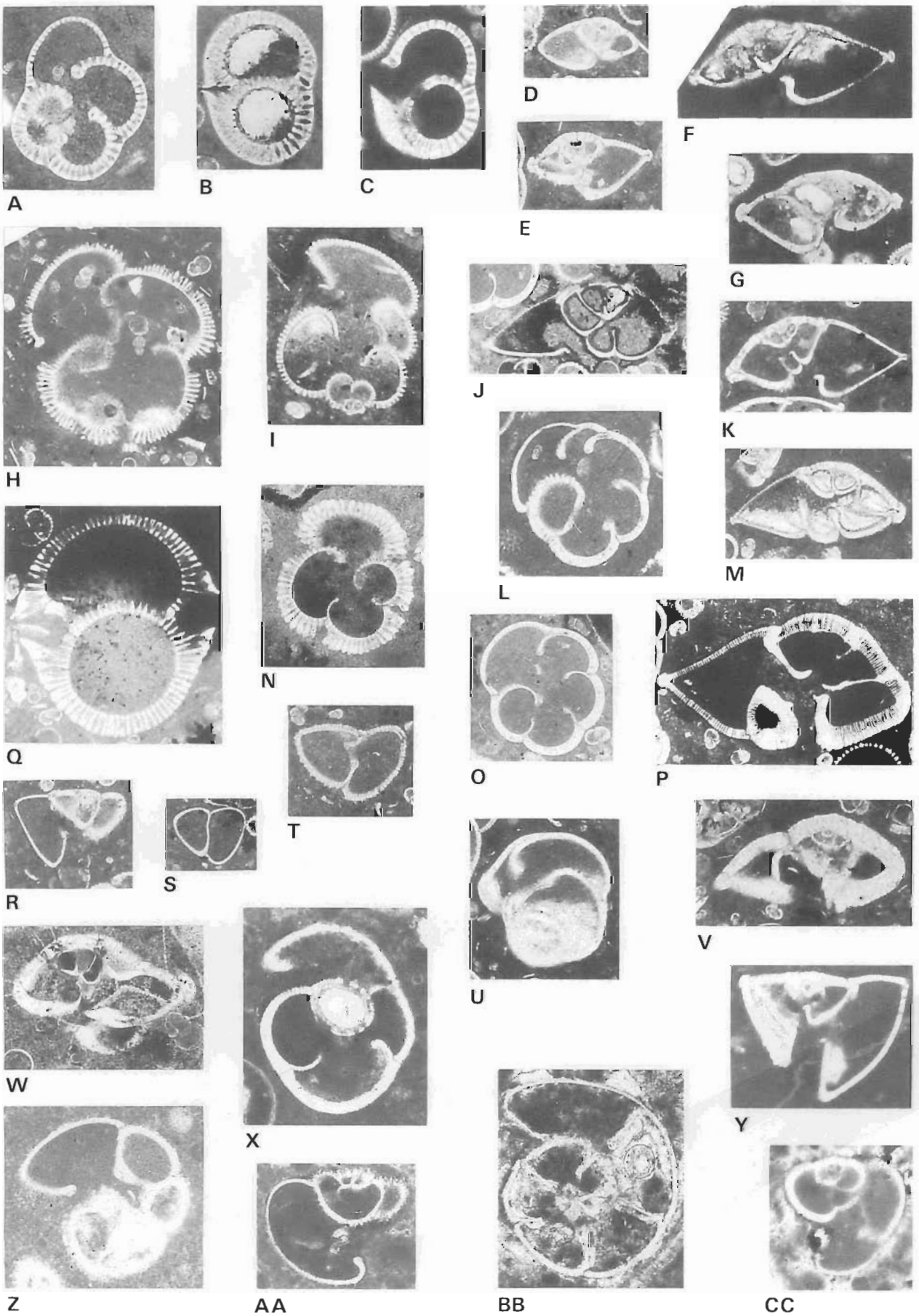
A
B
C
D
E
F
G
H
I
J
K
L
M
N
O
P
Q
R
S
T
U
V
W
X
Y
Z
AA
BB
CC

Genera and Their Classification. *Van Nostrand Reinhold, New York.*

Okada, H. & Bukry, D., 1980 — Supplementary modification and introduction of code numbers to the low-latitude coccolith biostratigraphic zonation (Bukry, 1973; 1975). *Marine Micropaleontology,* 5, 321–325.

Pigram, C.J., Davies, P.J. & Chaproniere, G.C.H., in press — Cement stratigraphy and the demise of the early–middle Miocene carbonate platform on the Marion Plateau. *In* Davies, P.J., McKenzie, J., Palmer-Julson, A.A., & others, Proceedings of the Ocean Drilling Program, Scientific Results, 133. *College Station, Texas (Ocean Drilling Program).*

Pigram, C.J., Davies, P.J., Feary, D.A., & Symonds, P.A., 1992 — Absolute magnitude of the second-order middle to late Miocene sealevel fall, Marion Plateau, northeast Australia. *Geology*, 20, 858–862.

Postuma, J.A., 1971 — Manual of Planktonic Foraminifera. *Elsevier, Amsterdam.*

Quilty, P.G., in press — Tasmantid and Lord Howe seamounts: Biostratigraphy and palaeoceanographic significance. *Alcheringa.*

Sartorio, D. & Venturini, S., 1988 — Southern Tethys Biofacies. *AGIP S. p. A., S. Donato Milanese, Italy.*

Figure 11. A to R, Planktic foraminiferids from the infilled cavities developed in the middle Miocene rudstone of the M1 platform phase.

A, *Sphaeroidinellopsis seminulina seminulina*. Oblique near-equatorial section. CPC30957, sample 75DR03III-7, x 50. **B**, *Sphaeroidinellopsis paenedehiscens*. Off-centre axial section. CPC30958, sample 75DR03III-2, x 50. **C**, *Sphaeroidinellopsis paenedehiscens*. Off-centre axial section. CPC30959, sample 75DR03III-1, x 60. **D**, *Globorotalia (Obandyella) scitula*. Axial section. CPC30960, sample 76DR02-16, x 60. **E**, *Globorotalia (Globorotalia) tumida plesiotumida*. Axial section. CPC30961, sample 76DR02-16, x 60. **F**, *Globorotalia (Globorotalia) cultrata cultrata*. Oblique axial section. CPC30962, sample 75DR03III-1, x 65. **G**, *Globorotalia (Globorotalia) tumida plesiotumida*. Off-centre axial section. CPC30963, sample 76DR02-16, x 65. **H**, *Globigerinoides conglobatus*. Oblique equatorial section. CPC30964, sample 75DR03III-3, x 50. **I**, *Dentoglobigerina altispira*. Axial section. CPC30965, sample 76DR02-16, x 70. **J**, *Globorotalia (Obandyella) margaritae*. Oblique axial section. CPC30966, sample 76DR02-5, x 50. **K**, *Globorotalia (Globorotalia) tumida plesiotumida*. Axial section. CPC30967, sample 75DR03III-2, x 50. **L**, *Pulleniatina primalis*. Oblique equatorial section. CPC30968, sample 75DR03III-1, x 70. **M**, *Globorotalia (Globorotalia) tumida plesiotumida*. Oblique axial section. CPC30969, sample 75DR03III-1, x 50. **N**, *Globigerinoides conglobatus*. Oblique equatorial section. CPC30970, sample 75DR03III-1, x 60. **O**, *Pulleniatina ?primalis*. Oblique equatorial section. CPC30971, sample 76DR02-5, x 65. **P**, *Globorotalia (Globorotalia) tumida tumida*. Off-centre axial section. CPC30972, sample 75DR03III-1, x 50. **Q**, *Sphaeroidinella dehiscens*. Off-centre axial section. CPC30973, sample 76DR03II-4, x 50. **R**, *Globorotalia (Truncorotalia) crassaformis*. Off-centre axial section. CPC30974, sample 75DR03II-4, x 50. **S to W**, Planktic foraminiferids from borings within both the rudstone and cavity fill in the M1 platform phase. **S**, *Globorotalia (Truncorotalia) crassaformis*. Axial section. CPC30975, sample 75DR02-1, x 50. **T**, *Globorotalia (Truncorotalia) crassaformis*. Off-centre axial section. CPC30976, sample 75DR03II-4, x 50. **U**, *Pulleniatina obliquiloculata*. Oblique equatorial section. CPC30977, sample 75DR03II-4, x 50. **V**, *Globorotalia (Globorotalia) tumida tumida*. Axial section. CPC30978, sample 75DR03II-4, x 50. **W**, *Globorotalia (Globorotalia) tumida tumida*. Oblique axial section. CPC30979, sample 76DR02-3, x 50. **X to CC**, Planktic foraminiferids from Pleistocene samples. **X**, *Pulleniatina obliquiloculata*. Oblique equatorial section. CPC30980, sample 76DR04, x 50. **Y**, *Globorotalia (Truncorotalia) truncatulinoides*. Axial section. CPC30981, sample 76DR04, x 50. **Z**, *Globorotalia (Truncorotalia) ?tosaensis*. Oblique equatorial section. CPC30982, sample 76DR04, x 65. **AA**, *Globorotalia (Truncorotalia) crassaformis*. Axial section. CPC30983, sample 76DR04, x 55. **BB**, *Globorotalia (Truncorotalia) truncatulinoides*. Oblique equatorial section. CPC30984, sample 76DR04, x 55. **CC**, *Globorotalia (Truncorotalia) ?crassaformis*. Oblique axial section. CPC30985, sample 76DR04, x 65.


A

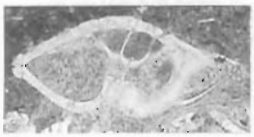
B


E

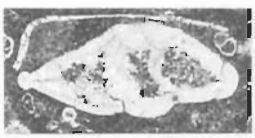
J

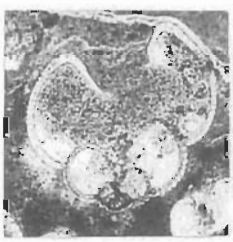
L


P


Q


T


X


C


F

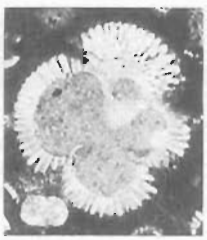
K

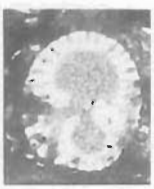
N


G

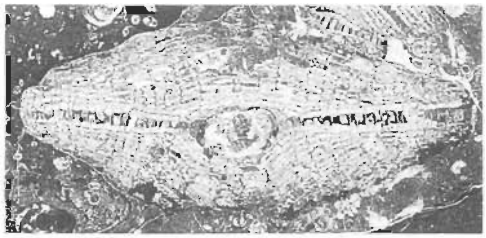
D


H


I


O


R


S


U

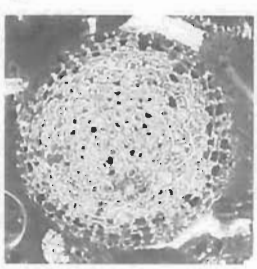
Y

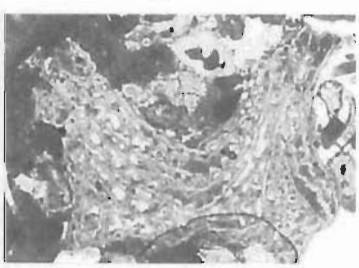
V


M


W

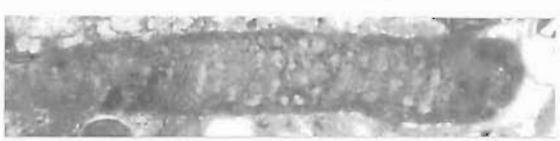
Z

Figure 12. A to K, Planktic and benthic foraminiferids from the hemipelagic sediments with the floatstone lithologies of the younger M2 platform.

A, *Globorotalia (Globorotalia) tumida plesiotumida*. Axial section. CPC30986, sample 76DR09-1, x 50. **B**, *Globorotalia (Globorotalia) tumida ?plesiotumida*. Axial section. CPC30987, sample 76DR09-1, x 50. **C**, *Sphaeroidinellopsis paenedehiscens*, Oblique section. CPC30988, sample 76DR09-1, x 50. **D**, *Lepidocyclina (Nephrolepidina) howchini*, near median section. CPC30989, sample 76DR09-3, x 15. **E**, *Globorotalia (Globorotalia) tumida plesiotumida*. Axial section. CPC30990, sample 76DR09-3, x 50. **F**, *Sphaeroidinellopsis paenedehiscens*. Oblique section. CPC30991, sample 76DR09-3, x 55. **G**, *Operculina complanata*. Vertical section. CPC30992, sample 76DDR03-9, x 30. **H**, *Amphistegina radiata*. Oblique vertical section. CPC30993, sample 76DR09I-C2-2, x 20. **I**, *Cycloclypeus (Cycloclypeus) ?carpenteri*. Off centre vertical section. CPC30994, sample 76DR09I-C2-2, x 30*. **J**, *Globorotalia (Globorotalia) tumida tumida*. Oblique axial section. CPC30995, sample 76DR09-3, x 50. **K**, *Globigerinoides conglobatus*. Oblique axial section. CPC30996, sample 76DR09-3, x 50. **L to P**, Planktic and larger benthic foraminiferids within the hemipelagic sediments overlying the floatstone. **L**, *Dentoglobigerina altispira*. Oblique axial section. CPC30997, sample 76DR09-3, x 55. **M**, *Acervulina inhaerens*. Section through encrusting mass over echinoid spine. CPC30998, sample 76DR03-9, x 35. **N**, *Sphaeroidinellopsis ?paenedehiscens*. Oblique section. CPC30999, sample 76DR09I-C2-2, x 55. **O**, *Lepidocyclina (Nephrolepidina) howchini*. Median section. CPC31000, sample 76DR09-1, x 15. **P**, *Globorotalia (Globorotalia) tumida tumida*. Oblique axial section. CPC31001, sample 76DR09I-C2-2, x 50. **Q to Z**, Larger and planktic foraminiferids from the mounds. **Q**, *Globorotalia (Truncorotalia) crassaformis*. Axial section. CPC31002, sample 76DR07-12, x 65. **R**, *Globorotalia (Truncorotalia) truncatulinoides*. Axial section. CPC31003, sample 76DR07-10, x 60. **S**, *Pulleniatina obliquiloculata*. Axial section. CPC31004, sample 76DR07-3, x 60. **T**, *Sphaeroidinella dehiscens*. Off-centre axial section. CPC31005, sample 76DR07-12, x 50. **U**, *Globorotalia (Truncorotalia) ?tosaensis*. Axial section. CPC31006, sample 76DR07-10, x 60. **V**, *Homotrema rubra*. Section through branching specimen. CPC31007, sample 76DR07-8, x 15. **W**, *Operculinella venosa*. Median section. CPC31008, sample 76DR07-8, x 30. **X**, *Globorotalia (Globorotalia) tumida tumida*. Off-centre axial section. CPC31009, sample 76DR07-3, x 50. **Y**, *Sphaerogypsina globulus*. Random section. CPC31010, sample 76DR07-1, x 15. **Z**, *Marginopora vertebralis*. Oblique section through fragment. CPC31011, sample 76DR07-12, x 30.

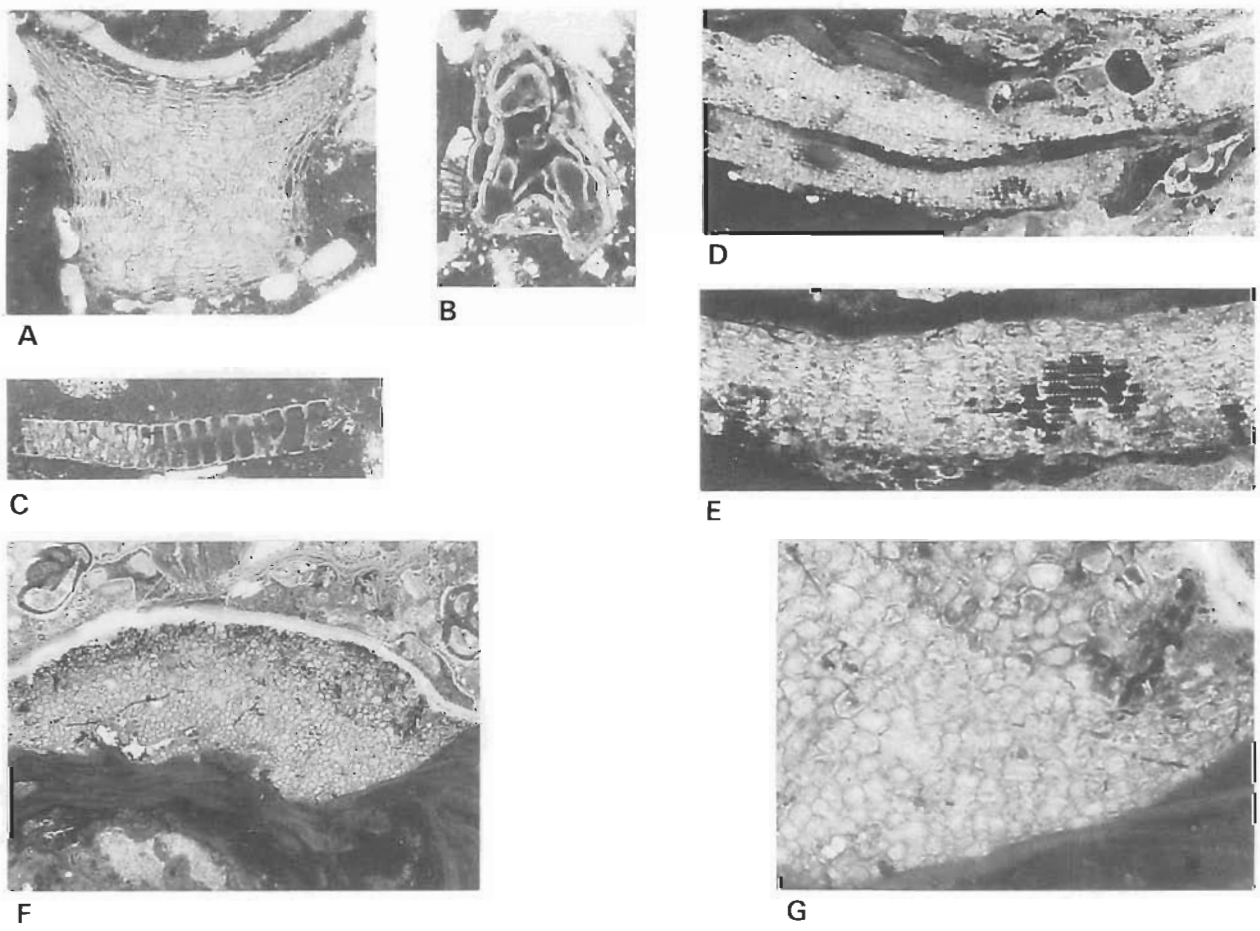

Figure 13. A to C, Larger benthic foraminiferids from the mounds in front of the M2 platform.

A, *Baculogypsina sphaerulata*. Oblique section. CPC31012, sample 76DR07-3, x 30. **B**, *Acervulina inhaerens*. Oblique section. CPC31013, sample 76DR07-3, x 30. **C**, Fragment of *Sorites* sp., or *Peneroplis* sp. Oblique section. CPC31014, sample 76DR07-3, x 35. **D to G**, *Gypsina plana*. Sections through encrusting mass. **D and E**, Same specimen; E detail of D. Vertical section showing chamber arrangement. CPC31015, sample 76DR09-2, x 15 and 50. **F and G**, Same specimen; G detail of F. Section showing arrangement of chambers perpendicular to the vertical. CPC31016, sample 76DR09-1, x 15 and 25.

AGSO Journal of Australian Geology & Geophysics, 14, 21–34

Architecture of the Queensland Trough: implications for the structure and tectonics of the Northeastern Australia Margin

Deborah L. Scott[1]

The Queensland Trough is a 155°-trending bathymetric deep, located just seaward of the Great Barrier Reef of northeast Australia. The trough reaches a maximum depth of 2800 m, separating the continental shelf and the submerged Queensland Plateau. It is underlain by extended continental crust. This preliminary interpretation of the trough's deep structure uses 3700 km of 1970's vintage seismic data, supplemented by gravity and magnetic data from the same surveys. The main seismic profile grid has a spacing of approximately 50 km. However, another survey shot in a zigzag pattern provides line spacing locally as close as a few kilometers.

Acoustic basement, characterized by a chaotic and indistinct seismic signature with rare, discontinuous steeply dipping reflections, is overlain by two main acousto-stratigraphic megasequences within the trough: (1) The post-rift section comprises flat-lying, continuous reflections and extends up to two seconds two-way travel time (TWT) below the water bottom. (2) The syn-rift section consists of moderately dipping semi-continuous reflections, separated by zones of chaotic reflections and diffractions. The reflection separating the syn- and post-rift packages is quite distinct, characterized by angular discordances and truncated reflections. No wells have penetrated the syn-rift package.

Seismic profiles in all orientations reveal tilted basement fault blocks. Many bounding faults are clearly listric. Half-graben form a series of syn-rift depocenters with up to 5 km of syn-rift fill. Syn-rift depocenters appear to be elongate along the axis of the trough, suggesting rift-parallel bounding faults and orthogonal extension. However, no structures parallel or perpendicular to the trough axis have been recognized. Most of the syn-rift depocenters are composed of two or more smaller "deeps".

Two rifting models provide alternative syn-rift structural interpretations: (1) Curvilinear faults, based on a model derived from the East African Rift where the tectonic transport direction has been shown to be oblique to the rift axis, define a series of half-graben. Accommodation zones and half-graben polarity switches are identified from profile and plan-view geometries. (2) Nearly rectilinear 110°- and 020°-striking faults, based on orthogonal extension models, predominate. However, both of these trends are oblique to the rift axis contrary to predicted geometries. "Transfer faults" provide a structural basis for the apparent compartmentalization the syn-rift isopach cells into the "deeps".

The data are insufficient to unequivocally support either model, although the orthogonal extension fault geometry better explains the distribution of the depocenters. Both interpretations, combined with limited basement dip information suggest that the structure underlying the Queensland Trough is the product of oblique rifting. Extension is aligned obliquely to the trough at 110°, rather than perpendicular to the rift elongation at 065°. The proposed kinematics suggest that formation of the trough pre-dates either the Coral or Tasman Sea taphrogenesis.

Introduction

The Queensland Trough is a bathymetric deep located just seaward of the Great Barrier Reef of northeast Australia (Fig. 1). Its present-day axis trends northwest-southeast at 155°. The trough defines the boundary between the continental shelf and the submerged Queensland Plateau, considered to be continental crust (Ewing & others, 1970). The deeper northern end of the trough has a maximum depth of 2800 m, and is linked to the Coral Sea Basin to the north by the Osprey Embayment, which appears to be underlain in part by oceanic crust (Symonds & others, 1984). The southern terminus of the trough shallows to 800 m at the intersection with the approximately east-west-trending Townsville Trough, separating the Queensland and Marion Plateaux. Previous interpretations of the Queensland Trough (Falvey & Taylor, 1974; Falvey & Mutter, 1981; Falvey & others, 1990; Gardner, 1970; GSI, 1980; Karig, 1971; Mutter, 1977; Mutter & Karner, 1978; Pinchin & Hudspeth, 1975; Symonds & others, 1983; Symonds & others, 1984; Symonds & Davies, 1988; Taylor & Falvey, 1977) invoked either Early to Late Cretaceous extension associated with the creation of the Tasman Sea spreading ridge to the south, or Paleocene to Eocene extension associated with the Coral Sea spreading ridge to the north, as mechanisms for trough formation. However, no reliable dating of the deep sediments is available. Refraction data (Ewing & others, 1970; Falvey & Taylor, 1974) suggest a sediment package at least 4 km thick in the trough.

The present study complements other, largely AGSO-sponsored ongoing work, that addresses the evolution of Australia's northeast margin. The Queensland Trough is a little known major depocenter, yet its evolution and architecture is critical to understanding the long-term petroleum potential of this region. Previously unpublished data are presented. Profile-specific geometries demonstrate that both "dip" and "strike" lines exhibit substantial

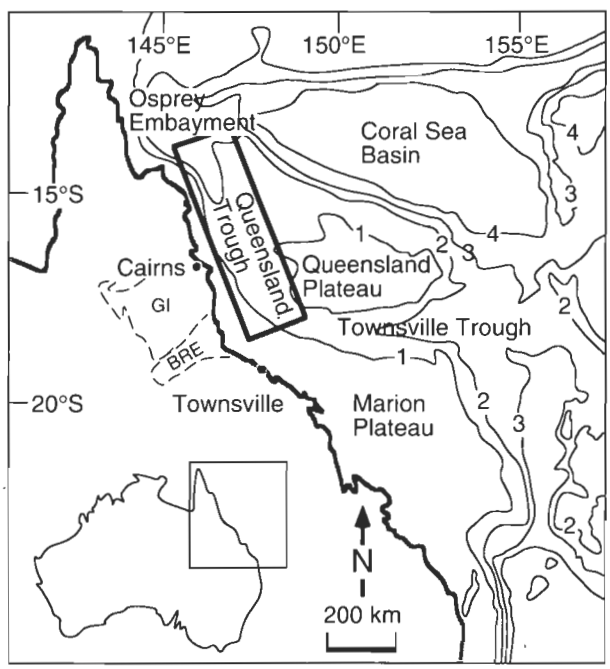

Figure 1. Location map of study area (heavy box) on the northeast margin of Australia and major physiographic features. Contours are in 1000's of meters. GI = Georgetown Inlier. BRE = Broken River Embayment.

[1] Research School of Earth Sciences, The Australian University, Canberra, ACT 2601

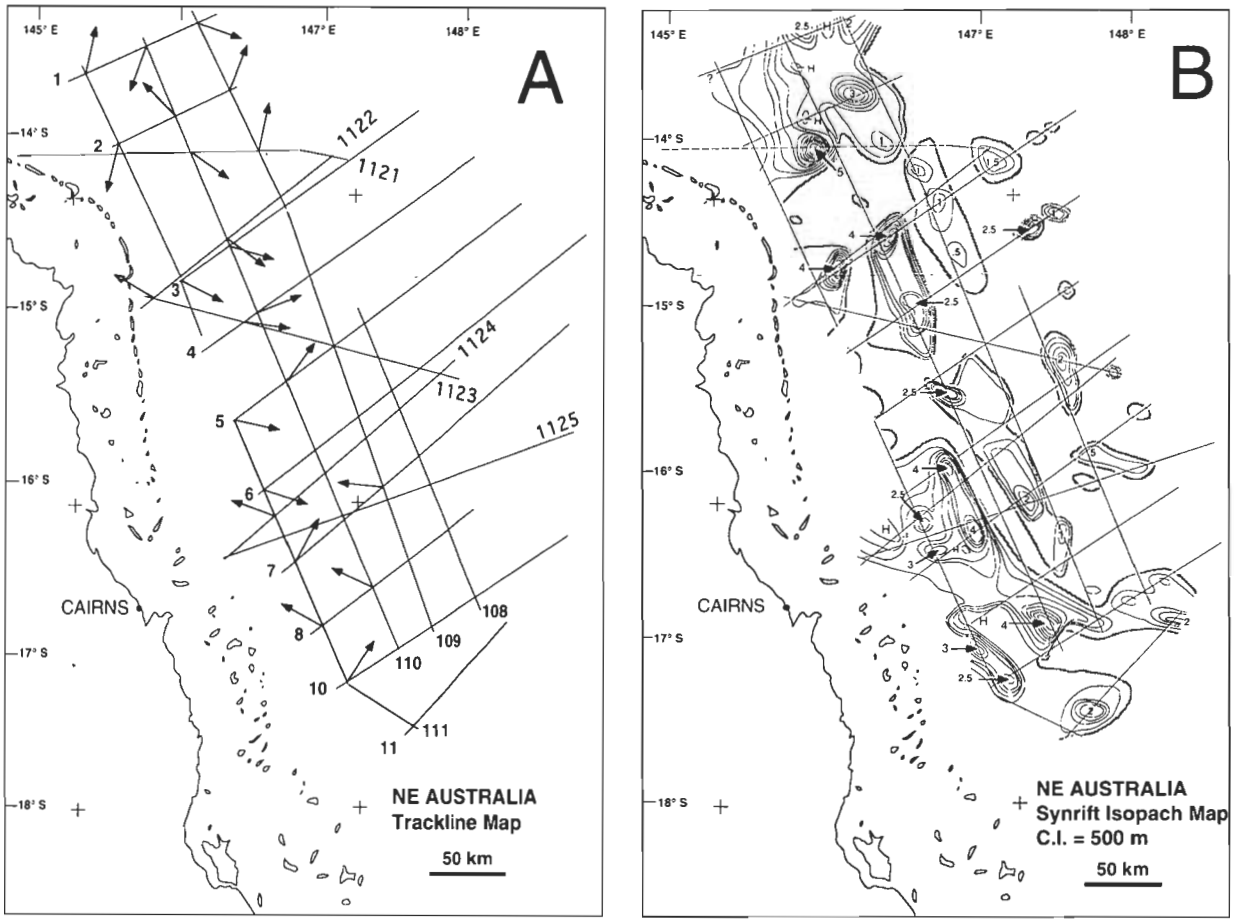

Figure 2. (A) Trackline map of data coverage over the Queensland Trough used in this study. Shaded segments are shown in the line drawings in Figures 4 through 7. Arrows indicate computed azimuth of basement dip. (B) Syn-rift isopach map of the Queensland Trough. Syn-rift depocenters appear to occur in elongate trough-parallel depressions. However, each depocenter appears to be composed of a number of deeps.

rotation of extended basement blocks.

The wide grid spacing of the presently available data makes it impossible to precisely constrain the structural geometry of the Queensland Trough. However, two extension models can be fitted to the observed structures, thus providing insights into the underlying rift architecture. Both alternative fault patterns, combined with measured basement rotation directions, indicate that the Queensland Trough formed by oblique rifting. Further, the proposed direction of extension appears to be incompatible with plate motion vectors involved in the seafloor-spreading phases responsible for opening either the Coral or Tasman Seas. It is suggested that the extension which produced the Queensland Trough pre-dates the extension episodes preceding the opening of both the Coral or Tasman Seas. A similar suggestion by earlier workers (Mutter & Karner, 1980; Symonds & others, 1987) is supported by this analysis.

The data

Figure 2A shows the location of approximately 3700 km of multi-channel seismic data collected by (GSI, 1974, 1979). The 1979 rectilinear grid over the trough has a spacing of approximately 50 km. The 1974 grid was shot in a zigzag pattern, thus providing line spacing locally as close as a few kilometers. The seismic data were processed using standard industry parameters of the time. The interpretation presented here is supplemented by gravity and magnetic data collected during the same surveys (GSI, 1980). Profiles perpendicular to the trough axis are conventionally referred to as "dip" lines and profiles parallel to the trough axis as "strike" lines and this usage is retained here. However, as will be demonstrated, these terms are misleading in the context of oblique rifting.

Two acousto-stratigraphic megasequences can be recognized in the seismic data (Fig. 3). The post-rift section comprises flat-lying, very continuous reflections and extends up to two seconds (TWT) below the water bottom. The syn-rift section is characterized by semi-continuous, moderately dipping, diverging reflections that are separated by zones of chaotic reflections and diffractions. The megasequence boundary separating the syn- and post-rift packages is distinct, characterized by onlap above and angular truncation below. The pre-rift or basement section is commonly chaotic or incoherent, but steeply dipping, discontinuous reflections are recognizable locally, especially in areas of high-standing basement within the rift and on the adjacent plateau. The boundary between the syn-rift and underlying basement is sometimes quite distinct, but is more commonly defined by a gradual loss of seismic character and/or a velocity jump. No wells have penetrated the syn-rift package, but 1000 m of the post-rift section were cored in the central Queensland Trough during Leg 133 of the Ocean Drilling Program (Davies & others,

1991). The hole was drilled near the intersection of Lines 7 and 111 (Fig. 2A). Its total depth corresponds to 3.2 TWT, well above the interpreted boundary between the post- and syn-rift megasequences interpreted herein (Fig. 3), and the oldest sediments intersected have been dated at Early Miocene.

Line drawings of the "dip" lines are shown in Figure 4. In each case, the dashed line is the seafloor. The majority of these profiles trend northeasterly (Fig. 2), but profile trends range from northeast, to due east, to southeast. The dotted line is the boundary between the flat-lying reflections of the post-rift megasequence and the dipping reflections of the syn-rift megasequence. The syn-rift reflection configuration can vary substantially. They are sometimes quite continuous, as in the half-graben on the right end of the profile in Figure 3, but also can be semi-continuous dipping reflections or diffractions as in the half-graben imaged on the left. As the focus of this article is the syn-rift megasequence and its tectonic significance, none of the flat-lying post-rift reflections have been digitized in the line drawings for clarity.

As noted earlier, water depths increase to the north along the axis of the Queensland Trough. However, there is no similar systematic increase in the thickness of the post-rift sediments; rather, they thicken over areas underlain by the dipping reflections of the syn-rift section and thin over basement highs. This may indicate either increased subsidence due to greater sedimentary loads or later fault movement in some places. Where there is no evidence of an underlying syn-rift section or where basement shallows, profile sections have been omitted from the line drawings.

Structural style

A striking feature of the profiles is the predominance of half-graben morphology along the entire rift. The majority of the half-graben deepen to the east and are bounded by west-dipping faults. Exceptions are the isolated half-graben deepening westward on the right end of Line 1122 (Fig. 4A) and a system of likewise westward-deepening half-graben in the southern-central portion of the rift on the right end of Lines 1124, 1125 & 7 (Fig. 4B). The northern profiles (Lines 1 & 2, Fig. 4A) image distinctly more chaotic and less coherent reflections below the post-rift megasequence. To the south on Lines 1121, 1122 & 3 (Fig. 4A), the deep structure of the trough is characterized by one or two half-graben, separated by apparently undeformed high-standing basement blocks. Farther south still, most profiles show a series of tilt-blocks that define larger composite half-graben (Lines 1123, 4, 5, 6, 1124, 1125, 7, & 8, Figs 4A & B). Finally, in the southernmost profile (Line 10, Fig. 4B), extensional strain is manifested by two widely separated half-graben which lie on both sides of the bathymetric trough. Examining each of these zones in more detail and including some "strike" or rift axis parallel profiles, one can establish the geometry of the syn-rift structure.

The three most northern dip lines (Fig. 4A) are tied by strike lines shown in Figure 5. Similarly to the two most northern profiles (Lines 1 and 2), the left end of the strike profiles have very discontinuous and chaotic reflection character beneath the post-rift megasequence. The sense of half-graben polarity and the presence of tilted fault blocks is ambiguous, although some dipping reflections

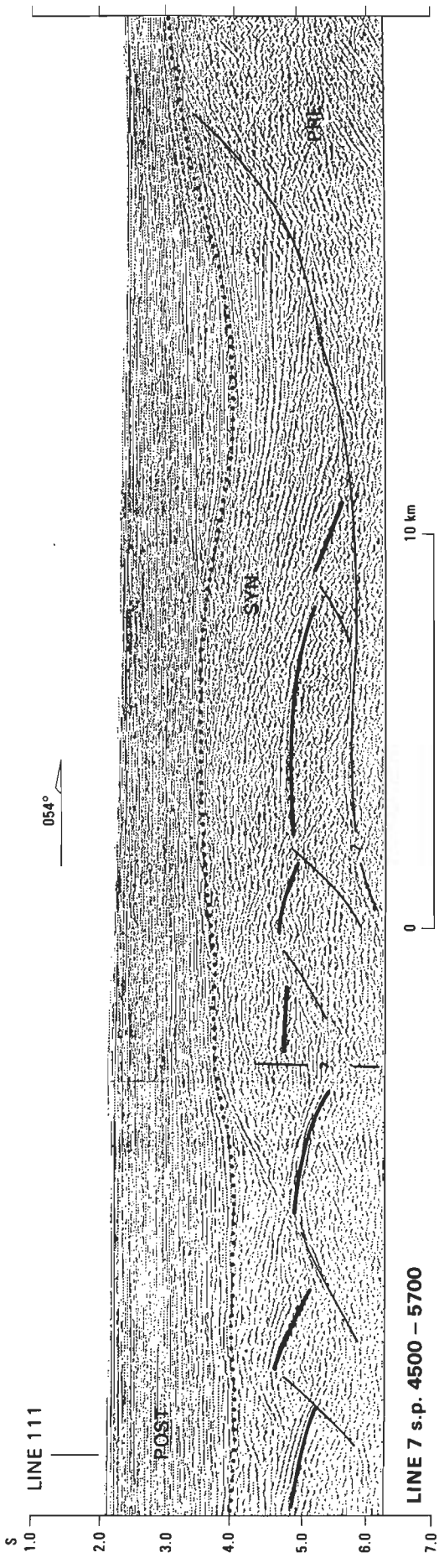

Figure 3. An example of the seismic data from the Queensland Trough. Two megasequences (referred to as the pre- and syn-rift) overlying acoustic basement (post-rift) are recognizable throughout the data set. Dotted line represents the boundary between flat-lying continuous reflections of the post-rift section and the dipping, semi-continuous reflections, separated by chaotic zones and diffractions of the syn-rift section. Solid line separates the base of the syn-rift from the chaotic, discontinuous reflections of the pre-rift basement. Note the variable rotation of tilted fault blocks on this NE trending "dip" line. For location see Figures 2A and 4B.

do extend deep into the section. The next line to the south (1121) records a clear, albeit isolated, half-graben that is manifested on the strike profiles (Lines 110 and 111, Fig. 5) by a thickening of the post-rift section in this locale.

Although it is not clear from these line drawings, the northern syn-rift reflections tend to be of higher amplitude than those to the south. The highly diffractive character of the reflections suggests the presence of volcanics; this is supported by the proximity to interpreted oceanic crust to the north in the Osprey Embayment (Symonds & others, 1984). Likewise, very high-amplitude events within the post-rift section, such as the example on the right end of Line 1 (Fig. 4A; labelled "V") between the intersections with Lines 110 and 109, may be interpreted as flows.

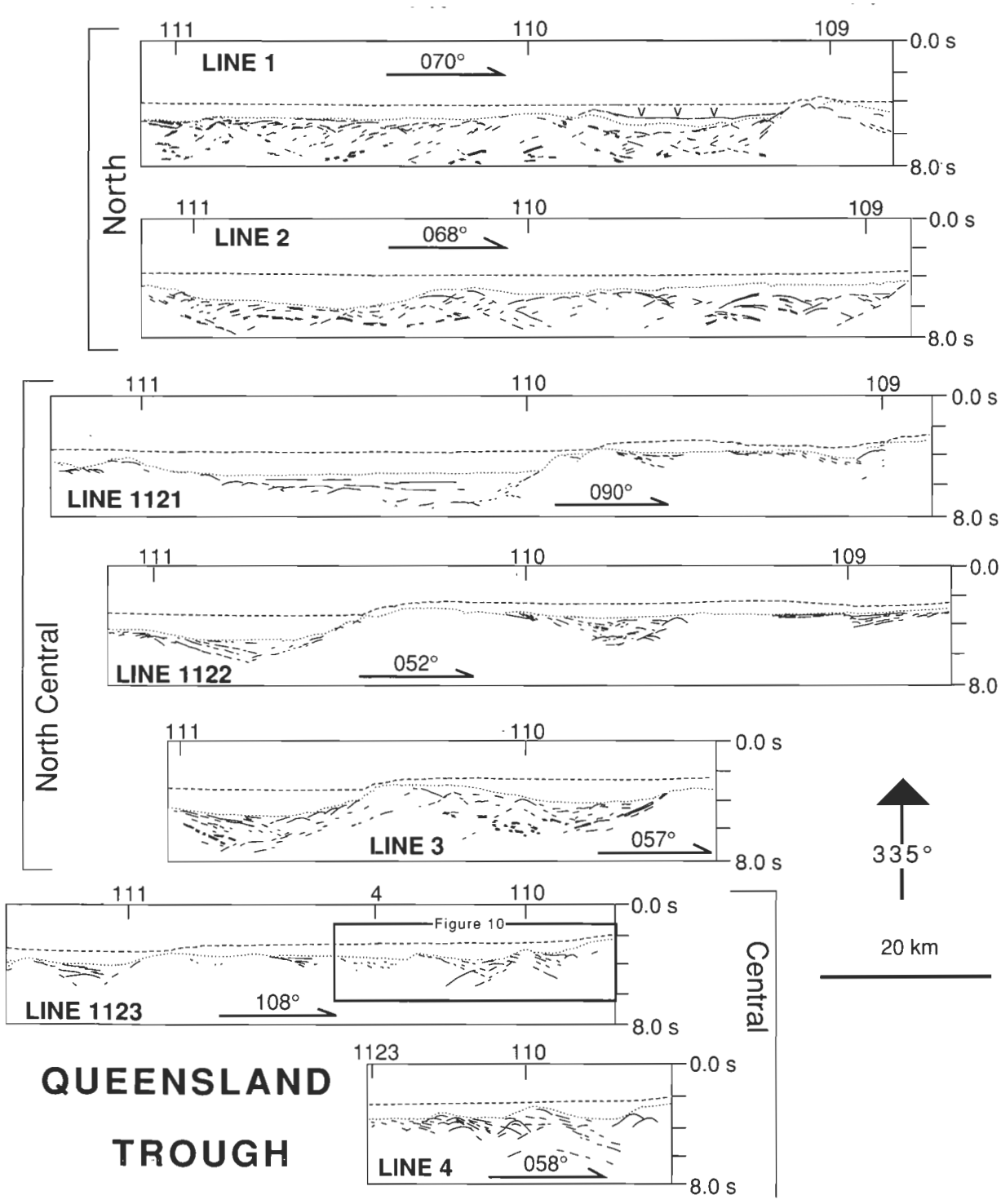

Figure 4. Line drawings of the (A) northern "dip" lines and the (B) southern "dip" lines in the Queensland Trough. Orientations of profiles are indicated by arrows and azimuths. Profiles are "hung" on the strike Line 110 and view is NW (335°). Profile ties are indicated. Boxes indicate portions of seismic profiles shown in Figures 3, 8 and 10 for comparison of seismic character to line drawings. Dashed lines represents the water/sediment interface. Dotted lines represent the boundary between the post- and syn-rift megasequences. See Figure 2A for locations.

Dip Lines 1121 and 1122 (Fig. 4A) show well-defined half-graben, isolated from each other by seemingly undeformed, planated basement. These isolated half-graben average 10–15 km in width. On Line 3, there is some evidence for a series of tilted fault blocks joining the two half-graben on either end of the profile. On the eastern end of Line 1122 on the Queensland Platform, the half-graben which deepens to the west does not extend to either undeformed so is not shown in the line drawings. An isolated half-graben with the opposite polarity is imaged on Line 1121 to the north, suggesting that an unrecognized structure (?transfer fault) must be present between the two profiles to allow for the different rotation of basement.

Strike profiles (Fig. 6) that tie dip Lines 1122 and 3 record dipping reflections, but individual half-graben are not well

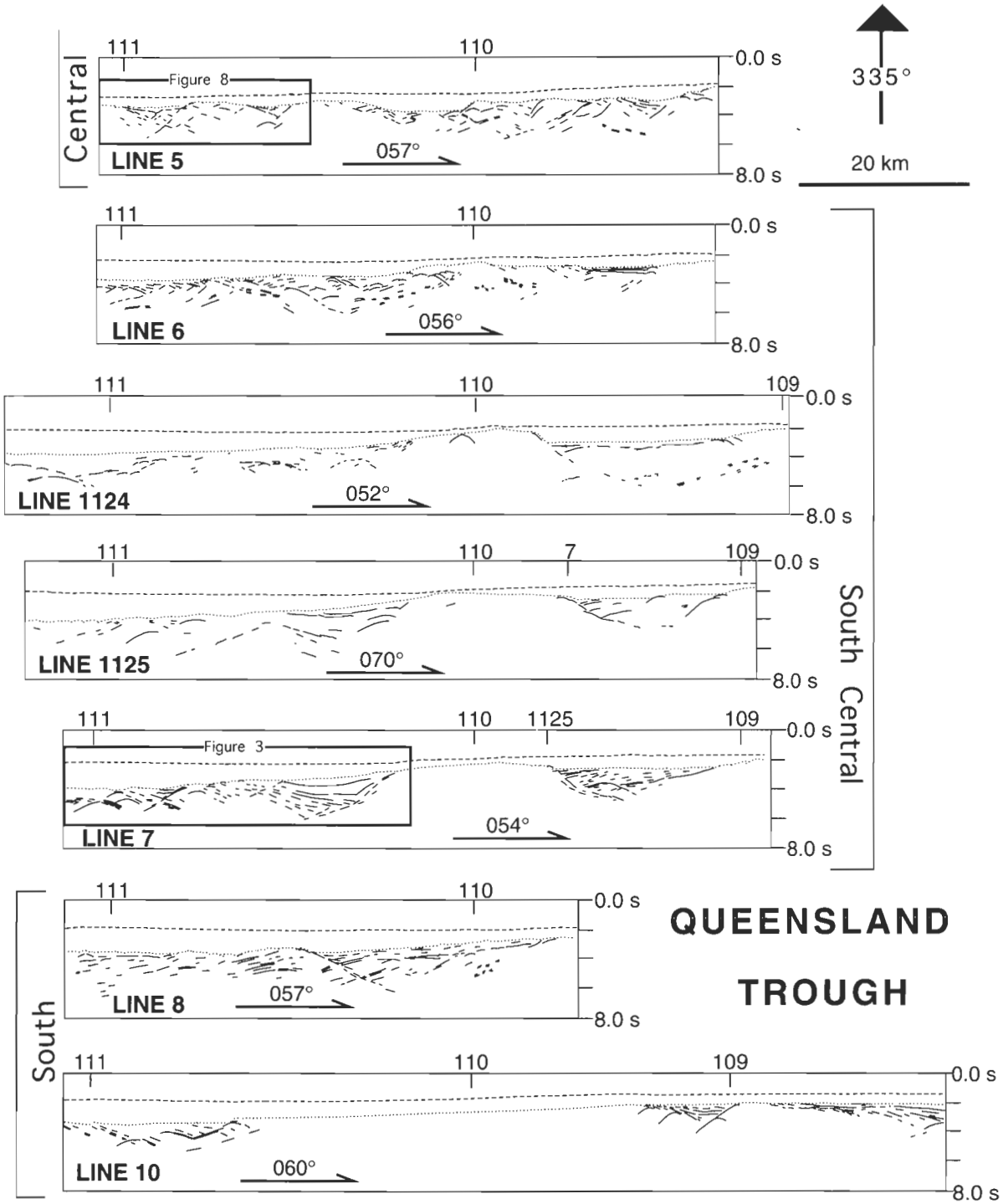

adjacent profile and is apparently totally isolated from the main trough. To the south on Line 3, no half-graben is present, and plateau basement to the east appears to be defined. On Line 110, a full-graben morphology is suggested by inward-dipping faults and outward-dipping syn-rift reflections at either end of the profile. These

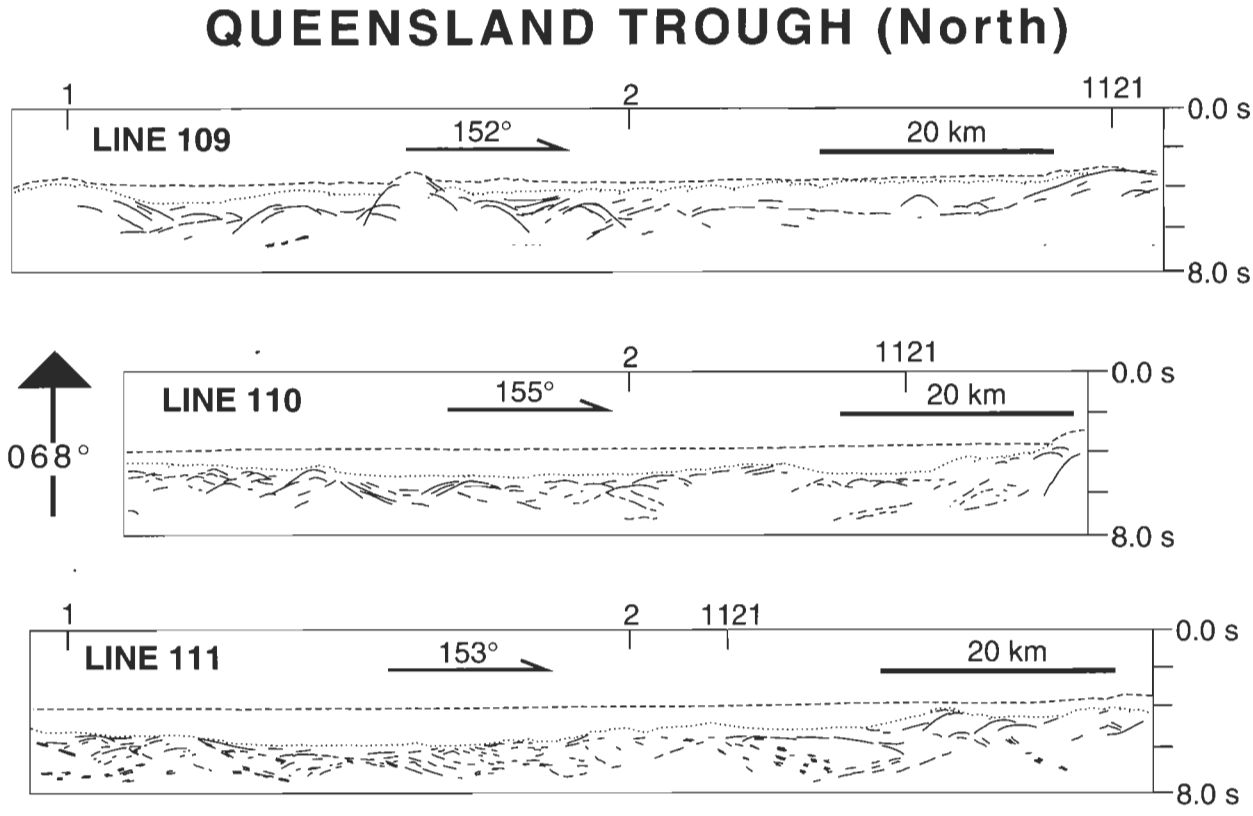

Figure 5. Line drawings of the northern "strike" lines of the Queensland Trough. Notations and locations as in Figure 4.

reflection/fault geometries are consistent with our traditional view of "dip" versus "strike" lines. That is, the data record higher rotation of syn-rift reflections, and more clearly imaged extensional features, such as tilted fault blocks, on dip profiles rather than on strike profiles. This relationship is predicted if extension has been aligned perpendicular to the rift axis or northeast–southwest. However, to the south, this relationship does not hold up and is not consistent throughout the rift zone.

In the central part of the trough, dip Lines 1123, 4 and 5 (Figs 4A & B) image series of tilted fault blocks combining to form composite half-graben rather than the single isolated half-graben that characterized the northern part of the trough. The composite half-graben morphology is typical of rifted basins elsewhere (e.g. Florensov, 1969; de Charpal & others, 1978; Ramberg & Neumann, 1978; Chenet & others, 1982; Logatchev & others, 1983; Bally, 1984; Ramberg & Morgan, 1984; Skilbeck & Lennox, 1984; Etheridge & others, 1985; Rosendahl, 1987). The size of tilted fault blocks is smaller, averaging 5–10 km. The post-rift section thins and thickens over each fault block. The only strike line through this part of the trough with recognizable syn-rift section is the one that runs down the axis of the trough (Line 110, Fig. 7A). It has all the characteristics one expects to see: that is, reflection packages with a variety of dips separated by sub-vertical reflection disruptions. The post-rift section undulates near the ties with Lines 4 and 1123, but is fairly constant in thickness and depth south of the tie with Line 5. The thickness of the post-rift section along this strike line does not vary as diagnostically as on the dip lines, where changes in thickness reflect the asymmetry of deeper structures.

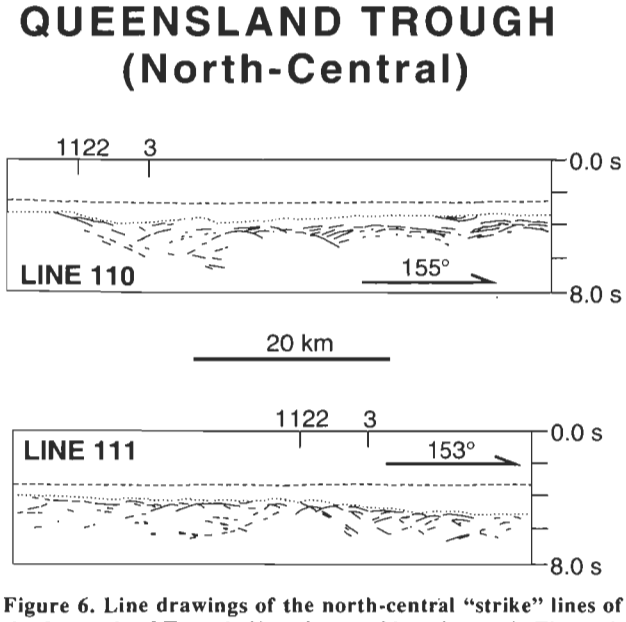

Figure 6. Line drawings of the north-central "strike" lines of the Queensland Trough. Notations and locations as in Figure 4.

Seismic profiles over the half-graben on the western end of Line 5 and the section of a strike line that it crosses are shown in Figure 8. Although there is apparent rotation of basement into a west-dipping fault on the western end of Line 5, there is clearly as much — if not more — rotation and higher subsidence to the south along Line 111. Likewise, the relationship of the post-rift thickness and underlying structure noted above is clearer on the strike line (111) than on the dip line (5). This example highlights the fact that seismic profiles of all orientations in the data set reveal tilted basement fault blocks, and there does not seem to be a consistent relationship between basement rotation and orientation of the profiles as one might

expect in simple extensional regimes (see later discussion section).

In the next "dip" profile to the south (Line 6, Fig. 4B), tilted fault blocks are locally as small as 1 to 3 km across. Lines 1124, 1125 and 7 to the south image the only observed linked polarity switch along the rift axis. On these three adjacent profiles, a basement horst separates opposing polarity half-graben, both deepening toward the horst. The westernmost strike profile (Line 111, Fig. 7B) also

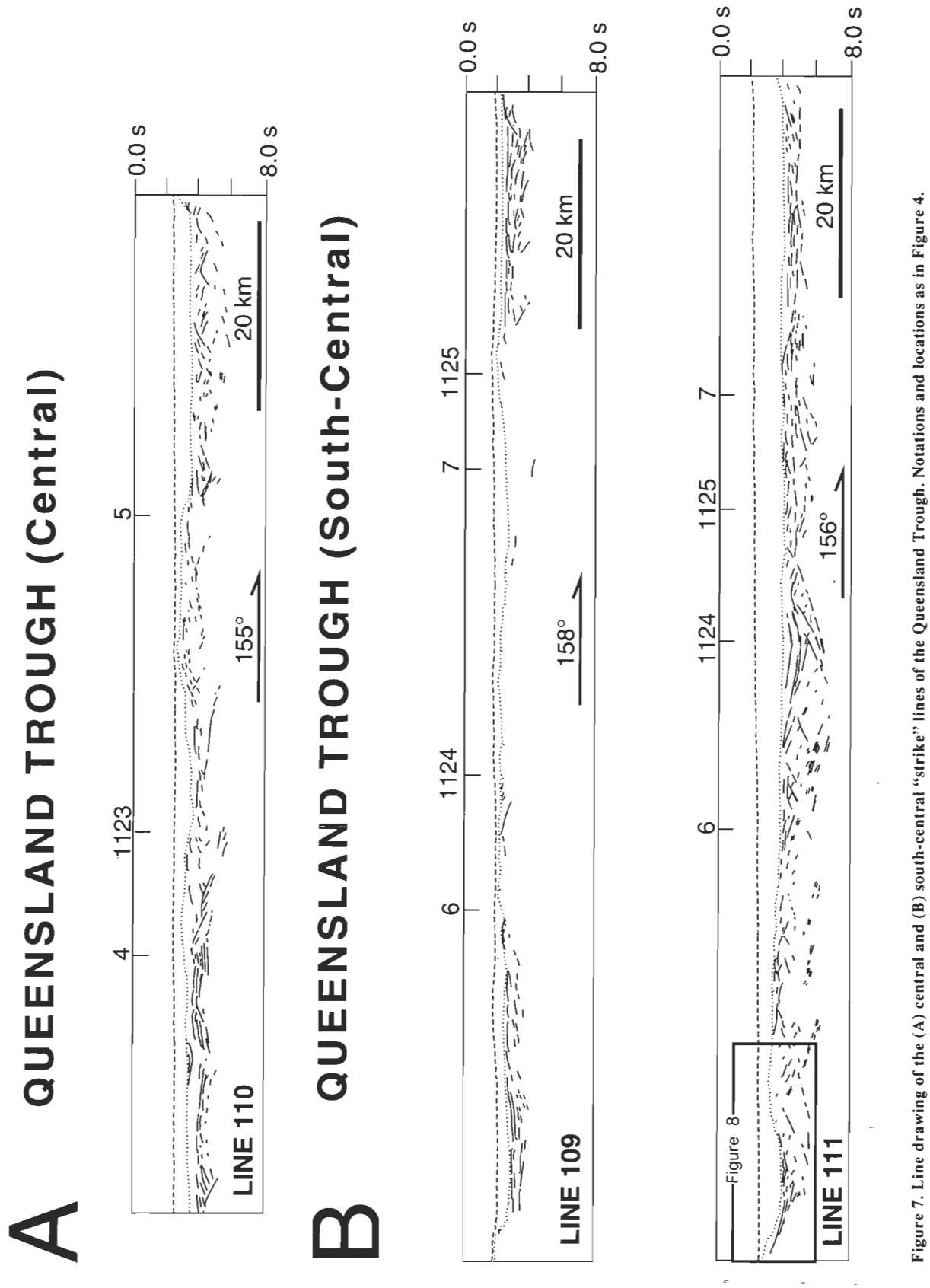

Figure 7. Line drawing of the (A) central and (B) south-central "strike" lines of the Queensland Trough. Notations and locations as in Figure 4.

images both tilted fault blocks and diverging syn-rift reflections, in contrast to what is expected from a "strike" line in simple rift-perpendicular extension. In fact, the half-graben imaged at the tie with Line 1124 is clearly more highly rotated on the strike profile (Line 111). The easternmost strike line (Line 109, Fig. 7b) sits almost entirely on the western edge of the Queensland Plateau. However, where the syn-rift section is imaged to the right of the tie with the dip profile (Line 1125), it also has a significant dip. The middle strike profile is not shown, because it images only the apparently undeformed basement horst seen in the "dip" lines. Although the horst appears to be a continuous feature, crossing Lines 1125 and 7 near their intersection and continuing north a distance of approximately 40 km to Line 1124, it is not seen on Line 6 farther north. Likewise, the horst is not imaged on Line 8 to the south. On the western end of Line 8 (Fig. 4B), westward-dipping syn-rift reflections and eastward-dipping fault plane reflections, continue through the intersection of Line 110 where one expects to see the continuation of the horst. Eastward of the expected location of the horst, a platform begins and continues seemingly undeformed to the eastern end of the line, where one might expect to see evidence of the half-graben imaged on Line 7 or the opposite polarity half-graben on Line 10.

On Line 10 (the southernmost profile, Fig. 4B), a large block of apparently undeformed basement is substantially broader than the horst described above. The absence of either the horst or this broad expanse of undeformed basement on Line 8 is evidence that they are not continuous. Well-defined half-graben on either side of the undeformed block on Line 10 are of the same polarity, in contrast to the opposite polarity half-graben adjacent to the

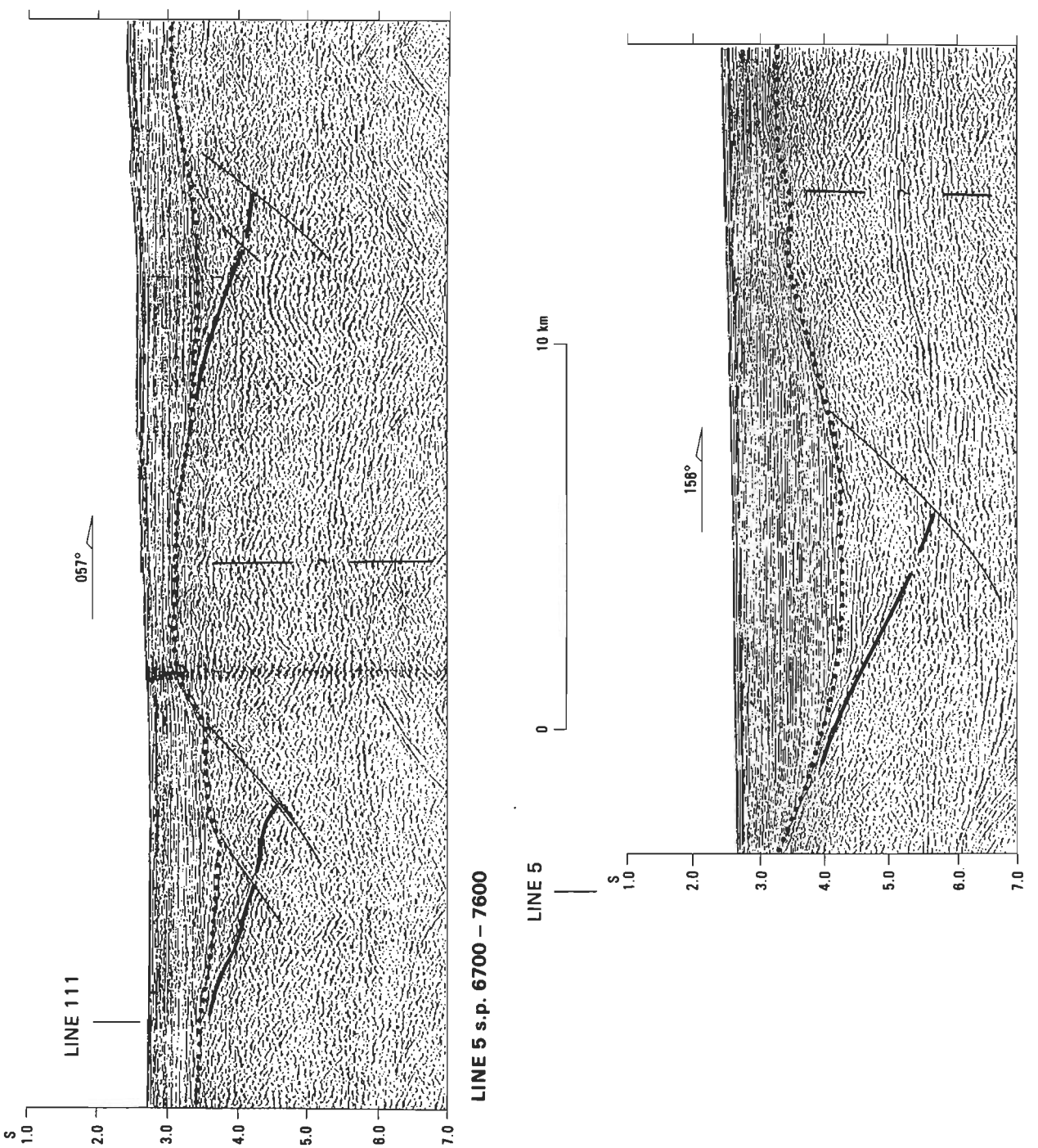

Figure 8. Tying seismic profiles. Line 5 is a "dip", or trough perpendicular profile. Line 111 is a "strike", or trough parallel profile. Apparent rotation of the half-graben near the profiles intersection is greater on the "strike" line than on the "dip" line. Note also the thicker post-rift section on the "strike" line indicating greater subsidence adjacent to the bounding fault. Notations and locations as in Figure 3.

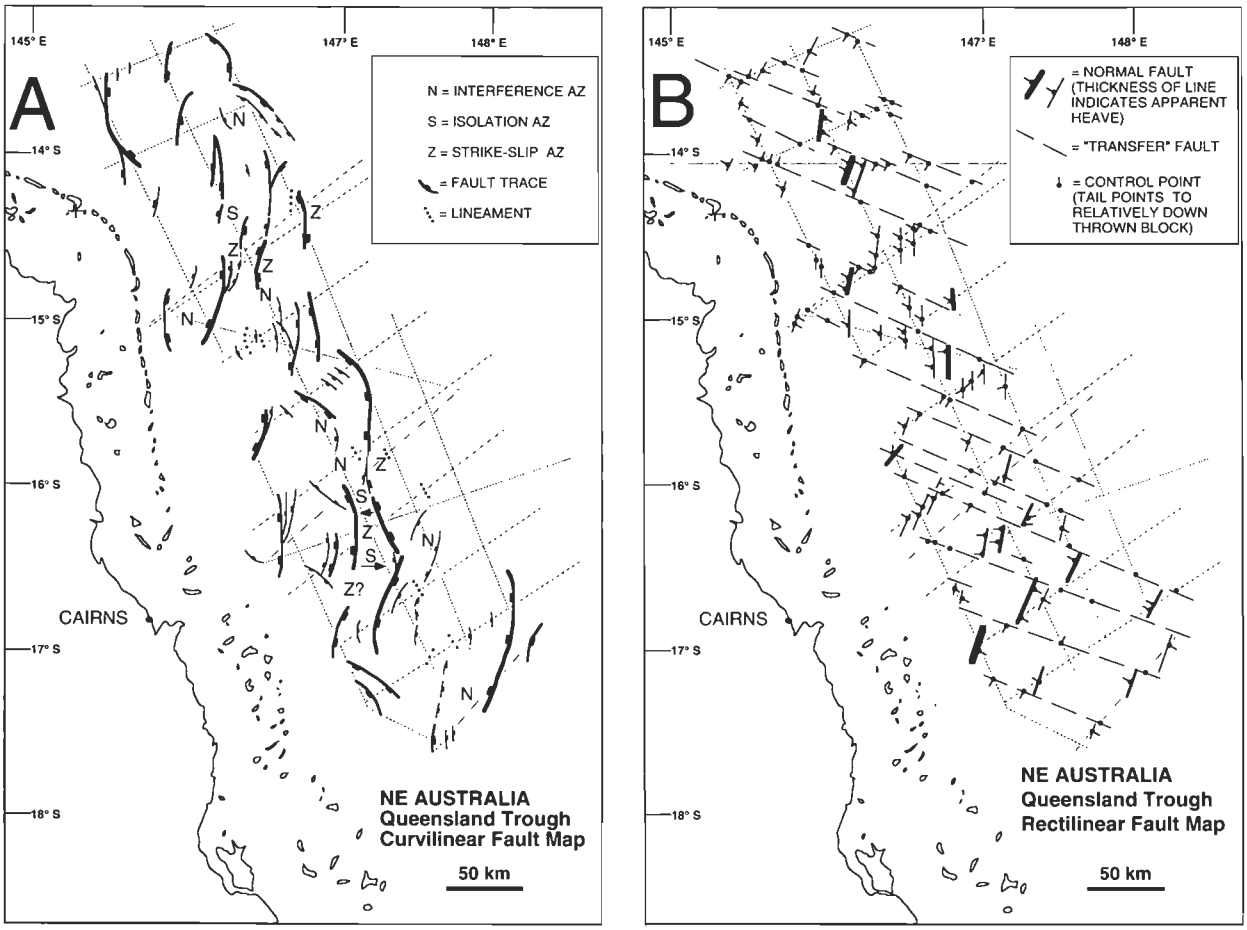

Figure 9. (A) Curvilinear fault map of the Queensland Trough using model concepts from the East African Rift (Rosendahl, 1987). Shaded strip indicates a possible zone of required structures for rift-perpendicular extension and to decouple mapped normal faults of varying orientation or opposing polarity. Structures of this orientation are not recognized in the available data. AZ = accommodation zone. (B) Rectilinear fault map of the Queensland Trough after concepts of the model presented by Lister & others (1986). Note that in both interpretations fault correlations adjacent to profile intersections are oblique to the axial trend of the rift.

horst to the north. The half-graben are widely separated, suggesting that the extensional strain has been more widely distributed. At this location, the trough is merging with the nearly east–west Townsville Trough, and the half-graben on the right end of the profile may be continuous with this system.

Architecture models of the Queensland Trough

The curvilinear interpretation. The above data show that seismic profiles of all orientations contain tilted basement fault blocks. Many bounding faults are clearly listric (Fig. 3), but there seems to be no consistent "dip" versus "strike" line relationship. The dip inconsistency is analogous to data collected from the East African Rift (EAR), where half-graben are thought to be bounded by arcuate or curvilinear faults connected by various types of accommodation zones (Rosendahl, 1987) into a sinusoidal system. In fact, the crustal scale analogy between the Tanganyika/Rukwa/Malawi Rift bending around the Tanzanian Craton and the Queensville/Townsville Trough system bounding the continental block of the Queensland Plateau was, in part, the motivation for this study. In the EAR, field measurements of slip on rift faults (Chorowicz & Sorlien, 1992) and dip analysis (Scott & others, 1990; Scott & others, 1992) indicate that extension is oblique to the rift axis. In addition, the horst in the south-central part of the Queensland Trough (Lines 1124, 1125 & 7, Fig. 4B) has a profile geometry described as an isolation accommodation zone by Rosendahl (1987).

With the EAR sinusoidal geometry as a model, the curvilinear fault interpretation shown in Figure 9A was derived from the available data. The half-graben bounding faults form a series of syn-rift depocenters with up to 5 km of fill, as shown in the isopach map of syn-rift section (Fig. 2B), that appear to be elongated along the axis of the trough at 155°–160°. This apparent structural grain suggests rift parallel bounding faults and orthogonal extension. However, the available data yield no evidence for major linear structures parallel or perpendicular to the trough axis. The series of arcuate half-graben north of 14° S in the Queensland Trough (Fig. 9A) are elongate more or less parallel to the trough trend; that is, the tangent to their point of maximum curvature is parallel to the rift trend. However, farther south fault patterns become more rhombohedral, indicating a strike-slip mechanism for the formation of the half-graben. Note also that most of the syn-rift depocenters are composed of two or more smaller "deeps" (Fig. 2B) that cannot be explained by the curvilinear fault model interpretation presented in Figure 9A.

The main criticism of the sinusoidal rift model (Reynolds,

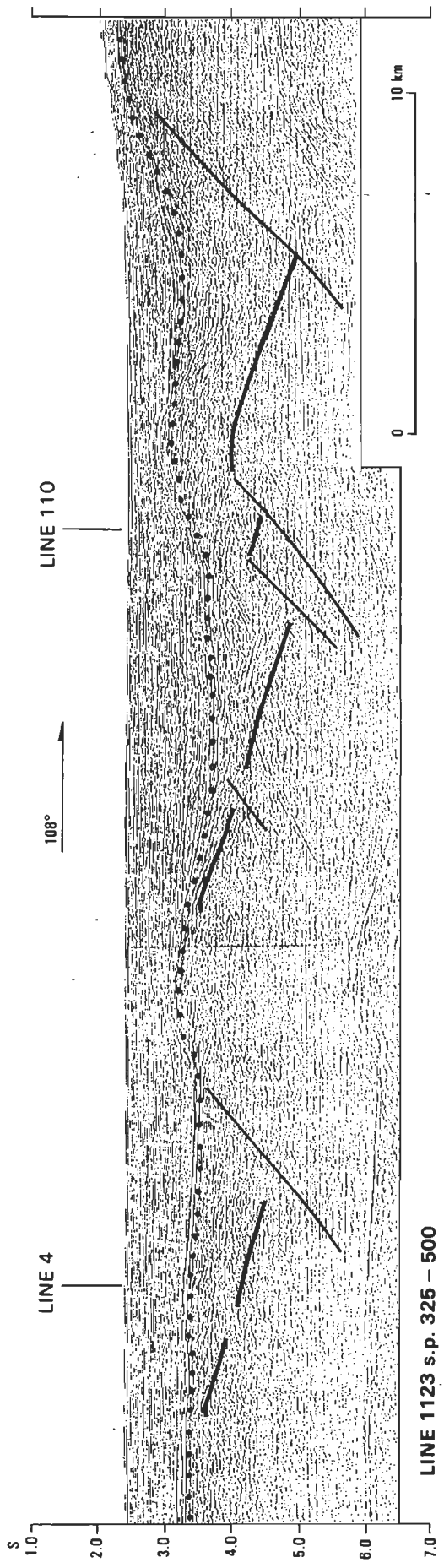

Figure 10. Southeast trending seismic profile 1123 exhibiting similar rotation of three tilted fault blocks. Compare this geometry with the variable rotation of tilted blocks imaged on northeast trending Line 7 shown in Figure 3. Notation and location as in Figure 3.

1984; Rosendahl, 1987) proposed for the EAR is that it does not provide structures whereby consistent regional kinematics can occur and has no predictive value for tectonic reconstructions. In other words, linking structures aligned approximately parallel to the extension direction are required to "release" blocks bounded by variably oriented faults along the rift-axis strike to allow tectonic transport of the blocks. The sinusoidal model predicts at least two directions for half-graben linking structures, which do not have a consistent relationship with the direction of extension. Scott & others (1992) and Chorowicz & Sorlien (1992) both addressed this problem by analysing the kinematics from two different data sets both concluding that such structures must exist. It is possible that either intracontinental rifts do not extend sufficiently to develop these structures or are ill-defined in early stages of rifting. However, sufficient evidence exists in both the East African Rift and the Queensland Trough that the structures are present and provide a consistent regional kinematic history.

The rectilinear interpretation. In a simple, ideal orthogonal extension model, a "dip" line shot parallel to the direction of extension images a series of tilted fault blocks with similar rotation and recoverable fault/base syn-rift relationships. Likewise, a "strike line" images flat-lying to shallowly-dipping syn-rift reflections and vertical faults. Profiles in any other orientation are predicted to image complex geometries which cannot be reconstructed in the plane of the profile simply by movement along the imaged faults. The rift axis will align perpendicular to the direction of extension, although deeps may shift their lateral position from the axis or switch polarity across extension parallel, rift perpendicular transfer faults.

Line 1123 (Fig. 10) most closely resembles the series of "balanceable" tilt blocks within a single profile that is predicted to be on a dip line in an orthogonal extension system. Note the morphology of the base of the syn-rift section. Block dips are consistent with each other. Profile orientation, however, is southeast at 108° rather than northeast as are the majority of the trough-perpendicular "dip" lines (Fig. 2A). The southeast direction is compatible with the basement rotation dip azimuths in Figure 2A. Line 4, which intersects Line 1123, also images tilted fault blocks, but they are not as clear, and there is considerable disruption of syn-rift reflections within each apparent fault block. Changes in the thickness of the post-rift section indicate that both profiles consist of three tilted fault blocks starting at their intersection and proceeding eastward. However, correlation of the bounding faults does not produce parallel structures. The easternmost block on Line 1123 appears to be smaller than the middle block, but the reverse relationship seems to be the case in Line 4. Any attempt at correlating faults on these two intersecting profiles requires at least two fault trends. The strike line that intersects these profiles (Line 110, Fig. 7A) images flat to dipping reflectors, which are truncated on a 1 to 3 km scale versus the 5 to 10 km scale of blocks in the "dip" lines. Interpretation of these profiles suggests that the normal faults accommodating extension in the rift trough are aligned roughly perpendicular to Line 1123 or at about 018° and that tilted blocks are separated from each other by "transfer" or oblique- to strike-slip faults aligned sub-parallel to the profile. This interpretation can accommodate all the observed faults as well as explain the chaotic nature of reflections within the half-graben imaged in Line 4.

It is also instructive to examine the geometry of the two

opposing half-graben and the horst block located on Lines 1124, 1125 and 7 (Fig. 4B) interpreted as an isolation accommodation zone in the previous section. Line 110 (not shown) is trough axis-parallel and images continuous elevated basement from just south of Line 7 to just north of Line 1124. Given the similarity in profile morphology, and the proximity and orientations of the lines, the interpretation of a trough parallel elongate horst shown in the curvilinear fault map (Fig. 9A) seems reasonable. However, attempting to correlate the rest of the faults within either of the adjacent half-graben leads to a variety of interpreted fault trends, as was the case for structures imaged on Lines 4 and 1123. Also, the opposing polarity half-graben on Line 6 (Fig. 4B) requires an intervening structure between the profiles to allow the asymmetry reversal.

Close inspection of the morphology of the horst reveals that basement dips atop the horst vary from profile to profile. In Line 7, the apex of the horst is east of the intersection with Line 110, with a wider westward-dipping surface. On Line 1125, the apex has shifted to the west of the intersection with Line 110 and has a distinctly wider eastward-dipping surface. The relationship of the apex to Line 110, and between the widths of the dipping surfaces, again reverses on Line 1124. In addition, a strong diffraction to the west of the intersection of Line 1124 with Line 110 suggests a possible structure or structures running through the horst at an angle with Line 110 rather than parallel to it. Correlation of these horst features yields a zigzag pattern whose segment trends are both oblique to the rift axis and suggests that this basement high is not a continuous unbroken feature but may be cut by sub-vertical strike-slip faults.

Where half-graben or tilted fault blocks are discernable, and where correlations of faults very near the profile ties is possible, faults trend NNE–SSW striking between 010° to 025° or WNW–ESE with strikes between 100° to 120° (Fig. 9B). These strikes are compatible with those predicted by the reflector dip/fault geometry interpretation done on Lines 1123, 4 and 110 (Figs 4A and 7A) based on orthogonal extension models, even though these trends are both oblique to the rift axis trend as in Figure 9B.

Discussion

The oblique relationship between the fault trends in the rectilinear fault map (Fig. 9B) and the rift axis are nearly identical to an interpretation of the western branch of the EAR system (Scott & others, 1992). Determination of the tectonic transport direction, based on dip analysis in the African basins, confirms that oblique rifting has been operative in the EAR. This conclusion is supported by landbased fault-slip analysis by Chorowicz & Sorlien (1992). A similar dip analysis on the Queensland Trough data is limited due to the small number of profile intersections (Fig. 2A). However, of the 22 profile ties where underlying basement rotation can be measured with reasonable confidence, 15 yield a true dip direction of WNW–ESE implying that tectonic transport direction or extension direction is aligned along this azimuth. The seven northeast–southwest dips are either found in the north, where the presence of volcanics obscures rift-related structures, or are adjacent to proposed northeast–southwest trending "transfer" faults which may affect subsidence locally.

It is likely that the structural pattern in the Queensland Trough is neither as regular and rectilinear, nor as perfectly arcuate and unlinked, as that shown in the two alternative interpretations in Figure 9. Rather, it is more likely that the actual structural style lies somewhere in between as modelled for the EAR by Chorowicz & Sorlien (1992), wherein extensional rift-bounding normal faults are arcuate and are compartmentalized by transfer faults aligned approximately in the direction of of extension, which is oblique to the rift axis (Fig. 11).

By incorporating arguments based on predicted orthogonal extension geometries and observations of geometries within the data, it is possible to construct an interpretation which provides a linked fault system consistent with a stable stress regime (Fig. 11). The underlying syn-rift extension of the Queensland Trough appears to have been accommodated by somewhat variably-trending NNE–SSW normal, possibly curvilinear, faults. The normal faults are truncated by pervasive WNW–ESE oblique- to strike-slip, steeply dipping faults in this interpretation. The structural architecture presented in Figure 11 also fits with the compartmentalization of the syn-rift isopach cells into smaller "deeps". Further, the interpretation is consistent with our current understanding of strain distribution in extensional systems, with the enigmatic qualification that both normal and transfer faults are aligned oblique to the trough axis.

In Figure 11, there is a noticeable change in the trend of the normal faults at 15° 15′ S from NNE–SSW in the north to north-south in the south. The normal faults appear to revert to a NNE–SSW trend at latitudes south of Cairns. The northwest–southeast-trending structures that separate the variable normal fault trends are approximately aligned with changes in the continental shoreline trend from north–south to northwest–southeast. Further, north–south-trending residual negative bouger gravity anomalies onshore are truncated by northwest–southeast-trending relative highs which align with these bounding structures (Murray & others, 1989; his fig. 1). It is proposed that these trends are major crustal anisotropies that have partitioned the strain along the axis of the Queensland Trough.

Tectonic implications

It is proposed that extension in the Queensland Trough was directed WNW–ESE at an oblique angle to the northwest–southeast (155°) trend of the rift axis. The axis of the trough may be so aligned in response to the regional grain of the Paleozoic Tasman Fold Belt (Mutter, 1977). The structural pattern of NNE-trending normal faults and WNW-trending transfer faults is broadly consistent with interpretations of recently collected seismic data from the Townsville Trough (Falvey & others, 1990; Symonds & others, 1987; 1988). Analysis of the Townsville Trough data suggests northwest-trending extension resulting in a ENE set of normal faults with northwest-trending transfer faults. As an alternative to the WNW-extension direction proposed above, it may be that northwest-trending extension indicated by Townsville Trough structural interpretations, reactivated a WNW crustal anisotropy suggested by the strain partitioning along the Queensland Trough and onshore gravity signatures (Murray & others, 1989).

As mentioned earlier, the regional crustal morphology of rift zones wrapped around a craton is similar to both the Tanganyika/Rukwa/Malawi Rift and the Queensland/Townsville Trough. However, the large-scale similarity ends there. The Tanganyika and Malawi rift zone axes are

sub-parallel and do not intersect; rather, they are joined by the strike-slip Rukwa rift zone (e.g. Rosendahl & others, 1992). The Queensland and Townsville Troughs intersect at their southern and western termini, respectively. Further, the troughs strike radially from their point of intersection at an angle of approximately 115° to each other. This configuration is very suggestive of an incipient triple junction (McKenzie & Morgan, 1969). There is some evidence that a third arm of the system extends inboard of the Marion Plateau. White (1961; 1965) first proposed that northeast-trending structures bounding the Broken River Embayment (Fig. 1) represent an intra-continental rift. Mutter & Karner (1980) also hypothesize a possible Paleozoic three-branch system of which only the Queensland and Townsville branches were reactivated in the Mesozoic. As evidence, they cite prominent structural lineaments of the appropriate trend in the Broken River Embayment and the Georgetown Inlier (Fig. 1). Arnold & Fawkner (1980) argued that these half-graben structures were active during deposition of Ordovician and Silurian sediments. However, their figure 4 suggests that the structures existed in pre-Silurian time. If this is true, then southeastward movement of the Queensland and Marion Plateaus is consistent with the creation of a possible incipient "triple junction" and explains the relationship between the Queensland and Townsville Troughs. Given the corroborating structural patterns mapped in the Townsville Trough, this seems to be the most plausible explanation for the creation of these troughs and resolves the kinematic difficulties of opening them with Mesozoic plate motion vectors determined from spreading centers in the Coral and Tasman Seas.

This interpretation differs radically with the many previous structural interpretations of the northeast margin of Australia with regards to implications for large-scale tectonic evolution. Whether or not extension within the Queensland/Townsville Trough was directed northwest or WNW, the structural interpretations presented herein and from the Townsville Trough (Symonds & others, 1987; 1988) imply that extension at basement levels in this system is not kinematically consistent with either the spreading direction of the Coral Sea to the north or the Tasman sea to the south as is commonly stated in other studies. Since we have no age constraints on the extension for the Queensland/Townsville Troughs system, it is possible, or probable, that extension here predates tectonism in either of the adjacent spreading centers. A (?pre-) Paleozoic triple junction, reactivated in the Mesozoic, is supported by the kinematics suggested here by the structural interpretation of the Queensland Trough as being the product of oblique rifting.

Acknowledgements

The Australian Geological Service Organization (AGSO) is gratefully acknowledged for providing the data for this study. M. Etheridge, D. Feary and P. Symonds provided thoughtful reviews which greatly improved an earlier version of the manuscript. Members of the Marine Division (AGSO), in particular P. Symonds, are especially thanked for many stimulating discussions and constructive input. Conscientious and expeditious reviews by C. Pigram and J. Colwell are appreciated.

References

Arnold, G.O. & Fawckner, J.F., 1980 — The Broken River and Hodgkinson Provinces. *In* Henderson, R.A. & Stephenson, P.J. (editor), The Geology and Geophysics of Northeastern Australia. *Geological Society of Australia, Queensland Division, Brisbane,* 175–190.

Bally, A.W. (editor), 1984) — Seismic Expression of Structural Styles — A Picture and Work Atlas. *Stud. in Geol. No. 15. American Association of Petroleum Geologists, Tulsa, Okla.*

Chenet, P.W., Montadert, L., Gairaud, H. & Roberts, D., 1982 — Extension ratio measurements on the Galicia, Portugal and Northern Biscay continental margins: implications for evolutionary models of passive continental margins. *American Association of Petroleum Geologists Bulletin,* 34, 703–715.

Chorowicz, J. & Sorlien, C., 1992 — Oblique extensional tectonics in the Malawi Rift, Africa. *Geological Society of America Bulletin,* 104, 1015–1023.

Davies, P.J., McKenzie, J.A. & Palmer-Julson, A., 1991 — Proceedings of the Ocean Drilling Program, Initial Reports. *Ocean Drilling Program, College Station, TX.*

de Charpal, O., Guennoc, P., Montadert, L. & Roberts, D.G., 1978 — Rifting, crustal attenuation and subsidence in the Bay of Biscay. *Nature,* 275, 706–711.

Etheridge, M.A., Branson, J.C. & Stuart-Smith, P.G., 1985 — Extensional basin-forming structures in Bass Strait and their importance for hydrocarbon exploration. *Australian Petroleum Exploration Association Journal,* 25, 344–361.

Ewing, M., Hawkins, L.V. & Ludwig, W.J., 1970 — Crustal structure of the Coral Sea. *Journal of Geophyscial Research,* 75(11), 1953–1962.

Falvey, D.A. & Mutter, J.C., 1981 — Regional plate tectonics and the evolution of Australia's passive continental margins. *Bureau of Mineral Resources Journal of Australian Geology and Geophysics,* 6, 1–29.

Falvey, D.A., Symonds, P.A., Colwell, J.B., Willcox, J.B., Marshall, J.F., Williamson, P.E. & Stagg, H.M.J., 1990 — Australia's deepwater frontier petroleum basins and play types. *Australian Petroleum Exploration Association Journal,* 30, 238–262.

Falvey, D.A. & Taylor, L.W.H., 1974 — Queensland Plateau and Coral Sea Basin structural and time stratigraphic patterns. *Australian Society of Exploration Geophysicists Bulletin,* 5, 123–126.

Florensov, N.A., 1969 — Rifts of the Baikal mountain region. *Tectonophysics,* 8, 443–456.

Gardner, J.V., 1970 — Submarine geology of the western Coral Sea. *Geological Society of America Bulletin,* 81, 2599–2614.

GSI, 1974 — Geophysical Services International — Coral Sea Roving Seismic Survey. (Housed in Sydney, accessed via AGSO Canberra, ACT.)

GSI, 1979 — Geophysical Services International — Coral Sea Scientific Investigation Survey. (Housed in Sydney, accessed via AGSO Canberra, ACT.)

GSI, 1980 — Geophysical Service International — Coral Sea Scientific Investigation 1974. *BMR P(SL)A Report 79/10 (Unpublished), Australia.*

Karig, D.E., 1971 — Origin and development of marginal basins of the western Pacific. *Journal of Geophysical Research,* 76, 2542–2561.

Figure 11. Interpreted tectonic architecture of the Queensland Trough. Grayed contours are the syn-rift isopachs shown in Figure 2B. Note the change in the orientation of the normal faults just south of 15° S latitude. This interpretation is consistent with the syn-rift isopach data, the dips of basement rotations (Fig. 2A), profile geometries discussed in the text and correlated structural trends close to profile intersections. XXX = westward extent of relatively highstanding basement blocks. V = volcanic seismic signature.

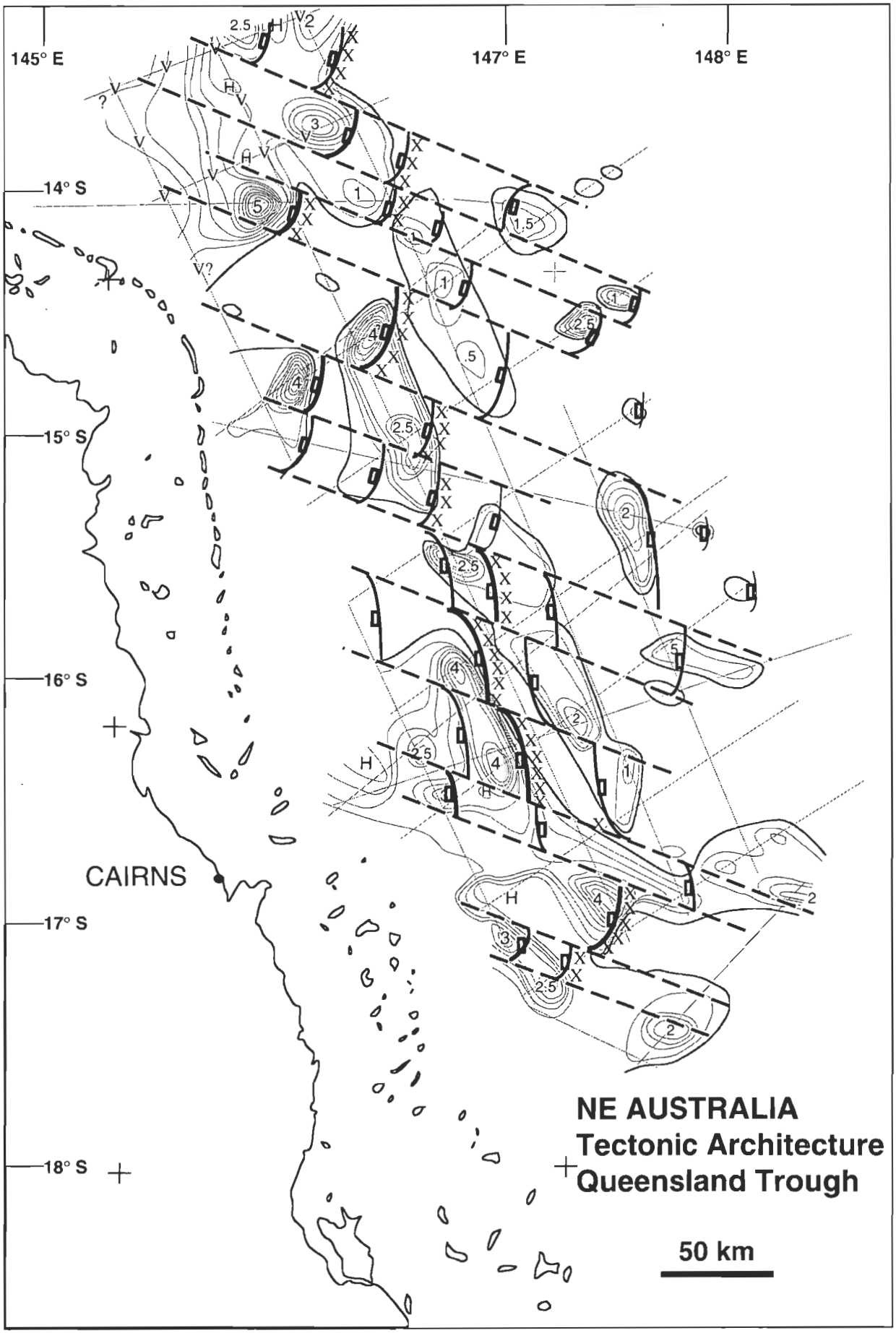
145° E
147° E
148° E
14° S
15° S
16° S
17° S
18° S
CAIRNS
NE AUSTRALIA
Tectonic Architecture
Queensland Trough
50 km

Lister, G.S., Etheridge, M.A. & Symonds, P.A., 1986 — Detachment faulting and the evolution of passive continental margins. *Geology*, 14, 245–250.

Logatchev, N.A., Zorin, Y.A. & Rogozhina, V.A., 1983 — Cenozoic continental rifting and geologic formations (as illustrated by the Kenya and Baikal rift zones). *Geotectonics*, 17, 83–92.

McKenzie, D. & Morgan, W.J., 1969 — Evolution of Triple Junctions. *Nature*, 224, 125–133.

Murray, C.G., Scheibner, E. & Walker, R.N., 1989 — Regional geological interpretation of a digital coloured residual Bouguer gravity image of eastern Australia with a wavelength cut-off of 250 km. *Australian Journal of Earth Sciences*, 36, 423–449.

Mutter, J.C., 1977 — The Queenlsand Plateau. *Bureau of Mineral Resources, Australia, Bulletin*, 179, 55.

Mutter, J.C. & Karner, G.D., 1978 — Cretaceous taphrogeny in the Coral Sea. *Bulletin of the Australian Society of Exploration Geophysicists*, 9, 82–87.

Mutter, J.C. & Karner, G.D., 1980 — The continental margin of northeast Australia. *In* Henderson, R.A. & Stephenson, P.J. (editor), The Geology and Geophysics of Northeastern Australia. *Geological Society of Australia, Queensland Division, Brisbane*, 47–70.

Pinchin, J. & Hudspeth, J.W., 1975 — The Queensland Trough: its petroleum potential based on some recent geophysical results. *Australian Petroleum Exploration Association Journal*, 15((1)), 21–31.

Ramberg, I.B. & Morgan, P., 1984 — Physical characteristics and evolutionary trends of continental rifts. *Tectonics*, 7, 165–216.

Ramberg, I.B. & Neumann, E.R. (editor), 1978) — Tectonics and Geophysics of Continental Rifts. *Reidel, Dordrecht.*

Reynolds, D.J., 1984 — Structural and dimensional repetition in continental rifts. *Duke Univ., Durham, N. C.*

Rosendahl, B.R., 1987 — Architecture of continental rifts with special reference to East Africa. *Annual Review of Earth & Planetary Sciences*, 15, 445–503.

Rosendahl, B.R., Kilembe, E. & Kaczmarick, K., 1992 — Comparison of the Tanganyika, Malawi, Rukwa and Turkana rift zones from analyses of seismic reflection data. *Tectonophysics*, 213, 235–256.

Scott, D., Etheridge, M. & Rosendahl, B., 1990 — Oblique Extension within the East African Rift System Abstract. *Eos Transactions, American Geophysical Union*, 71(43), 1605.

Scott, D.L., Etheridge, M.A. & Rosendahl, B.R., 1992 — Oblique-slip deformation in extensional terrains: a case study from the Lakes Tanganyika and Malawi rift zones, East Africa. *Tectonics*, 11(5), 998–1009.

Skilbeck, C.G. & Lennox, M.J., 1984 — The Seismic Atlas of Australian and New Zealand Sedimentary Basins. *The Earth Resources Foundation, University of Sydney, Sydney, N. S. W., Australia*, 301.

Symonds, P.A., Capon, D., Davies, P.J., Pigram, C.J. & Feary, D.A., 1987 — Structural style of the Townsville Trough and its implications for the development of the northeast Australian margin. *Bureau of Mineral Resources Research Symposium: Applied Extension Tectonics, Canberra, Bureau of Mineral Resources*, 165–172.

Symonds, P.A. & Davies, P.J., 1988 — Structure, stratigraphy, evolution and regional framework of the Townsville Trough and Marion Plateau region. *Bureau of Mineral Resources Research Cruise Proposal, Record 1988/48* (Unpublished).

Symonds, P.A., Davies, P.J. & Parisi, A., 1983—Structure and stratigraphy of the central Great Barrier Reef. *Bureau of Mineral Resources Journal of Australian Geology and Geophysics*, 2, 284–303.

Symonds, P.A., Fritsch, J. & Schluter, J.U., 1984 — Continental margin around the western Coral Sea Basin: Structural elements, seismic sequences and petroleum geological aspects. *Transactions of Third Circum-Pacific Energy and Mineral Resources Conference, Hawaii, American Association of Petroleum Geologists, Tulsa*, 143–252.

Taylor, L.W.H. & Falvey, D.A., 1977 — Queensland Plateau and Coral Sea Basin: stratigraphy, structure and tectonics. *Australian Petroleum Exploration Association Journal*, 17(1), 13–29.

White, D.A., 1961 — Geological history of the Cairns-Townsville hinterland, north Queensland. *Report of the Bureau of Mineral Resources Geology and Geophysics, Australia* 59.

White, D.A., 1965 — The geology of the Georgetown/Clarke River area, Queensland. *Bulletin of the Bureau of Mineral Resources Geology and Geophysics, Australia* 71.

AGSO Journal of Australian Geology & Geophysics, 14, 35–46

Application and extension of the ML earthquake magnitude scale in the Victoria region

J.Wilkie[1], G.Gibson[2] & V.Wesson[2]

A new function for –logAo has been deduced, and parameters determined using nonlinear regression analysis of data from the Victorian seismograph network. The formula for local magnitude:

$$ML = \log A - \log S - \log Ao$$

where $-\log Ao = 0.7 + \log R + 0.0056Re^{-0.0013R}$

S = site amplification

has been adopted for the Victoria region. The values of –logAo closely follow the trend of Richter's values at medium hypocentral distances. The features of Bakun & Joyner's (1984) formula at close range, which were found to be applicable in Victoria, have been retained. The formula is applicable for distances from a few kilometers, and the maximum distance has been extended from 600 to 1000 km.

The value of logS is closely related to the seismometer foundation, varying from about 0.0 at a bedrock site to more than 0.7 at soft sedimentary sites. The determination and application of site corrections is examined in detail.

Introduction

Magnitude is one of several measures of the earthquake source. The local earthquake magnitude is a single scalar value determined from the peak recorded body wave (P or S) ground motion, corrected for attenuation by a simple function of distance from the source. Ground motion displacement, velocity or acceleration may be used.

The original scale of local earthquake magnitude implemented by Richter (1935, 1958) was based on the maximum amplitude recorded on a standard displacement seismograph. The magnitude ML is related to the log of this amplitude (A) by

$$ML = \log(A/Ao) = \log A - \log Ao \quad (1)$$

where Ao includes an arbitary reference amplitude chosen to set the zero point on the ML magnitude scale. Sites where surface motion has been amplified, for example by soft sediments, require the application of a site correction.

Richter's data were acquired using Wood–Anderson torsion seismometers. Ao was defined as 10^{-6}m at a distance of 100 km from the epicentre; i.e. an earthquake registering a trace amplitude of 1 mm at a distance of 100 km from the epicentre would be assigned an ML magnitude of 3.0. The magnitude was determined independently for each of the horizontal components and the mean was taken.

Richter defined distance corrections empirically for southern California, and these are not necessarily valid for other regions. The applicability of the scale elsewhere depends upon the establishment of standard values of –logAo as a function of epicentral distance in each region. Richter's values of –logAo for southern California (Richter, 1958) enable the determination of an ML magnitude for earthquakes to an epicentral distance of 600 km. The mean depth of southern Californian earthquakes studied by Richter was thought to be 16 km (Richter, 1958). Richter points out that his –logAo corrections, because of the variation of recorded amplitude with crustal structure and distance, cannot be applied to deep-focus earthquakes.

1 Applied Physics Dept. Victoria University of Technology, Ballarat Rd., Footscray, 3011

2 Seismology Research Centre, Royal Melbourne Institute of Technology, Plenty Rd., Bundoora, 3083

At the Seismology Research Centre, Victoria, where the research was carried out, ML magnitudes are obtained from measurements of peak seismogram amplitude and the frequency at this peak, and are computed by an earthquake location program. The response of each seismograph is parametrically defined by transducer output, damping and natural frequency, the recording system gain and filter orders and frequencies. This information is stored on a file, and is automatically accessed using the earthquake date. System response can be checked by curve fitting a calibrating pulse. A calibration pulse at the start and end of each record is used to detect changes in system response.

The Victorian network of seismographs is essentially of two types:

- Sprengnether MEQ–800 single component analogue recorders, and
- triggered digital three-component recorders developed by the Seismology Research Centre.

These recorders are coupled to either Sprengnether S6000, S7000 or Mark Products L4C seismometers. All systems are optimised to record local micro-earthquakes which have dominant frequencies in the 4 to 20 Hertz range. Earthquakes can be located with uncertainties from less than 2 km for events within the network up to tens of kilometers for distant events outside the network. The trigger algorithm on the digital seismographs is designed to record nearby earthquakes, so it is not common for events at a distance greater than a few hundred kilometers to be recorded on these instruments. Figure 1 shows the geographical distribution of the Victorian seismograph sites.

The measured zero-to-peak amplitude is in millimeters from an analogue record, or counts from a digital record, for the larger of P or S motion. For triaxial instruments this is from the component which gives the highest peak value. The frequency corresponding to this peak is measured or estimated and the corresponding ground displacement is then computed. It is assumed that this is the displacement that would give peak response on the standard Wood Anderson seismograph used in the Richter ML definition (gain 2800, period 0.8s, damping 0.8), and this Wood Anderson seismograph response in millimeters and its logarithm (logA) are computed. The gain value of 2800 is a design value and there is evidence that the effective gain of Wood Anderson seismographs is actually about 2000

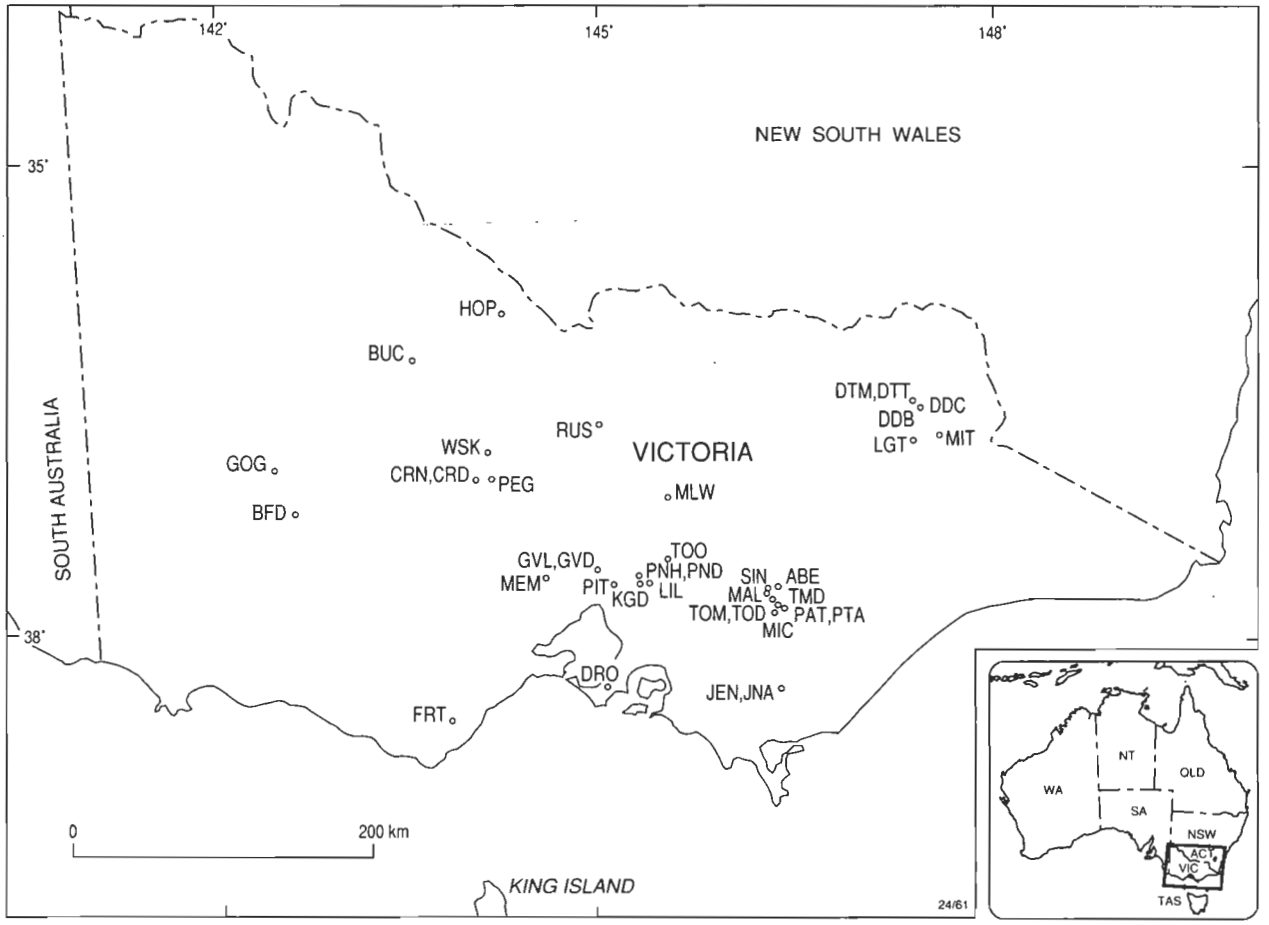

Figure 1. Victorian Seismograph Network.

(Boore, 1989; and Gaull & Gregson, 1991). There appears to be no reason to assume that Richter's instruments had the accepted standard gain of 2800 and standardization to this gain; for example using a multiplier of 1.346 (Gaull & Gregson, 1991) would introduce an error of 0.1 in the assigned magnitudes.

Prior to 1985 at the Seismology Research Centre, the Richter attenuation terms were approximated by a function based on a numerical fit to the Richter values by McGregor & Ripper (1976), but corrected for use with hypocentral distance:

$$-\log Ao = 2.26 + 0.00746R - 0.0000051R^2 \qquad (2)$$

R is the hypocentral distance given by $\sqrt{\Delta^2 + h^2}$, where Δ and h are, respectively, the epicentral distance and depth in kilometres. This was valid only for distances up to 600 km; and the R^2 term gave significant errors if the function was used at greater distances.

Cuthbertson (1977), in a study of earthquakes in central Victoria, found no significant variation of ML with epicentral distance, suggesting that the variation in attenuation of seismic waves is similar to that of southern California.

In a study of earthquakes of central California, Bakun & Joyner (1984) found the Richter values of –logAo generally applied, that is, the attenuation characteristics of the crust and upper mantle were similar to those of southern California. Bakun & Joyner found that for hypocentral distances from a few tens of kilometers to over 400 km the values of –logAo were consistent with Richter's values. However, for distances less than 30 km their values of –logAo were significantly greater than those of Richter.

Considering geometrical spreading and anelastic attenuation terms, Bakun & Joyner (1984) derived, by regression analysis, a parametric expression for –logAo:

$$-\log Ao = 0.7 + \log R + 0.00301R \qquad (3)$$

Figure 2(a) shows the relation between Richter's values of –logAo and –logAo calculated from Bakun's expression. It is obvious from Figure 2(a) that Bakun's expression is only consistent to about 475 km and beyond that distance deviates from the Richter values.

Figure 2(b) illustrates the deviation of Bakun & Joyner's (1984) values of –logAo from Richter's values at small values of R. Because Richter's values of –logAo are applicable to earthquakes of mean depth 16 km, the minimum value of R for which a Richter value of logAo exists is 16 km. However, earthquakes in California are in general much shallower than 16 km; for example, the earthquakes used in the study by Bakun & Joyner (1984) had a mean depth of approximately 7 km. If this value is used there is a closer fit between Bakun & Joyner and Richter's values of –logAo [Figure 2(c)] indicating that Richter's estimate of average depth was not accurate.

To provide more consistent magnitude values from nearby seismographs, the expression (3) for –logAo for the central

Californian region was adopted at the beginning of 1985 for the calculation of ML magnitudes in Victoria. This reduced the standard deviation of the calculated ML magnitude values for earthquakes, which included epicentral distances less than 30 km and generally increased the magnitude assigned to these earthquakes.

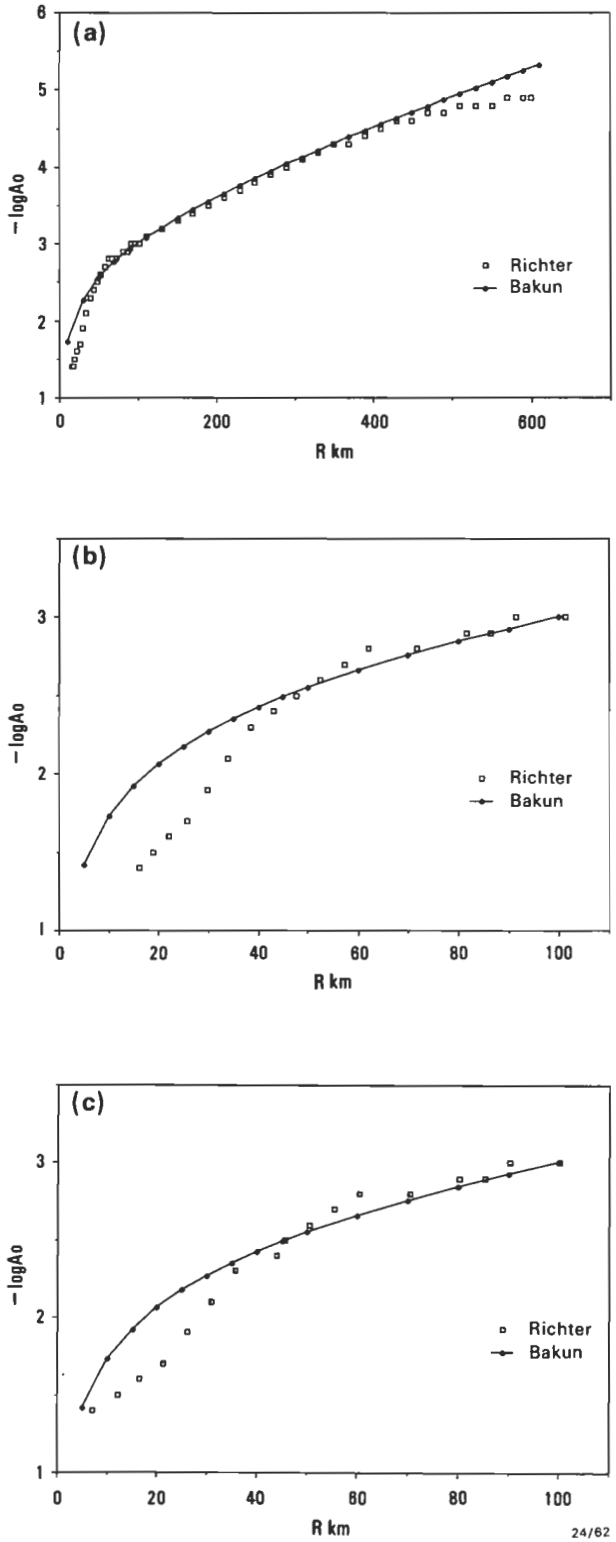

Figure 2(a). Comparison of –logAo from Bakun & Joyner's (1984) expression (3) with Richter's values of –logAo.
Figure 2(b). Comparison of –logAo from Bakun & Joyner's expression (3) with Richter's values (average depth 16 km) at close range.
Figure 2(c). Comparison of –logAo from Bakun & Joyner's expression (3) with Richter's values (average depth 7 km) at close range.

The major seismological recording centres and networks in Australia are for geographic reasons separated by large distances, in many cases of the order of 1000 km. Various organizations, including governments and universities, contribute to the over-all pattern of recording sites (Fig. 3). The recorded seismicity of Australia and the derived seismic risk has in the past been strongly influenced by this distribution (Denham, 1979). In order to have overlap between networks in the assignment of ML magnitudes, thus unifying the scale, it is highly desirable to extend the equivalent of Richter's –logAo values to distances of at least 1000 km.

The length of time for which the Seismology Research Centre Victorian seismographs have been installed varies considerably. The earliest seismographs GVL, PNH, LIL, KGD and TOM were installed in 1976–77 and it is on these seismographs that most of the data relating to earthquakes at ranges greater than 600 km have been recorded. The most recently installed (triggered digital) seismographs have been triggered by few distant earthquakes. Several of the original analogue seismographs PEG, LIL and KGD are no longer operational.

The aims of the following analysis were:

- to extend the use of the Bakun-type parametric magnitude expression (3) to a range of 1000 km
- to derive parameters for the Bakun-type expression which are based on Australian earthquake data, and
- to determine site corrections.

The magnitude function

Examining Bakun & Joyner's (1984) expression for –logAo, the term which significantly contributes to the deviation between Bakun & Joyner and Richter values for large epicentral distances is the term related to the anelastic attenuation, 0.00301R. If the trend followed by Richter's values at large epicentral distances is extrapolated, the term above would have to reduce to approximately 0.0015R at 1000 km.

The relation between the recorded amplitude A of ground motion at a range R from an earthquake hypocentre can be expressed as

$$A = \frac{ESe^{-\gamma R}}{R^n} \qquad (4)$$

where E is a parameter related to the earthquake size, S is site amplification, γ is the coefficient of anelastic attenuation and n is a geometrical spreading coefficient (Greenhalgh & Singh, 1986; Nuttli, 1973; Bakun & Joyner, 1984).

$$\gamma = \frac{\pi f}{uQ} \qquad (5)$$

where u is the wave speed, f is the frequency of the wave and Q is the specific quality factor (Bullen & Bolt, 1985, p101).

Taking the logarithm of A, we obtain an expression of the form:

Figure 3. Australian Seismographic Stations, 1989.

$$\log A = \log E + \log S - n\log R - \frac{\gamma R}{\ln 10}$$

Defining $M = \log E + C$ will give a logarithmic magnitude scale, where C is a scaling term adjusting the magnitude to the Richter magnitude values.

$$M = \log A - \log S + C + n\log R + \frac{\gamma R}{\ln 10}$$

$$M = \log A - \log S + C + n\log R + KR \qquad (6)$$

$$\text{where } K = \frac{\gamma}{\ln 10} = \frac{\pi f}{\ln 10 u Q} \qquad (7)$$

From (6) and considering the Richter magnitude scale (1), Richter's attenuation term $-\log Ao$ is in the form used by Bakun & Joyner (1984)

$$-\log Ao = C + n\log R + KR \qquad (8)$$

In this paper we regard the site term, logS, as a correction to ground surface amplitude to give the equivalent motion for an ideal seismograph site. This means that the attenuation term $-\log Ao$ is simply a function of distance, and does not involve a site correction.

The geometrical spreading coefficient n equals 1 for the spherical spreading of body waves through a homogeneous medium. Regression analysis by Bakun & Joyner (1984) determined n to be close to 1 and they adopted this value. Greenhalgh & Singh (1986), in a study of South Australian earthquakes, determined a value for n of 1.09. In the present study, to avoid a proliferation of parameters, a value of 1 for n was adopted. The other terms then give the difference from spherical spreading.

Using expression (6) and regression analysis Bakun & Joyner (1984) derived the parametric expression (3) for $-\log Ao$. Greenhalgh & Singh (1986) determined values of n and K for the South Australian region and obtained the following expression for $-\log Ao$

$$-\log Ao = 0.7 + 1.1\log\Delta + 0.0013\Delta \qquad (9)$$

In the studies by Greenhalgh & Singh (1986) and Bakun &

Joyner (1984), K, the parameter in (6) related to anelastic attenuation, was considered to be a constant. However, it is seen from (7) that K is a function of both frequency and wave speed. As R increases, the higher frequency waves are attenuated most, so that the waves determining magnitude decrease in frequency with R. Also, as R increases the waves penetrate to a greater depth near or into the mantle, and consequently the mean wave speed for the wave path increases with R. Both these factors decrease γ and possibly account for the change in K needed to generate Richter's values of –logAo beyond 475 km using Bakun's expression. Other factors, such as guided waves, may also be involved.

Q values depend upon frequency and radial displacement in the earth, varying from the order of 10,000 in the core to a few hundred in the aesthenosphere. Considerable variation in Q even within the lithosphere occurs, varying, for example, from approximately 1000 in the eastern United States to 200 in western United States (Aki, 1980). The frequency dependence of Q also varies from region to region. For seismically active regions there is a peak in Q^{-1} between 0.5 and 1 Hz, but for seismically stable areas, such as eastern and central United States, Q^{-1} is a constant or decreases monotonically with frequency (Aki, 1980). Rautian & Khalturin (1978) experimentally determined $Q = 360\sqrt{f}$. In other studies, Q proportional to f^m has been used, where m is between 0 and 1 (Bullen & Bolt, 1985, p.451). It appears that a reasonable assumption would be that either Q can be taken as independent of frequency or Q varies as some fractional power of frequency. In either case, since frequency is a term in the numerator in expression (5), γ will decrease with decreasing frequency which is the required trend.

Thus, we can anticipate that K will decrease with increasing R and also depend upon the regional attenuation characteristics. The variation of K with R is evident when the values of K from the various parametric expressions for –logAo are examined with respect to the maximum values of R for which the expressions were derived:

K	Maximum R	
0.00301	475 km	Bakun & Joyner (1984)
0.0013	600 km	Greenhalgh & Singh (1986)
0.00189	700 km	Hutton & Boore (1987)
0.000657	2000 km	Gaull & Gregson (1991)

In accordance with our aim to extend the use of the parametric expression to 1000 km, the 0.00301R of (3) was replaced by an exponent term giving the new expression:

$$-\log Ao = p_1 + \log R + p_2 R e^{-p_3 R} \qquad (10)$$

with parameters p_1, p_2 and p_3.

The choice of the form of the term $p_2 R e^{-p_3 R}$ was made to give the minimum and simplest change to the term KR, yet accommodate the trend of the decreasing proportional contribution of the term with R shown in the above values of K and the trend of the Richter values with distance beyond 500 km (Fig. 2a).

Assuming the parameters p_2 and p_3 are related to the seismic wave path, p_1 includes the site term logS which adjusts the value of logA to accommodate the site characteristics, and the constant C , from (8), adjusting the magnitude so that it is numerically equivalent to the original Richter magnitude.

ML magnitudes were obtained using measurements of peak seismogram amplitude and the frequency at this peak, and were computed using

$$ML = \log A + p_1 + \log R + p_2 R e^{-p_3 R} \qquad (11)$$

where A is the amplitude which would have been registered by Richter's standard Wood–Anderson seismograph and

$$p_1 = -\log S + C \qquad (12)$$

Evaluation of parameters

Non-linear regression analysis was applied to the earthquake data for each seismograph site, giving values of the parameters p_1, p_2 and p_3 which minimise the standard deviation of the assigned and calculated values of ML magnitude. The magnitude assigned to an earthquake was the mean of the values available from the Victorian network, calculated using the Bakun & Joyner (1984) expression (3) for –logAo, and those determined by other seismograph networks.

Table 1 gives the values of the parameters resulting from the regression analysis of the data for each seismograph with the standard deviation of the values of ML magnitude calculated using expression (11) from the values of ML magnitude assigned to the earthquakes used. This analysis included all data with epicentral distances ranging from a few kilometers to over 1000 km. For the seismograph stations MEM, BUC, HOP, and TMD, no data for earthquakes with epicentral distances greater than 475 km were available. The seismograph station MIC had no data for earthquakes beyond 295 km and this accounts for the negative value for p_3, and station MAL, which had a very small negative value for p_3, had only one earthquake in its data set beyond 400 km; hence application beyond this distance is invalid.

When Bakun & Joyner's (1984) expression in the form

$$ML = \log A + p_1 + 0.7 + \log R + 0.00301R \qquad (13)$$

(where p_1 can be regarded as a statistical station correction) was applied to the data from the analogue, stations which included significant numbers of earthquakes with epicentral distances greater than 475 km, the average standard deviation of the Bakun & Joyner ML values from (13) with respect to the assigned ML value was approximately 0.55, emphasizing the inappropriateness of (3) for values of R greater than 475 km. Also, when regression analysis was used to find a value of K appropriate for data to 1000 km range, a value of K less than 0.00301 was obtained, but the standard deviation for data with R less than 475 km then significantly increased.

Table 2 shows the results of regression analysis of the application of Bakun & Joyner's expression (13) to the data for all seismographs restricted to only those earthquakes whose epicentral distance from the seismograph was less than 475 km, i.e. selecting the range of epicentral distances over which the Bakun expression should apply.

Table 1. Parameter values and standard deviations derived using nonlinear regression analysis with expression (11).

SITE CODE	*p1*	*p2*	*p3*	*SD*	*N*
GVL	0.538	0.00563	0.00128	0.20	51
PNH	0.488	0.00710	0.00153	0.26	52
TOM	0.685	0.00491	0.00114	0.29	50
LIL	0.417	0.00747	0.00166	0.26	35
KGD	0.223	0.00834	0.00167	0.20	29
JEN	0.748	0.00456	0.00117	0.28	31
PEG	0.431	0.00503	0.00121	0.29	49
FRT	0.420	0.00453	0.00103	0.27	29
ABE	0.500	0.00369	0.00117	0.28	100
TOD	0.216	0.00426	0.00064	0.35	107
PAT	0.271	0.00386	0.00049	0.38	94
MEM	0.268	0.00520	0.00131	0.23	13
BUC	0.582	0.00637	0.00234	0.32	22
HOP	0.553	0.00765	0.00168	0.27	50
MIC	0.140	0.00083	–0.00383	0.36	63
MAL	0.860	0.00087	–0.00062	0.31	41
TMD	0.104	0.01450	0.01633	0.26	29

(i) SD is the standard deviation of the calculated values of ML magnitude and the assigned ML values for each earthquake.

(ii) N is the number of earthquakes used for each site analysis.

(iii) Epicentral distance range, 0 to 1000 km.

(iv) The first eight seismographs are analogue instruments, the others digital.

Table 3 allows a direct comparison of the standard deviations achieved with the revised expression (11) (henceforth for clarity called the Wilkie expression) from Table 1 for all data , with the standard deviations resulting from the application of Bakun & Joyner's expression (13) to the restricted (less than 475 km) data set (Table 2).

Table 2. Values of parameter and standard deviation resulting from regression analysis using Bakun & Joyner's expression (13) with R<475 km.

SITE CODE	*p1*	*SD*	*N*
GVL	0.070	0.19	30
PNH	0.133	0.28	40
TOM	0.079	0.32	41
LIL	0.079	0.30	28
KGD	0.017	0.19	23
JEN	0.066	0.28	24
PEG	–0.105	0.22	30
FRT	–0.184	0.25	22
ABE	–0.185	0.29	98
TOD	–0.401	0.35	105
PAT	–0.383	0.38	93
MEM	–0.293	0.24	13
BUC	–0.024	0.33	22
HOP	–0.011	0.30	50
MIC	–0.682	0.36	63
MAL	–0.031	0.37	40
TMD	–0.535	0.30	29

For the analogue seismographs, where from 20 to 40% of the data for each site were for earthquakes with epicentral distances from 475 to 1000 km, the standard deviations in most cases are less for the Wilkie expression applied to all data compared to the Bakun & Joyner expression applied to the restricted data. In the case of the digital seismographs, where almost 100% of the data were for earthquakes whose epicentral distance was less than 475 km, for which the Bakun & Joyner expression is applicable, the Wilkie expression gave a lower standard deviation in all cases compared to the Bakun & Joyner expression standard deviation.

Attenuation for Victoria

In Table 1, the positive correlation between p_2 and p_3 is obvious for the analogue stations and if the term $p_2Re^{-p_3R}$ in (11) is to be a general attenuation term for the Victorian or southeastern Australian region, constant values of p_2 and p_3 need to be adopted. The mean values of p_2 and p_3 were approximately 0.0056 and 0.0013, respectively, and coincide with the values computed for the seismograph station GVL, which is the seismograph with the greatest percentage of earthquakes with epicentral distances greater than 475 km.

The above values for p_2 and p_3 were adopted, and further regression analysis of the data was computed using

$$ML = \log A + p1 + \log R + 0.0056Re^{-0.0013R} \qquad (14)$$

Table 4 shows the computed values of the parameter p_1 and the standard deviations of the calculated ML values with respect to the assigned ML values for each site. The adoption of the values of p_2 and p_3 resulted in all cases in a minimal increase in the standard deviation relative to the values in Table 3.

Table 3. Comparison of the standard deviations achieved with the Wilkie expression (11) for R from a few km to 1000 km, with the standard deviations resulting from the application of the Bakun & Joyner expression (13) to data with R less than 475 km.

SITE CODE	*WILKIE FORMULA SD from Table 1 (all data)*	*Bakun & Joyner FORMULA SD from Table 2 (data <475 km)*
GVL	0.20	0.19
PNH	0.26	0.28
TOM	0.29	0.32
LIL	0.26	0.30
KGD	0.20	0.19
JEN	0.28	0.28
PEG	0.29	0.22
FRT	0.27	0.25
ABE	0.28	0.29
TOD	0.35	0.35
PAT	0.38	0.38
MEM	0.23	0.24
BUC	0.32	0.33
HOP	0.27	0.30
MIC	0.36	0.36
MAL	0.31	0.37
TMD	0.26	0.30

The Bakun standard deviations from Table 2 have been included in Table 4 enabling a rough comparison of the performance of the two expressions: Wilkie applied to all

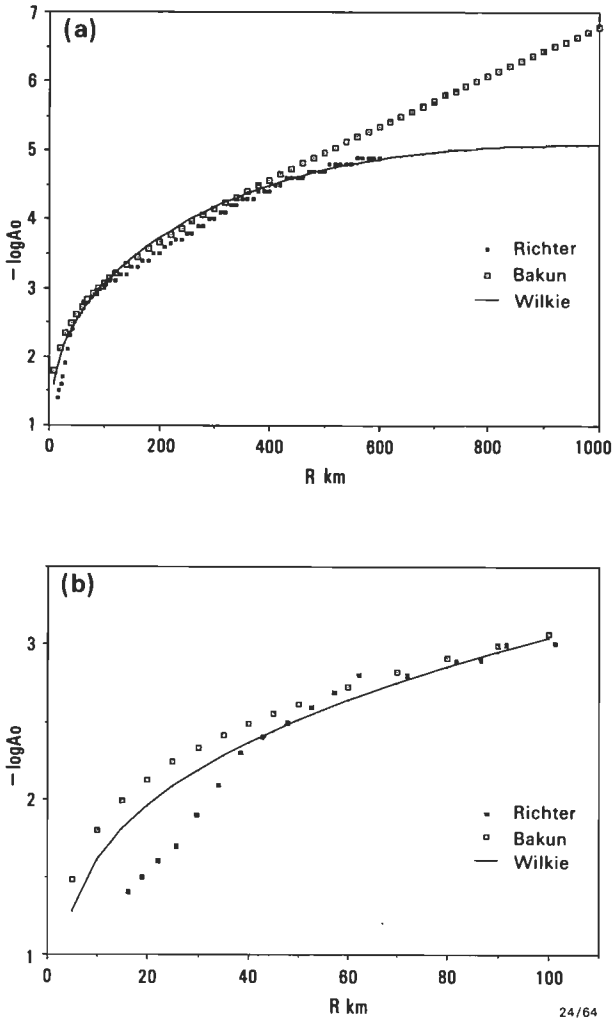

Figure 4(a). Comparison of Richter (1958), Bakun & Joyner (1984) and Wilkie (present study) expressions to a range of 1000 km.
Figure 4(b). Comparison of Richter, Bakun & Joyner and Wilkie expressions at close range.

data to 1000 km and Bakun & Joyner applied to data restricted to epicentral distances less than 475 km. The mean of the standard deviations for the former was 0.30 and for the latter 0.29. As described above, if the Bakun & Joyner formula was used with all data to 1000 km, the standard deviation was 0.55.

Figures 4(a) and 4(b) show plots, for the GVL seismograph, of the three estimates of –logAo considered, including the site corrections (GVL site correction 0.07, for Bakun & Joyner, is taken from Table 2):

$$-\log Ao \quad \text{empirical values} \quad \text{Richter, 1958}$$

$$-\log S - \log Ao = 0.07 + 0.7 + \log R + 0.00301R \quad \text{Bakun \& Joyner (modified)}$$

$$-\log S - \log Ao = 0.55 + \log R + 0.0056Re^{-0.0013R} \quad \text{Wilkie (present study)}$$

The Wilkie expression retains the features of Bakun & Joyner's expression at short epicentral distances giving higher values of –logAo than Richter. It agrees closely with Richter (1958) and Bakun & Joyner (1984) to approximately 450 km, but then follows the required trend of the Richter values out to 600 km. The Wilkie expression then extends the estimate of –logAo to 1000 km, achieving over the whole range of epicentral distance the same standard deviation for computed ML magnitudes with respect to the assigned ML magnitude as the Bakun & Joyner expression gave for the data restricted to epicentral distances less than 475 km.

Table 4. Values of p_1 and standard deviations resulting from the application of expression (14). Standard deviations from the application of Bakun & Joyner's expression (13) with R <475 km has been included for comparison.

WILKIE FORMULA ($p_2 = 0.0056$, $p_3 = 0.0013$) *(applied to all data to 1000 km)*				*Bakun & Joyner FORMULA (restricted data <475 km)*
SITE	p_1	*ERROR*	*SD*	*SD*
GVL	0.55	0.05	0.20	0.19
PNH	0.66	0.07	0.26	0.28
TOM	0.62	0.08	0.29	0.32
LIL	0.58	0.09	0.27	0.30
KGD	0.53	0.08	0.22	0.19
JEN	0.59	0.10	0.29	0.28
PEG	0.36	0.08	0.29	0.22
FRT	0.33	0.10	0.28	0.25
ABE	0.36	0.06	0.29	0.29
TOD	0.17	0.07	0.36	0.35
PAT	0.19	0.08	0.38	0.38
MEM	0.21	0.13	0.23	0.24
BUC	0.58	0.14	0.33	0.33
HOP	0.62	0.08	0.27	0.30
MIC	–0.11	0.10	0.38	0.36
MAL	0.52	0.12	0.38	0.37
TMD	0.04	0.12	0.34	0.30
		Mean	0.30	0.29

ERROR = 2* standard error in p_1

Site corrections

In determining magnitudes, Richter (1958) applied station corrections which were determined statistically from the systematic deviation of the magnitude determined by a particular seismograph from the mean magnitude. Richter associated this correction with the local ground and installation conditions. Likewise associated with their parametric expression for –logAo, Bakun & Joyner (1984) applied station corrections which ranged from –0.6 to +0.4 and closely associated these corrections with local geology, rock sites giving positive corrections and sedimentary sites giving negative corrections.

ML magnitudes calculated for individual sites and recorded in the earthquake location files at the Seismology Research Centre, were used to calculate a site correction with respect to the adopted ML magnitude. The initial analysis used data for 1984–86. Only earthquakes whose magnitude was computed at three or more sites were included.

The range of magnitude (approximately 0 to 3) for which the corrections were calculated for Victoria varied from site to site, depending on the seismic activity in the vicinity and the proximity of other recording sites to enable an estimate of earthquake magnitude. However, plots of site

correction against magnitude for the sites TOD, TMD, GVL and FRT, respectively, showed no statistically justifiable variation in the correction with respect to magnitude.

This conclusion is also supported by evidence from Bougainville Island, New Guinea, where Seismology Research Centre seismographs were operated at several sites. The range of ML magnitude, 3 to 6, and depth range, 0 to 500 km, associated with plate subduction in one of the most seismically active regions of the world, are in strong contrast to the intraplate Victorian micro-earthquakes. Plots of site corrections, which were of the order of −1.0, against magnitude showed in all cases corrections independent of magnitude.

Table 5. Mean ML magnitude site corrections 1984–86

SITE CODE	*CORRECTION*	*SD*	*N*	
MLW	0.14	0.28	207	
PNH	0.27	0.26	262	
TMD	−0.61	0.28	60	
GVL	0.13	0.18	251	
FRT	−0.52	0.18	45	
TOD	−0.26	0.25	96	
TOM	−0.17	0.22	222	Jan'84–Nov'85
TOM	0.05	0.21	123	Nov'85–Dec'86
PEG	−0.22	0.23	154	
JEN	0.19	0.30	188	
MEM	−0.43	0.15	7	
HOP	0.43	0.12	14	Jan'84–Sept'84
HOP	0.28	0.25	33	Oct'84–Dec'86
BUC	−0.01	0.23	31	
MAL	0.28	0.27	41	
PAT	−0.41	0.25	87	
ABE	−0.04	0.20	77	
MIC	−0.50	0.21	45	

Over the range of the first few tens of kilometres there is a rapid change in the frequencies recorded during an earthquake and a special investigation of the possibility of variation of site correction with R at small values of R was made; however, no evidence of variation was found.

Therefore, considering the above, it appears that a site correction, independent of magnitude, can be applied in the computation of ML magnitude for each seismograph. There is considerable evidence that ground motion is amplified at sedimentary foundation sites, especially the horizontal components (Phillips & Aki, 1986). On a logarithmic magnitude scale any amplification will appear as a constant correction and site amplification appears to be the main contribution to site corrections.

The site corrections with the number of earthquakes used and standard deviations for 1984–86 data are shown in Table 5. In order to confirm these corrections, the 1987–89 Victorian earthquake ML magnitude data were analysed for site corrections. The results are shown in Table 6, which includes the 1984–86 site corrections for comparison. In most cases, the corrections are closely confirmed. The change at MAL is due to the conversion in January 1988 from a vertical component to a triaxial seismograph, the change at HOP is due to the installation of some nearby seismographs thereby influencing the magnitudes assigned to earthquakes. However, no reason can be found for the change in site correction at PEG and FRT.

Further investigation of mean ML site corrections was carried out to try to eliminate the effects of site groupings; for example, where most nearby sites record only the vertical component or nearby sites are mainly on sediment and consequently register higher ML magnitudes due to amplification. Only earthquakes for which at least eight values of ML magnitude had been computed were used. This gave, for each earthquake, an assigned magnitude derived from seismographs with a wide variety of foundations, thus minimising local effects.

Table 6. Mean ML magnitude site corrections 1984–86 and 1987–89.

SITE	*1984–86*	*1987–89*
MAL	0.28	0.08
HOP	0.28	0.11
PNH	0.27	0.25
JEN	0.19	0.12
GVL	0.13	0.15
TOM	0.05	0.00
BUC	0.00	−0.05
ABE	−0.04	−0.09
PEG	−0.22	−0.46
TOD	−0.26	−0.30
PAT	−0.41	−0.50
MIC	−0.50	−0.51
FRT	−0.52	−0.14
TMD	−0.61	−0.66

The mean ML site corrections 1987–89 can be compared with the corrections for 1987–89 using only earthquakes with at least 8 computed ML magnitudes in Table 7. The sites with analogue recorders, detecting only the vertical component, have had their mean ML correction increased by approximately 0.1, whereas the corrections for sites with triaxial seismographs have generally remained constant.

An interpretation of this is that the smaller earthquakes, normally recorded at fewer than eight sites, can be detected by the analogue seismographs, but do not trigger the triaxial digital instruments. When the triaxial seismographs are triggered by the larger earthquakes, the horizontal components are used to determine the ML magnitude. Since the amplitude of the vertical component is generally less than the horizontals, the triggering of the triaxial instruments results in a higher magnitude being assigned to the earthquake and as a consequence the mean ML site correction for each analogue site will be increased. Implications of this will be discussed in a later paper.

Likewise when the triaxial sites are considered, both HOP and WSK have the largest increase in site correction. Often these seismographs are triggered by nearby earthquakes which are usually recorded only by the analogue seismographs. When larger earthquakes are considered, the increase in mean ML site correction can be attributed to the triggering of most of the triaxial seismographs and a consequent increase in the ML magnitude assigned to the earthquake.

Considering the above, the mean ML site corrections adopted were those indicated by using more than 8 ML magnitude values.

Table 7. Comparison of site corrections (1987–89) determined using three or more magnitude values with site corrections calculated when eight or more magnitude values were available.

SITE	*>=8 ML values*	*>=3 ML values*	*site foundation*	*components*
GVL	0.22	0.15	granite	Z
TOM	0.07	0.00	weathered granite	Z
TOD	–0.30	–0.30	weathered granite	ENZ
ABE	–0.07	–0.09	Palaeozoic sediment	ENZ
BEL	–0.23	–0.31	Palaeozoic sediment	ENZ
JEN	0.17	0.12	Cretaceous sediment	ENZ
WSK	0.02	–0.10	Palaeozoic sediment	ENZ
MLW	0.33	0.19	granite	Z
HOP	0.23	0.11	granite	ENZ
PAT	–0.53	–0.50	Palaeozoic sediment	ENZ
DRO	–0.02	–0.07	weathered granite	Z
PNH	0.37	0.25	Silurian sediment	Z
FRT	–0.12	–0.14	Cretaceous sediment	Z
BUC	0.01	–0.05	granite	ENZ
MIC	–0.53	–0.51	weathered granite	ENZ
TMD	–0.67	–0.66	rock fill dam	ENZ
CRN	0.35	0.11	granite	Z
RUS	–0.30	–0.32	Palaeozoic sediment	ENZ
MAL	0.16	0.08	hornfels	ENZ
PEG	–0.35	–0.46	Tertiary sediment	Z

E East–West component
N North–South component
Z Vertical component

The mean ML magnitude site corrections with their corresponding geological foundation are shown in Table 7. Phillips & Aki (1986) found an inverse relationship between site amplification and the age of sediment. There is no evidence of such a relationship in Table 7, apart from granite bedrock sites being in general the sites corresponding to the least amplification and a rock fill dam, representing very recent sediment, giving the greatest site amplification.

Figure 5 shows the mean ML site correction plotted against the corresponding value of p_1 from Table 4. The approximate linear nature of this plot indicates a direct relationship between the parameter p_1 and the mean ML site correction. It was previously assumed that p_2 and p_3 in expression (11) were related to path and p_1 to seismograph foundation. Figure 5 confirms the validity of this assumption.

It appears that the maximum value of p_1 is about 0.7. The triaxial sites which have a value of p_1 close to 0.7 are the rock foundation sites (Table 7); therefore, a value of 0.7 for p_1 can be thought of as the value corresponding to the ideal rock seismograph site. Since $p_1 = -\log S + C$ (12) and defining logS for an ideal site to be 0.0, the value of C is 0.7.

$$ML = \log A - \log S + 0.7 + \log R + 0.0056Re^{-0.0013R} \quad (15)$$

The attenuation function for Victoria is

$$-\log Ao = 0.7 + \log R + 0.0056Re^{-0.0013R} \quad (16)$$

The site term, logS, is a correction relative to the ideal hard rock site and is related to the site foundation amplification used in many earthquake building codes.

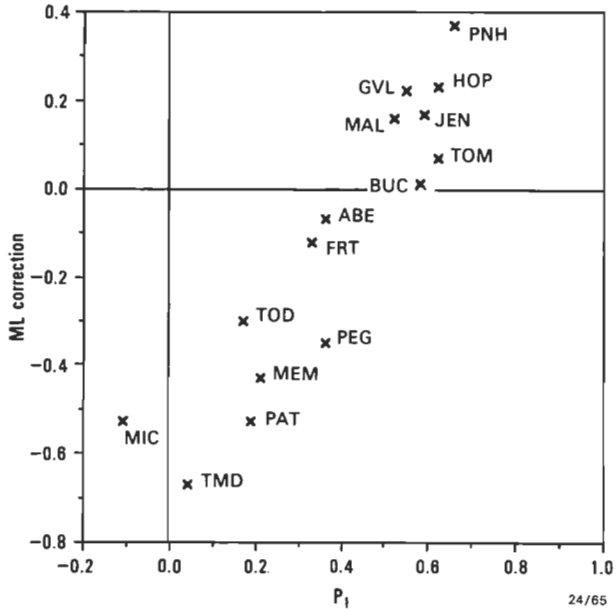

Figure 5. Plot of seismograph site correction versus p_1 from (14). Corrections for each site are the average differences between the magnitudes computed using the original Bakun & Joyner expression (13) and the assigned magnitude for each earthquake.

The site term can be determined for new sites as soon as a statistically reliable mean ML magnitude site correction can be determined. The site terms for the seismograph sites in this study are listed in Table 8.

The expressions of Greenhalgh & Singh (1986), Gaull & Gregson (1991), and Wilkie (this study) for –logAo are shown below for comparison:

$$-\log Ao = 0.7 + 1.1\log\Delta + 0.0013\Delta \quad \text{Greenhalgh \& Singh (1986)}$$

$$-\log Ao = 0.66 + 1.137\log R + 0.000657R \quad \text{Gaull \& Gregson (1991)}$$

$$-\log Ao = 0.7 + \log R + 0.0056Re^{-0.0013R} \quad \text{Wilkie (present study)}$$

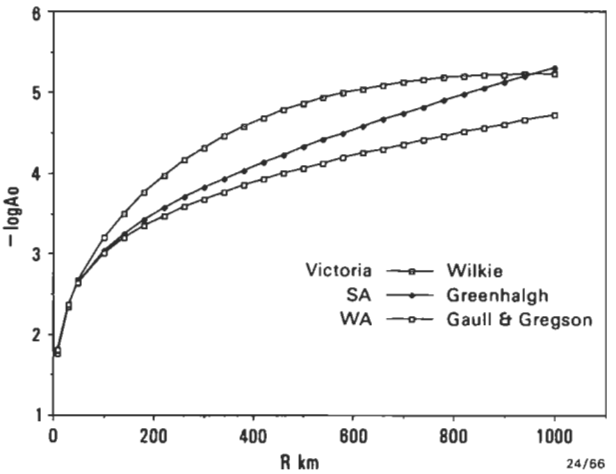

Figure 6. Comparison of Australian attenuation expressions.

Table 8. Site terms, logS, to be applied in expression (15) for the calculation of ML magnitudes.

SITE	*SITE TERM (logS)*
GVL	0.15
PNH	0.04
TOM	0.08
LIL	0.12
KGD	0.17
JEN	0.11
PEG	0.34
FRT	0.37
ABE	0.34
TOD	0.53
PAT	0.51
MEM	0.49
BUC	0.12
HOP	0.08
MIC	0.81
MAL	0.18
TMD	0.66

Figure 6 shows a comparison of the Australian expressions for –logAo, emphasising the lower attenuation for South Australia and Western Australia compared with that for Victoria. Part of the difference is due to the different definition of the site correction. Both Greenhalgh & Singh and Gaull & Gregson relate the site correction to an 'average' site, while the Wilkie expression relates it to a typical bedrock site, giving a difference of about 0.2, depending on the nature of the 'average' site in South Australia or Western Australia. The near-linear variation of –logAo with R at large distances for the South Australian and Western Australian expressions shows the dominance of the KR term in (6).

In order to confirm the correctness of the above formula and corrections, magnitudes were recalculated for a fresh sample of 35 earthquakes, most of which had a magnitude of 2 and above to ensure that a reasonable number of seismographs recorded each event. The results were:

- Comparing the old and new values of mean magnitude for each earthquake, it was found that the mean difference over all earthquakes in the sample was less than 0.04, the new values being less than the old. This result would be expected, because by choosing the larger events many were recorded at the high amplification sites in the Thomson Reservoir area and hence had their mean magnitude reduced.

- Those earthquakes recorded at a set of sites with low magnification had their magnitude increased, and those recorded at a set of sites including some high magnification sites had their magnitude decreased. Some events had a change of –0.2, when high amplification sites such as MIC and TMD were involved. Remembering that overall the old magnitudes assigned depend upon the subset of seismographs recording a particular event, but the site corrections are with respect to the total set of Victorian seismographs with a range of site amplifications involved, the above result would be expected

- The standard deviation of the magnitude values for the sites recording a particular earthquake was on average reduced by a factor of 0.7, and in many cases where the high amplification sites were involved the standard deviation was halved.

Table 9 shows two examples of the reassessment of magnitude described above, one for an event at Mt Selma close to the Thomson Reservoir higher amplification sites, and the other at Benambra in eastern Victoria. In both cases, the standard deviation of the individual magnitude values was substantially reduced. In the case of the Benambra event, the new mean magnitude is greater than the old, and for the Mt Selma event the new magnitude is less than the old, consistent with the application of site corrections adopted with respect to the total set of Victorian seismograph sites.

Table 9. Reassessment of magnitudes for two Victorian earthquakes showing substantial reduction in the standard deviation of individual magnitude values.

	Mt Selma		*Benambra*	
SITE	*ML old*	*ML new*	*ML old*	*ML new*
GVL	1.8	1.9	2.3	2.4
PNH	1.6	1.8	2.1	2.4
TOM	2.0	1.9	2.2	2.3
TOD	1.9	1.5		
MIC	2.5	1.8		
PAT	2.3	1.9		
ABE	2.1	1.9		
MAL	1.8	1.7		
TMD	2.3	1.7		
JEN	1.4	1.5	2.3	2.5
PEG	1.9	1.9	3.0	2.9
MLW			2.3	2.5
DRO			2.2	2.3
mean	1.96	1.77	2.34	2.47
stand. dev.	0.32	0.16	0.30	0.20

The extended range of the formula was tested on two well-documented earthquakes:

- The Lithgow earthquake on 13th February 1985, magnitude 4.3 (Michael-Leiba & Denham, 1987).
  It was possible to measure the magnitude of this earthquake at six Victorian network sites with ranges extending from 586 to 667 km.
  The mean magnitude was 4.4 (standard deviation 0.19) compared with a value of 4.3±0.2 assigned to the earthquake.

- The Newcastle earthquake on 28th December 1989, magnitude 5.6 (McCue & others, 1990).
  This earthquake was offscale on most of the Victorian network analogue seismographs, but eight magnitude values could be computed, with site ranges extending from 708 to 940 km. The mean magnitude was 5.9 (standard deviation 0.32) compared with a value of 5.6 adopted from a variety of sources (mainly conversions from other magnitude scales and indirect measures such as duration and isoseismal radii) with no estimate of error. The direction of the fault was northwest–southeast, giving a maximum of shear-wave radiation to the southwest in the direction of the Victorian seismograph sites.

One would expect that the Victorian network with its wide variety of site foundations, dictated to some extent by logistics associated with specialized projects, would give

higher values of magnitude compared with those from bedrock sites normally selected for seismic observatories, when more flexible site location is possible. This is an example of one of the features of the Richter scale which make its world wide portability difficult.

It must be noted that this study does not define the new Victorian scale to be consistent with that in southern California. Use of magnitudes as previously computed in the regression for p_1, p_2 and p_3 means that the Victorian datum remains essentially unchanged.

Discussion

The assignment of a magnitude to an earthquake is a simple concept: the magnitude is a number representing a measure of the earthquake 'size' determined from a seismogram according to a prescribed procedure. Complexity arises from the many factors influencing the propagation of seismic waves which are used to measure magnitude. These factors include asymmetry in the source radiation pattern, frequency dependent attenuation, variation in attenuation depending on the propagation path which varies with R, and seismograph site amplification.

Ideally, each seismograph recording of a particular earthquake should give the same magnitude irrespective of seismograph site foundation or R. This consistency will not be achieved in practice because of the many variables involved. Some of these variables have been studied in this investigation. By the separation of parameters which represent path and site, combined with a knowledge of the influence of the components used in the magnitude measurement, a reduction in the standard deviation of the computed magnitudes can be achieved, and a magnitude can be assigned keeping in mind the overall quality of the network sites used in the assessment.

The new expression for attenuation is:

$$-\log Ao = 0.7 + \log R + 0.0056Re^{-0.0013R}$$

This is a simple arbitary function used to fit the variation of amplitude with distance, and it is possible that other more complex functions will give a better fit. The constants 0.0056 and 0.0013 are appropriate for southeast Australian earthquakes, and may differ in other regions. The constant 0.7 is a scaling term, used to adjust magnitude values to the original Victorian magnitude values. Unification to the original Richter magnitude values depends on the difference in attenuation between California and Victoria, and on the difference in site amplification at average seismograph sites in California (1935) and Victoria (1987–89).

Extension of the parametric expression for –logAo to a range of 1000 km opens the possibility of other networks doing a similar analysis; thus, with the extended range, several networks can assign an ML magnitude to an earthquake giving a unification of the local magnitude scale Australia-wide.

We have seen that the seismograph sites have a major influence on ML magnitude assignment. At most sedimentary foundation sites there is amplification of the horizontal components, and a different magnitude will be determined for an earthquake depending on the combination of foundation conditions at the recording sites. For example, an ML magnitude assigned from seismographs all located on bedrock sites would be of the order of 0.5 less than that assigned by a network of seismographs on sedimentary sites. This difference can be very significant when site corrections are of the order of –1.0, as experienced in Bougainville.

The relationship in Figure 5 shows that the site term logS, which we define as a correction with respect to an 'ideal' site, could partially solve this problem. On the assumption that bedrock sites are normally sought by seismologists, then the local magnitude scale needs to be defined so that the assigned magnitude is that from the mean of equivalent bedrock sites in order to eliminate the lack of definition with respect to site combination choice.

The definition of the site term relative to a rock site, rather than an 'average' site, links this correction to site amplification as used in earthquake building codes.

Although the Richter local magnitude scale has been adopted world wide, it is not a portable scale and is only defined for southern California. The problem lies in the definition of the zero magnitude earthquake in terms of an earthquake at a distance of 100 km from the recording site. This immediately involves the southern Californian attenuation factors and therefore makes the portability of the scale difficult.

The result of using the new attenuation function and the site corrections defined is to give negligible change in the average magnitude for most Victorian earthquakes, a reduction in the standard deviation of magnitudes computed from different seismographs for each earthquake and the ability to compute magnitudes to a distance of 1000 km rather than 600 km.

Acknowledgments

The authors thank S. Greenhalgh and D. Denham for their detailed and helpful reviews of the paper, and AGSO for the supply of seismic information used in the project. J. Wilkie wishes to thank the Victoria University of Technology for supporting the research with a grant of PEP leave.

References

Aki,K., 1980 — Scattering and attenuation of Shear Waves in the Lithosphere. *Journal of Geophysical Research*, 85, no. B11, 6496–6504.

Bakun, W.H. & Joyner, W.B., 1984 —The ML Scale in Central California. *Bulletin of the Seismological Society of America*, 74, no.5, 1827–1843.

Boore, D.M., 1989 —The Richter Scale: its development and use for determining earthquake source parameters. *Tectonophysics* 166, 1–14.

Bullen, K.E. & Bolt, B.H., 1985 — An Introduction to the Theory of Seismology. *Cambridge University Press.*

Cuthbertson, R.J., 1977 — PIT Seismology Centre Network Calibration and Magnitude Determination. *B.Sc. honours thesis, Uni. of Melbourne.*

Denham, D., 1979 — Earthquake Hazard in Australia. *Proceedings of the Symposium on Natural Hazards in Australia, 1979. Australian Academy of Science, Canberra.*

Gaull, B.A. & Gregson, P.J., 1991 — A new local magnitude scale for Western Australian earthquakes. *Australian Journal of Earth Sciences*, 38, 251–260.

Greenhalgh, S.A. & Singh, R., 1986 — A revised magnitude scale for South Australian earthquakes.

Bulletin of the Seismological Society of America, 76, no.3, 757–769.

Hutton L.K. & Boore D.M., 1987 — The ML Scale in Southern California. *Bulletin of the Seismological Society of America*, 77, no.6, 2074–2094.

McCue, K., Wesson, V. & Gibson, G., 1990 — The Newcastle, New South Wales, earthquake of 28 December 1989. *BMR Journal of Australian Geology & Geophysics*, 11, 559–567.

McGregor, P.M. & Ripper, I.D., 1976 — Notes on earthquake magnitude scales. *Bureau of Mineral Resources, Australia, Record* 1976/56.

Michael-Leiba, M.O. & Denham, D., 1987 — The Lithgow earthquake of 13 February 1985: macroseismic effects. *BMR Journal of Australian Geology & Geophysics*, 10, 139–142.

Nuttli, O.W., 1973 — Seismic wave attenuation and magnitude relations for eastern North America. *Journal of Geophysical Research*, 78, no.5, 876–885.

Phillips, W.S. & Aki, K., 1986 — Site amplification of Coda Waves from local earthquakes in Central California. *Bulletin of the Seismological Society of America*, 76, no.3, 627–648.

Rautian, T.G. & Khalturin, V.I., 1978 — The use of the Coda for determination of the earthquake source spectrum. *Bulletin of the Seismological Society of America*, 68, 923–948.

Richter, C.F., 1935 — An instrumental magnitude scale. *Bulletin of the Seismological Society of America*, 25, 1–32.

Richter, C.F., 1958 — Elementary Seismology. *W.H. Freeman, San Francisco.*

AGSO Journal of Australian Geology & Geophysics, 14, 47–63

The "Geera Clay equivalent": a regressive marine unit in the Renmark Group that sheds new light on the age of the Mologa weathering surface in the Murray Basin

M.K. Macphail[1], J.R. Kellett[2], J.P. Rexilius[3] & M.E. O'Rorke[4]

Sandy clays deposited during the waning phase of Oligocene–Middle Miocene transgression of the Murray Basin conformably overlie the shallow to marginal marine Geera Clay and grade laterally into fluvio-lacustrine sediments of the Middle and Upper Renmark Group. These sandy clays (informally named "Geera Clay equivalent") and the Geera Clay preserve marine dinoflagellates that became extinct by middle to late Middle Miocene time. *If* the subsequent regression was due to a global drop in relative sealevel, then we propose that the unconformity developed across the Geera Clay and that the lateral equivalents during the Late Miocene (Mologa weathering surface) correlates with either the 13.8 Ma or (preferred) 10.5 Ma sequence boundary of Haq & others (1987).

Three pollen species of potential biostratigraphic value in the Murray Basin are illustrated and discussed. One new species is described: *Tetrapollis campbellbrownii*.

Introduction

One of the major low-permeability barriers to groundwater flow within the Murray Basin is the shallow to marginal marine Geera Clay. This formation extends from the Flinders Ranges, South Australia, in an arc about 100 km wide and 800 km long across the centre of the Murray Basin to the Grampians, Victoria (Fig. 1). It represents the maximum extent of Oligocene–Miocene marine transgression into the basin: progradation of the Geera Clay over platform carbonates of the Murray Group is widely assumed to reflect marine regression during the Miocene (Fig. 2).

Foraminifera have provided a moderately reliable age for the base of the Geera Clay, but because the upper section has only environmentally restricted faunas, a confident minimum age limit is neither available for the formation nor for the time of development of the Mologa weathering surface. For example, Lindsay (1983) proposed that the Geera Clay continued to accumulate into the early Middle Miocene in the western Murray Basin, although the youngest age obtained was Early Miocene.

Palynological age determinations in the Murray Basin are usually much less precise than those based on foraminifera, although marine dinoflagellates could provide a relatively detailed chronological control. Published time distributions (Table 1), suggest that *Pentadinium laticinctum* Gerlach 1961, recorded at Oakvale-1 by Truswell & others (1985), may range no higher than the early Middle Miocene; whereas *Apteodinium australiense* (Deflandre & Cookson) Williams 1978, and *Systematophora placacantha* (Deflandre & Cookson) Davey & others 1969, emend 1980, present in the SADME MC 63 borehole (Martin, 1991), range no higher than the late Middle Miocene. The absence of a reliable datum to compare palynosequences from widely separated boreholes complicates the situation (see Macphail & Truswell, 1989, p. 305).

Palynological analyses have revealed a number of instances where *Apteodinium australiense* + *Pentadinium laticinctum*, with *Systematophora placacantha* either present or absent, occur not only within the Geera Clay, but also in sandy clays within the Middle and Upper Renmark Group previously assumed to be entirely non-marine. The stratigraphic distribution of these dinoflagellates and associated spores and pollen in nine boreholes intersecting this sandy clay unit are discussed. Analyses of the underlying Geera Clay in one borehole revealed a sample which preserves a diverse assemblage of calcareous nannoplankton. The assemblage appears to have been deposited during marine flooding in basal Early Miocene time. If this event can be shown to be regional, then it may prove to be useful as a *datum* for correlating boreholes intersecting the Geera Clay and lateral marginal marine correlatives.

The present article is concerned mainly with the palynology and palaeontology; lithologic and geophysical data, supporting some of the environmental interpretations given here, are to be found in well-completion reports.

Geera Clay & marginal marine correlatives within the Middle and Upper Renmark Group

The Geera Clay [map symbol = T_{mg}] consists of dark greenish-grey to black silty muds, silts, clays and minor dark sands accumulated under complex paralic conditions. Goethitic and glauconitic faecal pellets and pyritic tubules may be frequent locally. Lithofacies analysis (Brown & Radke, 1989) indicate that the formation was deposited in micro-progradational (shoaling upwards) cycles during an *overall* rise in relative sea-level.

The formation greatly influences the regional hydrogeology and hydrogeochemistry of the central Murray Basin, e.g. the distribution of groundwater discharge zones (Evans & Kellett, 1989). It impedes lateral throughflow in the upper and middle Renmark Group aquifers and, where it grades laterally into the Middle and Upper Renmark Group, acts as a semi-confining bed on top of the lower Renmark Group aquifer (Kellett, 1989). In many places, the upper part of the Geera Clay is a sink for, and the lower part a source of, salts which diffuse into the regional groundwater system.

Boreholes adjacent to the northern limits of the Geera Clay often intersect sandy clay strata in the Middle and Upper Renmark Group [map symbol = T_{er2} and T_{er3}, respectively]

1 Consultant Palynologist, 20 Abbey St., Gladesville NSW 2111
2 Australian Geological Survey Organisation, GPO Box 378, Canberra ACT 2601
3 International Stratigraphic Consultants P/L, PO Box 26, Cottlesloe WA 6011
4 Rural Water Corporation of Victoria, 590 Orrong Rd., Armadale VIC 3143

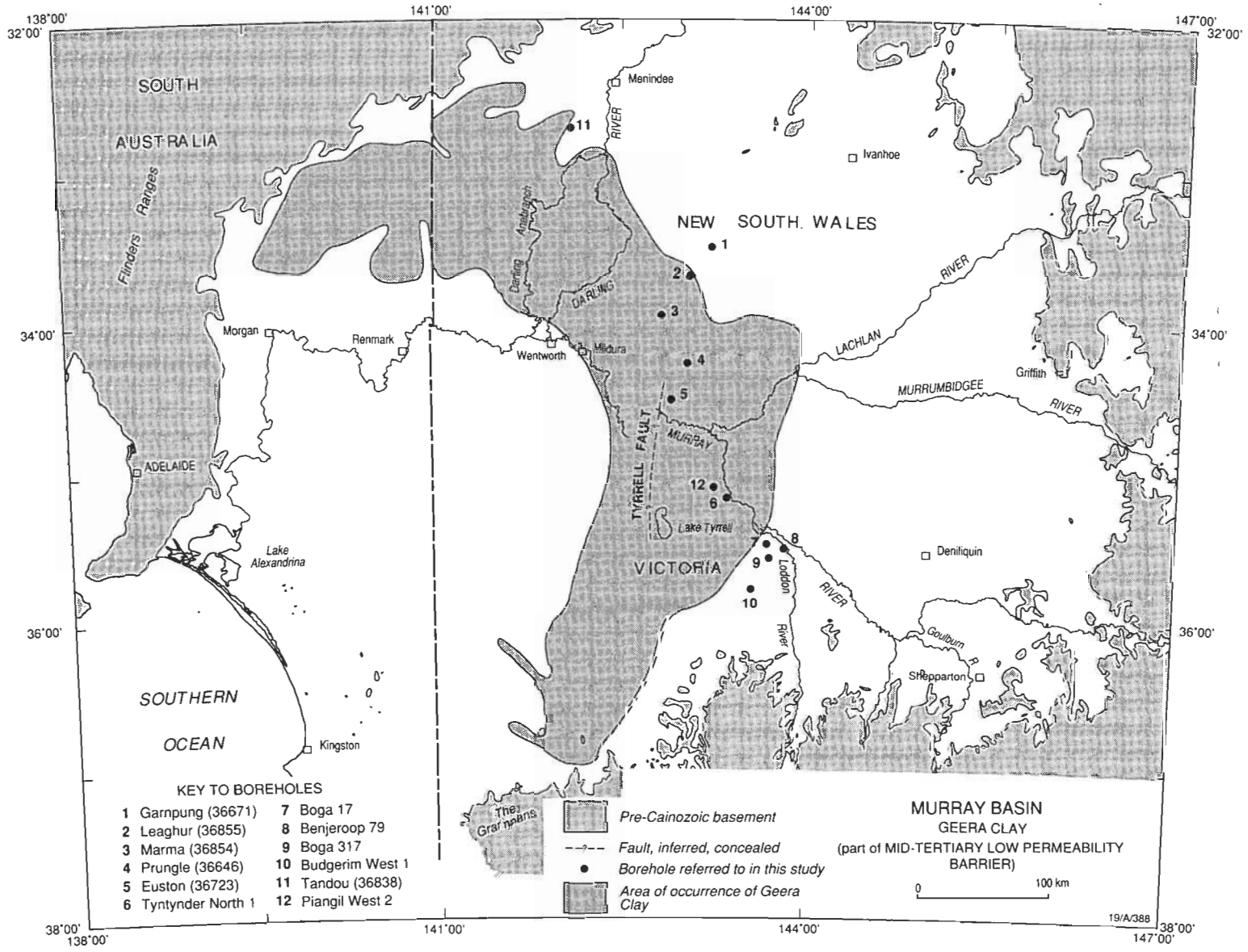

Figure 1. Isopachs of the Geera Clay mid-Tertiary Low Permeability Barrier in the central Murray Basin; numbers refer to the location of boreholes mentioned in the text.

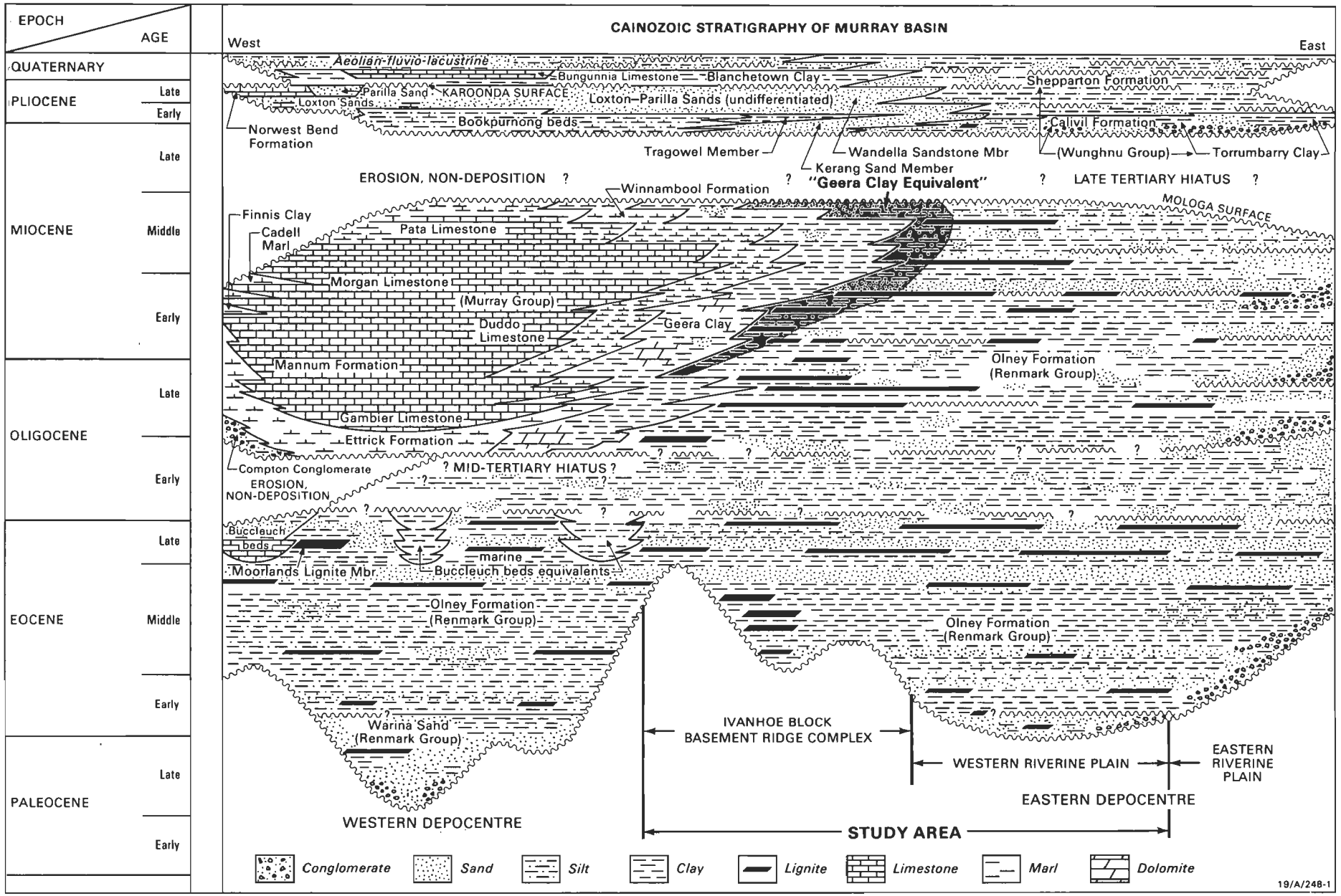

Figure 2. Cenozoic stratigraphy of the Murray Basin, showing the Geera Clay and "Geera Clay equivalent" wrapping around the Winnambool Formation marls and Murray Group limestones.

Table 1. Last appearance for selected marine dinoflagellates.

		Apteodinium australiense	*Pentadinium laticinctum*	*Systematophora placacantha*
Williams & Bujak (1985)	Planktonic Foram. Zone	N11/12	N15	N15
	Calc. Nanno. CN Zone	–	–	–
	Calc. Nanno. NN Zone	NN6	NN9	NN9
	Age+	mid. MIDDLE MIOCENE	Latest MIDDLE MIOCENE	Latest MIDDLE MIOCENE
Stover (1987)	Planktonic Foram. Zone	N12	N10	N13
	Calc. Nanno. CN Zone	CN5A	CN4	CN5B
	Calc. Nanno. NN Zone	–		–
	Age*	mid. MIDDLE MIOCENE	early MIDDLE MIOCENE	Late MIDDLE MIOCENE
Powell (1992)	Planktonic Foram. Zone	no data	N14	N12
	Calc. Nanno. CN Zone	no data	–	–
	Calc. Nanno. NN Zone	no data	NN8	NN6
	Age*	–	Latest MIDDLE MIOCENE	mid. MIDDLE MIOCENE

+ Timescale after Harland & others (1982)

* Timescale after Haq & others (1987)

that are lithologically indistinguishable from fluvio-lacustrine facies, but which preserve low to moderate numbers of marine dinoflagellates and chitonous remains of foraminifera (trochospiral liners). These sandy clays interfinger with and conformably overlie the Geera Clay: the upward coarsening nature of the sequence (in combination with the geophysical logs) demonstrates that the unit, here *informally* named "Geera Clay equivalent" [map symbol = T_{mge}], was deposited during one or more periods of waning marine influence during the Oligocene–Miocene.

Borehole sequences

Localities are shown in Figure 1. The three key bores are Leaghur (DWR 36855), Marma (DWR 36854), and Tandou (DWR 36838), all drilled as part of a joint program between the Bureau of Mineral Resources (now Australian Geological Survey Organisation, or AGSO) and the New South Wales Department of Water Resources (DWR). The first two drillsites lie within the Ivanhoe Block (Fig. 2), a faulted and uplifted, concealed basement ridge complex on the northeastern margin of the hydrogeologic divide separating the Riverine and Scotia groundwater Provinces (Evans & Kellett, 1989). The third bore, Tandou, is west of this divide in the Scotia Province.

Cutting samples only were available, but as the boreholes were fully flushed metre by metre between collection, all are considered to be reliable over the depth indicated. The New South Wales sites have been augmented by cuttings from boreholes drilled by the Victorian Department of Industry, Technology and Research (DITR) near the eastern margin of the Geera Clay in the Riverine Province, i.e. Benjeroop 1, Boga 17, Boga 317, Budgerim West 1, and Tyntynder North 1 in the Kerang–Nyah district of northern Victoria.

Formation boundaries are based on cutting samples taken at the time of drilling; age determinations and revisions of the borelog lithostatigraphy presented here are wholly based on fossil dinoflagellates, spores and pollen — except at Marma where five samples between 129–224 m were also analysed for foraminifera and calcareous nannoplankton. Only the Oligo-Miocene marine section of each bore is discussed. Full lithostratigraphic details are available from the relevant drilling authority. The palynological zonation scheme followed is that of Stover & Partridge (1973), as adapted for use in the Murray Basin by Macphail & Truswell (1989). *Triporopollenites bellus*, the nominate species of the late Early to Late Miocene *T. bellus* Zone (Stover & Partridge, 1973), was transferred to *Canthiumidites* by Mildenhall & Pocknall (1989). However, the name of the *Zone* has not been formally altered and is retained here. Ages cited in millions of years (Ma) are based on the timescale of Haq & others (1987).

(A) Northwestern Riverine Province

(1) Leaghur (DWR 36855) Fig. 4a

The drillsite is between Lakes Leaghur and Mungo, two in a chain of playa lakes (Willandra System) extending from swamps 50 km southwest of Ivanhoe in southwestern New South Wales to the Prungle Lakes about 40 km northeast of Euston on the Murray River. Geologically, the lakes lie within the Willandra Trough, a basement depression bounded by the two parallel south-southwest-trending basement Neckarboo and Iona Ridges (Fig. 3). The barrier action of these ridges on groundwater flow has resulted in the Willandra System being a prominent regional groundwater discharge zone since late Cenozoic time. The Leaghur (and Marma) bore was drilled to monitor movement of the regional water table. Units intersected by the bore are:

0–14 m	Undifferentiated Quaternary sediments
14–48 m	Loxton–Parilla Sands
48–84 m	Upper Renmark Group
84–121 m	Middle Renmark Group A
121–144 m	Geera Clay
144–196 m	Middle Renmark Group B
196–261 m	Lower Renmark Group

The interval indentified as Geera Clay is unusually sandy, of possible tidal channel origin. Marine dinoflagellates at 81–83 m, 95–97 m and 119–120 m indicate that the Middle Renmark Group A and basal 3 m of the Upper Renmark Group are "Geera Clay equivalent". Thin well-cemented siliceous and dolomitic/calcareous bands occur within the interval.

Proteacidites tuberculatus Zone (129–130 m) [T_{mg}]

This palynoflora is wholly dominated by long-ranging spore and pollen species, in particular Casuarinaceae and *Nothofagus (Brassospora)*. The age determination is based on (i) the absence of *T. bellus* Zone indicators, such as *Canthiumidites (=Triporopollenites) bellus*, and (ii) three species that are more typical of the *P. tuberculatus* than younger zones: *Aglaoreidia qualumis, Malvacearumpollis* sp. and *Tetrapollis campbellbrownii*. The dinocyst flora includes *Apteodinium australiense*. Dinoflagellates at 145–146 m, at the top of the Middle Renmark Group B, may be caved.

Triporopollenites bellus Zone (81–120 m) [T_{mge}]

Palynofloras within this interval are dominated by Araucariaceae and Myrtaceae. The age determination is based on *Canthiumidites bellus* at 119–120 m and 81–83 m, *Schizocolpus marlinensis* at 119–120 m, and *Hypolepis spinyspora* at 95–97 m. Dinoflagellates include *Apteodinium australiense* at 119–120 m and *Systematophora placacantha* at 119–120 m and 95–97 m.

(2) Marma (DWR 36854) Fig. 4b

The Marma drillsite is located in the Willandra Trough 40 km south-southwest of the Leaghur borehole. Units intersected by the bore are:

0–20 m	Undifferentiated Quaternary sediments
20–48 m	Loxton–Parilla Sands
(Mologa weathering surface at 48–58 m)	
48–125 m	Upper Renmark Group

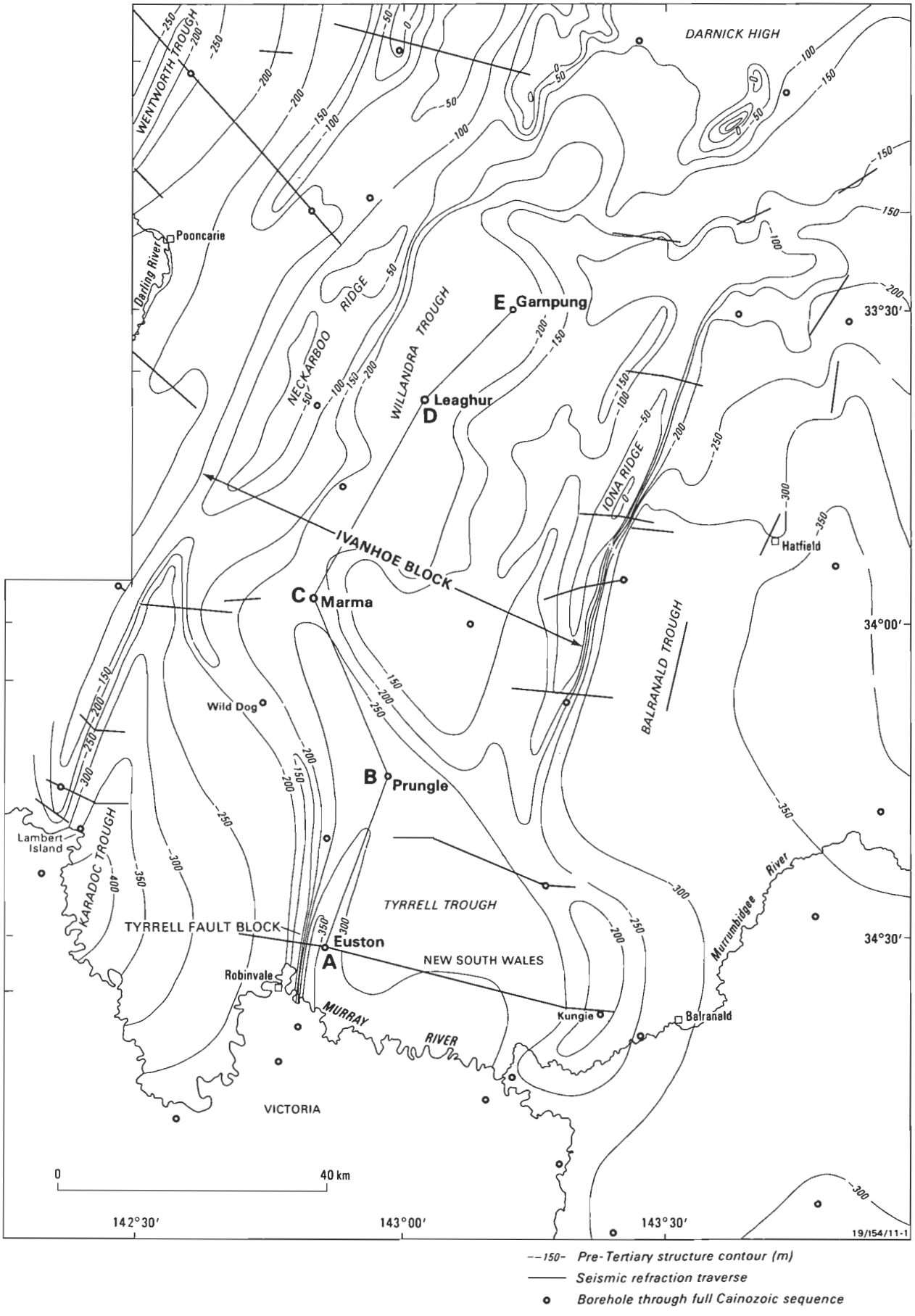

Figure 3. Structure contours of pre-Tertiary basement sediments on the Ivanhoe Block and under part of the western Riverine Plain; also showing location of cross-section in Figure 6.

125–178 m	Middle Renmark Group A
178–233 m	Geera Clay
233–267 m	Middle Renmark Group B
267–281 m	Lower Renmark Group

Samples of Geera Clay between 183–224 m yielded low to moderate numbers of calcareous nannoplankton, with one diverse assemblage at 223–224 m. Marine dinoflagellates at 63–65 m, 83–85 m, 102–103 m, 129–130 m, and 169–170 m indicate that both the Middle Renmark Group A and lower 63 m of the Upper Renmark Group are "Geera Clay equivalent". Siliceous and dolomitic/calcareous hardbands occur within the interval.

Proteacidites tuberculatus Zone (183–224 m) [T_{mg}]

The *P. tuberculatus* Zone age-determination is based on *Cyatheacidites annulatus, Acaciapollenites myriosporites,* and *Bluffopollis scabratus* at 223–224 m; *Granodiporites nebulosus* and *Foveotriletes crater* at 201–202 m; and *Tetrapollis campbellbrownii* in a *Nothofagus (Brassospora)*-dominated assemblage lacking *Canthiumidites bellus* at 183–184 m. *Apteodinium australiense* is present at 223–224 m, 201–202 m, 183–184 m, and (caved?) in many samples within the underlying Renmark Group B unit; *Pentadinium laticinctum* and *Systematophora placacantha* occur at 183–184 m.

Triporopollenites bellus Zone [129–130 m(?170 m)] [T_{mge}]

The palynoflora at 169–170 m includes *Foveotriletes crater,* which first appears in the *P. tuberculatus* Zone, and a single specimen of *Canthiumidites bellus.* The sample is the deepest in the subsurface to date in which *C. bellus* has been found in the Murray Basin. This raises the possibility that the specimen has been caved during drilling, i.e. the sample is from the *P. tuberculatus* Zone. A more reliable lower boundary for the *T. bellus* Zone is 129–130 m, based on *Glencopollis ornatus, Rugulatisporites cowrensis* and *Haloragacidites haloragoides.* The last two species are located in the sample provisionally picked as the top of the zone (63–65 m). Dinoflagellates present in the interval include *Apteodinium australiense* at 169–170 m and *Pentadinium laticinctum* at 129–130 m. Long-ranging species only occur above 130 m.

Nannoplankton and foraminifera 169–224 m

The calcareous nannoplankton *Cyclicargolithus floridanus* show that Geera Clay between 183–202 m is no younger than mid Middle Miocene, nannofossil Zone CN5a. The associated *P. tuberculatus* Zone palynofloras refine this limit to no younger than nannofossil Zone CN3 (see Fig. 5). *Zygrhablithus bijugatus* and *Cyclicargolithus abisectus* in an assemblage lacking *Dictyococcites bisectus* at 223–224 m demonstrate that the sample is basal Early Miocene, nannofossil Zone CN1a (see Okada & Bukry, 1980), consistent with the *P. tuberculatus* Zone age.

Planktonic foraminifera are sparse to absent throughout: no age-diagnostic species were recorded. Benthic foraminifera, such as *Globocassidulina subglobosa, Cibicides mediocris* and *Brizealina* sp., are sparsely distributed between 169–202 m; *Globocassidulina subglobulosa* and single specimens each of *Anomalina* spp., *Florilus* cf *japonicus, Discrobis* cf *balcombiensis* and *Glandulina* spp. occur at 223–224 m. Several of these are useful palaeoenvironmental indicators (see Discussion).

(B) Scotia Province

(1) Tandou (DWR 36838) Fig. 4c

The drillsite is close to the (southern) outflow of Lake Tandou, one of several playas above the Great Anabranch of the Darling River and lying within the most arid part of the Murray Basin. Like the Willandra System, the area is a fossil groundwater discharge zone. The bore occurs at the extreme northern limits of the Geera Clay, where the thin sand-rich nature of clay units make it difficult to separate this formation and the Renmark Group. Units intersected by the bore are:

0–27 m	Plio-Pleistocene sediments
27–62 m	Loxton–Parilla Sands
62–128 m	Upper Renmark Group
128–168 m	Middle Renmark Group A
168–235 m	Middle Renmark Group B
235–311 m	Lower Renmark Group

Marine dinoflagellates indicate that at least part of the Upper Renmark Group (81–83 m) is "Geera Clay equivalent".

Triporopollenites bellus Zone (81–83 m) [T_{mge}]

Canthiumidites bellus and *Rugulatisporites cowrensis* demonstrate that this sample is no older than *T. bellus* Zone. Late Miocene–Pliocene indicators are absent. Marine dinoflagellates are abundant and diverse: species recorded include *Areosphaeridium capricornum, Cleistosphaeridium* spp., and *Pentadinium laticinctum.* No marine dinoflagellates were found in a sample from the base of the Middle Renmark Group A unit (166–168 m).

(C) Central Western Riverine Province

(1) Euston (DWR 36723) Fig. 4d

The drillsite is on the northwestern side of Lake Benanee, a former playa now used as a reservoir for Murray River water. The bore lies superimposed on a basement depression (Tyrrell Trough) bounded on the west by the Tyrrell Fault Block and was drilled to establish whether hydraulic connection exists between this depression and the Willandra Trough. Units intersected by the bore are:

0–38 m	Quaternary sediments
38–78 m	Loxton–Parilla Sands
78–135 m	Upper Renmark Group
135–333 m	Geera Clay
333–371 m	Lower Renmark Group

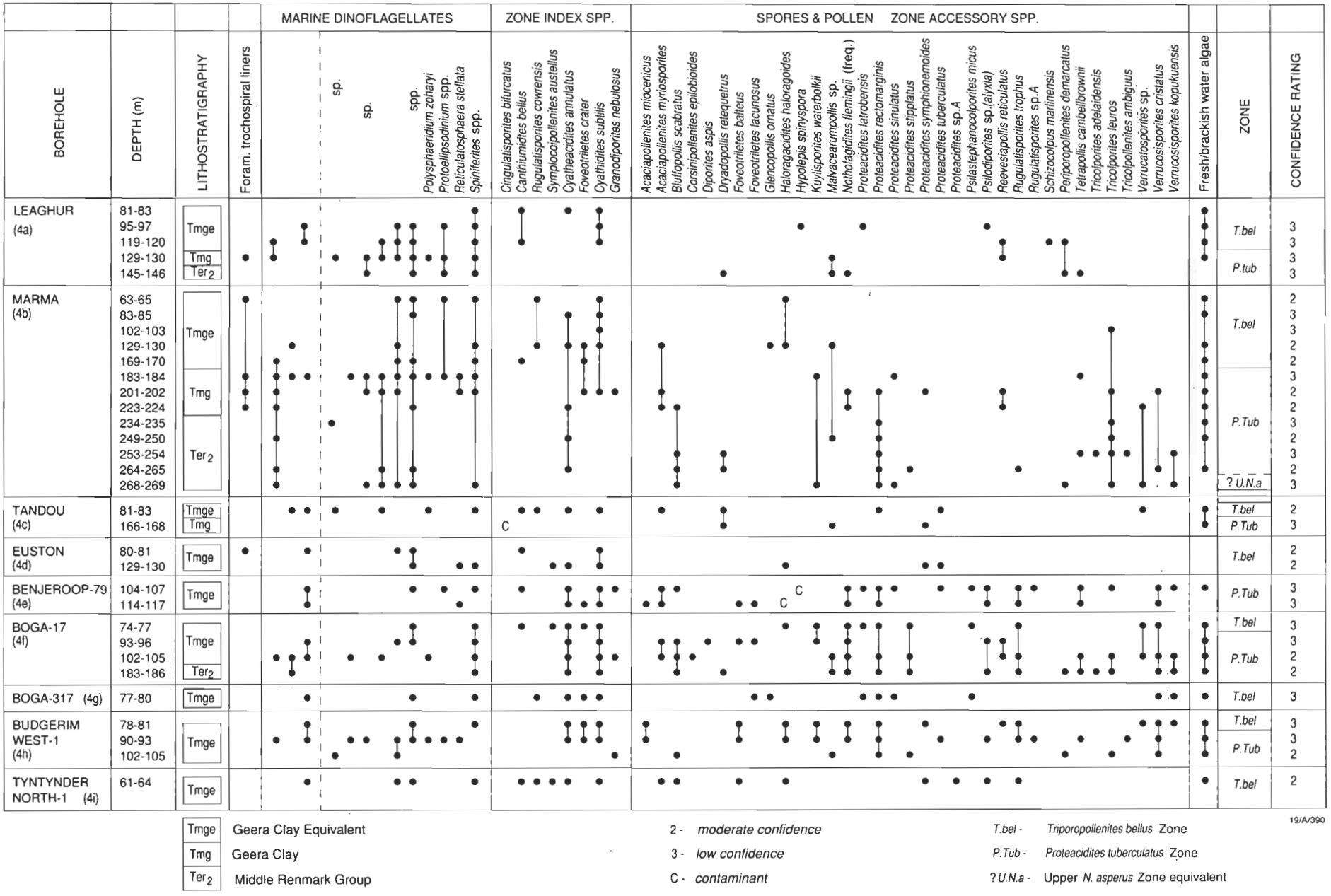

Figure 4. Stratigraphic distribution of selected spores, pollen and marine dinoflagellates.

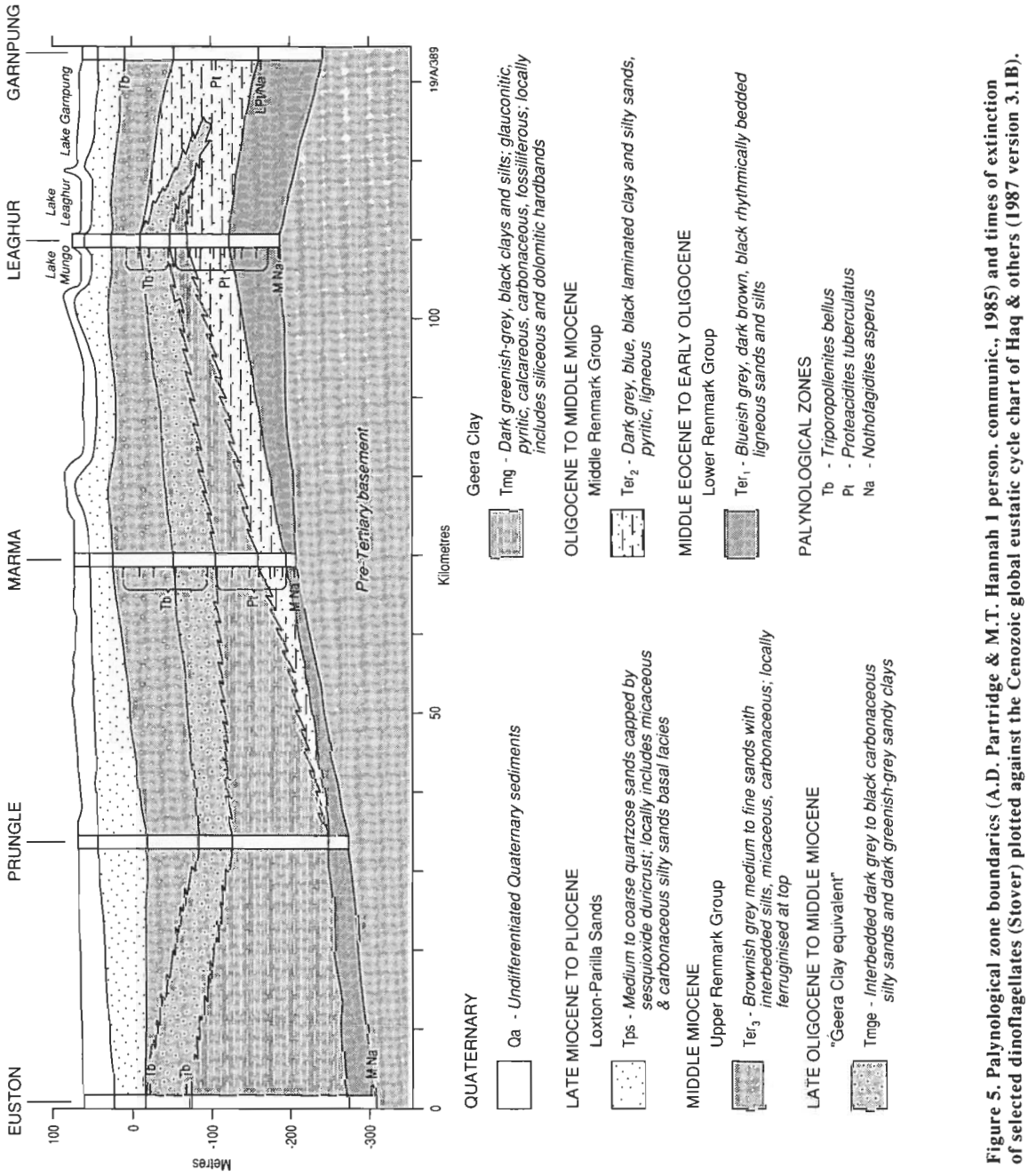

Figure 5. Palynological zone boundaries (A.D. Partridge & M.T. Hannah 1 person. communic., 1985) and times of extinction of selected dinoflagellates (Stover) plotted against the Cenozoic global eustatic cycle chart of Haq & others (1987 version 3.1B).

Marine dinoflagellates at 80–81 m and 129–130 m indicate that the interval identified as Upper Renmark Group is "Geera Clay equivalent".

Triporopollenites bellus Zone (80–130 m) [T_{mge}]

Symplocoipollenites austellus, *Rugulatisporites cowrensis*, and *Haloragacidites haloragoides* at 129–130 m and *Canthiumidites bellus* at 80–81 m confirm that this interval is no older than *T. bellus* Zone. Late Miocene–Pliocene indicator species are absent. Dinoflagellate numbers decrease upsection; *Systematophora placacantha* occurs at 80–81 m.

(D) Southwestern Riverine Province [Kerang–Nyah area]

Palynofloras recovered from boreholes in the Kerang–Nyah area differ from those in the northwestern Riverine and Scotia Provinces in two ways: the palynomorphs tend to be better preserved; and fern spores, including *Cyatheacidites annulatus*, are more frequent, presumably reflecting the close proximity of the Southeastern Highlands. Fossil and active playa lakes are present in the region.

(1) Benjeroop 79 (104–117 m) Fig. 4e

Units penetrated at this drillhole are:

0–63 m	Quaternary sediments
63–95 m	Loxton—Parilla Sands
95–187 m	Middle? Renmark Group

187–310 m	Lower Renmark Group

Marine dinoflagellates at 104–117 m indicate that part of the unit identified as Middle Renmark Group is "Geera Clay equivalent".

Proteacidites tuberculatus Zone (104–117 m) [T_{mge}]

The sample at 104–107 m yielded a "mixed" assemblage of species, including *Granodiporites nebulosus*, not known to range above the *P. tuberculatus* Zone, and *Canthiumidites bellus* (the latter being the index species of the *T. bellus* Zone). *Cyatheacidites annulatus* shows that the sample at 114–117 m is no older that *P. tuberculatus* Zone. *Systematophora placacantha* occurs in both samples.

A *P. tuberculatus* Zone age is preferred since it is more likely that cutting samples will be contaminated by caved species, in this case *Canthiumidites bellus*, in contrast to incorporated sedimentologically reworked specimens of rare species such as *Granodiporites nebulosus*.

(2) Boga 17 (74–184 m) Fig. 4f

Units penetrated at this drillhole are:

0–50 m	Plio-Pleistocene sediments
50–67 m	Loxton–Parilla Sands
67–123 m	Middle Renmark Group
123–184 m	Lower Renmark Group

Pratt (1988) identified a marginal marine unit, informally named "Boga Silt", at 81–99 m within the Middle Renmark Group. Marine dinoflagellates occur at 74–77 m, 93–96 m and 102–105 m, indicating that the "Boga Silt" is part of a thicker unit of "Geera Clay equivalent" within the Middle Renmark Group. Dinoflagellates at 183–184 m, at the base of the Lower Renmark Group, appear to be caved.

Proteacidites tuberculatus Zone (93–105 m) [T_{mge}]

Cyatheacidites annulatus, Granodiporites nebulosus, and *Bluffopollis scabratus* provide a reliable *P. tuberculatus* Zone date for the sample at 102–105 m. The sample at 93–96 m lacks *T. bellus* Zone indicators and is provisionally dated as *P. tuberculatus* Zone based on *Bluffopollis scabratus* and frequent *Cyatheacidites annulatus*. The dinoflagellate flora comprises *Systematophora placacantha* at 93–96 m and 102–105 m, and *Apteodinium australiense* and *Pentadinium laticinctum* at 105 m.

(3) Boga 317 (77–80 m) Fig. 4g

The lithostratigraphy of this borehole resembles Boga 17, except that the Renmark Group facies are thinner and the "Boga Silt" is not obviously present:

0–40 m	Plio-Pleistocene sediments
40–62 m	Loxton–Parilla Sands
62–100 m	Middle Renmark Group
100–169 m	Lower Renmark Group

Marine dinoflagellates indicate that at least part of the Middle Renmark Group (77–80 m) is "Geera Clay equivalent".

Triporopollenites bellus Zone (77–80 m) [T_{mge}]

The palynoflora, which includes *Systematophora placacantha* among others, is provisionally dated as *T. bellus* Zone based on *Cyatheacidites annulatus, Rugulatisporites cowrensis*, and *Psilatstephanocolporites micus*.

(4) Budgerim West 1 (78–105 m) Fig. 4h

Units penetrated at this drillhole are:

0–43 m	Plio-Pleistocene sediments
43–75 m	Loxton–Parilla Sands
75–148 m	Middle Renmark Group
148–200 m	Lower Renmark Group

Marine dinoflagellates indicate that the upper part of the Middle Renmark Group (78–105 m) is "Geera Clay equivalent". This interval encompasses a marginal marine unit correlated with the "Boga Silt" by Pratt (1988).

Proteacidites tuberculatus Zone (90–105 m) [T_{mge}]

The interval is provisionally dated as *P. tuberculatus* Zone, based on *Acaciapollenites myriosporites* and frequent *Cyatheacidites annulatus* at 90–93 m; and *Granodiporites nebulosus*, and frequent-to-common *Proteacidites rectomarginis*, and *Phyllocladidites mawsonii* at 102–105 m. The latter sample is no older than Upper *N. asperus* Zone based on *Granodiporites nebulosus*. *Apteodinium australiense* and *Systematophora placacantha* occur at 90–93 m.

Triporopollenites bellus Zone (78–81 m) [T_{mge}]

The sample is provisionally dated as *T. bellus* Zone based on *Proteacidites symphyonemoides* and *Perisyncolporites pokornyi*. Late Miocene–Pliocene index species are absent. The very sparse dinoflagellate flora includes *Systematophora placacantha*, among others.

(5) Tyntynder North 1 (71–74 m) Fig. 4i

Units penetrated at this drillhole are:

0–55 m	Undifferentiated Quaternary sediments/ Loxton–Parilla Sands
55–74 m	Upper/Middle Renmark Group A
74–218 m	Geera Clay
218–233 m	Middle Renmark Group B
233–296 m	Lower Renmark Group

Marine dinoflagellates at 71–74 m indicate that base of the Upper/Middle Renmark Group A is "Geera Clay equivalent".

Triporopollenites bellus Zone (71–74 m) [T_{mge}]

The sample is reliably dated as *T. bellus* Zone, based on *Cyatheacidites annulatus* (frequent), *Canthiumidites bellus*, *Rugulatisporites bellus*, and *Symplocoipollenites austellus* in an assemblage lacking Late Miocene—Pliocene indicators. *Systematophora placacantha* is one of the more frequent dinoflagellates.

Discussion and conclusions

This study underlines an intrinsic limitation in biostratigraphic research, which attempts to integrate palaeontological evidence from several different fossil groups, i.e. because the various source organisms have specific ecological preferences — thus, the various lines of evidence provide optimum information on age only in particular depositional environments. The problem becomes acute in sediments of paralic environments where there are rapid lateral changes in habitat during any given time period.

For example, in the Miocene land-locked Murray Basin, the sparse numbers and sporadic distribution of index dinoflagellate species found in the "Geera Clay equivalent" may be owing to one or more of (1) the sandy nature of the facies, thus poor preservation; (2) unfavourable local habitats, exemplified by variable salinity levels related to freshwater influx; and (3) reduced populations of species at the threshold of regional or global extinction. Macphail & Truswell (1989, p. 317) have commented on the complex controls on fossil spore and pollen assemblages in the central west Murray Basin: data presented in the present study confirm that the index species of the *P. tuberculatus* Zone, *Cyatheacidites annulatus*, is much less common in marine facies in the central west than in equivalent facies in areas of the basin adjacent to the Southeastern Highlands.

Nevertheless, the combined dinoflagellate, spore and pollen data are adequate to establish a marginal marine correlative of the Geera Clay within the Middle–Upper Renmark Group, and thus provide some indication of its lateral extent and stratigraphic relationships. In addition, foraminifera and calcareous nannoplankton (Marma) have strengthened our understanding of the depositional environment of the Geera Clay.

Palaeoenvironment

Calcareous nannoplankton and benthic formaminifera between 169–202 m in the Marma type locality show that part of the Geera Clay/basal "Geera Clay equivalent" accumulated under holomarine inner-neritic conditions. Micro-faunal evidence for any freshwater influx is absent, although freshwater algae are present — a contradiction that may be more apparent than real if it is accepted (see Macphail & Truswell, 1989, p. 321) that climates included at least one relatively dry season. The diversity and composition of the assemblage at 223–224 m is consistent with marine flooding.

Age control

The basal Early Miocene (Nannofossil Zone CN1a) age for Marma 223–224 m is not only one of the most firmly constrained dates for an interval of Geera Clay, but also for any Tertiary unit in the Murray Basin. The age agrees well with the *P. tuberculatus* Zone date based on spores and pollen, and with the correlation of this zone by A.D. Partridge & M.J. Hannah (person. communic., 1985) against the Haq & others (1987) time scale (see Fig. 5).

Based on presently available data, none of the spore or pollen species can be shown to have become extinct during the Early–Middle Miocene across the central west Murray Basin (see Macphail & Truswell, 1989), and correlation of the "Geera Clay equivalent" against the international time scale to a large degree depends on open marine/northern hemisphere records of *Apteodinium australiense*, *Pentadinium laticinctum*, and *Systematophora placacantha*. Whilst some variation exists in the published ranges (Table 1), in particular for *Pentadinium laticinctum*, there is consensus that none of the species survived into the Late Miocene. Based on range data presented in Figures 4a–4i, the following age constraints have been established:

(a) The maximum and minimum ages for "Geera Clay equivalent" samples (with *Apteodinium australiense*, and *Pentadinium laticinctum*, with *Systematophora placacantha* present or absent, **and** *T. bellus* Zone index pollen species) are late Early Miocene and late Middle Miocene respectively (Budgerim West 1, Boga 17, Boga 317, Euston, Leaghur, Marma, Tandou, Tyntynder North 1).

It must be emphasised that, with the possible exception of Tandou (see below), none of the samples in (a) are at or close to the top of the interval identified as "Geera Clay equivalent", i.e. no sample provides a precise date for the final retreat of the sea from any locality during the Oligocene–Miocene transgression, nor for the development of the Mologa Weathering Surface. For example, at the Marma drillsite, the stratigraphically highest sample found to preserve age-diagnostic dinoflagellates (129–130 m) is at least 66 m below the top of the "Geera Clay equivalent" and about 71 m below the Mologa Weathering Surface.

(b) In Tandou, a relatively thin sandy interval (12 m) separates the interbedded silts and clays with the age-diagnostic dinoflagellate *Pentadinium laticinctum* (at 81–83 m) from reddish-brown mottled and ferruginised silty clays presumed to represent the Mologa weathering surface (56–62 m). If correct, then the unconformity is unlikely to be substantially older than either late Middle Miocene (see Table 1) or younger than Late Miocene–Early Pliocene based on macrofossils in the overlying Bookpurnong beds elsewhere in the basin (Brown & Stephenson, 1991, p. 427).

(c) *Apteodinium australiense*, *Pentadinium laticinctum*, and *Systematophora placacantha* first appear in the Eocene, and occurrences in *P. tuberculatus* Zone palynofloras do little to improve the dating of "Geera Clay equivalent" samples in, for example, Benjeroop 79, Budgerim West 1, and Boga 17. Nevertheless, the combined data are valuable in that they confirm one or

more episodes of waning marine influence in the Kerang area during the Oligocene–late Early Miocene. It is possible that the drop in sealevel was due to high rates of sediment influx, leading to shoreline progradation in areas adjacent to the Southeastern Highlands (see below).

Geological correlations

The revised lithostratigraphies for the Leaghur, Marma and Euston drillsites can be tested using data from other boreholes in the Willandra and Tyrrell Troughs, i.e. Lake Garnpung (DWR 36671) and Prungle Lakes (DWR 36646) (Fig. 1). A cross-section from Lake Garnpung to Euston is shown in Figure 6. Based on this correlation we propose:

(1) The marine influence responsible for deposition of the "Geera Clay equivalent" in Leaghur and Marma may not have extended as far north as Lake Garnpung, although the three palynofloras examined by Truswell (1987) came from widely spaced lignitic sections.

(2) The boundary between the Geera Clay and "Geera Clay equivalent" in the Willandra Trough appears to coincide with the *P. tuberculatus/T. bellus* Zone boundary and may represent a local? erosional surface.

(3) The "Geera Clay equivalent" separates the Geera Clay and Upper Renmark Group at Prungle in the north of the Tyrrell Trough. No palynological data are available, but the (DWR) borelog records "calcareous fragments" in an interval of grey carbonaceous clays between 153–195 m. Farther to the south in the Tyrrell Trough, the Upper Renmark Group sediments are replaced by "Geera Clay equivalent". This differs from the Kerang area where the "Geera Clay equivalent" replaces part of the Middle Renmark Group.

On present indications, the "Geera Clay equivalent" is a time-transgressive facies 'replacing' the Geera Clay where the supply of coarse clastics was high during the Oligocene–late Early Miocene, prograding over this formation during the late Early and Middle Miocene (Fig. 2).

Relationship to global eustacy

Although there is general agreement that the stratigraphy of the Murray Basin records fluctuations in relative sealevel, the exact association remains uncertain owing to the poorly understood tectonic relationship between uplift of the Southeastern Highlands and subsidence in the basin (see Jones & Veevers, 1982). For example, there is no reason to doubt that the "Geera Clay equivalent" is part of the same depositional sequence as the Geera Clay, Winnambool and Ettrick Formations, all of which accumulated during an overall rise, then fall, in sealevel (Fig. 2). However, it is less clear whether the succession in its entirety was deposited during one transgressive–regressive cycle, predominantly within one to several cycles, or whether it is a stacked sequence reflecting a large number of geologically short-term eustatic cycles, i.e. the ca. 11 (third-order) cycles recognised by Haq & others (1987) for the Oligo-Miocene. Complicating the issue is the proposal concerning a possible tectonic origin for third-order cycles in general (see Miall, 1991).

Interestingly, it is possible to interpret the major Tertiary formations infilling the Murray Basin as *one* eustatic cycle in which: (i) the Compton Conglomerate and basal Ettrick Formation represent, repectively, the updip (incised valley fill) part of the lowstand wedge cycle and early transgressive cycle; (ii) the main body of the Ettrick Formation, Winnambool Formation and Geera Clay represent backstepping prograding deposits originated during the main transgressive cycle; and (iii) the upper units of Winnambool Formation and Geera Clay/"Geera Clay equivalent" and Upper Renmark Group terrestrial sediments reflect a basinward progradation during the late highstand cycle. This scenario, however, is highly unlikely given that the depositional sequence spans some 20 m.y. — a period encompassing three second-order eustatic cycles [Supercycles TA4, TB1, TB2, of Haq & others (1987)].

An alternative hypothesis (Jones & Veevers, 1982) that the depositional sequence reflects uplift of the Southeastern Highlands (influencing sediment supply and subsidence in the Murray Basin) is supported by the lack of evidence for major downward shifts in relative sealevel during the Oligocene–Early Miocene. However, stratigraphic evidence that the sequence comprises many system tracts, as implied by Brown (1989, p. 132), also is weak — a number of hardgrounds implying periodic sub-aerial exposure occur within the Geera Clay in Piangil West 2 in the Tyrrell Trough (Brown & Radke, 1989). Here, five lithofacies representing different marginal marine conditions suggest cyclical patterns of sediment accumulation, but changes are subtle.

Although poor resolution of palynostratigraphic units within the Geera Clay/"Geera Clay equivalent" makes it impossible to identify individual transgressive–regressive cycles, let alone relating these to global changes in relative sealevel, this study has identified two *possible* exceptions outlined in the next sections. It must be emphasised that the correlations are wholly based on local data and must be viewed as a working hypothesis to be tested when detailed regional correlations become available.

(A) Geera Clay at 223–224 m in Marma

The well-established basal early Miocene date and high diversity of calcareous nannoplankton at 223–224 m in Marma suggest a correlation with the 24.8 Ma maximum transgressive event of Haq & others (1987). To date, little attention has been paid to the nannoplankton in the Murray Basin; it is thus unknown whether the flooding event recorded in this sample can be recognised elsewhere in the basin.

(B) Mologa weathering surface in Tandou

The magnitude of the regression leading to the development of the Mologa weathering surface suggests that this event is more likely to reflect a *global* decrease in relative sealevel rather than localised events, such as either (i) a "rise" in the lowlands surrounding the basin associated with "settling" of the Southeastern Highlands (Jones & Veevers, 1982, p. 5), or (ii) intraplate stresses generated by plate margin processes (Cloetingh, 1988). If correct, then this unconformity should be correlatable with sequence boundaries in basins developed on passive margins elsewhere.

Based on age limits deduced for the Mologa weathering surface at the Tandou drillsite, only two correlations are probable in terms of the Haq & others (1987) global eustatic cycles chart. These are: (a) TB2.4/2.5 (13.8 Ma) — a sequence boundary related to a rapid drop in sealevel

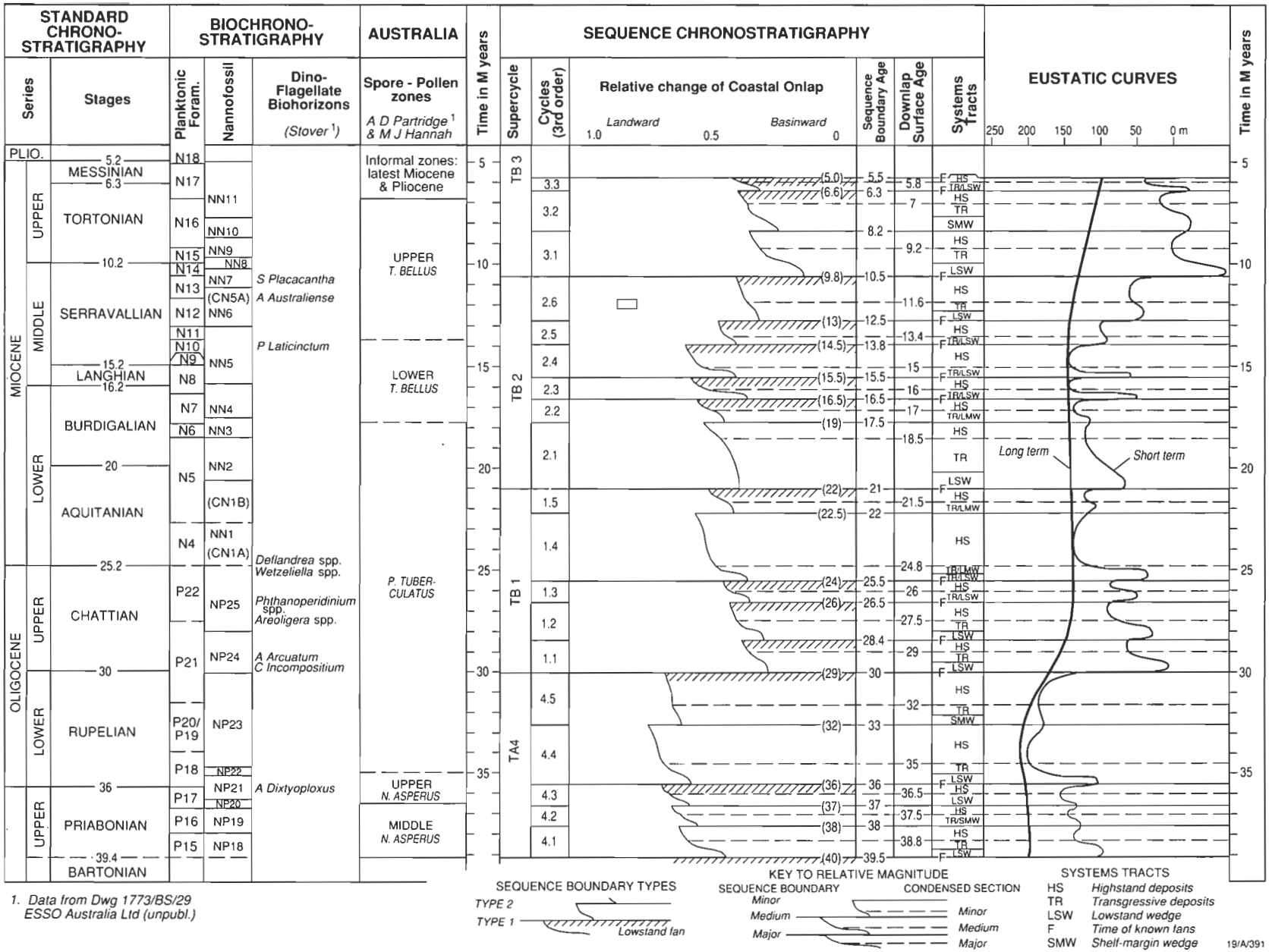

1. Data from Dwg 1773/BS/29 ESSO Australia Ltd (unpubl.)

Figure 6. Stratigraphic section through the Willandra Trough.

from its (Late Oligocene–Middle Miocene) maximum extent, coinciding with the last appearance of *Pentadinium laticinctum*; and (b) TB2.5/TB3.1 (10.5 Ma) — a sequence boundary coinciding with the last appearance of *Apteodinium australiense* and *Systematophora placacantha*, according to Stover (in Haq & others 1987). Unfortunately, dinoflagellates within the "Geera Clay equivalent" are too sporadic to allow the sequential extinction criteria proposed by Stover (Fig. 5) to be used for identifying sediments deposited between 13.8 and 10.5 Ma. At present, we can only state a preference for the 10.5 Ma correlation, based on the "magnitude" of this sequence boundary relative to that at 13.8 Ma (Fig. 5).

Acknowledgments

We are grateful to Clinton Foster for his assistance in preparing photomicrographs and to Alan Partridge, Neil Marshall and Helene Martin for their thorough reviews of an earlier version of this paper. We thank Karl Wolf (AGSO editor) for his helpfull comments.

References

Brown, C.M., 1985 — Murray Basin, southeastern Australia: stratigraphy and resource potential–a synopsis. *Bureau of Mineral Resources, Australia, Report* 264.

Brown, C.M., 1989 — Structural and stratigraphic framework of groundwater occurrence and surface discharge in the Murray Basin, southeastern Australia. *BMR Journal of Australian Geology and Geophysics*, 11 2/3, 127–146.

Brown, C.M. & Radke, B.M., 1989 — Stratigraphy and sedimentology of mid-Tertiary permeability barriers in the subsurface of the Murray Basin, southeastern Australia. *BMR Journal of Australian Geology and Geophysics*, 11 2/3, 367–385.

Brown, C.M. & Stephenson, A.E., 1991 — Geology of the Murray Basin. *BMR Journal of Australian Geology and Geophysics*, 235, 1–430.

Cloetingh, S., 1988 — Intraplate stress; a new element in basin analysis. *In* Kleinspehn, K.C. & Paola, C. (editors)–New Perspectives in Basin Analysis. *Springer-Verlag, Berlin, New York*, 205–230.

Dudgeon, M.J., 1983 — Eocene pollen of probable proteaceous affinity in the Yamba Basin, central Queensland. *In* Roberts, J. & Jell, P.A. (editors)–Dorothy Hill Jubilee Memoir. *Association of Australasian Palaeontologists, Memoir* 1, 339–362.

Evans, W.R. & Kellett, J.R., 1989 — The hydrogeology of the Murray Basin, southeastern Australia. *BMR Journal of Australian Geology and Geophysics*, 11 2/3, 147–166.

Haq, B.U., Hardenbol, J. & Vail, P.R., 1987 — Mesozoic and Cenozoic chronostratigraphy and cycles of sealevel change. *Science*, 235, 1156–1166.

Hekel, H., 1972 — Pollen and spore assemblages from Queensland Tertiary sediments. *Geological Survey of Queensland Publication*, 355, 1–33.

Jones, J.G. & Veevers, J.J., 1982 — A Cainozoic history of Australia's Southeast Highlands. *Journal Geological Society of Australia*, 29, 1–12.

Kellett, J.R., 1989 — The Ivanhoe Block—its structure, hydrogeology and effect on groundwaters of the Riverine Plain of New South Wales. *BMR Journal of Australia Geology and Geophysics*, 11 2/3, 333–354.

Lindsay, J.M., 1983 — Oligo-Miocene transgressive events in Geera Clay, Oakvale-1, northern Murray Basin. *Geological Survey of South Australia, Quarterly Geological Notes*, 85, 5–12.

Macphail, M.K., Colhoun, E.A., Kiernan, K. & Hannan, D., 1993 — Glacial climates in the Antarctic region during the late Palaeogene: evidence from northwest Tasmania, Australia. *Geology* (in press).

Macphail, M.K. & Truswell, E.M., 1989 — Palynostratigraphy of the central west Murray Basin. *BMR Journal of Australian Geology and Geophysics*, 11 2/3, 301–331.

Martin, H.A., 1973 — The palynology of some Tertiary and Pleistocene deposits, Lachlan River Valley, New South Wales. *Australian Journal of Botany, Supplementary Series* 6, 1–57.

Martin, H.A., 1991 — Dinoflagellate and spore pollen biostratigraphy of the S.A.D.M.E. MC63 bore, western Murray Basin. *Alcheringa*, 15, 107–144.

Miall, A., 1991 — Stratigraphic sequences and their chronostratigraphic correlation. *Journal of Sedimentary Petrology*, 61, 497–505.

Mildenhall, D.S. & Harris, W.F., 1971 — Status of *Haloragacidites* (al. *Triorites*) *harrisii* (Couper) Harris comb. nov. and *Haloragacidites trioratus* Couper, 1953. *New Zealand Journal of Botany*, 9, 297–306.

Mildenhall, D.S. & Pocknall, D.T. 1989 — Miocene-Pleistocene spores and pollen from Central Otago, South Island, New Zealand. *New Zealand Geological Survey Palaeontological Bulletin*, 59, 1–128.

Milne, L.A., 1988 — Palynology of a late Eocene lignite sequence from the western margin of the Eucla Basin, Western Australia. *In* Jell, P.A. & Playford, G.A. (editors)–Palynological and Palaeobotanical Studies in Honour of Basin E. Balme. *Association of Australasian Palaeontologists, Memoir* 5, 285–310.

Okada, H. & Bukry, D., 1980 — Supplementary modification and introduction of code numbers to the low-latitude coccolith zonation (Bukry, 1973; 1975). *Marine Micropalaeontology*, 5, 321–325.

Powell, A.J., 1992 — Dinoflagellate cysts of the Tertiary System. *In* Powell, A.J. (editor)–A stratigraphic index of dinoflagellate cysts. *British Micropalaeontological Society Publications*, Chapman & Hall, 155–229.

Pratt, M., 1988 — Hydrogeological assessment of the Loddon and Avoca Plains. *Victorian Department of Industry, Technology and Resources*, unpublished report.

Radke, B.M., 1987 — Sedimentology and diagenesis of sediments encountered by Vic. D.M. Piangil West 1 Murray Basin, southeastern Australia. *Bureau of Mineral Resources, Australia, Record 1987/25.*

Stover, L.E., & Partridge, A.D., 1973 — Tertiary and Late Cretaceous spores and pollen from the Gippsland Basin, southeastern Australia. *Royal Society of Victoria, Proceedings*, 85(2), 237–286.

Truswell, E.M., 1987 — Reconnaissance palynology of selected boreholes in the western Murray Basin, New South Wales. *Bureau of Mineral Resources, Australia, Record 1987/24.*

Truswell, E.M., Sluiter, I.R. & Harris, W.K., 1985 — Palynology of the Oligocene-Miocene sequence in the Oakvale-1 corehole, western Murray Basin, South Australia. *BMR Journal of Australian Geology and Geophysics*, 9, 267–295.

Vail, P.R., Hardenbol, J. & Todd, R.G., 1984 — Jurassic unconformities, chronostratigraphy and sea-level changes from seismic stratigraphy and biostratigraphy. *In* Interregional Unconformities and Hydrocarbon Accumulation. *American Association Petroleum Geologists, Memoir* 36, 129–144.

Williams, G.L. & Bujak, J.P., 1985 — Mesozoic and Cenozoic dinoflagellates. *In* Bolli, H.M., Saunder, J.B.

& Perch-Nielsen, K. (editors)–Plankton Stratigraphy Volume 2, *Cambridge University Press*, 847–964.

Appendix 1. Taxonomic, phytogeographic and biostratigraphic notes on selected species

M.K. Macphail & E.M. Truswell[2]

Previous studies (Martin, 1973; Truswell & others, 1985; Truswell, 1987; Macphail & Truswell, 1989) have shown that the Murray Basin preserves an exceedingly diverse pollen flora. Whilst the overwhelming majority of species are found elsewhere, a few of the records represent a significant extension in the known time distribution or geographic range.

In this section, we describe one new species and provide brief notes on another three taxa for which the Murray Basin records extend existing knowledge.

Angiosperm pollen

Genus *Tetrapollis* Pflug 1953

Type species *Tetrapollis validus* (Pflug) Pflug 1953

Tetrapollis campbellbrownii n. sp. (pl. 1, figs 1–7)

1989 *Tetrapollis* sp. Macphail & Truswell, p.330, fig. 11L)

Description. Pollen isopolar, strongly oblate, amb quadrangular to irregular polygonal, sides between apertures straight to convex. Tetraporate, rarely triporate or pentaporate. Exine 1.0 to 1.5 microns thick, clearly differentiated into two layers approximately equal in thickness, columellae indistinct; nexine ca. 0.8 microns and thickening around apertures, nexinous annuli 4 microns in diameter, often showing channelling on inner surface of nexine, reduced to granules or absent; sexine ca. 0.6 microns thick, sometimes crumpled, surface weakly scabrate, breaking down around apertures to produce annuli. Pores equatorial, aspidate, 1.2–2.0 microns in diameter, pore margins concave in polar view. Dimensions 16 (21) 28 microns, 22 specimens measured.

Holotype. Hay 3 at 268–269 m. Specimen within double ring inscribed on coverslip: England finder coordinate H 55.0: *Proteacidites tuberculatus* Zone, Late Oligocene–late Early Miocene.

Paratypes. J43.1 and J53.1 (triporate), K61.0 (tetraporate, pentaporate) and N31.3 (tetraporate).

Type locality. Hay 3 (Maude DWR 36797) borehole, grid reference 6179531N 802927E, at 153–154 m; *Proteacidites tuberculatus* Zone, Late Oligocene–late Early Miocene.

Stratigraphic range. Middle *Nothofagidites asperus* Zone to *Triporopollenites bellus* Zone inclusive, Late Eocene–Middle Miocene (Murray Basin, Otway Basin).

Etymology. Named after Mr. Campbell Brown, senior research scientist in Bureau of Mineral Resources (now AGSO) who conducted the first integrated surface and subsurface geological survey of the entire Murray Basin; tragically killed during field work in the Darling Basin, 2 June 1991.

Comments. *Tetrapollis campbellbrownii* differs from *Polyorificites oblatus* Martin 1973 (jnr. synonym *Helciporites astrus* Stover & Partridge, 1973) in having an angular rather than sub-circular amb as well as narrower and few pores. The species may superficially resemble tri- and tetraporate specimens within the *Casuarinidites cainozoicus — Haloragacidites harrisii* complex (pl. 1, fig. 8), but is flat-lenticular and lacks the micro-apiculate sculpture of the latter (see Mildenhall & Harris, 1971; Mildenhall & Pocknall, 1989).

The species is consistently present in Oligo-Miocene sediments from the eastern (Riverine) and northwestern (Scotia) groundwater Provinces of the Murray Basin. The few records from the southwestern (Limestone) province are restricted to the Late Oligocene–late Early Miocene, *Proteacidites tuberculatus* Zone. Isolated specimens are present in (onshore) southeastern Otway Basin. One specimen, possible reworked, occurs in Pliocene calcarenites in the (offshore) Gippsland Basin.

Botanical affinity. Unknown Angiosperm (*Haloragaceae*?).

Genus *Proteacidites* Cookson ex Couper 1953 emend Martin & Harris 1974.

Type species *Proteacidites adenanthoides* Cookson 1950 subsequent designation by Couper, 1953.

Proteacidites sinulatus Dudgeon 1983 (pl. 1, Figs 9–11).

This species was first described from specimens recovered from Eocene sediments in the Yamba Basin, central Queensland by Dudgeon (1983). Since then, it has been recorded in Late Eocene sediments in the western Eucla Basin of Western Australia (Milne, 1988). The Murray Basin records link these widely separated regions and extend the known distribution of this uncommon species into the late Early–Late Miocene *Triporopollenites bellus* Zone and younger sediments.

The species resembles *Proteacidites reflexus* Stover & Partridge, 1973 and *P. bremerensis* Stover & Partridge, 1982, in having strongly thickened nexine in the interapertual areas, but is strongly anisopolar and, at 24–34 microns diameter, is about half the size of these species. Like *Proteacidites reflexus*, the exine thins markedly around the apertures in *P. sinulatus*.

Genus *Striasyncolpites* Germeraad, Hopping & Muller, 1968

Type species *Striasyncolpites zwaardi* Germeraad, Hopping & Muller, 1968

Striasyncolpites laxus Mildenhall & Pocknall, 1989 (pl. 1, Figs 12–15)

This species, first described from Early to Middle Miocene sediments in New Zealand, has been recorded as early as Early Oligocene in Tasmania, and possibly as recently as Middle Miocene in the onshore Gippsland Basin. The Murray Basin records range from *Proteacidites tuberculatus* to *Triporopollenites bellus* Zones.

[2] Australian Geological Survey Organisation, GPO Box 378, Canberra ACT 2601

The type closely resembles modern Menyanthaceae pollen, although the striate sculpture is more variable than pollen of, e.g. the three taxa present in Tasmania, *Liparophyllum gunnii* Hook f., *Nymphoides crenata* (F. Muell.) Kuntze or *Villarsia exaltata* (F. Muell.) Kuntze. *Liparophyllum gunnii* is restricted to upper sub-alpine lakes and *Striasyncolpites laxus* occurs in the earliest known Tertiary palynoflora with cold climate associations in Tasmania (Macphail & others, 1993).

Genus *Tricolpites* Cookson 1947 ex Couper 1953

Type species *Tricolpites reticulatus* Cookson 1947 (subsequent designation by Couper, 1953).

Tricolpites trioblatus Mildenhall & Pocknall 1989 (pl.1, Figs 17–20)

This species, which was described from Late Miocene to Early Pliocene sediments in New Zealand, occurs sporadically from Late Eocene, Middle *Nothofagidites asperus* Zone to at least the late Early–Late Miocene, *Triporopollenites bellus* Zone in the Murray Basin. It is probable that Australian Tertiary pollen referred to the New Zealand Paleocene species *Tricolpites aspermarginus* McIntyre 1968, e.g. by Hekel (1972), are *T. trioblatus*.

The type resembles pollen of the modern Scrophulariaceae genera *Euphrasia* and *Hebe*.

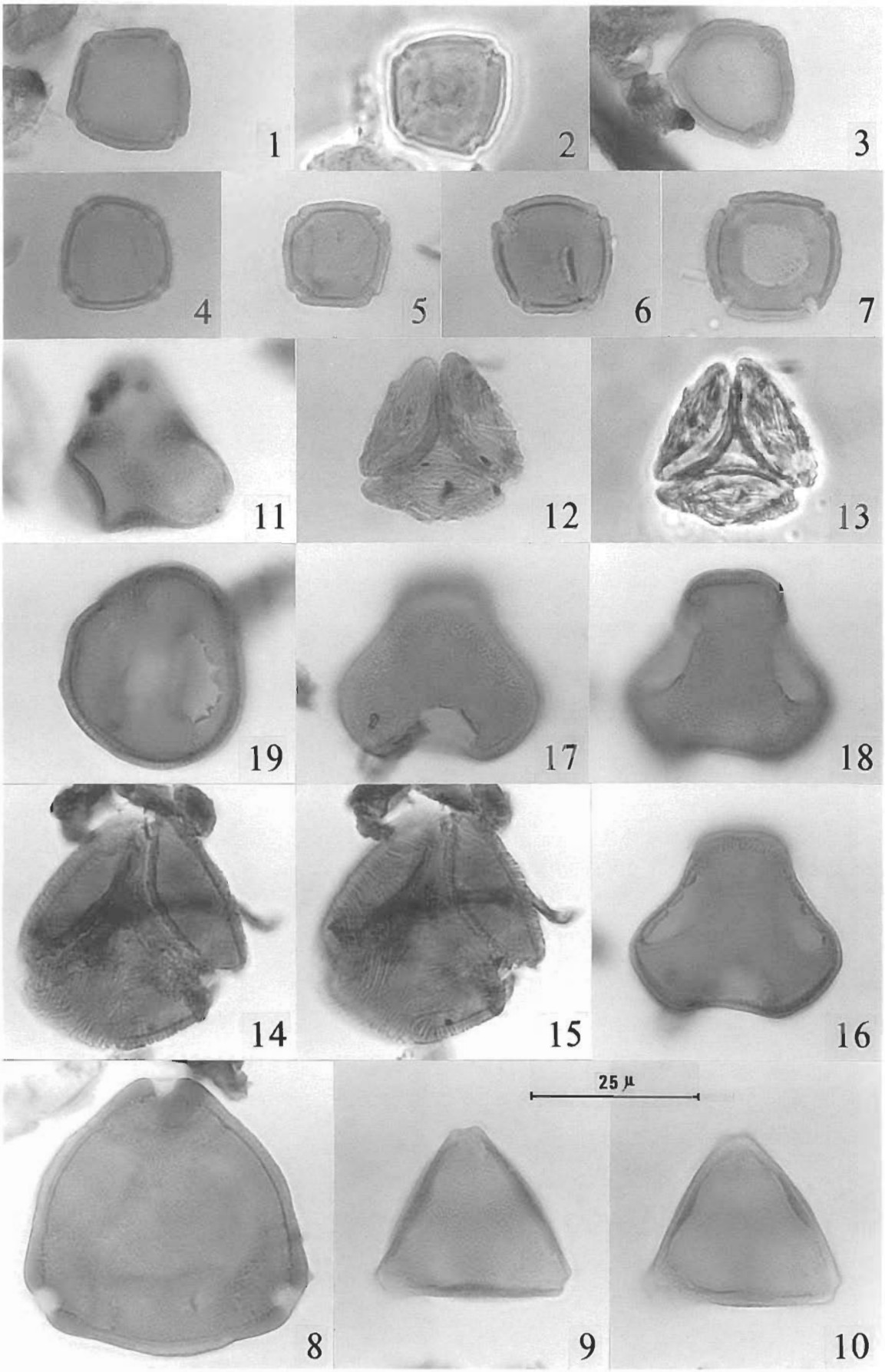
1
2
3
4
5
6
7
11
12
13
19
17
18
14
15
16
25 μ
8
9
10

AGSO Journal of Australian Geology & Geophysics, 14, 65–76

Revised stratigraphy of the Ordovician (Late Tremadoc–Arenig) Prices Creek Group and Devonian Poulton Formation, Lennard Shelf, Canning Basin, Western Australia

Robert S. Nicoll[1], John R. Laurie[1] & Michael T. Roche[2]

The Early Ordovician (late Tremadoc to Arenig) Prices Creek Group outcrops only on the northern margin of the Canning Basin in a small area centred on Prices Creek, 60 km southeast of Fitzroy Crossing. Recent hydrocarbon and mineral exploration has shown that the Prices Creek Group, previously defined as consisting of a lower Emanuel Formation and an upper Gap Creek Formation can now be subdivided into four formations. The new formations comprise a basal transgressive sandstone unit, here named the Kunian Sandstone, which is overlain by a dolomitic carbonate-dominated unit, here named the Kudata Dolomite. The Kunian Sandstone does not outcrop, but the Kudata Dolomite, which was formerly included in the Emanuel Formation, is exposed at the base of the type section of that unit along Emanuel Creek. The Kudata Dolomite is conformably overlain by the revised Emanuel Formation.

The Gap Creek Formation is informally divided into a lower fossil-rich dolomitic unit and an upper fossil poor unit that shows evidence of a hypersaline depositional regime near the top. The Poulton Formation is recognised in outcrop, paraconformably above the Gap Creek Formation and unconformably below the Pillara Formation.

The sandstone–dolomite–shale sequence of the lower Prices Creek Group has some economic potential, both for hydrocarbons and minerals. Oil shows are common in shallow wells drilled into the Emanuel Formation and both live oil and bitumen have been found in cores from the Kudata Dolomite. The oil is probably sourced from the Emanuel Formation which also serves as an effective regional seal. Traces of lead and zinc have been found in the Kudata Dolomite, but the depth of the unit below the surface may reduce the economic value of any significant mineralisation that might be found.

Introduction

Ordovician sediments are widely distributed in the Canning Basin (Forman & Wales, 1981), but outcrop is limited to a small area in the vicinity of Prices Creek, 60 km southeast of Fitzroy Crossing and to a number of small sandstone exposures, known as the Carranya Beds, located south of Halls Creek (Fig. 1).

Re-examination of outcrop sections, mineral exploration core holes and petroleum exploration wells on the shelf and shelf margin has provided the essential data for a revision of the lithostratigraphy of these Ordovician sediments on the eastern end of the Lennard Shelf. In general, these revisions of the stratigraphy formalise the observations of Henderson (1963), and they form the basis of a lithological correlation of the Lennard Shelf sediments to the classic Ordovician Nambeet–Willara–Goldwyer–Nita Formations succession in the subsurface Canning Basin.

Previous work

The Ordovician age of rocks in the Prices Creek area on the northern margin of the Canning Basin was first recognised from fossils found in 1949 by D.J. Guppy and A.W. Lindner (Guppy & Öpik, 1950) during the mapping of rocks previously considered to be of Devonian age. These rocks were the first Ordovician sediments to be recognised in the basin and still represent the largest exposure of Ordovician age sediments. The discovery was reported by Guppy & Öpik (1950) when they established the Prices Creek Group, which was subdivided into a lower Emanuel Limestone and an upper Gap Creek Dolomite. The type section of the Emanuel Limestone was measured along Emanuel Creek (Guppy & Öpik, 1950, p. 205), just south of the Emanuel Range (Fig. 2), and was reported to be 509 m (1670 feet) thick.

The name of the Emanuel Limestone was changed to the Emanuel Formation by Guppy & others (1958, p. 17). The type section was re-measured at 595 m (1950 feet) in outcrop and extended by an additional 56 m (182 feet) from sediments intersected in a shallow drill hole associated with a seismic survey (Smith, 1955; Guppy & others, 1958, p. 18). The exact location of the 1955 BMR Test Drill Hole (Guppy & other, 1958, p. 87) is not known, but the thickness of the 'crystalline brown limestone' at the base of the outcrop section combined with an additional 22 m (72 feet) from the top of the test hole gives a thickness of 95 m (312 feet) for this dolomitic interval. The basal part of the section in the test hole consisted of 34 m (110 feet) of sandstone. It is not clear from their text if Guppy & others (1958, p. 18) considered this sandstone as part of the Emanuel Formation or as part of a separate, but undefined, stratigraphic unit.

Veevers & Wells (1961) briefly discussed the Prices Creek Group. They placed the sandy dolomite and arkosic sediments found in the BMR 3 Prices Creek (now renamed Noonkanbah No. 3) drillhole in the base of the Emanuel Formation.

Henderson (1963) further described the sequence in this stratigraphic drillhole, located adjacent to Emanuel Creek and near the base of the Emanuel Formation type section (Fig. 2). He interpreted the sequence as consisting of an upper 10.6 m (35 feet) of sandy limestone belonging to the Emanuel Formation overlying an 88 m (290 feet) interval of sandy dolarenite and dolomitic shale with basal quartz sandstone which, in turn, overlies 82 m (268 feet) of arkose forming the base of the sedimentary sequence. The hole bottomed in Precambrian tuffs and metamorphics. Henderson (1963, p. 49) considered both the dolarenite and arkose units as separate formations, distinct from the Emanuel Formation, but because they were known only from the single drillhole they were not formally named.

Exposures in the vicinity of Gap Creek and north of the Emanuel type section (Fig. 2) were named the Gap Creek Formation by Guppy and Öpik (1950). The type section

1 Australian Geological Survey Organisation, GPO Box 378, Canberra ACT 2601

2 Exploration Department, BHP–Utah, 3 Plain Street, East Perth, W.A. 6004

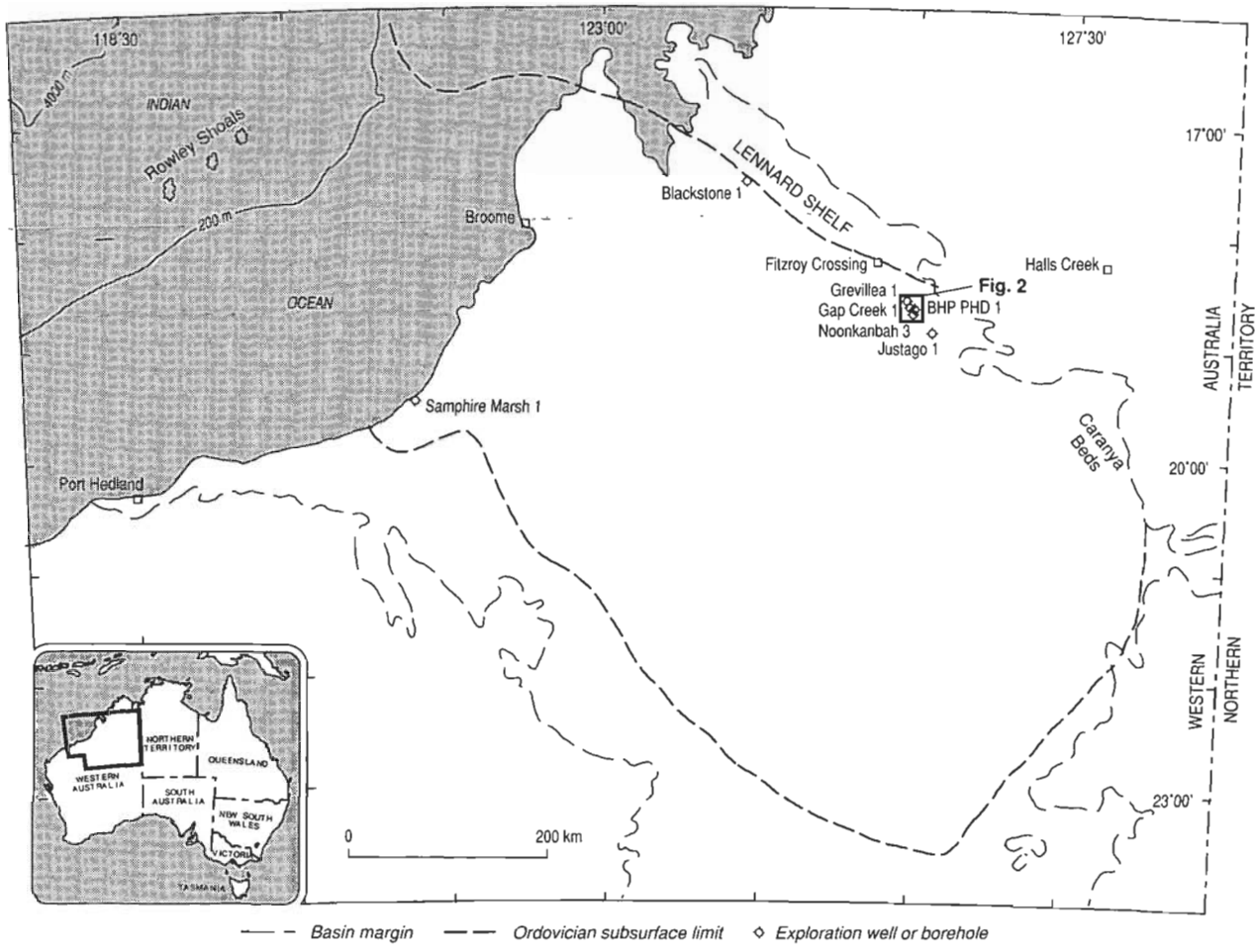

Figure 1. Locality map showing location of the Canning Basin (inset), the subsurface distribution of Ordovician sediments in the basin, and the location of wells discussed in the text. Caranya Beds' outcrop area indicated south of Halls Creek. For Prices Creek outcrop area, see Fig. 2.

was detailed by Guppy & others (1958) and a lower Trenton (Late Ordovician) age was indicated for the unit. McTavish (1973) included the lower part of the Gap Creek Formation (*sensu* herein) in the top of the Emanuel Formation. The lithologic analysis of the formation in this study indicated that the boundary between the Emanuel and Gap Creek Formations lies well below the base of section RM 10.

A thick Ordovician section on the eastern part of the Lennard Shelf has been intersected in three petroleum exploration wells (Fig. 1) near the shelf margin and in numerous shallow mineral exploration coreholes in the Prices Creek area (Fig. 2). These data considerably increase knowledge of the extent and nature of Ordovician sedimentation in this part of the basin beyond that of the restricted exposures. The penetration of both the dolomitic and sandstone units in a number of recent petroleum and mineral exploration holes (Fig. 4) demonstrates that both of these units have regional distribution and should be recognised as formal stratigraphic units.

Revised Lennard Shelf Stratigraphy

Kunian Sandstone (new name)

The Kunian Sandstone (Roche, 1990) is the basal transgressive Ordovician sandstone on the eastern portion of the Lennard Shelf (Fig. 3). The type section, 82 m thick, is in BMR Noonkanbah No. 3 drillhole (Henderson, 1963) from where cores 4–6 were supposedly taken in this unit. These were described as consisting of "medium hard pale grey and pale brown very fine to coarse-grained arkose" with glauconite and pyrite (Henderson, 1963, pl. 3). We have examined cores 4–6, and because they are vastly different from the original descriptions of the drillsite geologist, we can only assume that they have become confused with cores from other drillholes (see Appendix). We therefore assume the original descriptions to be essentially accurate because they conform with observations made in nearby core holes. Examination of several BHP coreholes indicates that the unit is not so much an arkose but a quartz–lithic arenite with occasional glauconite-rich units throughout.

The Kunian Sandstone has been intersected in the petroleum exploration wells Grevillea No.1 (90.5 m thick), Gap Creek No. 1 (77 m), Justago No. 1 (in excess of 100 m), and in several BHP stratigraphic coreholes (Fig. 4), the most complete section of which is to be found in BHP's diamond drillhole PHD 1 where it is 112 m thick (Handley, 1991). This latter hole was drilled in 1990 by BHP Minerals Ltd as part of their Lennard Shelf base metal exploration program.

The name of the unit is taken from Kunian Gap which passes through the Emanuel Range north of the type locality.

Kudata Dolomite (new name)

The Kudata Dolomite (Roche, 1990; Fig. 3 herein) is named for Kudata Gap, a water gap through the Emanuel Range (west of Kunian Gap) located about 6 km north of the type section. The type section is located along Emanuel Creek and in the adjacent BMR 3 Prices Creek (= Noonkanbah No. 3) drillhole where the unit is 88 m thick and represented by cores 1–3. In outcrop, the formation consists of brown to brownish-grey recrystallised dolomite and dolomitic limestone which is medium to thick bedded in the lower part, becoming silty to shaly with thin dolomite beds in the upper part.

Unlike those purported to be from the underlying unit, the cores (1–3, see Appendix) identified as coming from BMR Noonkanbah No. 3, agree more closely with the description of those cores and cuttings in the drilling report (Henderson & others, 1963, pl. 3). We therefore assume that they are probably correctly identified.

The Kudata Dolomite has also been intersected in the petroleum exploration wells Grevillea No. 1 (69 m thick), Gap Creek No.1 (84 m), Justago No.1 (160.5 m), and in several BHP stratigraphic coreholes, the most complete section of which is to be found in BHP's drillhole PHD 1 where it is 85 m thick.

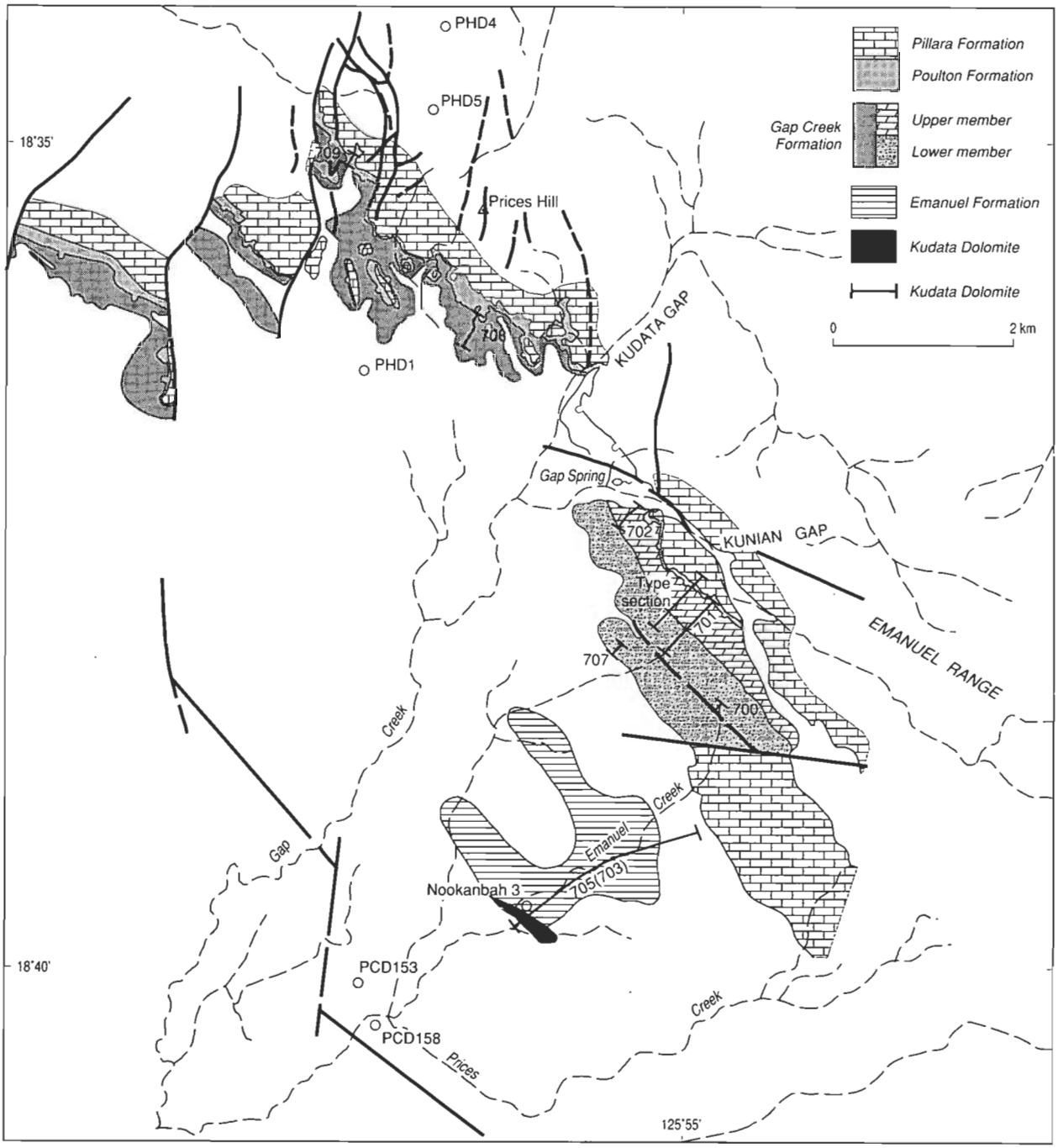

Figure 2. Geological map of the Prices Creek outcrop area showing the location of wells and outcrop section (see locality information).

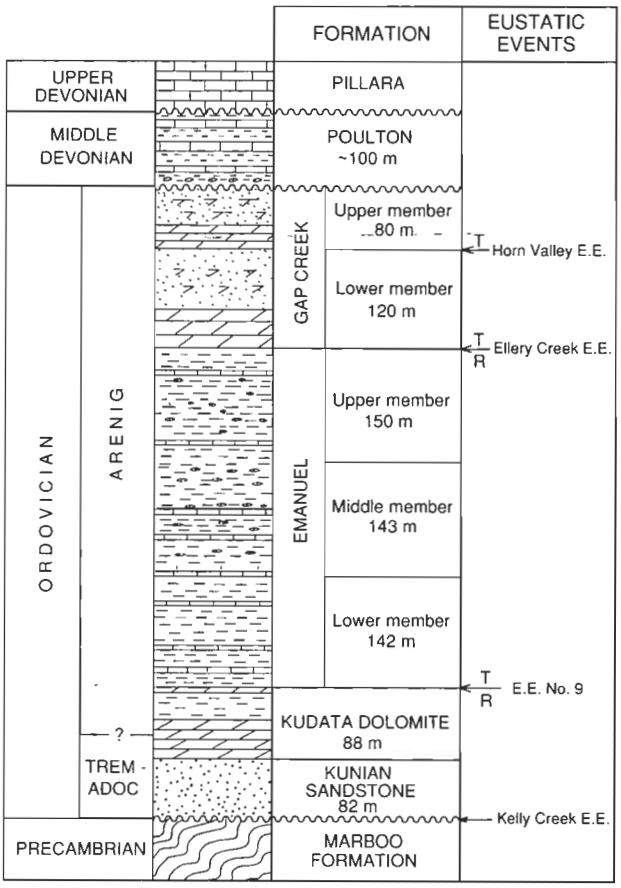

Figure 3. Stratigraphic column showing lithostratigraphic units of the Prices Creek area and the position of the eustatic events. The vertical scale is based on thicknesses of measured sections. Transgressive (T) and regressive (R) trends are indicated.

Emanuel Formation (revised)

The Emanuel Formation (Fig. 3) is redefined to exclude the basal Kunian Sandstone and the Kudata Dolomite that were included, in whole or in part, in the formation by both Guppy & others (1958) and Veevers & Wells (1961). The type section of the Emanuel Formation is located in and alongside Emanuel Creek, as originally measured by Guppy & Öpik (1950). In this study, the base of the Emanuel Formation is placed at the top of the highest dolomitic limestone of the Kudata Dolomite. In the type section, the Emanuel Formation can be subdivided into three informal members:

- The basal member is 142 m thick and very poorly exposed with only a few intervals of shale and siltstone and a few thin limestone beds outcropping in the section. The first significant fossiliferous exposure is 23 m above the base of the formation.

- The middle member of the Emanuel Formation is 143 m thick and is distinguished from the underlying unit by the relatively continuous exposure, the abundance of bedded limestone or beds of large (>100 mm) diameter carbonate nodules, interbedded with siltstone and shale. This middle member of the formation is abundantly fossiliferous.

- The upper member of the Emanuel Formation is in excess of 150 m thick and extends upward to the base of the Gap Creek Formation. This member is not well exposed and is characterised by shale, siltstone and small diameter limestone nodules. In the upper part of this member, the abundance of nodular limestone decreases and exposure becomes poorer. The upper part of the formation consists of shale and siltstone with only occasional beds of nodular limestone. On the measured section the uppermost exposure of the Emanuel Formation consists of 1.5 m of shale below a thick caliche deposit with exposures of Devonian limestone a short distance upstream.

The transition to the dolomitic carbonates of the overlying Gap Creek Formation is not exposed, but can be seen in BHP's diamond drillholes PHD 2 and PHD 3. Here, it is an apparently transitional contact, with the degree of dolomitisation determining the position of the actual contact. McTavish (1973) placed the upper boundary of the Emanuel Formation at the base of a thick dolomite bed near the crest of a hogback ridge. However, our interpretation of the exposure is that the entire McTavish RM 10 section should be placed in the Gap Creek Formation.

The Emanuel Formation has been intersected in the petroleum exploration wells Grevillea No.1 (234 m thick), Gap Creek No. 1 (204 m), Justago No. 1 (315 m), and in several BHP stratigraphic coreholes, the best section of which is to be found in BHP PHD 1 where an incomplete section is 405 m thick.

Gap Creek Formation

The Gap Creek Formation (Fig. 3) conformably overlies the Emanuel Formation and the two units are apparently in a transitional relationship. The Gap Creek Formation is a silty to sandy calcarenite and siltstone that has been secondarily dolomitised. The base of the Gap Creek Formation is taken at the incoming of a significant amount of dolomitic siltstone replacing the predominant shale of the upper part of the Emanuel Formation.

The type section of the Gap Creek Formation (Fig. 2) is east of Gap Creek and about 1.5 km southeast of Gap Spring (Guppy & Öpik, 1950). The type section corresponds to a series of traverse section conodont samples (WCB 701) collected for this study. An additional section, WCB 708, was measured by BMR 2.5 km west of Gap Spring. This section starts low in the Gap Creek Formation, but above the Emanuel Formation which is not exposed at the locality. The top of section WCB 708 is in the Poulton Formation. A third section, WCB 707, was measured 0.5 km west of the type section and is from near the stratigraphic base of the formation.

The Gap Creek Formation can be divided into two informal members in the exposures adjacent to Gap Creek. The lower 120 m of the formation consist of dolomitic siltstones and sandstones, and dolomites. A rich macrofossil fauna can be found in this lower part of the formation, but the faunal diversity is low when compared with the underlying Emanuel Formation. Principal components of this fauna include trilobites (*Lycophron sp.*), brachiopods (*Spanodonta hoskingiae*), gastropods (*Teiichispira* sp.), and conodonts (*Oepikodus communis, Bergstroemognathus hubeiensis*).

The upper member of the formation is about 80 m thick and consists of similar rock types but has a greater percentage of siltstone. Fossils are rare in the upper member and

nodules in the upper half of the unit are pseudomorphs after evaporitic minerals, indicating probable elevated salinity at the time of deposition. Large macluritacean gastropods are found in the upper 20 m of formation in section WCB 708.

The Gap Creek Formation has been intersected in the petroleum exploration wells Grevillea No.1 (212 m thick), Gap Creek No. 1 (114.5 m), Justago No. 1 (297.5 m), and in several BHP stratigraphic coreholes, the most complete section of which is to be found in BHP PHD 2 where an incomplete section is 93 m thick.

Poulton Formation

The Gap Creek Formation is paraconformably overlain by a previously unnamed stratigraphic unit that is here correlated with the Poulton Formation (Playford & others, 1975) found in the subsurface of the western part of the Lennard Shelf (Fig. 3). The type section of the Poulton

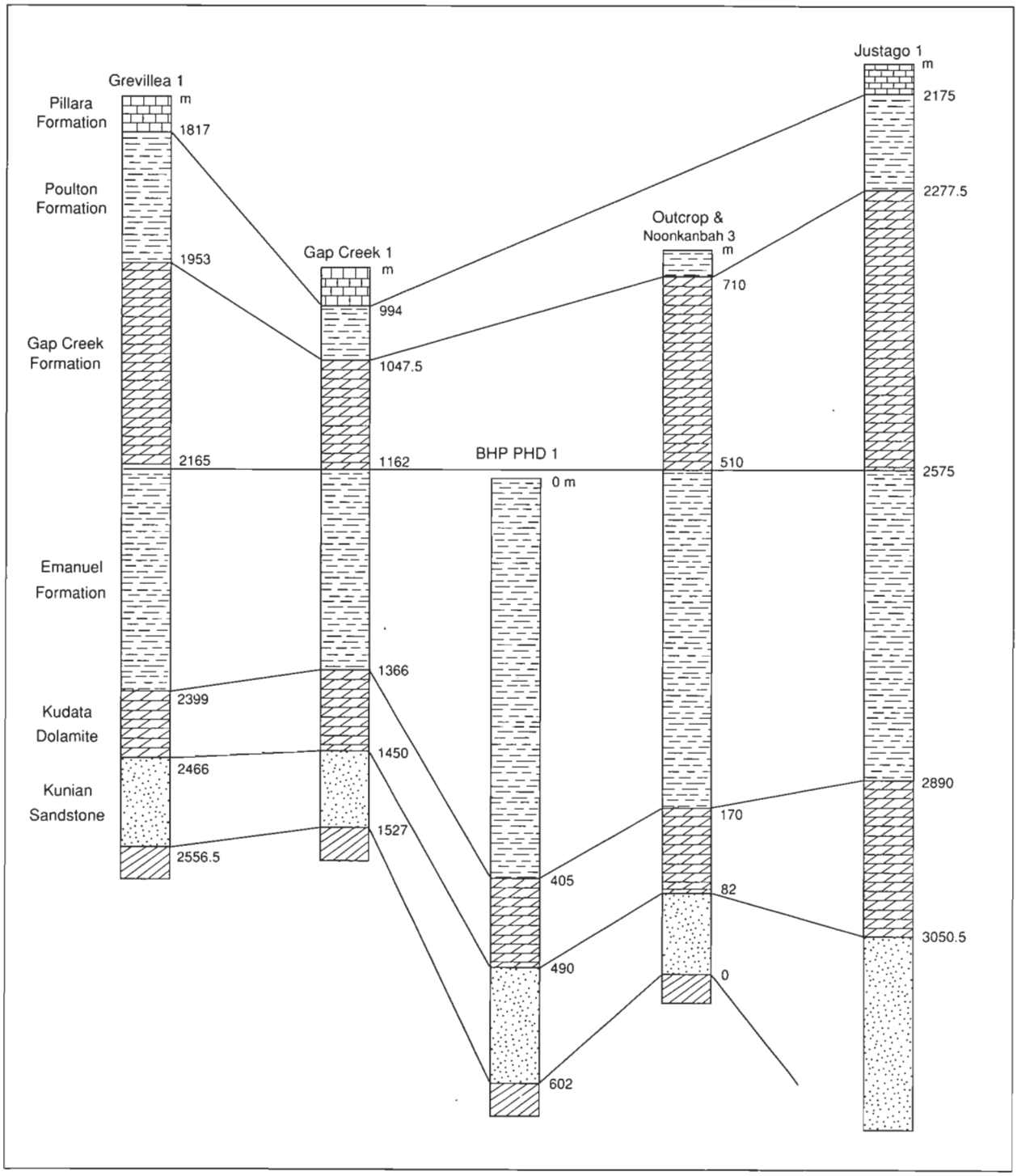

Figure 4. Stratigraphic correlation of the Kunian Ss, Kudata Dol. and Emanuel Fm. in petroleum exploration wells (Grevillea No. 1, Gap Creek No. 1 and Justago No. 1), stratigraphic drill holes (BHP PHD 1, Noonkanbah No. 3) and the outcrop in the Prices Creek area. See Figure 1 for the location of the line of section.

Formation is located in Blackstone No. 1 (1941–2220 m) and the unit has also been reported in nearby wells, such as Meda No. 1 and Napier No. 1 (Towner & Gibson, 1983). The Poulton Formation has not previously been reported from outcrop. Based on both lithologic similarity and stratigraphic relationships, we extend the Poulton Formation to include the outcrop exposures in the Prices Creek area.

In outcrop sections, the Poulton Formation consists of dolomitic siltstone, dolomite, and dolomitic sandstone with some shale intervals. The base of the unit is marked by pebble conglomerates in some localities and quartz pebbles are found in the lower part of the unit at several locations. Some of the dolomites appear to be algal laminates, and halite pseudomorphs were found in dolomite in measured section WCB 708 (sample 144 A). Apart from two beds containing unidentified gastropods located near the base of the unit in traverse section WCB 709, no macrofossils or phosphatic microfossils have been recovered from the unit. Based on microfloras, a Middle Devonian age has been ascribed to the Poulton Formation (Playford & others, 1975).

In the type section (Blackstone No.1), and in outcrop, the Poulton Formation is overlain by the Lower Dolomite of the Pillara Formation with angular unconformity. This same angular relationship is indicated in the subsurface of the western part of the Lennard Shelf (Playford & others, 1975). However, near Cadjebut Mine, the basal arkose of the Devonian sequence (possibly the Poulton Formation) is apparently conformably overlain by the lower dolomite of the Pillara Formation. Hence, the angular unconformity in the type and other sections may be due to a local tectonic event.

The Poulton Formation has been intersected in the petroleum exploration wells Grevillea No. 1 (136 m thick), Gap Creek No. 1 (53.5 m), and Justago No. 1 (102.5 m).

Age relationships

An Ordovician age for the Prices Creek Group was not recognised until 1949 (Guppy & Öpik, 1950). At that time, Guppy & Öpik (1950) correlated the Ordovician of the Canning Basin with stages of the North American succession. They correlated the base of the Emanuel Formation with the Upper Ozarkian, the top of the Emanuel Formation with the Chazyan, and the Gap Creek Formation with the Lower Trenton. Teichert & Glenister (1954), using cephalopods, concluded that the upper part of the Emanuel Formation was of Canadian age, or slightly older than the age indicated by Guppy & Öpik (1950), but they had no cephalopod control on the age of the base of the Gap Creek Formation.

More recent palaeontological studies by McTavish (1973), McTavish & Legg, (1976) and Legg (1976, 1978) suggested that the top of the Prices Creek Group is older than the Lower Trenton age proposed by Guppy & Öpik (1950). McTavish (1973) examined conodont faunas from the Emanuel Formation and the base of the Gap Creek Formation (his top Emanuel Formation, see above) and compared them with the conodont biozonation of the Baltic. On this basis, McTavish (1973) concluded that the Emanuel Formation represented the entire interval of the Latorp Stage, that is the lower part of the Arenig. Legg (1976, 1978) also concluded that the Emanuel–Gap Creek interval was essentially Latorpian in age, but suggested that the base of the Emanuel might extend down into the upper part of the Tremadoc.

Analysis of biostratigraphic collections made in 1990 in the Prices Creek area are now in progress, and preliminary analysis of conodont and trilobite faunas indicate some revision of the age determinations given by previous authors is needed.

There is no faunal evidence for the age of the Kunian Sandstone. No macrofossils were observed in any of the core examined, and glauconitic and friable sands examined for phosphatic microfossils were barren. New K-Ar dates of 515±4 and 504±4 Ma obtained from the Spielers Shear in the Oscar Range Inlier (Shaw & others, 1992) suggest that tectonism in the northern margin was active as late as about the Cambrian–Ordovician boundary. Shaw & others (1992) apply the term Spielers Event to this period of apparent crustal shortening and uplift. As the Kunian Sandstone and Kudata Dolomite show no evidence of metamorphism, and conodonts from the Kudata Dolomite have a low conodont color alteration index (CAI = 1), it is probable that sedimentation in the basin was initiated in the Early Ordovician. The Kunian Sandstone is thus most likely to be of Warendian (=Tremadoc) age, and to represent the major transgressive phase following the Kelly Creek Eustatic Event (Nicoll & others, 1992) in the Amadeus and Canning Basins.

The Kudata Dolomite contains no datable macrofossils, but conodonts recovered from both surface and subsurface samples indicate a Tremadoc age for the unit. Taxa recovered include *Scolopodus bolites* and *Drepanoistodus* sp. This fauna is similar to the conodont fauna described by Repetski (1982) from the lower part of the El Paso Formation in Texas and correlated with conodont fauna *D. deltifer* Zone of the North American conodont zonation.

In the Emanuel Formation, as defined in this study, both the conodont and trilobite faunas indicate that the unit is of early Arenig age. The conodont fauna includes *Prioniodus oepiki, Paracordylodus gracilis, Bergstroemognathus extensus*, and *Serratognathus bilobatus*.

The top of the Emanuel Formation and the base of the Gap Creek Formation have not been adequately sampled to determine their age because this contact does not outcrop. However, conodonts from the base of sections WCB 707 and WCB 708, which are presumed to begin low in the Gap Creek Formation, indicate an Arenig age based on the recovery of species such as *Oepikodus communis* and *Bergstroemognathus hubeiensis*. This same fauna appears to extend through the lower member of the Gap Creek Formation. The upper member of the Gap Creek Formation has only a very sparse macrofauna and an apparently non-diagnostic conodont fauna.

The Poulton Formation, as noted above, lacks age diagnostic fossils in the outcrop sections, but palynomorphs from subsurface samples (Playford & others, 1975) indicate that the unit is most probably of Middle Devonian age.

Canning Basin outcrop to subsurface correlation

Precise correlation of the Prices Creek Group with the subsurface Ordovician of the rest of the Canning Basin (Fig. 5) is difficult because adequate faunal studies are

available only from the Emanuel Formation (Legg, 1973; McTavish, 1973). Subsurface biostratigraphy has been based primarily on petroleum exploration wells, and is limited to work by Legg (1976, 1978) and McTavish & Legg (1972, 1976). Re-evaluation of the conodont biostratigraphy of the subsurface (Nicoll, 1992b) now provides a general framework against which to correlate the new outcrop collections.

The Kunian Sandstone is lithologically correlated with the basal transgressive sands of the Nambeet Formation (McTavish & Legg, 1976). There is no direct palaeontological evidence on which to establish an age for either sandstone unit, but biostratigraphic control provided by the overlying Kudata Dolomite and the non-sandstone facies of the lower part of the Nambeet Formation suggest equivalence.

The Kudata Dolomite correlates with the lower part of the Nambeet Formation. Conodont faunas from the lower part of the Nambeet Formation in Samphire Marsh No. 1 are the same age as the conodont fauna from BHP PCD 158 and are assigned to the Drepanoistodus–Paltodus Zone (Nicoll, 1992b).

The revised Emanuel Formation is correlated with the upper part of the Nambeet Formation on the presence of elements of the *Prioniodus elegans–Bergstroemognathus extensus* Zone in both units (Nicoll, 1992b). The Gap Creek Formation is correlated with part of the Willara Formation, but there is no faunal evidence presently available for the age of the upper part of the Gap Creek Formation. In the outcrop area, near Prices Creek, the top of the Gap Creek Formation is marked by an eroded, unconformable surface overlain by the Poulton Formation which has elsewhere been dated as Middle Devonian (Playford & others, 1975). This indicates that on at least the eastern part of the Lennard Shelf, there is no equivalent of the Goldwyer or Nita Formations preserved. It is possible that sediments equivalent to these units were deposited in the area, but were removed subsequently by erosion.

The Ordovician section in the western part of the Lennard Shelf is intersected in the WAPET Blackstone No. 1 petroleum exploration well and has been interpreted by McTavish & Legg (1976) as consisting of 444+ m of the Goldwyer Formation (2606.7–3050.3 m = TD) overlain by 386 m of the Nita Formation (2221–2606.7 m). The Poulton Formation was named by Playford & others (1975) for the interval 1941–2220 m in the Blackstone No. 1 well. Lehmann (1984) interpreted the Blackstone No. 1 section to include 134 m of the Worral Formation (2102–2236 m) and 168 m of the Poulton Formation equivalent units (1934–2102 m). However, conodonts from core 16 (2220–2229 m) are of Ordovician age (e.g. *Drepanoistodus*) and belong with the underlying unit. This review places the Poulton Formation in Blackstone No. 1 between 1934–2221 m, a thickness of 287 m, much as indicated by Playford & others (1975) and correlates this interval with the lithologies of the exposures in the Prices Creek area.

Examination of the conodont faunas from Blackstone No. 1

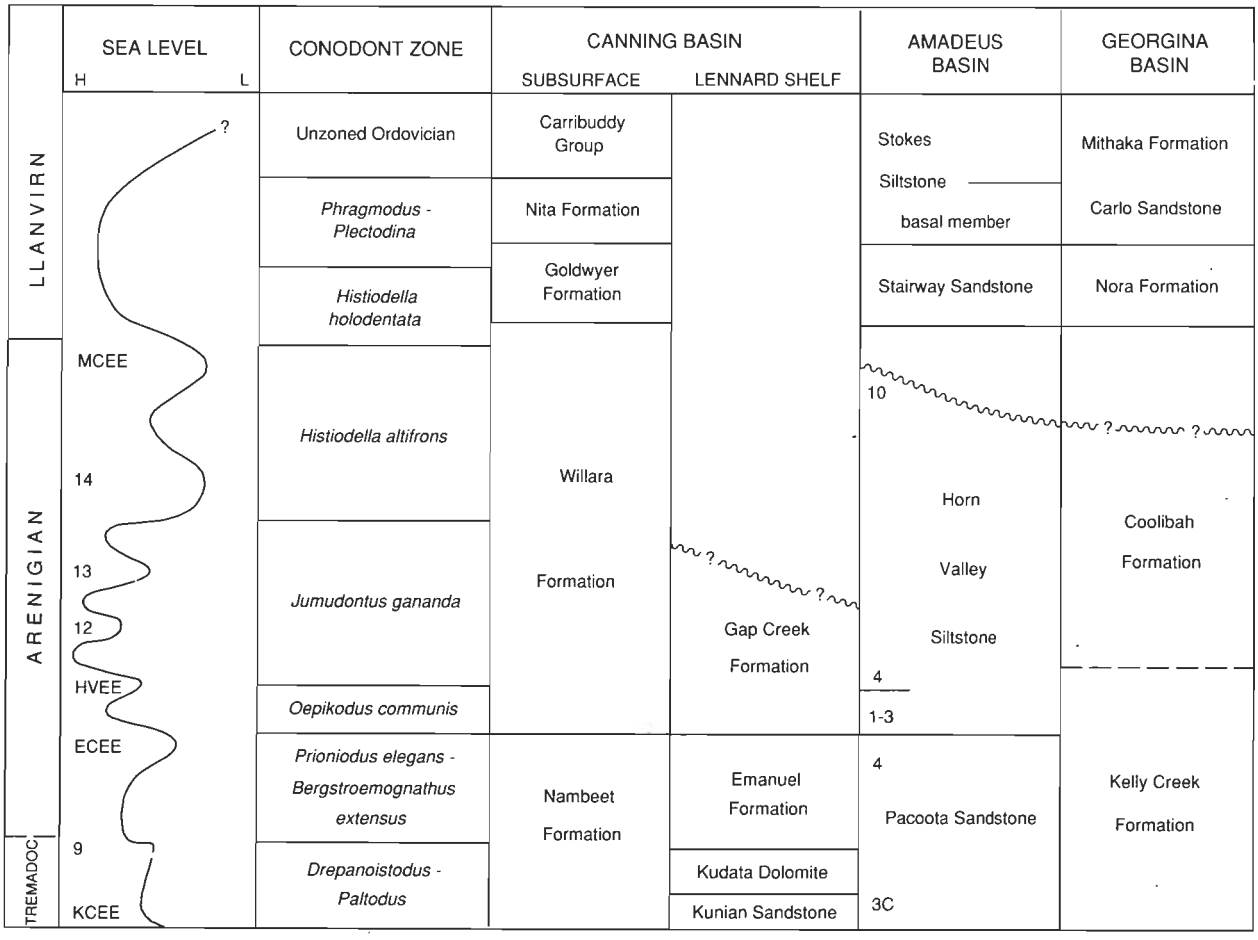

Figure 5. Correlation of the Canning Basin subsurface and Lennard Shelf areas with the Amadeus and Georgina Basin Ordovician succession. The sea-level curve is modified from Nielsen (1992). The vertical scale is time linear.

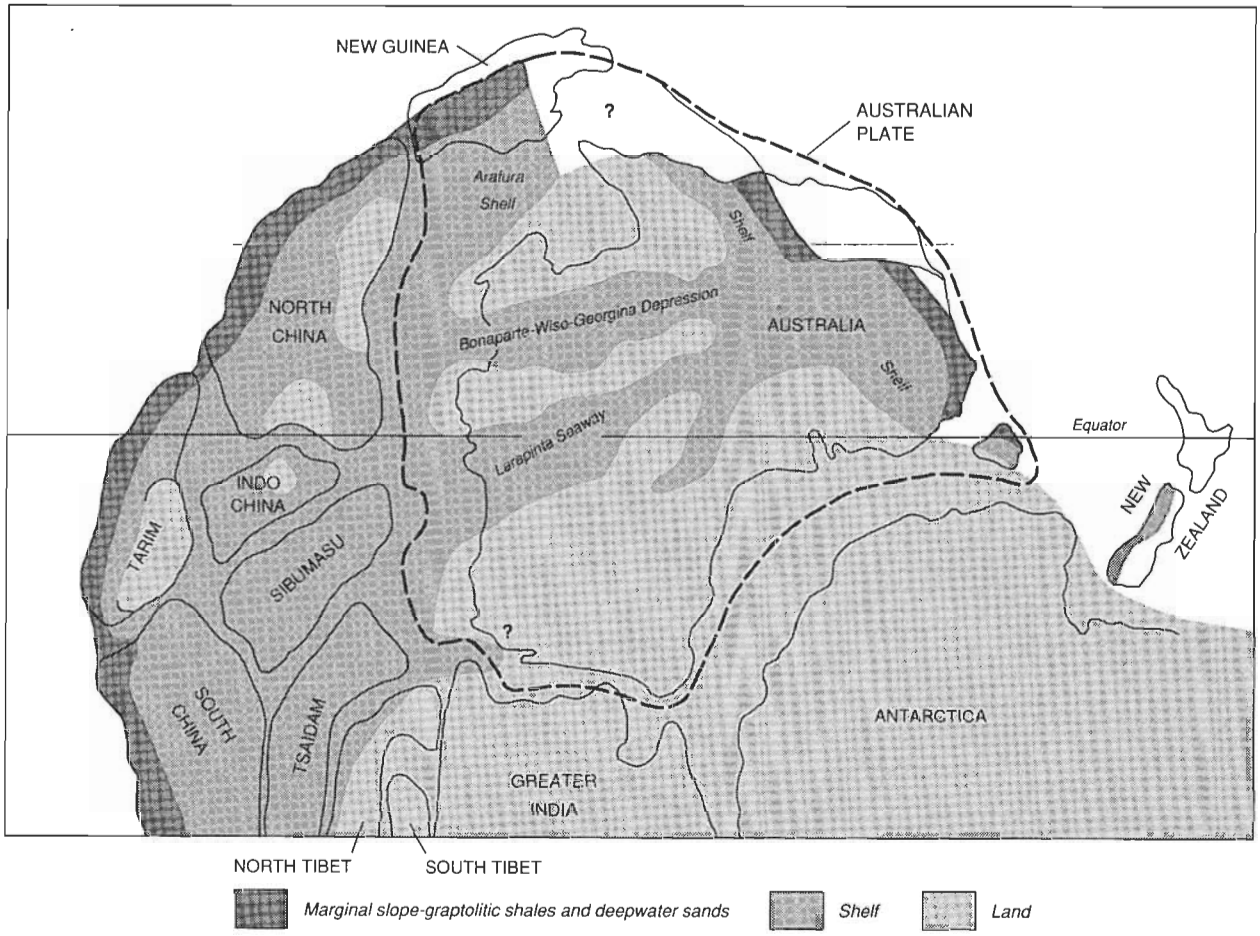

Figure 6. Map showing the position of the Larapinta Seaway and the position of basins in the middle Arenig time. After Nicoll & others, 1989.

cores 16 to 19 (2221–2460) indicates that the conodont fauna from this interval of the Nita Formation belongs to the *Phragmodus–Plectodina* Zone. This zone is found in the upper part of the Goldwyer Formation and in the Nita Formation in the subsurface throughout the basin and confirms the stratigraphic interpretation of McTavish & Legg (1976).

Interbasin correlation and palaeogeography

Correlation of the Ordovician sedimentary sequences of the Canning, Amadeus and Georgina Basins (Fig. 5) is here revised from the scheme proposed by Nicoll & others (1988) following the results of ongoing biostratigraphic studies in the three basins. The relationship of the sedimentation pattern between the Canning and Amadeus Basins (Fig. 6) is very close, because the two basins were thought to be physically linked as a single depositional system throughout much of Ordovician time (Webby, 1978; Nicoll & others, 1988, 1989; Cook & Totterdell, 1991). The Georgina Basin is more remote and is only indirectly linked to the Canning Basin, but all three basins were subjected to essentially the same tectonic and eustatic controls on depositional patterns.

The Canning Basin in Ordovician time was located in Eastern Gondwanaland (Fig. 7) in an equatorial position (Webby, 1978) on what became the Australian Plate (Nicoll & Totterdell, 1990). West of the present continental margin were what were to become the Tsaidam, Sibumasu, South China, Indochina, Tarim and North China Blocks (Fig. 6).

The Larapintine Seaway, one of several subparallel depressions that extended across the northern part of Eastern Gondwanaland (Nicoll & Totterdell, 1990), was apparently not the site of Cambrian sedimentation in the area of the present Canning Basin as no record of Cambrian rocks has been found in the major part of the basin. The Middle Cambrian rocks of the Ord Basin (Mory & Beere, 1985), extending south to the vicinity of Halls Creek, are not known to extend into the Canning Basin proper. Cambrian sediments are also known in the western Amadeus Basin (Wells & others, 1965) and on the Shan-Thai Block to the west (Burrett et al., 1990).

Ordovician sedimentation was initiated in the Canning Basin in the latest Tremadoc by the Kelly Creek transgression, following the Kelly Creek Eustatic Event (Nicoll & others, 1992). The inundation was probably from the west and the oldest dated sediments are in the Samphire Marsh No 1 and Prices Creek areas. Initial Ordovician sedimentation (basal Nambeet Formation = Kunian Sandstone = Carranya Beds) spread across the Canning Basin and the Larapintine Seaway was established when the connection through the Amadeus and Warburton Basins to the eastern Australian marginal shelf was completed. For most of the

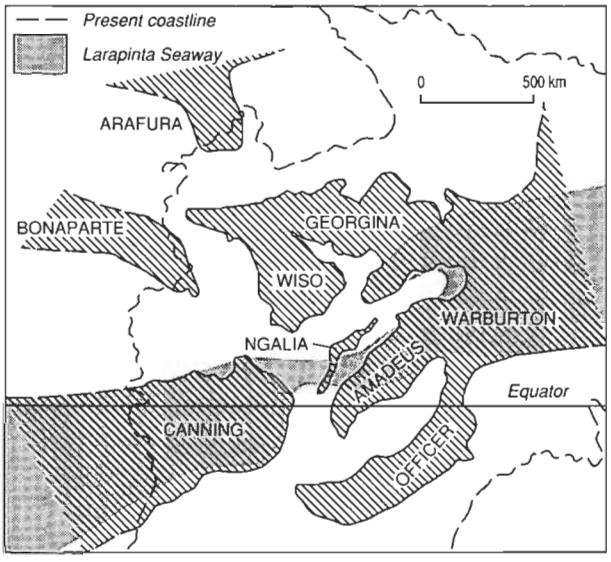

Figure 7. Palaeogeographic reconstruction of Eastern Gondwanaland in the Early Ordovician showing land areas, major seaways and shelves and continental margin slope deposits. After Nicoll & Totterdell, 1990.

remainder of the Ordovician, a series of regressive and transgressive couplets, bounding major eustatic events, can be identified in the Canning, Amadeus and Georgina Basins (Nicoll & others, 1992; Nielsen, 1992). The depositional environment was shallowest in the Amadeus Basin and usually deeper during the corresponding time in the Canning and Warburton Basins. Thus, time correlative units, such as the Willara Formation = Horn Valley Siltstone, or the Emanuel Formation = Pacoota Sandstone (unit 4) record deeper-water sediments in the Canning Basin than in the adjacent Amadeus Basin.

Eustatic event 9 of Nicoll & others (1992) is interpreted to occur in the Canning Basin between the Kudata Dolomite and the overlying Emanuel Formation. In the Amadeus Basin, this is equivalent to the break recognised between Pacoota Sandstone units 3C and 4. The following transgression led to the deposition of the Emanuel Formation and Pacoota Sandstone unit 4 and is represented by the *Prioniodus elegans–Bergstroemognathus extensus* Zone conodont fauna.

Based on conodont correlations, the Ellery Creek Eustatic Event (new name = event 10 of Nicoll & others, 1992) is considered to lie between the Emanuel Formation and the Gap Creek Formation in the Canning Basin and between the Pacoota Sandstone unit 4 and the Horn Valley Siltstone in the Amadeus Basin. In the Canning Basin, this eustatic event interval is not well exposed; but the interval is well exposed in the Amadeus Basin, at sections on Ellery Creek and Maloney Creek (Laurie & others, 1991). There may be little or no recognisable depositional break in the Canning Basin sequence, but a major hiatus can be demonstrated in parts of the Amadeus Basin, as at Maloney Creek section (Laurie & others, 1991). This Ellery Creek regression marks the end of the *Prioniodus elegans–Bergstroemognathus extensus* Zone fauna and the introduction of the *Oepikodus communis* Zone fauna on the following transgression.

The basal dolomitic beds of the Horn Valley Siltstone (units 1–3, Fig. 5) are correlated with the base of the Gap Creek Formation (section RM 10 of McTavish, 1973) on the basis of the presence of *Oepikodus communis* and *Bergstroemognathus hubeiensis* in both units. The lower part of the Gap Creek Formation also contains specimens of the asaphid trilobite *Lycophron* similar to *Lycophron howchini* (Etheridge, 1894) found in the lower trilobite assemblage of the Horn Valley Siltstone. Also found at this level in the Gap Creek Formation is the peculiar macluritacean gastropod *Teiichispira* sp., which also occurs in the Coolibah Formation in the Georgina Basin (Gilbert-Tomlinson, 1973, p. 70) and in the Karmberg Limestone of southern Tasmania (Laurie, 1991, p. 21).

The Horn Valley Eustatic Event (HVEE) of Gorter (1992) was first recognised in the Amadeus Basin where it is marked by the abrupt lithologic change in the lower part of the Horn Valley from the dolomitic limestone unit at the base of the formation, units 1–3 of Elphinstone & Gorter (1991) or unit 15 of Gorter (1991), to the shale and siltstone dominated unit that overlies it. Palaeontological evidence suggests that this event is located in the Gap Creek Formation at the abrupt faunal shift between the lower and upper members, at about 110 m (section WCB 708) above the base of the formation. In the subsurface, this event is identified by the boundary of the *Oepikodus communis* and *Jumudontus gananda* Zones.

Events 12 through 14 are not recognised in the outcropping Canning Basin sequence. They are established from the Horn Valley Siltstone curve of Nielsen (1992), but have not yet been detailed in the Canning Basin subsurface and may not have been preserved in the Gap Creek Formation.

The Maloney Creek Eustatic Event (Nicoll & others, 1991) is marked in the Amadeus Basin by the abrupt incursion of clastic sedimentation seen in the Stairway Sandstone. In the Canning Basin, this event is not as clearly defined but appears to occur with the shift from predominantly carbonate deposition in the upper part of the Willara Formation to the mixed shale–carbonate depositional pattern of the lower part of the Goldwyer Formation (McTavish & Legg, 1976).

With the possible exception of the section in the Blackstone No. 1 well area (discussed earlier), no record exists of sediments equivalent to the Goldwyer or Nita Formations on the Lennard Shelf. There is no reason to believe equivalent sediments were not deposited in the area, but they may have been removed prior to Middle Devonian deposition of the Poulton Formation.

Economic implications

The interest in the economic potential of Ordovician sediments in the Canning Basin dates to 1919 when a well drilled at Prices Creek recovered traces of oil (Guppy & others, 1958). In 1921, the Western Australian Government drilled a hole to 90 feet in the same area and recovered traces of hydrocarbons. On the basis of these reports, the Freney Oil Company Limited drilled a series of four holes in the years 1922–23 in the Prices Creek area (Guppy & others, 1958). Three of these holes, all in Ordovician rocks, recovered traces of oil. The deepest of these holes, drilled to a depth of 1008 feet (307.3 m), was drilled entirely in the Emanuel Formation and produced shows of oil. This was the last initiative in the early phase of interest in the Ordovician on the Lennard Shelf.

In the second round of exploration drilling in the 1980s, the

Ordovician section in the Prices Creek area was penetrated in three wells: IEDC Grevillea No. 1 (1982), IEDC Justago No. 1 (1984/85) and Kufpec Gap Creek No. 1 (1988). Two of these wells, Grevillea No.1 and Gap Creek No. 1, bottomed in Precambrian basement. None of the holes encountered significant hydrocarbons, but minor shows were reported in Grevillea No. 1 (Weaver, 1983).

The economic importance of the pre-Gap Creek Formation sediments on the Lennard Shelf is related to its source and reservoir potential for hydrocarbon accumulation. The 500 to 700 m thick Emanuel Formation acts as a regionally extensive seal and source for hydrocarbons that can be reservoired in the underlying sandstone and dolomite units. This situation is analogous to the Amadeus Basin where the slightly younger Horn Valley Siltstone acts as both source and seal for the Pacoota Sandstone (Gorter, 1984)

Despite the lack of significant hydrocarbons in the few existing wells that have penetrated Ordovician sediments on the Lennard Shelf, the lower part of the Prices Creek Group is still believed to be prospective and worth investigation. This optimism is based on the frequency of hydrocarbon shows in shallow mineral exploration drilling of the Emanuel Formation, and because existing petroleum exploration holes have been sited to target plays in the overlying Devonian sediments; hence they may not have been in the optimum position to evaluate structures in the Ordovician succession.

The distribution of *Gloecapsomorpha prisca*, commonly thought to have served as the source of most of the Ordovician hydrocarbon shows in the Canning Basin and deposits in the Amadeus Basin, appears to be controlled by water depth or factors related to water depth. In the Canning Basin, *G. prisca* is most abundant in the upper part of the Nambeet Formation and in the Goldwyer Formation (Foster & others, 1986; Taylor, 1992). The upper Nambeet Formation occurrence would correlate with the lower part of the Emanuel Formation. In the Amadeus Basin, *G. prisca* is most abundant in the Horn Valley Siltstone (Foster & others, 1986; Taylor, 1992).

There are also some minor lead–zinc traces in some of the mineral exploration cores that intersect the Kudata Dolomite, but for the most part the depth of the unit below the surface precludes most economic mineral interest.

Conclusions

The Early Ordovician (late Tremadoc to Arenig) Prices Creek Group outcrops only in the Prices Creek area of the Lennard Shelf. Recent exploration has shown that the Prices Creek Group, previously defined as consisting of a lower Emanuel Formation and an upper Gap Creek Formation, can now be subdivided into four formations. The new formations comprise a basal transgressive sandstone unit, here named the Kunian Sandstone. This unit does not outcrop but has been penetrated in several drillholes. It is overlain by a dolomitic carbonate-dominated unit, here named the Kudata Dolomite, which was formerly included in the Emanuel Formation and is exposed at the base of the type section of that unit along Emanuel Creek. The Kudata Dolomite is apparently conformably overlain by the Emanuel Formation.

The Gap Creek Formation is informally divided into a lower more fossiliferous dolomitic member and an upper less fossiliferous member that shows evidence of a hypersaline depositional regime near the top. The Poulton Formation is recognised for the first time in outcrop, paraconformably above the Gap Creek Formation and unconformably below the Pillara Formation.

The sandstone–dolomite–shale sequence of the lower Prices Creek Group has some economic potential, both for hydrocarbons and minerals. The oil is probably sourced from the Emanuel Formation, which also serves as an effective regional seal. Traces of lead and zinc have also been found in the Kudata Dolomite.

Acknowledgements

The authors wish to thank Chris Handley (BHP) and John Shergold (BMR) for their assistance, and Broken Hill Proprietary Company Limited for their assistance with logistics and permitting access to drill core. M.T. Roche publishes with the permission of the Broken Hill Proprietary Company Limited.

References

Burrett, C.F., Long, J.A. & Stait, B.A., 1990 — Early-Middle Palaeozoic biogeography of Asian terranes derived from Gondwana. *Geological Society Memoir* 12, 163–174.

Cook, P.J. & Totterdell, J.M., 1991 — Palaeogeographic atlas of Australia. Volume 2–Ordovician. *Bureau of Mineral Resources, Geology and Geophysics, Canberra.*

Elphinstone, R. & Gorter, J.D., 1991 — As the worm turns: implications of bioturbation on source rocks of the Horn Valley Siltstone. *Bureau of Mineral Resources, Geology and Geophysics, Bulletin* 236, 317–332.

Etheridge, R., 1894 — Official contributions to the palaeontology of South Australia, No.7. Further additions to the Lower Silurian fauna of central Australia. *South Australian Parliamentary Paper* No.25, 23–26, pl. 3.

Forman, D.J. & Wales, D.W. (compilers), 1981 — Geological evolution of the Canning Basin, Western Australia. *Bureau of Mineral Resources, Geology and Geophysics, Bulletin* 210, 1–91.

Foster, C.B., O'Brien, G.W. & Watson, S.T., 1986 — Hydrocarbon source potential of the Goldwyer Formation, Barbwire Terrace, Canning Basin, Western Australia. *The APEA Journal*, 26, 142–155.

Gilbert-Tomlinson, J., 1973 — The Lower Ordovician gastropod *Teiichispira* in Northern Australia. *Bureau of Mineral Resources, Geology and Geophysics, Bulletin* 126, 65–88, pls 29–34.

Gorter, J.D., 1984 — Source potential of the Horn Valley Siltstone, Amadeus Basin. *The APEA Journal*, 24, 66–90.

Gorter, J.D., 1991 — Palaeogeography of Late Cambrian to Early Ordovician sediments in the Amadeus Basin, central Australia. *Bureau of Mineral Resources, Geology and Geophysics, Bulletin* 236, 253–275.

Gorter, J.D., 1992 — Ordovician petroleum in Australia in relation to eustasy. *In* Webby, B.D. & Laurie, J.R. (editors)–Global Perspectives on Ordovician Geology. *Balkema, Rotterdam*, 433–443.

Guppy, D.G. & Öpik, A.A., 1950 — Discovery of Ordovician rocks, Kimberley Division, W.A. *Australian Journal of Science*, 12, 205–206.

Guppy, D.G., Lindner, A.W., Rattigan, J.H. & Casey, J.N., 1958 — The geology of the Fitzroy Basin, Western Australia. *Bureau of Mineral Resources, Geology and*

Geophysics, Bulletin 36, 116 p.

Handley, C., 1991 — Prices Hill MO4/171–175, EO4/437, West Kimberley Mineral Field, Annual Report, 1990. *Unpublished internal BHP Company Report* CR 7112.

Henderson, S.D., 1963 — Bore BMR 3 Prices Creek. *In* Henderson, S.D., Condon, M.A. & Bastian, L.V. Stratigraphic drilling, Canning Basin, Western Australia. *Bureau of Mineral Resources, Geology and Geophysics, Report* 60, 46–51.

Laurie, J.R., 1991 — Articulate brachiopods from the Ordovician and Lower Silurian of Tasmania. *Memoir of the Association of Australasian Palaeontologists*, 11, 1–106.

Laurie, J.R., Nicoll, R.S. & Shergold, J.H., 1991 — Ordovician siliciclastics and carbonates of the Amadeus Basin, Northern Territory. Guidebook for Field Excursion 2, Sixth International Symposium on the Ordovician System. *Bureau of Mineral Resources, Geology and Geophysics, Record* 1991/49, 74 p.

Legg, D.P., 1973 — Ordovician stratigraphy and palaeontology (Trilobita, Graptolithina), Canning Basin, Western Australia. *Unpublished Ph.D. thesis, University of Western Australia.*

Legg, D.P., 1976 — Ordovician trilobites and graptolites from the Canning Basin, Western Australia. *Geologica et Palaeontologica*, 10, 1–58.

Legg, D.P., 1978 — Ordovician biostratigraphy of the Canning Basin, Western Australia. *Alcheringa*, 2, 321–334.

Lehmann, P.R., 1984 — The stratigraphy, palaeogeography and petroleum potential of the Lower to lower Upper Devonian Sequence in the Canning Basin. *In* Purcell, P.G. (editor), The Canning Basin, W.A. *Proceedings of Geological Society of Australia/Petroleum Exploration Society Australia Symposium, Perth, 1984.*

McTavish, R.A., 1973. — Prioniodontacean conodonts from the Emanuel Formation (Lower Ordovician) of Western Australia. *Geologica et Palaeontologica*, 7, 27–58.

McTavish, R.A. & Legg, D.P., 1972 — Middle Ordovician correlation — conodont and graptolite evidence from Western Australia. *Neues Jahrbuch für Geologie und Paläontologie, Monatshefte* 1972, 465–474

McTavish, R.A. & Legg, D.P., 1976 — The Ordovician of the Canning Basin, Western Australia. *In* Bassett, M.G. (editor)–The Ordovician System: proceedings of a Palaeontological Association symposium. *National Museum of Wales,* 447–478.

Mory, A.J. & Beere, G.M., 1985 — Geology of the Onshore Bonaparte and Ord Basins in Western Australia. *Geological Survey of Western Australia Bulletin,* 134, 1–184.

Nicoll, R.S., 1992a — Analysis of conodont apparatus organisation and the genus Jumudontus (Conodonta), a coniform — pectiniform apparatus structure from the Early Ordovician. *BMR Journal of Australian Geology & Geophysics*, 13, 213–228.

Nicoll, R.S., 1992b — Ordovician conodont distribution in selected petroleum exploration wells, Canning Basin, Western Australia. *Bureau of Mineral Resources, Australia (Unpublished Professional Opinion 1992/005).*

Nicoll, R.S., Gorter, J.D., & Owen, M., 1991 — Ordovician sediments in the Waterhouse Range Anticline, Amadeus Basin, central Australia: their interpretation and tectonic implications. *In* Korsch, R.J. & Kennard, J.M. (editors)–Geological and Geophysical studies in the Amadeus Basin. *Bureau of Mineral Resources, Geology and Geophysics, Bulletin* 236, 277–284.

Nicoll, R.S., Nielsen, A.T., Laurie, J.R. & Shergold, J.H., 1992 — Preliminary correlation of Payntonian (Latest Cambrian) to earliest Arenig (Early Ordovician) sealevel events in Australia and Scandinavia. *In* Webby, B.D. & Laurie, J.R. (editors), Global Perspectives on Ordovician Geology. *Balkema, Rotterdam,* 381–394.

Nicoll, R.S., Owen, M., Shergold, J.H., Laurie, J.R. & Gorter, J.D., 1988 — Ordovician event stratigraphy and the development of a Larapintine Seaway, central Australia. *Bureau of Mineral Resources, Geology and Geophysics, Record* 1988/42, 72–77.

Nicoll, R.S., Owen, M., Shergold, J.H., Laurie, J.R. & Gorter, J.D., 1989 — Larapintine Seaway. *BMR 89,* 52–53.

Nicoll, R.S. & Totterdell, J.M., 1990 — Conodonts and the distribution in time and space of Ordovician sediments in Australia and adjacent areas. *Tenth Australian Geological Convention, Geological Society of Australia. Abstracts* 25, 46.

Nielsen, A.T., 1992 — Intercontinental correlation of the Arenigian (Early Ordovician) based on sequence and ecostratigraphy. *In* Webby, B.D. & Laurie, J.R. (editor), Global Perspectives on Ordovician Geology. *Balkema, Rotterdam,* 367–379.

Playford, P., Cope, R.N., Cockbain, A.E., Lowe, G.H. & Lowry, D.C., 1975 — Canning Basin. *In* The Geology of Western Australia. *Geological Survey of Western Australia, Memoir* 2, 319–368

Repetski, J.E., 1982. — Conodonts from El Paso Group (Lower Ordovician) of westernmost Texas and southern New Mexico. *New Mexico Bureau of Mines and Mineral Resources, Memoir* 40, 121 p.

Roche, M.T., 1990. — Proposed stratigraphic nomenclature for the Lower Ordovician Lennard Shelf, W.A. *Unpublished internal BHP Company Memorandum* CM 4321.

Shaw, R.D., Tyler, I.M., Griffin, T.J. & Webb, A., 1992 — New K-Ar constraints on the onset of subsidence in the Canning Basin, Western Australia. *BMR Journal of Australian Geology & Geophysics,* 13, 31–35.

Smith, E.R., 1955 — Seismic survey of the Poole Range, Prices Creek area, Kimberley Division, Western Australia. *Bureau of Mineral Resources, Geology and Geophysics, Record* 1955/35.

Taylor, D., 1992 — A Review of Ordovician source rocks, Canning Basin, Western Australia. *Bureau of Mineral Resources, Geology and Geophysics, Record* 1992/43.

Teichert, C. & Glenister, B.F., 1954 — Early Ordovician cephalopod fauna from northwestern Australia. *Bulletin of American Paleontology*, 35, 1–130.

Towner, R.R. & Gibson, D.L., 1983 — Geology of the onshore Canning Basin, Western Australia. *Bureau of Mineral Resources, Geology and Geophysics, Bulletin* 215, 1–51.

Veevers, J.J. & Wells, A.T., 1961 —The geology of the Canning Basin, Western Australia. *Bureau of Mineral Resources, Australia, Bulletin* 60, 323 p.

Weaver, P.A., 1983 — Well completion report Grevillea No.1, EP 102, Canning Basin, Western Australia. *International Energy Development Corporation of Australia Pty. Limited (unpublished).*

Webby, B.D., 1978 — History of the Ordovician continental platform and shelf margin of Australia. *Journal of the Geological Society of Australia,* 25, 41–68.

Wells, A.T., Forman, D.J. & Ranford, L.C., 1965 — The geology of the north-western part of the Amadeus Basin, Northern Territory. *Bureau of Mineral Resources, Geology and Geophysics, Report* 85, 1–45, pls 1–11.

Locality information

Eight BMR measured or traverse sections were collected as part of the faunal studies associated with this investigation. The locality information and stratigraphic information for each locality is given below. In addition a number of BHP–Utah mineral exploration core-holes were examined and biostratigraphic samples were selectively collected.

WCB 700 Gap Creek Formation, lower member. Traverse section. 125°55′15"E, 18°38′25"S

WCB 701 Gap Creek Formation, lower & upper members. Traverse section. Traverse is parallel to and approximates the line of the type section of Guppy & Öpik (1950). Base: 125°55′00"E, 18°38′10"S; Top: 125°55′15"E, 18°37′53"S

WCB 702 Gap Creek Formation, mostly upper member. Traverse section. Base: 125°54′45"E, 18°37′30"S; Top: 125°54′50"E, 18°37′23"S

WCB 703 Emanuel Formation, Traverse section. Follows line of type section. See WCB 705 for coodinates.

WCB 705 Emanuel Formation, Measured section. Follows the line of the type section of Guppy & Öpik (1950). Base: 125°54′00"E, 18°39′50"S; Top: 125°55′05"E, 18°39′12"S

WCB 707 Gap Creek Formation, lower part lower member. Measured section, correspond approximately to McTavish section RM 10. Base: 125°54′38"E, 18°38′10"S; Top: 125°54′42"E, 18°38′07"S

WCB 708 Gap Creek (lower & upper members) and Poulton Formations. Measured section. Base: 125°53′40"E, 18°36′20"S; Top: 125°53′47"E, 18°36′05"S

WCB 709 Poulton Formation. Traverse section. 125°52′55"E, 18°35′10"S

BHP PHD 1 Emanuel Formation. 125°53′00"E, 18°36′30"S

BHP PCD 153 Kunian Sandstone. 125°53′00"E, 18°40′12"S

BHP PCD 158 Kunian Sandstone and Kudata Dolomite. 125°53′10"E, 18°40′25"S

Appendix 1

Description of cores from BMR 3 Prices Creek (=Noonkanbah No. 3)

Examined by J.R. Laurie & R.S. Nicoll, March, 1992.

Core 1:

50′–51′9" — light grey micaceous siltstone with wispy fragments and laminae of dark-grey fine siltstone/mudstone.

51′9"–58′3" — buff to pale-brown medium to fine-grained sandy dolomite with occasional laminae and very thin beds of medium to dark-grey micaceous siltstone becoming more common toward bottom.

58′3"–58′4" — breccia (flat pebble conglomerate?) with rounded pebble sized clasts incorporated into a crystalline carbonate groundmass.

58′4"–60′ — light grey fine to medium-grained dolomite with wispy interlaminae of medium grey to greenish grey micaceous siltstone/mudstone. Lower 15 cm bioturbated by well-developed burrows.

Core 2:

148′–154′9" — light grey fine to medium-grained dolomite with wispy interlaminae of dark to medium grey micaceous mudstone/siltstone with occasional bioturbation.

154′9"–156′4" — light grey, fine to medium-grained dolomite of saccharoidal appearance

156′4"–156′7" — light grey, coarse-grained dolomite.

Core 3:

250′—259′2" — light brownish grey to pinkish grey, fine to coarse grained, cross-bedded carbonate cemented quartz sandstone with occasional greenish grey, micaceous, shaly partings.

The remaining cores 4–6 are so vastly different from the original descriptions of the drillsite geologist, we can only assume that they have become confused with cores from other drillholes.

Core 4 is a fine to medium-grained light greygreen or light chocolate brown clay cemented quartz-lithic sandstone. Core 5 mostly consists of a heavily slickensided and silicified, and in some places brecciated, siltstone or mudstone in the top portion of the core with a well-developed mylonite near the base.

The pieces of core tentatively identified as Core 6? consist of a light grey clayey friable siltstone to fine sandstone containing many fragments of vascular plants. We believe this last core is possibly Permian.

AGSO Journal of Australian Geology & Geophysics, 14, 77–95

A stream-sediment geochemical orientation survey of the Davenport Province, Northern Territory

B.I. Cruikshank[1], D.M. Hoatson[1] & J.G. Pyke[1]

A geochemical orientation study in the Davenport Province, Northern Territory, indicates that stream-sediment sampling is an effective geochemical technique for mineral assessment, despite overall poor drainage development.

Bismuth, Mo, Sn and W from vein-type deposits appear to be dispersed by mechanical weathering, giving rise to well-defined anomalies in both sieved samples and heavy mineral concentrates. Dispersion trains exceed 10 km downstream from mineralisation, and for regional surveys the analysis of a coarse sieved fraction at a sample spacing of 1 to 2 km is recommended.

Dispersion of U and Cu appears to be chemically controlled, and anomalies near known mineralisation in both sieved and heavy mineral samples are either less well defined or absent. Dispersion trains rarely extend more than 1 km from mineralisation, and sample spacing of 0.5 to 1 km, or less, would be necessary.

Introduction

A geochemical orientation survey (Hoatson & Cruikshank, 1985) of the Davenport Province study was undertaken as part of a combined Bureau of Mineral Resources (BMR) and Northern Territory Geological Survey (NTGS), to define the province's stratigraphy, structure, sedimentological history, tectonic setting, and economic potential. The aims of this survey were to determine the most suitable geochemical sampling type(s) that characterise the different styles of known Au, Bi, Cu, Mo, Sn, U and W mineralisation, the mechanisms of secondary dispersion, and the characteristics of secondary dispersion including the identification of pathfinder elements, and the sample spacing required to detect mineralisation.

The Davenport Province, about 180 km south of Tennant Creek (Fig. 1) and covering approximately 15 000 km^2, is centred near the conjunction of the Bonney Well, Frew River, Elkedra and Barrow Creek 1:250 000 sheet areas at longitude 135°E and latitude 21°S.

The region has a semi-arid climate with an average annual rainfall of about 300 mm, largely during December to March, and is characterised by marked diurnal and seasonal fluctuations in temperature with average maximum–minimum ranges for December and July of 38–24°C and 24–11°C, respectively (Perry & others, 1962).

The region is dominated by the northwest–southeast trending Murchison and Davenport Ranges, with the Younghusband Range forming a westerly extension of the latter (Fig. 1). The ranges consist of rocky strike ridges rising up to 597 m above sea level at Mt Cairns, and commonly 200 m above the surrounding plains. The ridges are formed of sandstone, quartzite and conglomerate, with intervening flat to gently undulating depressions on carbonate and argillaceous sediments, intermediate-mafic lavas, pyroclastic flows, and intrusions. Granite outcrops commonly have spectacular tor development, most notably at the Devils Marbles National Park on the Stuart Highway (Twidale, 1980).

The two main drainage systems are those of the east-flowing Elkedra River in the south and the north-flowing Frew River on the northeastern flank of the Murchison Range. Drainage elsewhere is largely controlled by long strike ridges of sandstone and quartzite. All drainage terminates in the sandy plains surrounding the ranges. Run off after rain is very rapid, and for most of the year surface water is restricted to semi-permanent waterholes along the main watercourses and to small rockholes in the ranges.

The ranges have a sparse cover of spinifex and small trees (e.g. snappy gum). Isolated stands of acacia and eucalypts occur along drainage channels. Open grasslands are scattered with several varieties of spinifex. Soils are generally immature and poorly developed, varying from shallow and stony on the ridges to either coarse alluvial soils or red aeolian sands on low-lying areas. Aeolian sands cover most of the plains in the Davenport Province.

Geology and mineralisation

Prior to 1981, the geological and economic features of the Davenport Province had been discussed by, amongst others, Sullivan (1952), Ryan (1961), Smith & others (1961), Smith (1964, 1970), Smith & Milligan (1964, 1966), and Roarty (1977). During the BMR–NTGS survey, the province was remapped at 1:100 000 scale, resulting in the publication of four special map sheets: Devils Marbles region (Wyche & others, 1987), Kurundi region (Stewart & Blake, 1986), Hatches Creek region (Blake & others, 1986) and Elkedra region (Blake & Horsfall, 1987), the boundaries of which, along with the generalised geology of the region, are shown in Figure 2. The results of the survey are synthesised in BMR Bulletin 226 and the accompanying 1:250 000 geological map (Blake & others, 1987).

The Davenport Province forms the southern part of the Proterozoic Tennant Creek Inlier, and lies to the north of the Proterozoic Arunta Inlier. The eastern and western margins of the province are masked, respectively, by lower Palaeozoic platform cover of the Georgina and Wiso Basins. The oldest rocks exposed in the Davenport Province are turbidites and minor 1880–1870 Ma felsic volcanics of the Warramunga Group (Blake & Page, 1988; Le Messurier & others, 1990). The Warramunga Group, which extends north to Tennant Creek, consists of tightly folded greywacke and siltstone with subordinate jaspilitic chert and minor felsic volcanics. It was deformed and intruded by granite (Hill of Leaders Granite) before being unconformably overlain by the Hatches Creek Group, a sequence of shallow-water sediments of predominantly quartz arenites, feldspathic quartz arenites, conglomerates and argillites with minor carbonates, interspersed with bimodal mafic–felsic volcanics of both lava flow and pyroclastic origin. Blake & others (1984, 1987) have subdivided the Hatches Creek Group into the Ooradidgee

[1] Australian Geological Survey Organisation, GPO Box 378, Canberra ACT 2601

Subgroup (lower), the Wauchope Subgroup (middle) and the Hanlon Subgroup (upper), which collectively contain twenty formations totalling about 10 000 m in thickness (Table 1). Uranium-Pb zircon data for felsic extrusives from the Epenarra and Treasure Volcanics formations indicate probable ages of 1820 to 1810 Ma for volcanism in the basal Ooradigee Subgroup (Blake & Page, 1988).

Multiple sill-like intrusions of granophyre, feldspar porphyry and gabbro occur within the Ooradidgee and lower Wauchope subgroups. Small stock-like bodies of granite occur throughout the province, while areally larger muscovite–biotite granites form extensive intrusions marginal to the outcropping area. The larger granite complexes are the Devils Marbles, Hill of Leaders and Elkedra Granites, with the latter two in particular displaying local greisenisation and quartz–aplite veining. Regional metamorphic grade of the Hatches Creek Group is mainly lower greenschist facies, but upper greenschist facies may have been attained locally (Blake & others, 1987).

The Cainozoic surficial sediments consist largely of ferricrete and lateritic gravel, silcrete, calcrete, and poorly consolidated to unconsolidated gravels, sands, silts and clays (Blake & others, 1986). The Fe-rich gravels form cappings up to 3 m thick on Proterozoic and Cambrian rocks and are believed to represent remnants of the upper parts of probable Tertiary weathering profiles. Silcrete occurs on the tops of ridges, hills and mesas. Calcrete, as inorganic cellular limestone, is widespread as patches and probably formed by evaporation of groundwater during the Cainozoic. The poorly consolidated Cainozoic sediments form colluvial, alluvial and aeolian deposits covering most plains and valley floors (Blake & others, 1986).

Gold, Cu, Pb, U and W (± Bi, Cu, Mo and Sn) mineralisation are known in the region, but only Au and W, with minor associated Bi and Cu, have been mined, and this

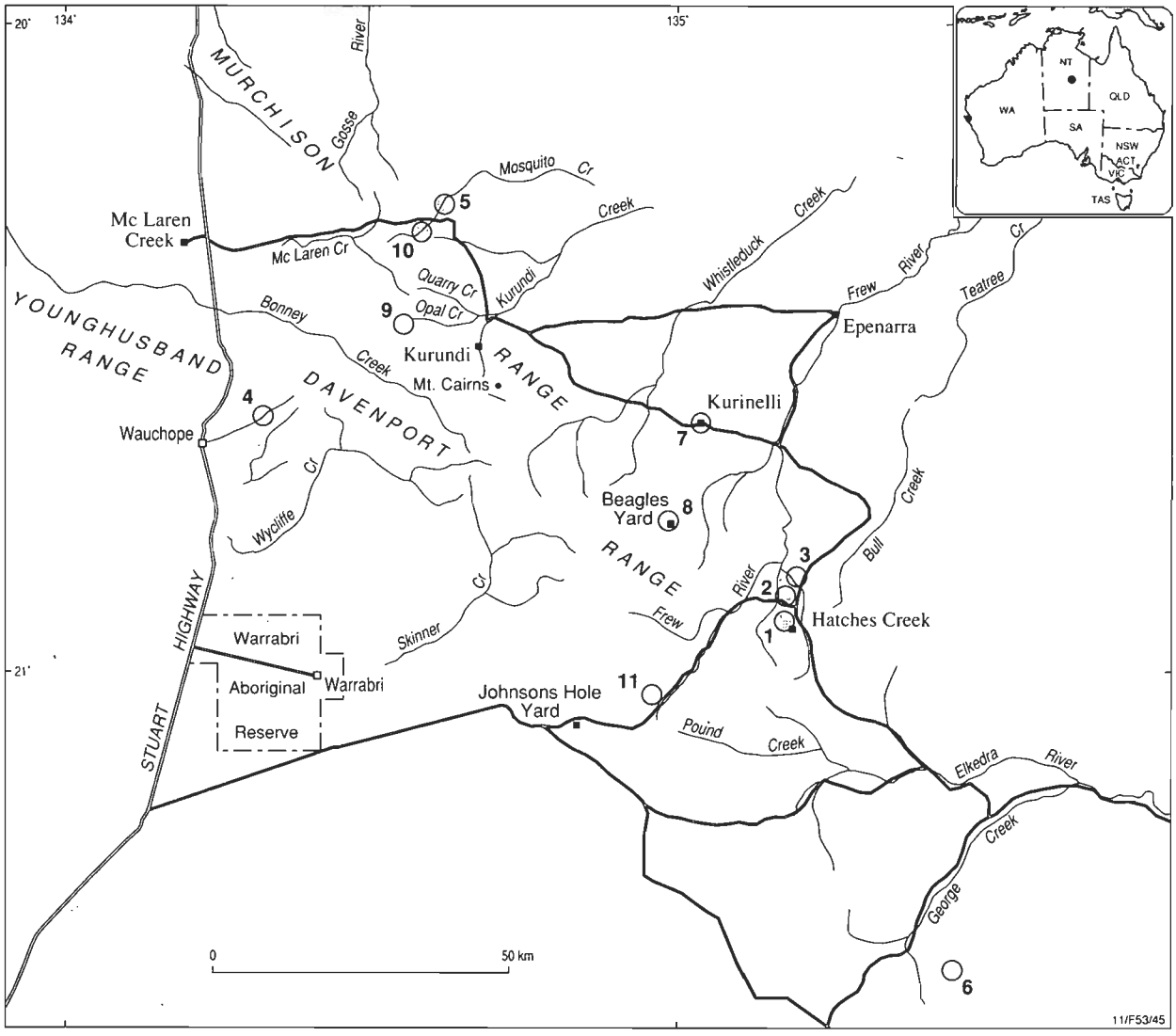

Figure 1. Physiographic map of the Davenport Province showing areas covered in the survey.

(1) Hatches Creek Wolfram Field
(2) Pioneer Mine
(3) Wolfram Hill mines
(4) Wauchope Wolfram Field
(5) Hill of Leaders/Mosquito Creek Wolfram Field
(6) Juggler Wolfram Mine (Elkedra Granite)
(7) Kurinelli Goldfield
(8) Great Davenport Gold Mine and Cairns Gold Prospect
(9) Power of Wealth Gold Mine
(10 Munadgee Uranium Prospect
(11) Silver Valley Lead Prospect

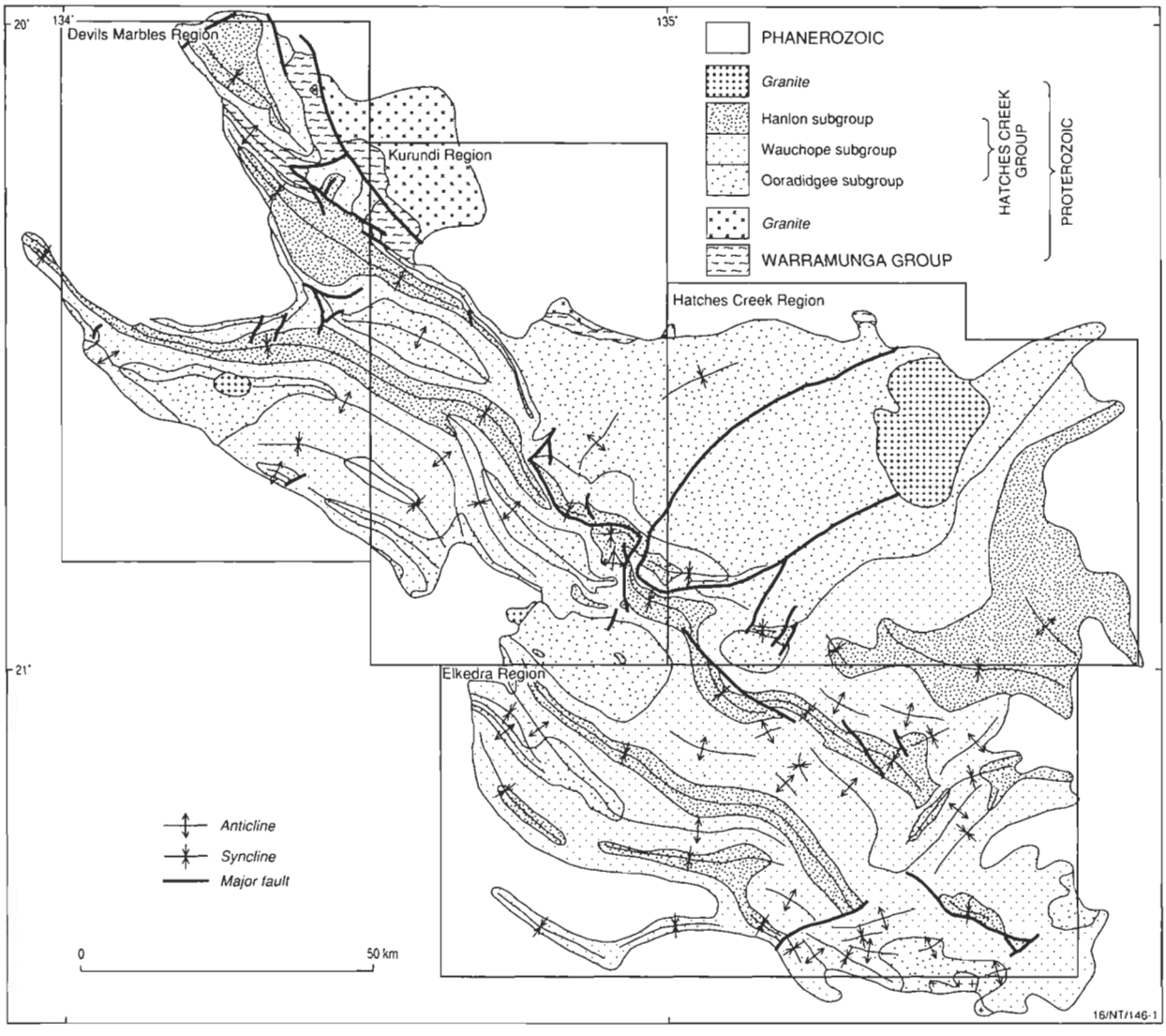

Figure 2. Geological map of the Davenport Province showing the boundaries of the special 1:100 000 map sheet areas.

was intermittent and of small scale. Tungsten mineralisation occurs in a number of styles and settings, ranging from concordant vein swarms within sedimentary–volcanic and/or hypabyssal hosts, to simple vein systems within the upper levels of granitic bodies. Total production of W concentrates from the Hatches Creek and Wauchope Fields has amounted to approximately 4500 tonnes (62–65% WO_3), with about 70 tonnes of Cu and 6 tonnes of Bi concentrates also produced at the Hatches Creek Field (Sullivan, 1952; Ryan, 1961). Other W workings include the Hill of Leaders–Mosquito Creek Field, The Juggler Mine (Elkedra Granite) and the Woodenjerrie Mine (Blake & others, 1987), but no production records are known for these areas.

Gold mineralisation is widely distributed throughout the province but, with the exception of the Kurinelli Goldfield (total recorded production 13.6 kg–Roarty, 1977), the Power of Wealth Gold Mine and the Great Davenport Gold Prospect (Yeaman, 1965: total recorded production 4.7 kg –Smith, 1970; Roarty, 1977), it is isolated and of low tenor.

Minor U mineralisation occurs at the Munadgee Prospect (Lord, 1955; Livingstone, 1957), minor Pb at the Silver Valley Mine/Prospect (Smith & Milligan, 1964), and minor Cu at the Copper Show Mine near Hatches Creek (Ryan, 1961).

Geochemical sampling and analytical procedures

The principal objective of geochemical orientation surveys is to define the patterns of primary and secondary dispersion which occur in the survey area, particularly those of economically or environmentally interesting elements. In geochemical orientation studies, samples from areas of known mineralisation are collected to establish such behaviour, while samples from unmineralised areas are collected to define normal background variations (Hawkes & Webb, 1962). Stream-sediment sampling, involving both sieved fractions and heavy mineral concentrates, is generally considered the most effective technique for regional studies as some form of drainage-dispersal pattern is almost always developed.

In the Davenport Province, stream-sediment sampling was often hindered by confined catchment areas, the restricted length of many streams, and the paucity of fine detritus within the drainage channels because of the dominance of

Table 1. Proterozoic stratigraphy of the Davenport Geosyncline. Data from Blake & others (1987).

Group	*Subgroup*	*Formation (Members)*	*Lithologies*	*Thickness (m)*
		Yaddanilla Sandstone	Quartz arenite, feldspathic quartz arenite	1000?
		Vaddingilla Formation	Siltstone, shale, arenite	ca. 800
		Canulgerra Sandstone	Quartzose-feldspathic arenite, siltstone, mudstone	ca. 500
	Hanlon	Lennee Creek Formation	Siltstone, shale, arenite, calcareous beds	700–1500
		Alinjabon Sandstone	Quartz-feldspathic arenite, siltstone, shale, mafic lava	300–840
		Errolola Sandstone	Quartz-feldspathic arenite	100–1200+
	Conformable contact			
		Kudinga Basalt	Basalt, tuffaceous siltstone, arenite	50–770
		Frew River Formation	Kaolinitic–quartz–feldspathic arenite, dolomite	0–600
		Coulters Sandstone	Quartz–feldspathic–lithic arenite, siltstone, basalt	140–1000+
	Wauchope	Arabulja Volcanics	Felsic lava, tuff	0–500
Hatches Creek		Newlands Volcanics	Dacite, rhyolitic ignimbrite, tuff, agglomerate, arenite	0–2000+
		Yeeradgi Sandstone	Arenite, mudstone, shale, slate, phyllite, felsic lava	0–800
		Unimbra Sandstone	Quartz–lithic arenite, conglomerate	100–1500
	Conformable locally to unconformable contact			
		Mia Mia Volcanics	Felsic ignimbrite, tuff, rhyolitic lava, arenite	2000+
		Treasure Volcanics	Felsic lava, basalt, tuff, arenite	0–1800+
		Taragan Sandstone	Quartz–feldspathic–lithic arenite, siltstone, felsic lava	0–1000+
	Ooradidgee	Edmirringee Volcanics	Basalt, dacite, rhyolite, arenite, siltstone	0–2500
		Kurinelli Sandstone	Feldspathic–lithic–quartzose arenite, siltstone, minor volcanics	0–2600
		Rooneys Formation	Siltstone, arenite, greywacke	0–1200+
		Epenarra Volcanics	Felsic lavas, tuff, agglomerate, arenite	0–3000+
	Unconformity			
Warramunga			Greywacke, siltstone, jasper, chert	10 000+

quartz-rich lithologies throughout the province and the flushing effect of the heavy summer rains. However, soil profiles in areas visited were found to be poorly developed with potentially high aeolian components and this, coupled with the limited mobility of many elements (e.g. Pb, Sn, W, etc) in arid, high pH soils, was considered to preclude soil sampling as part of the regional geochemical survey. Similarly, the style of known mineralisation in the region (i.e. mostly localised small-scale vein systems with weak hydrothermal alteration haloes) renders rock chip sampling impractical because of the high sampling density necessary. Therefore, stream-sediment sampling remains the most effective approach for regional geochemical surveys in the Davenport Province.

Samples were collected from streams draining mineralisation in Hit or Miss Gully, Treasure Gully, Copper Show Mine and the Wolfram Hill mines in the Hatches Creek Field, the Wauchope Field, the Munadgee Uranium Prospect, the Great Davenport and Cairns Gold Prospects, the Power of Wealth Gold Mine, the Juggler Tungsten Mine and the Elkedra Granite, the Hill of Leaders Granite and associated mines, the unconformity between the Warramunga and Hatches Creek Groups in the northwest of the province, and several unmineralised and potentially mineralised areas. Sampling densities near mineralisation generally were one sample per 0.5–1 km of run in the main drainage channel with most well-defined tributaries also sampled. Remote from mineralisation as well as in unmineralised areas, the density was reduced to one sample per 1–2 km of stream run. The Kurinelli Goldfield was not sampled owing to absence of suitable drainage and dominance of aeolian material.

Samples were collected by teams in 4-wheel drive vehicles, although it was often necessary to walk to the actual sample site. Each sample was a 3–5 kg composite from several sites within the stream bed to minimise the effects of local variations due to stream flow/sedimentation mechanics. Coarse material (i.e. >1 mm) was sieved off and discarded. The samples were sent to BMR's laboratories in Canberra for final sieving, grinding and analysis (Hoatson & Cruikshank, 1985).

To determine the most appropriate grain-size ranges for analysis, several samples from sites close to mineralisation were sieved into eight size fractions using aluminium-bodied sieves fitted with nylon bolting cloth (710 μm, 500 μm, 355 μm, 250 μm, 180 μm, 118 μm and 75 μm mesh sizes). In all samples there was insufficient +710 μm

fraction for analysis. Each fraction was finely ground and analysed for As, Bi, Mo, Nb, Pb, Rb, Sn, Sr, Th, U, W, Y and Zr by X-ray fluorescence spectrometry, and for Ag, Be, Co, Cr, Cu, Fe, Li, Mn, Ni and Zn by atomic absorption spectrometry (Table 2). Details of methods are given in Cruikshank & Pyke (1993). The geochemical contrast for most elements was greatest in either the +250–500 μm fraction or the –75 μm fraction (see Results). The remaining samples were sieved for these two grain-size ranges and analysed as above.

The remainder of each sample was passed over a Wilfley table and the light fraction discarded. The resulting concentrate was separated using tetrabromoethane (SG 2.96), after which the heavy fraction was separated on a Carpco Magnetic Separator into magnetic and non-magnetic fractions. Although a low magnet current was used to allow for the moderate magnetic susceptability of wolframite, repeated passes through the separator removed nearly all magnetite, most martite, and also some ilmenite, tourmaline, mica and amphibole. Both the magnetic and non-magnetic fractions were retained for examination under the stereoscopic microscope, and the non- magnetic fraction was also examined under short-wavelength ultraviolet light to check for the presence of scheelite, carbonates, and phosphate- bearing minerals. Grains which could not be identified under the stereoscopic microscope were identified using a petrographic microscope or by X-ray diffraction. Selected samples were qualitatively analysed by optical emission spectrography. The basic technique is labour intensive in comparison to analysis of sieved fractions and requires a high level of skill to identify some minerals, especially when in low abundance.

Results

Stream-sediment sampling effectively defined the area of W and associated Sn (±Bi and Mo) mineralisation at the Hatches Creek and Wauchope Fields where extensive, well-defined dispersion trains were identified. However, there were marked differences in the behaviour of W and Sn due to the mechanical properties of their minerals present in the mineralisation and, therefore, in the stream sediments. Molybdenum and Bi were detected only in close proximity to mineralisation owing to their low abundances in the lodes. Copper, although present in significant concentrations in some ore bodies, showed restricted dispersion, whereas U was not detected even adjacent to exposed, but low-level, U mineralisation. The poor chemical signatures of Cu and U are possibly due to the dominance of chemical weathering processes and greater mobilities of these elements.

The mass of data accumulated during a geochemical survey can be assimilated and interpreted more easily using statistical methods. Such treatments usually assume that sampling is random or unbiased, whereas, in the present orientation survey sampling was deliberately biased towards mineralised areas which have been subjected to mining activity or intensive exploration, thereby greatly increasing the number of 'anomalous' samples, or outliers, in the sample population. Despite this limitation, a number of useful observations can be drawn from an analysis of the available data. Means and standard deviations for the –75 μm fraction are listed in Table 2, and Pearson correlation coefficients in Table 3. A number of elements (i.e. As, Fe, Nb, Pb, Sr, Th, U, Y and Zr) show little variation over the total sample population indicating the absence of 'anomalous' populations of these elements. In contrast, W, Sn and Cu, the principal elements in much of the known mineralisation, show large ranges and standard deviations. Cumulative frequency plots (Sinclair, 1974) of W, Sn and Cu are shown in Figure 3 and suggest background and anomalous populations for each element with threshold values, corresponding to the breaks in slope of the plots, of 7, 4 and 20 ppm, respectively. Threshold values are element concentrations above which geochemical values may be of particular interest for exploration purposes. For Ag, Bi and Mo 'not detected' values (detection limits of 2, 2 and 1 ppm, respectively) formed the greater part of the datasets and hence few parameters have been recorded, but for these elements detected values may be of interest.

Strong mutual correlations ($r>0.60$ and $r<-0.60$) were found between the members of the following three groups:

(i) Rb, W, Bi, Sn, Mo, Be, Cu and Li,

(ii) Co, Cr, Fe, Mn, Ni and Zn, and

(iii) Th, Y, U and Nb

Of these associations, only (i) appears to be of economic significance. Association (ii), and any variation in these elements, appears to be due to the presence of two populations, the low values derived from the ubiquitous quartz–feldspathic sediments and higher values from the mafic volcanics. Association (iii) is usually associated with the presence of resistant detrital minerals, such as monazite and xenotime weathered from granites (Rossiter, 1975).

Heavy mineral concentrates were useful in delineating W-Sn-Cu mineralisation in the province (Hoatson & Cruikshank, 1985). However, because of the complex nature of the bedrock geology, the predominance of quartz-rich arenites (e.g. Unimbra, Errolola, Taragan and Kurinelli Sandstones), and a general absence of diagnostic metamorphic minerals, the heavy mineral samples were not as useful in discriminating geological units in the province as in the Forsayth area of north Queensland (Rossiter, 1983). Heavy minerals of direct economic significance identified in concentrates from the Davenport Province are wolframite, scheelite, cassiterite, bismuthinite, molybdenite, malachite, azurite, chrysocolla, and a molybdenum-bearing variety of scheelite (Table 4), while those of indirect significance are topaz, two varieties of tourmaline, and fluorapatite.

Tungsten

Tungsten mineralisation occurs at Hatches Creek within steeply dipping quartz lodes. The larger deposits (>200 tonnes WO_3) are generally associated with quartz veins cutting the Treasure Volcanics, Kurinelli Sandstone and Taragan Sandstone, dolerite and gabbro, whereas the smaller deposits are usually confined to sedimentary rocks. The lodes are structurally controlled by shears, fracture zones, and intersections of favourable host lithologies. Wolframite is usually the dominant W mineral, but scheelite becomes prominent where gabbro is the host. Associated minerals are tungstite, native bismuth, bismuthinite, bismutite, chalcopyrite, chalcocite, covellite, bornite, tetrahedrite, malachite, azurite, chrysocolla, cuprite, native copper, molybdenite, wulfenite, galena, gold and cassiterite (Ryan, 1961).

At Wauchope, the W mineralisation is in thin quartz veins

Table 2. Summary statistics for analysed elements in all (N = 415) –75 μm fractions of stream-sediment samples collected in the Davenport Province. Concentrations in parts per million (ppm).

Element	*Arithmetic Mean (AM)*	*Standard Deviation (SD)*	*Geometric Mean (GM)*	*Geometric Deviation (GD)*	*Maximum value (X)*	*Median (M)*	*Analytical Method (DL)#*
Ag*	–	–	–	–	2	–	AAS (1)
As	3.30	1.26	3.12	1.390	12	4	XRFS (1)
Be	1.67	1.19	1.46	1.648	10	1	AAS (1)
Bi**	–	–	–	–	48	–	XRFS (2)
Co	6.99	3.53	6.29	1.658	26	7	AAS (3)
Cr	35.0	28.1	30.9	1.510	286	28	AAS (3)
Cu	21.5	32.3	15.2	1.917	322	13	AAS (2)
Fe	19000	5026	18410	1.284	58000	17500	AAS (–)
Li	14.2	10.6	12.5	1.572	143	12	AAS (1)
Mn	203.9	100.0	184.4	1.550	897	179	AAS (2)
Mo***	–	–	–	–	14	–	XRFS (2)
Nb	11.6	2.20	11.3	1.248	24	11	XRFS (2)
Ni	11.2	9.84	9.33	1.720	88	9	AAS (2)
Pb	12.5	2.72	12.1	1.299	25	12	XRFS (2)
Rb	96.6	49.0	87.1	1.640	328	80	XRFS (2)
Sn	4.41	10.0	2.72	2.558	96	2	XRFS (2)
Sr	59.0	20.4	56.4	1.385	282	56	XRFS (2)
Th	16.0	4.24	15.4	1.369	44	16	XRFS (2)
U	3.85	1.19	3.67	1.390	9	4	XRFS (1)
W	24.4	136.2	4.34	3.980	2188	4	XRFS (3)
Y	36.7	8.50	35.4	1.387	83	36	XRFS (2)
Zn	30.8	13.9	28.5	1.463	115	28	AAS (2)
Zr	1297	364.9	1228	1.586	3320	1250	XRFS (3)

* Ag content below detection limit (1 ppm) in 347 samples.

** Bi content below detection limit (2 ppm) in 324 samples.

*** Mo content below detection limit (2 ppm) in 408 samples.

\# XRFS = X-ray fluorescence spectrometry
AAS = Atomic absorption spectrophotometry
DL = 'Detection Limit' in ppm.

which are generally conformable with bedding in sediments of the Hatches Creek Group. No volcanic rocks or gabbro–dolerite have been recorded. Host rocks belong to the Taragan Sandstone and include gently dipping silty mudstones, laminated siltstones with sandy lenses, arenites and various hornfelsed variants of these. Kaolinisation wallrock alteration is locally intense, and some tourmaline, topaz and hematite have been introduced. Ore minerals are wolframite, trace scheelite, pyrite, chalcopyrite, molybdenite and bismuthinite (Sullivan, 1952).

Stream-sediment samples from the Hatches Creek area (Fig. 4) and from Wauchope Creek downstream from the Wauchope Field (Fig. 5) usually gave W values much higher than the 7 ppm threshold, and the anomaly persisted for at least 10 km down Wauchope Creek. Adjacent to the Wauchope mine, high W values occur in both fine and coarse sieve fractions with a pronounced minimum centred on the 118–180 μm fraction. About 3.5 km downstream from the mine, W has disappeared from the coarser fractions due to the pulverising of the brittle W-bearing minerals during alluvial transport (Fig. 6). Similar profiles were found in size fraction plots for samples from Hit or Miss Gully at Hatches Creek (Fig. 7). This behaviour during transport and the presence of much detrital wolframite and scheelite in heavy mineral concentrates indicates that dispersion occurs by mechanical, rather than chemical, processes (Rossiter, 1975). Wolframite and scheelite are both relatively insoluble under the conditions prevailing in most surface waters (Krauskopf, 1970). Also, in streams draining the Devils Marbles near the Wauchope Field, banks of coarse stream sediment contained copious quantities of unweathered feldspar grains, thus confirming the importance of mechanical weathering processes.

Detrital wolframite was the dominant W mineral in heavy mineral concentrates from Wauchope and Hatches Creek (Table 4). However, where W- rich quartz vein lodes cut granite as at Wolfram Hill (1–2 km north of Hatches Creek), the Hill of Leaders mines in the north of the province, and near the Juggler Mine on the Elkedra Granite in the south, scheelite is the dominant W-bearing mineral.

The strong statistical correlation between W and Cu, Bi, Sn, Mo, Rb, Li and Be (Table 3) is reflected in an equally strong spatial correlation of values for these elements in samples from the Hatches Creek and Wauchope areas (Figs 4 & 5–Li and Be are not shown for Hatches Creek Field). Copper and Bi minerals — and at Hatches Creek, Sn and Mo-bearing minerals — have been identified in the mineralisation (Sullivan, 1952; Ryan, 1961). Correlations with Rb, Li and Be suggest that the mineralisation was derived from a pegmatitic or other fractionated granitic source (Levinson, 1974), as does the widespread occurrence in heavy mineral concentrates from both locations of topaz and two varieties of tourmaline (i.e. schorl and

Table 3. Pearson correlation coefficients (raw data) for elements in the –75 μm fractions of the Davenport stream-sediment samples (N=415). Strong correlations (r>0.60) are in bold and indicate possible geochemical associations.

Th	*Rb*	*Pb*	*Y*	*U*	*As*	*W*	*Bi*	*Sr*	*Sn*	*Nb*	*Zr*	*Mo*	*Ag*	*Be*	*Co*	*Cr*	*Cu*	*Fe*	*Li*	*Mn*	*Ni*	*Zn*	
0.25	0.42	**0.80**	**0.70**	0.18	0.05	–.03	0.08	0.13	**0.67**	0.53	0.03	0.04	0.19	–.08	–.20	–.02	0.00	0.16	–.01	–.23	–.04	Th
	0.20	0.27	0.19	0.05	0.51	**0.67**	0.35	**0.82**	0.44	–.13	0.43	0.12	**0.86**	0.19	–.07	**0.70**	0.39	**0.72**	0.41	–.07	**0.65**	Rb
		0.46	0.38	0.34	0.23	0.18	0.34	0.17	0.39	0.05	0.24	0.11	0.18	0.27	–.02	0.02	0.19	0.30	0.19	0.00	0.18	Pb
			0.70	0.23	0.07	0.09	0.10	0.16	**0.64**	0.48	0.07	0.07	0.22	0.10	–.12	0.07	0.19	0.17	0.19	–.13	0.10	Y
				0.25	0.10	0.06	0.04	0.12	0.54	0.48	0.10	0.01	0.12	–.08	–.15	0.01	–.03	0.15	0.03	–.19	–.07	U
					0.25	0.01	0.28	0.03	0.30	0.05	0.15	0.21	0.01	0.20	0.04	–.03	0.23	0.25	0.14	0.04	0.10	As
						0.67	0.51	**0.65**	0.31	–.03	**0.84**	0.08	0.43	0.06	–.02	0.30	0.13	**0.73**	0.24	–.02	0.35	W
							0.29	**0.77**	0.25	0.04	**0.64**	0.02	**0.61**	0.08	–.04	**0.67**	0.24	0.53	0.29	–.04	0.55	Bi
								0.41	0.30	–.16	0.41	0.11	0.32	0.31	0.06	0.11	0.22	0.56	0.31	0.10	0.29	Sr
									0.33	0.01	**0.60**	0.05	**0.73**	0.09	–.05	**0.68**	0.27	0.09	0.35	–.06	0.56	Sn
										0.40	0.24	0.07	0.41	0.03	–.19	0.15	0.16	0.38	0.16	–.20	0.23	Nb
											–.01	–.08	–.11	–.29	–.18	0.01	–.25	–.15	–.14	–.22	–.18	Zr
												0.02	0.37	0.04	–.02	0.30	0.13	0.51	0.18	–.02	0.30	Mo
													0.05	0.08	0.00	0.00	0.05	0.17	0.10	–.03	0.07	Ag
														0.23	–.02	**0.65**	0.42	**0.63**	0.46	0.00	**0.66**	Be
															0.55	0.18	**0.74**	0.27	**0.67**	**0.85**	0.50	Co
																0.05	0.42	0.07	0.36	**0.94**	0.16	Cr
																	0.38	0.38	0.39	0.06	**0.62**	Cu
																		0.31	**0.67**	0.51	**0.68**	Fe
																			0.45	0.08	0.50	Li
																				0.42	**0.64**	Mn
																					0.23	Ni
																						Zn

dravite). The two tourmalines appear to coexist, and topaz is abundant, only near W–Sn mineralised areas at Hatches Creek and Wauchope. They are probably derived from wall rock alteration (e.g. greisenisation) associated with the hydrothermal veining. The schorl–dravite–topaz association, therefore, appears to be a useful indicator for W–Sn mineralisation.

Tungsten values are low (20–25 ppm) immediately downstream from the Hill of Leaders Field and the Juggler Mine. At Hill of Leaders, strong spatial and statistical correlations were apparent between W, Sn, Bi and Cu, but these associations are weaker and more diffuse at the Juggler Mine. Scheelite was the dominant W mineral in heavy mineral concentrates from both areas and while schorl and dravite were abundant, topaz was rare or not observed. Fluorapatite was confined to samples from these areas and, although its relationship to the mineralisation is not clear, it appeared to be associated with scheelite. No enrichment in Sn, Cu, Bi, Mo, Rb, Li or Be was evident in stream sediments from Hill of Leaders. Low level Sn, Bi and Be anomalies occurred over the Elkedra Granite, although not immediately downstream from the Juggler Mine.

Sampling programs for W can be based on collection and analysis of fine (–75 μm) or coarse (+180 –500 μm) sieved sediment, or on visual examination of heavy mineral concentrates for W-bearing and associated minerals. Visual examination of heavy mineral concentrates is labour intensive and, therefore, analysis of the fine sieved fraction is probably the most efficient and economical approach. Given the rather lengthy dispersion trains from the Wauchope and Hatches Creek Fields, a sample spacing of 1 to 2 km should be adequate to define W mineralisation in the province.

Tin

The dispersion of Sn is also controlled by the mechanical and chemical stability of its major mineral, cassiterite. Cassiterite is abundant and widespread in heavy mineral concentrates from Wauchope, and from Treasure Gully at Hatches Creek. At both locations, Sn initially concentrates in the coarser fractions of the sieved sediments, but moves to finer fractions with transport as shown down Wauchope Creek (Fig. 8), due to the mechanical pulverising of the cassiterite grains.

Although there is a shift in abundance of Sn to finer fractions with distance from mineralisation, the highest values were found in the coarser fractions. Thus, a program seeking Sn mineralisation should be based on coarse sediment (+180 –500 μm) sampling at spacing of 1 to 2 km. Visual examination of heavy minerals for cassiterite can also be used, but is considered to be less economical.

Bismuth and molybdenum

Bismuthinite and minor amounts of molybdenite were observed in heavy mineral concentrates from Hit or Miss Gully at Hatches Creek. Bismuth and Mo concentrated in the coarser fractions of the sieved sediments regardless of distance from mineralisation, possibly because of the ductility of the minerals. At Wauchope, Bi and Mo values are much lower than in Hit or Miss Gully, although anomalous levels of Bi persisted for some 3 to 4 km down Wauchope Creek.

The coarser fractions of sieved sediments are necessary for Bi (+250 –500 μm) and Mo (+180 –500 μm). Bismuthinite and molybdenite are easier to identify in heavy mineral

concentrates than wolframite, scheelite and cassiterite because of their platy form and metallic lustre.

Other elements associated with W mineralisation

Rubidium, Li and Be display similar distribution patterns to W and, along with Sn, Bi, Mo, and, to a lesser extent Cu (see below), can be used as pathfinder elements for W mineralisation. These elements are more prominent in the

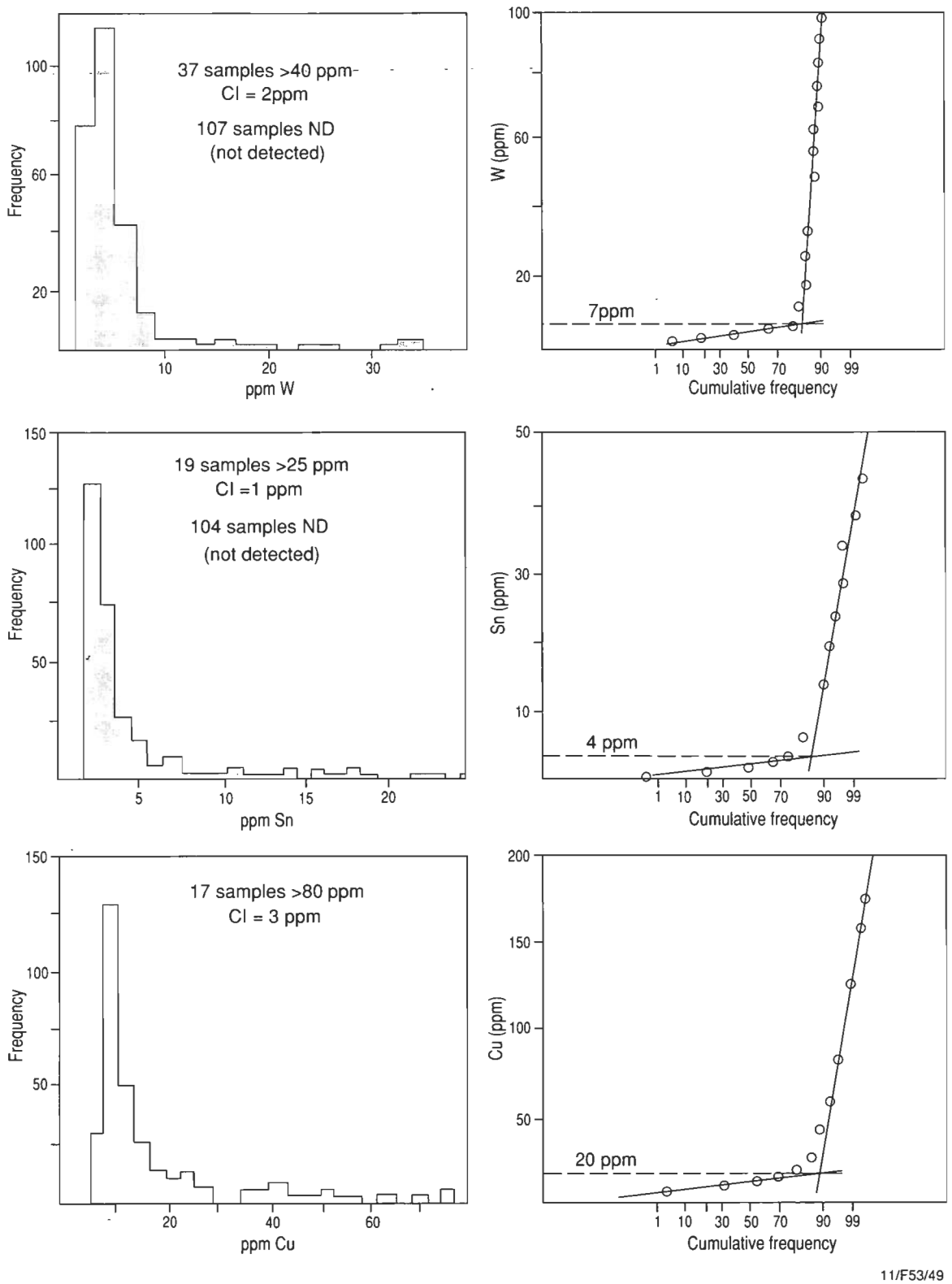

Figure 3. Histograms and cumulative frequency plots for W, Sn and Cu in the –75 μm fraction of all sieved stream-sediment samples collected. The break in the slope of the cumulative frequency plots is the 'threshold' value.

Table 4. Distribution of heavy minerals of economic significance.

Mining Centre	*Wolframite*	*Scheelite*	*Cassiterite*	*Bismuthinite*	*Molybdenite*	*Malachite*	*Azurite*	*Chrysocolla*	*Schorl*	*Dravite*	*Topaz*	*Fluorapatit*
(1) Hatches Creek												
Hit or Miss Gully	A	M	M	R	M	C	R	N/O	C	M	C	N/O
Treasure Gully	M	N/O	A	N/O	N/O	N/0	N/O	N/O	M	M	M	N/O
Copper Show Mine	M	R	R	N/O	N/O	M	M	R	R	R	N/O	N/O
(2) Wolfram Hill	C	A	N/O	R	M	M	C	N/O	M	M	N/O	N/O
(3) Wauchope	A	R	A	N/O	N/O	R	R	N/O	M	R	A	R
(4) Hill of Leaders	R	A	N/O	N/O	N/O	N/O	N/O	N/O	A	C	N/O	R
(5) Juggler Tungsten Mine	N/O	A	N/O	N/O	N/O	N/O	N/O	N/O	A	M	R	M
(6) Power of Wealth Gold Mine	N/O	N/O	N/O	N/O	N/O	N/O	N/O	N/O	R	M	N/O	N/O
(7) Great Davenport Gold Prospect	N/O	N/O	N/O	N/O	N/O	N/O	N/O	N/O	C	A	N/O	N/O

A = abundant
C = common
M = minor
R = rare
N/O = not observed

coarser sieved fractions (Table 5).

Copper

Copper mineralisation is scattered throughout the Davenport Province but, apart from the southern part of the Hatches Creek Field, the reported occurrences are of little economic significance. Copper minerals have been observed in vesicles in Kudinga Basalt, 19 km southeast of Kurundi Homestead (Smith, 1970). Secondary Cu minerals occur in quartz veins 19 km east of Murray Downs Homestead (Smith & Milligan, 1964), and a narrow vein of chalcocite has been reported west of Elkedra station (Smith & Milligan, 1966). Turquoise has been mined at the Tosca Mine in the Elkedra area (Blake & Horsfall, 1987).

Downstream from the Copper Show Mine at Hatches Creek (Fig. 4), and in Wauchope Creek (Fig. 5), Cu has a relatively short dispersion train of 2 km or less, beyond which values fall below the threshold value of 20 ppm. Proximal Cu values were low in both, surprisingly so near the Copper Show Mine (2.5–4.5 times threshold), although azurite, malachite and chrysocolla were identified in heavy mineral concentrates from these two areas (Table 4). No detrital Cu sulphide minerals were observed. The short dispersion train and low initial values could be due to Cu, released during oxidation of ore-body sulphide minerals, being largely flushed out during the wet season as these sediments appear to have little finely divided material (clays or hydrated oxides) to adsorb the Cu ions. The secondary minerals are very friable and would be quickly pulverised during alluvial transport.

During the survey, a small pocket of secondary Cu minerals was found in siltstones of the Rooneys Formation, close to the Elkedra Granite. Even though the mineralisation was exposed, no Cu anomaly was detected in a stream sediment less than 1 km downstream. The mineralisation has little economic significance, but its presence underlines the potential difficulties in interpretation caused, firstly, by such small pockets of mineralisation and, secondly, by the limited secondary dispersion of Cu.

Copper background levels are variable, with values usually less than 10 ppm in areas draining sedimentary rocks and felsic volcanics and 10 to 20 ppm where mafic volcanics are present.

In the immediate vicinity of mineralisation, Cu is equally present in both coarse and fine fractions of the sieved sediment — but at a distances greater than 1 km, the Cu response is very muted and virtually confined to the fine (–75 μm) fraction. For this reason, the fine fraction should be sampled at sample spacings of 0.5 to 1 km, or less. Heavy mineral concentrates are more useful, because the secondary Cu carbonate minerals are readily identified by their vivid colours (Table 6).

Gold

Gold-bearing quartz lodes are restricted to the Kurinelli Sandstone, Rooneys Formation and Epenarra Volcanics of the Hatches Creek Group, and to dolerite, gabbro and granophyre bodies intruding these units. Stream-sediment sampling was carried out downstream from the Great Davenport Mine and Cairns Prospect (Fig. 9), and the Power of Wealth Mine (Fig. 10).

At Great Davenport, patchy flake and coarse gold, the latter associated with pyrite and oxidised pyritic boxworks, occur in quartz veins cutting the Kurinelli Sandstone (Yeaman, 1965). At the Cairns Prospect, 6 km to the southeast, thin quartz and quartz–hematite–magnetite veins cut altered porphyritic granophyre, and arenite and siltstone of the Kurinelli Sandstone. The mineralisation at the Power of Wealth Mine is in intense quartz veining within the Kurinelli Sandstone and Epenarra Volcanics. Surface expression of the mineralisation is poor, and even at the 30 m level, where the highest grades occur, the mineralisation is patchy and discontinuous.

No free gold was observed in streams draining Great Davenport and the Cairns Prospect (Fig. 9). However, Au was detected by optical emission spectrographic analysis of heavy mineral concentrates from streams draining both

prospects. Interesting near Great Davenport is the concentration of low-level Au values to the southwest of the mine in streams draining rhyolite of the Treasure Volcanics and arenite of the Taragan Sandstone and Unimbra Sandstone. Of the other elements analysed, only As has any obvious spatial correlation with Au. Arsenic shows weak anomalies (up to 9 ppm) close to the mineralisation, but falls to background levels (3–4 ppm) within 1–2 km of the mineralisation. Hence, As appears to have limited application as a pathfinder for Au.

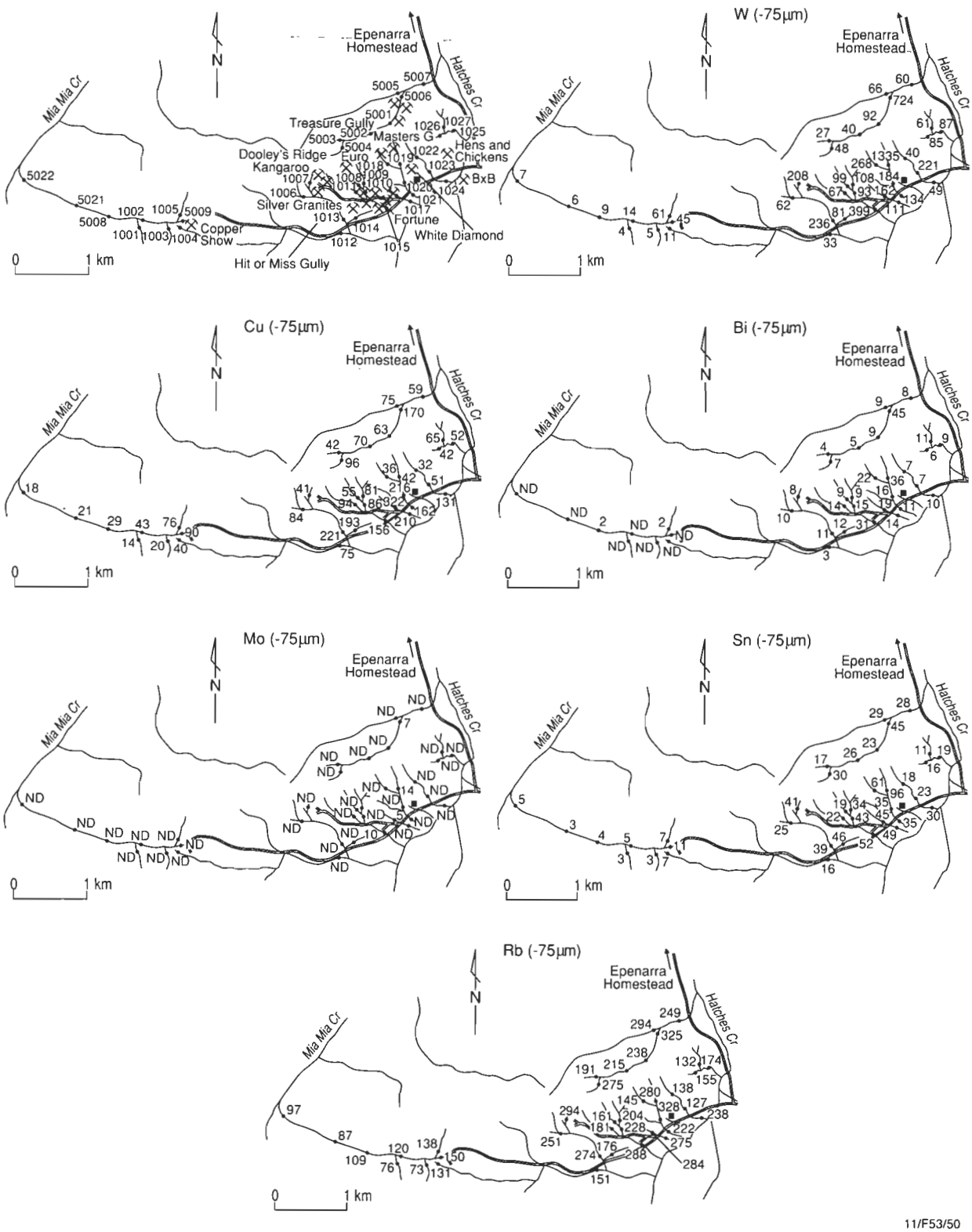

Figure 4. (a) Location of mines and sample sites in the area of the Hatches Creek Field. (b-g) Values for W, Cu, Bi, Mo, Sn and Rb, respectively. ND = 'Not detected'

Gold was also detected by emission spectrography in heavy mineral concentrates from streams draining the Power of Wealth Mine, in the headwaters of Opal Creek and in several streams draining the area of intense quartz veining (Fig. 10). Arsenic remains at background levels (3–4 ppm) in all samples from the survey area with no obvious enrichment near the Power of Wealth Mine. This is not surprising since the sulphide content of the Power of Wealth lode is much lower than the Great Davenport lode. Moderate local Cu anomalies (>10 ppm) are probably related to the Edmirringee and Kudinga Basalts, as samples from streams draining the Kurinelli Sandstone Formation and Epenarra Volcanics rarely exceed 10 ppm Cu.

Uranium

Autunite, torbernite and carnotite mineralisation occurs within a sheared porphyry intruding the Warramunga Group at Munadgee. The mineralisation occurs on a ridge, drained by short gullies on its western side only (Fig. 11). Uranium in all size fractions was low (generally <3 ppm), with slightly anomalous values (4 to 6 ppm) in some

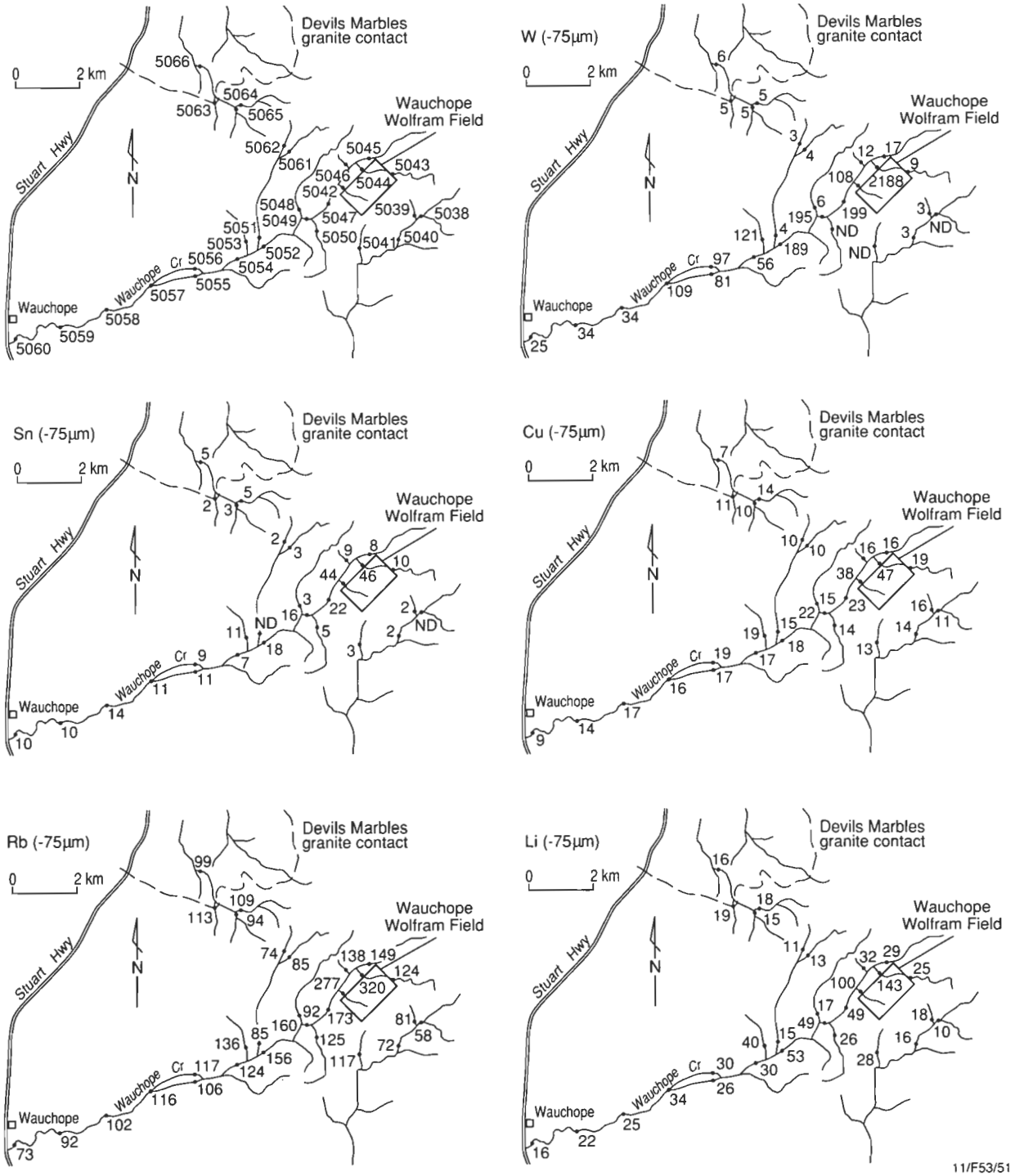

Figure 5. (a) Location of mineral field and sample sites in the area of the Wauchope Field. (b-f) Values for W, Sn, Cu, Rb and Li, respectively.

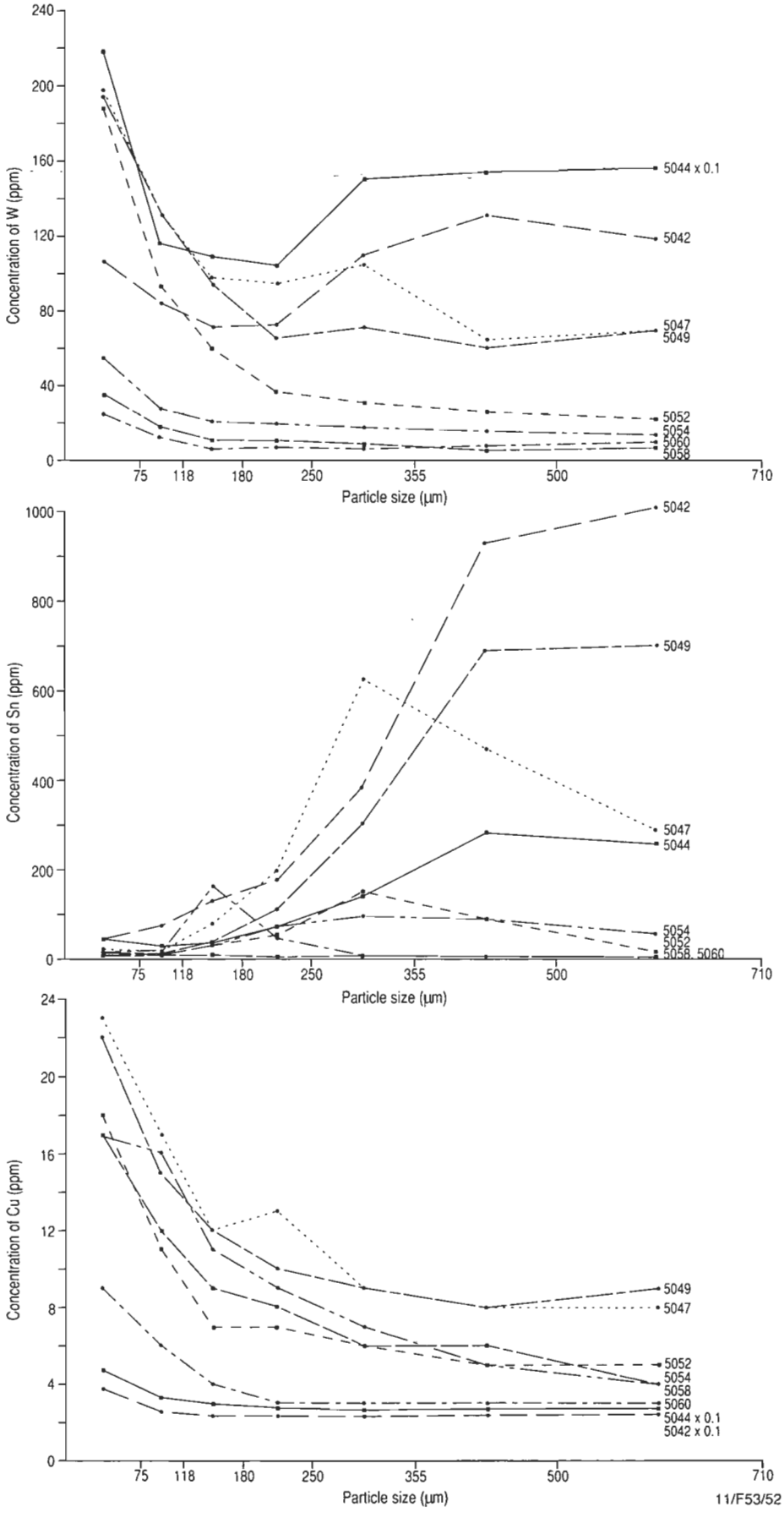

Figure 6. Concentration/particle size plots for the Wauchope Field for W (a), Sn (b), and Cu (c).

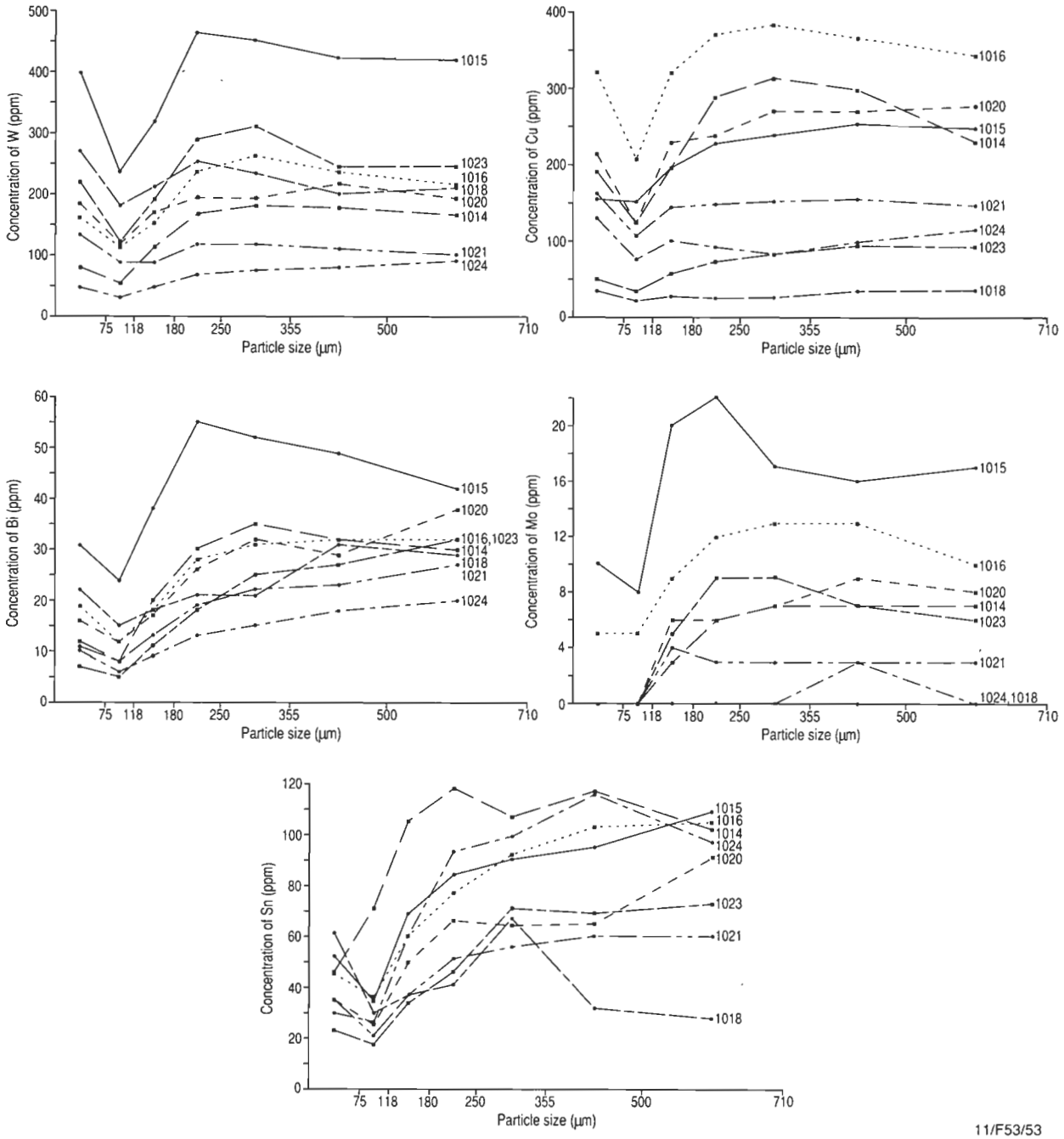

Figure 7. Concentration/particle size plots for the Hatches Creek Field for W (a), Cu (b), Bi (c), Mo (d), and Sn (e).

samples draining the ridge. The low levels in the sieved fractions can be attributed to the limited surface expression of the mineralisation and to the extreme solubility and mobility of the UO_{22+} ion in arid environments (Hawkes & Webb, 1962). Pathfinder elements characteristic of vein-type U deposits, such as As, Bi, Co, Cu, Mo and Ni (Levinson, 1974), give little indication of the Munadgee U mineralisation. No secondary U minerals were observed in the heavy mineral concentrates, and scans of the concentrates with a scintillometer gave no response.

One sample, from about 1 km to the southwest of the prospect, showed anomalous values for Bi, Cu, Sn and W, but the U value was about average for the area. The source of this anomaly is not known.

Neither sieved sediments nor heavy mineral concentrates defined the known mineralisation adequately or unambiguously, even in close proximity to the exposed mineralisation. Sample spacings of less than 0.5 km for fine (–75 μm) sieved sediments would be necessary to have any chance of detecting mineralisation.

Discussion

Despite limitations imposed by restricted drainage, stream-sediment sampling is a useful geochemical exploration technique in the Davenport Province. Both sieved fractions

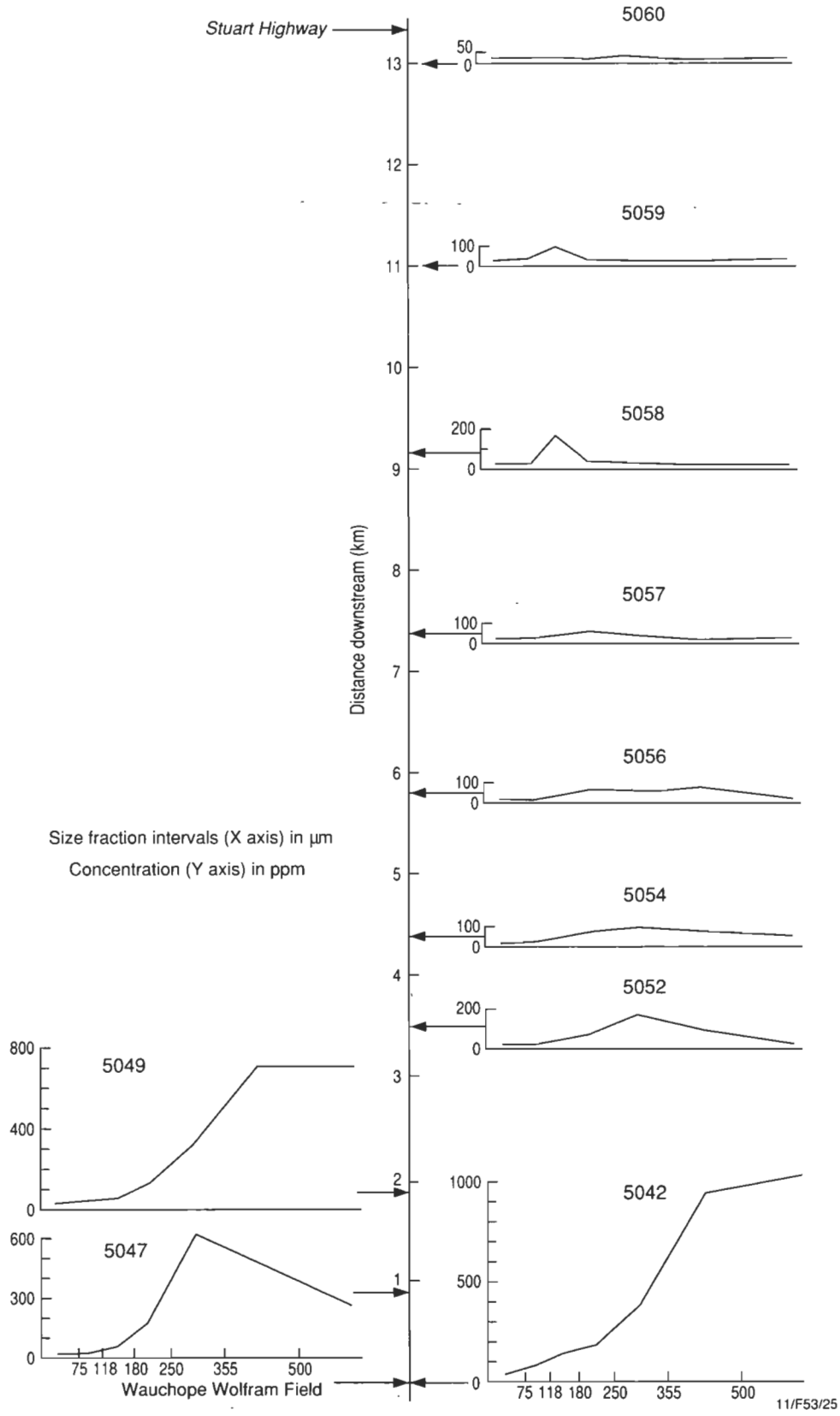

Figure 8. Longitudinal section showing the distribution of Sn in stream-sediment size fractions along Wauchope Creek. Arrows indicate approximate positions of samples downstream from the Wauchope Wolfram Field. Size fraction intervals (X-axis) in µm; concentration (Y-axis) in ppm.

Table 5. Summary of the stream-sediment geochemical survey, Davenport Province.

Styles of mineralisation	*Useful element associations*	*Optimum sieve fractions(μm)* *Near source*	*Remote from*	*Heavy mineral indicators (in order of frequency)*	*Application of heavy minerals*
(1) Wolframite/scheelite vein-type in sediment, or mixed sediment–volcanic/intrusive host	Cu, Bi, Mo, Sn, Be, Rb and Li	W –75, +180–500 Cu –75, +180–500 Bi +500 Mo +180–500 Sn +180–500 Li +180–500 Be +180 Rb +180	–75 (>13 km) –75 (1 km) –75 (3 km) +180–500 (>13 km) –75 (>13 km) –75 (3 km) –75 (>13 km)	Wolframite Malachite Cassiterite Topaz Schorl Dravite Scheelite Azurite Bismuthinite Molybdenite	Malachite and azurite readily identified by vivid green–blue colours: metallic lustre of the bismuth–molybdenum minerals assists rapid identification: cassiterite and topaz diagnostic of sediment host and, because of stability in secondary dispersion, are excellent indicators
(2) Scheelite vein, disseminated type, in granite host	Sn, U, Nb, and Bi	Sn +250–500 U –75 Nb –75 Bi +250–500		Scheelite Schorl Dravite Fluorapatite Topaz Wolframite Cassiterite (?)	Scheelite and fluorapatite readily identified by fluorescence under short wave length UV light
(3) Vein–type gold (Au) in sediment host	As (?)	As –75		Dravite (?) Schorl	Little application
(4) Vein–type gold (Au) in granophyre-sediment host	As(?)	As –75		–	

and heavy mineral concentrates should be considered.

Sieved fractions

Mechanical weathering processes appear dominant in the dispersion of W, Sn, Bi and Mo. This is indicated by the presence of W and Sn in the coarser of the sieved fractions in samples from near mineralisation and by their subsequent movement to the finer fractions during alluvial transport. Wolframite, scheelite and cassiterite are all relatively stable under the prevailing weathering conditions, but wolframite and scheelite are very brittle due to their perfect cleavage. Cassiterite is more resistant than the W minerals; hence Sn is less prominant in the finer fractions than W. Grains of wolframite in heavy mineral concentrates frequently show little evidence of rounding or solution. Tungsten and Sn have dispersion trains which persisted for more than 13 km down Wauchope Creek (Fig. 5), although the lengths of the trains were no doubt enhanced by the mining activity upstream. Bismuth and Mo appear to remain in the coarser fractions, possibly because their major minerals (bismuthinite and molybdenite) are ductile and hence not easily pulverised during transport, although they are relatively unstable in the weathering environment and may be oxidised releasing soluble Bi and Mo species. In the Davenport Province, stream-sediment samples at 1 to 2 km spacings along a drainage system should detect the presence of the W-Sn-Bi-Mo mineralisation, especially if more than one size fraction (e.g. –75 μm and +250 –500 μm) was separated and analysed.

Chemical processes appear to be dominant in the dispersion of Cu and U, as shown by relatively low values for these elements in stream sediments close to mineralisation and by short dispersion trains. This is evident at the Copper Show Mine where stream-sediment Cu values are surprisingly low, and at the Munadgee Uranium Prospect where no U anomalies were clearly defined, even adjacent to exposed mineralisation. These elements are probably taken into solution during weathering and flushed out of the stream sediment during the wet season. This effect would be compounded by the relative paucity in the sediments of finely divided clay material, organic matter, and hydrated oxides of Fe and Mn which otherwise might concentrate these elements by either adsorption or coprecipitation as in more tropical climates (Rossiter, 1975). Relatively high, but not anomalous, levels of Cu and U are found in many streams draining mafic volcanics and granites, respectively. Since Cu and U levels associated with mineralisation are only slightly anomalous, this factor tends to complicate delineation of anomalies. Hence, Cu and U anomalies are more difficult to detect than W or Sn anomalies, and their detection requires denser sample spacings of 0.5 to 1 km, or less.

Pathfinder elements are limited to Be, Li and Rb for W and Sn mineralisation and possibly As for Au mineralisation, especially for sulphide-bearing lodes.

A summary of the stream-sediment geochemistry is given in Table 5.

Heavy mineral concentrates

Heavy mineral concentrates are a valuable tool for defining W, Sn and Cu mineralisation in the Davenport Province (Hoatson & Cruikshank, 1985). The observed distribution of heavy minerals of economic importance is summarised in Table 4, together with that of a number of heavy minerals of indirect economic importance, namely topaz, two varieties of tourmaline and fluorapatite. Heavy minerals associated with each style of mineralisation are summarised in Table 5, and descriptions of typical grains of these minerals are given in Table 6. Gold was not observed in any of the heavy mineral concentrates, including those from streams draining Au mines or prospects. Similarly, no

secondary U minerals were found in concentrates from streams draining the Munadgee Prospect.

Table 6. Descriptions of heavy minerals found in concentrates from the Davenport region.

Mineral	*Description*
W minerals	
Wolframite	Grains generally brownish-black to black with brownish black streak and weakly magnetic. Grains from Hatches Creek commonly elongated (up to 3 mm in length) with a 'splintery' appearance. Grains from Wauchope have shorter and more prismatic, tabular habit. Small grains showed no evidence of rounding.
Scheelite	Forms small (generally less than 1 mm), irregularly shaped, honey-brown (volcanic hosts) to milky white (granitic hosts) grains with uneven fracture and vitreous lustre. Fluoresces blue-white and at Hatches Creek, yellowish blue (indicating a molybdic variety).
Cu minerals	
Malachite	Forms small (generally less than 1 mm) irregular, vivid green grains, easily seen under the microscope. Often with limonitic fragments.
Azurite	As for malachite except coloured blue.
Sn minerals	
Cassiterite	Grains prismatic in habit about 1 mm long; well shaped near the source, subrounded downstrean, indicating strong resistance to chemical and mechanical weathering. Colour ranges from almost colourless, through pinkish-red, reddish-brown and brownish-black to black. Some grains are colour zoned.
Bi and Mo minerals	
Bismuthinite	Rare, brittle platy grains found proximal to mineralisation.
Molybdenite	Rare, occurring as small (less than 1 mm), scaly plates which have burred, compressed margins due to abrasion during transport.
Minerals of indirect economic interest	
Tourmaline	Two types (schorl and dravite) noted. Schorl (Fe-rich) is invariably dark-brown to black and strongly pleochroic from reddish-brown to bluish-green (under polarising microscope). Dravite (Mg-rich) is clear to tan-brown and moderately pleochroic from yellow to brown. Grains near source are elongate, prismatic, have striated faces and are rarely terminated.
Topaz	Grains about 1 mm across; readily identified by coarse, blocky shape, frosted appearance and yellow, orange or red colour, or are colourless and glassy. Distinguished from ferruginised quartz by subhedral shape and coarser grain size.
Fluorapatite	Rare, readily identified by strong pale yellow to golden fluorescence, small irregular grains, usually transparent to milky white.

Conclusions

Stream-sediment sampling is an effective exploration technique for Au, Bi, Mo, Sn and W mineralisation in the Davenport Province, less effective for Cu mineralisation, and ineffective for U mineralisation.

For Bi, Mo, Sn and W, parallel analysis of the +180 –500 µm and –75 µm sieved fractions would be most informative, but would double the cost of any sampling and analytical program. On balance, the coarser (+180 –500 µm) sieved fraction at a spacing of one sample every 1 to 2 km of stream run is preferred. These elements appear to be dispersed by mechanical processes and enter the sediment in the coarser fractions but, with the exception of Sn, concentrate in finer fractions at distance from the source (Table 5). Prospective areas may be defined by Be, Li and Rb highs, indicating the possible presence of pegmatitic or fractionated granites.

While visual examination of heavy mineral concentrates is also a very effective technique, it is considered to be less cost effective than analysis of sieved fractions due to the level of skill necessary to identify the W and Sn minerals and the general labour intensiveness of the technique.

Stream-sediment sampling is less effective for Cu and U, which appear to be dispersed by chemical processes. For Cu, the fine (–75 µm) sieved fraction is preferred at a close spacing of one sample per 0.5 to 1 km, or less, of stream run. The vividly coloured secondary Cu minerals are easily identified in heavy mineral concentrates and this technique may be cost effective, if only to confirm sieved fraction anomalies. Uranium mineralisation could not be definitely defined by either sieved fractions or heavy mineral concentrates.

Free gold was not found in any of the heavy mineral concentrates, but was detected by optical emission spectrographic analysis of concentrates. Although not carried out in this study, it is considered that bulk cyanide leach followed by a sensitive analytical technique, such as either graphite furnace atomic absorption spectrophotometry (GF–AAS) or inductively coupled plasma-mass spectrometry (ICP–MS), would be highly effective for samples from the province. Arsenic is a pathfinder for gold/sulphide mineralisation.

Acknowledgements

The authors wish to acknowledge K. Mitchell, G. Newman, N. Young, B. Zimmerman (BMR), G. Stewart and G. Gric (NTGS) who assisted with the collection of samples, and W. Pappas, J.A. Haldane and T.I. Slezak (BMR) who assisted with sample preparation and analysis. The cooperation of D. Guy, who assisted with heavy liquid separations, and J. Kamprad and M. Duggan with identification of mineral grains, is acknowledged. D.H. Blake, J.W. Sheraton, A.J. Stewart and A.L. Whitaker (all AGSO) are thanked for their invaluable comments on the manuscript.

References

Blake, D.H., & Horsfall, C.L., 1987 — Elkedra region, Northern Territory. 1:100 000 Geological Map Commentary. *Bureau of Mineral Resources, Australia.*

Blake, D.H., & Page, R.W., 1988 — The Proterozoic Davenport Province, central Australia:regional geology and geochronology. *Precambrian Research*, 40/41, 329–340.

Blake, D.H., Stewart, A.J. Sweet, I.P. & Wyche, S., 1984 — Definitions of newly named and revised Precambrain rock units in the Davenport and Murchison Ranges of Central Australia. *Bureau of Mineral Resources, Australia, Report* 257.

Blake, D.H., Stewart, A.J., Sweet, I.P. & Hone, I.G., 1987 — Geology of the Proterozoic Davenport province,

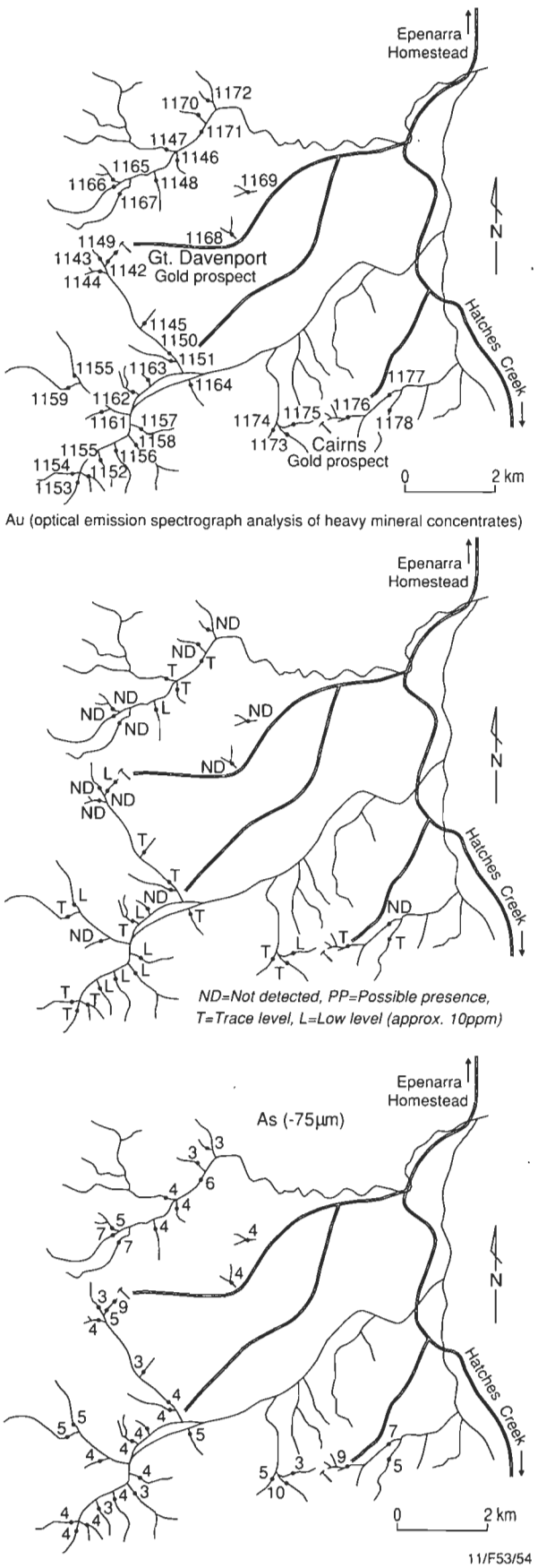

Figure 9. (a) Location of mines and sample sites in the Great Davenport area. (b & c) Values for Au and As, respectively.

central Australia. *Bureau of Mineral Resources, Australia, Bulletin* 226.

Blake, D.H. Wyche, S. & Hone, I.G., 1986 — Hatches Creek region, Northern Territory. 1:100 000 Geological Map Commentary. *Bureau of Mineral Resources, Australia.*

Cruikshank, B.I. & Pyke, J.G., 1993 — Analytical methods used in Minerals and Land Use Program's geochemical laboratory. *Australian Geological Survey Organisation, Australia, Record* (in press) (unpublished).

Hawkes, H.E. & Webb, J.S., 1962 — Geochemistry in Mineral Exploration. *Harper & Row, New York.*

Hoatson, D.M. & Cruikshank, B.I., 1985 — A stream sediment geochemical orientation survey of the Davenport Province, Northern Territory. *Bureau of Mineral Resources, Australia Record* 1985/44 (unpublished).

Krauskopf, K.B., 1970 — Tungsten. *In* Wedepohl, K.H. (editor)–Handbook of Geochemistry, Volume II–5, *Springer-Verlag.*

Le Messeurier, P. Williams, B.T. & Blake, D.H., 1990 — Tennant Creek Inlier — regional geology and mineralisation. *In* Hughes, F.E. (editor)–Geology of the Mineral Deposits of Australia and Papua New Guinea. *The Australian Institute of Mining & Metallurgy, Melbourne, Monograph* 14, 829–838.

Levinson, A.A., 1974 — Introduction to Exploration Geochemistry. *Applied Publishing Ltd., Calgary.*

Livingstone, D.F., 1957 — Airbourne scintillograph survey in the Mosquito Creek region, Northern Territory. *Bureau of Mineral Resources, Australia, Record* 1957/80 (unpublished).

Lord, J.H., 1955 — Report on an inspection of a uranium prospect near Mosquito Creek, Northern Territory. *Bureau of Mineral Resources, Australia, Record* 1955/62 (unpublished).

Perry, R.A. Mabbutt, J.A. Litchfield, W.H. Quinlan, T. Lazarides, M. Jones, N.O. Slatyer, R.O. Stewart, G.A. Bateman, W. & Ryan, G.R., 1962 — General report on lands of the Alice Springs area, Northern Territory, 1956–57. *CSIRO Land Research Series* No. 6.

Roarty, M., 1977 — The Kurundi Goldfield, Northern Territory. *Northern Territory Geological Survey, Report* GS 77/13 (unpublished).

Rossiter, A.G., 1975 — An orientation geochemical survey in the Georgetown area, north Queensland. *Bureau of Mineral Resources, Australia, Record* 1975/164 (unpublished).

Rossiter, A.G., 1983 — A heavy-mineral survey of the Forsayth area northeast Queensland. *BMR Journal of Australian Geology & Geophysics*, 8, 339–349.

Ryan, G.R., 1961 — The geology and mineral resources of the Hatches Creek Wolfram Field, Northern Territory. *Bureau of Mineral Resources, Australia, Bulletin* 6.

Sinclair, A.J., 1974 — Selection of threshold values in geochemical data using probability graphs. *Journal of Geochemical Exploration*, 3, 129–149.

Smith, K.G., 1964 — Frew River, Northern Territory 1:250 000 Geological Series. *Bureau of Mineral Resources, Australia, Explanatory Notes* SF/53–3.

Smith, K.G., 1970 — Bonney Well, Northern Territory 1:250 000 Geological Series. *Bureau of Mineral Resources, Australia, Explanatory Notes* SF/53–2.

Smith, K.G. & Milligan, E.N., 1964 — Barrow Creek, Northern Territory 1:250 000 Geological Series. *Bureau of Mineral Resources, Australia, Explanatory Notes* SF/53–6.

Smith, K.G. & Milligan, E.N., 1966 — Elkedra, Northern Territory 1:250 000 geological Series. *Bureau of Mineral Resources, Australia, Explanatory Notes* SF/53–7.

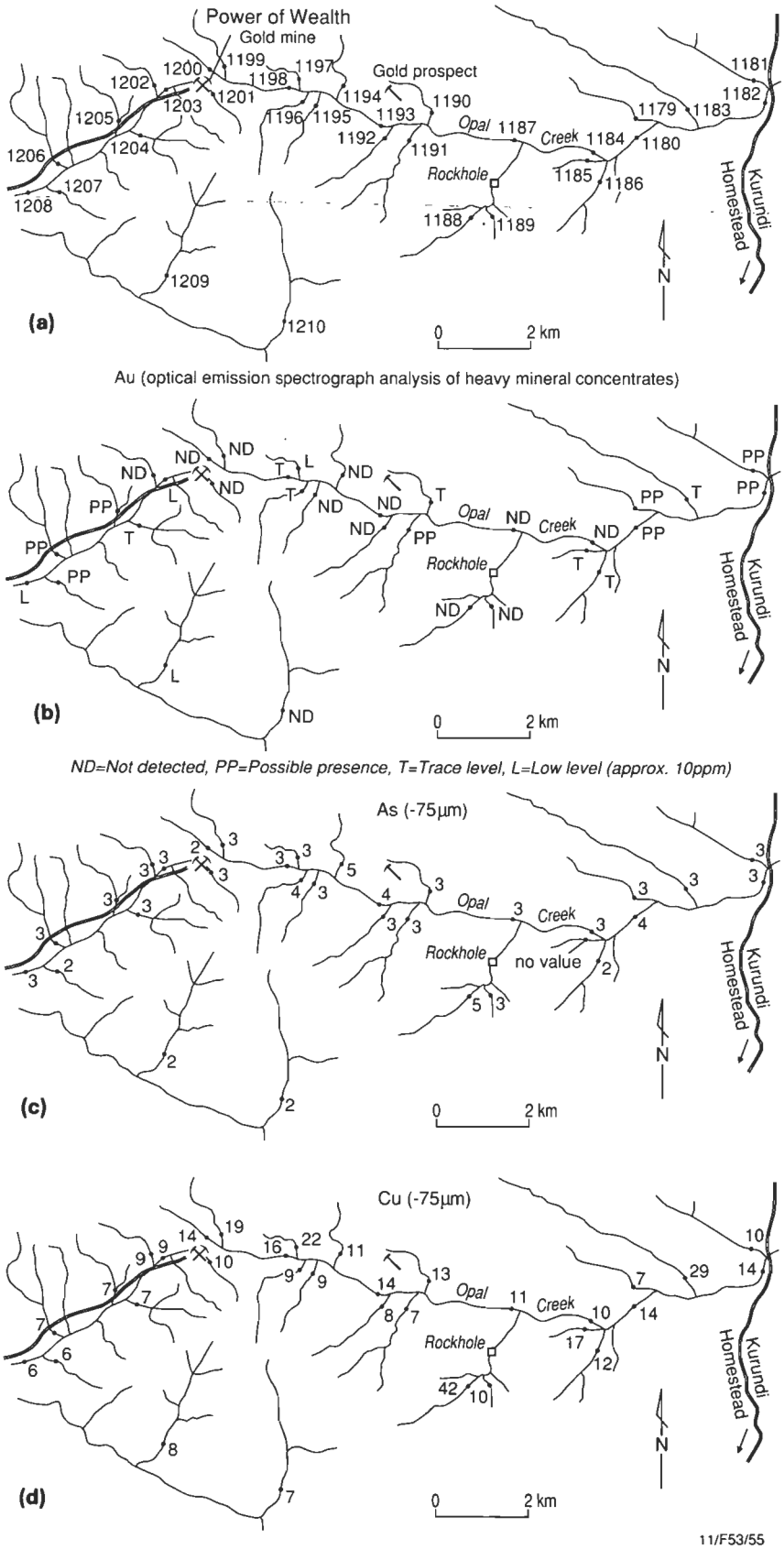

Figure 10. (a) Location of mines and sample sites in the Power of Wealth Mine area. (b-d) Values for Au, As and Cu, respectively.

Smith, K.G. Stewart, J.R. & Smith, J.W., 1961 — The regional geology of the Davenport and Murchison Ranges, Northern Territory. *Bureau of Mineral Resources, Australia, Report* 58.

Stewart, A.J. & Blake, D.H., 1986 — Kurundi region, Northern Territory. 1:100 000 Geological Map Commentary. *Bureau of Mineral Resources, Australia.*

Sullivan, C.J., 1952 — Wauchope Wolfram Field. *Bureau of Mineral Resources, Australia, Bulletin* 4.

Twidale, C.R., 1980 — The Devil's Marbles, Central Australia. *Transactions of the Royal Society of South Australia*, 104, 41–49.

Wyche, S. Blake, D.H. & Simons, B., 1987 — Devils Marbles region, Northern Territory. 1:100 000 Geological Map Commentary. *Bureau of Mineral Resources, Australia.*

Yeaman, W.S., 1965 — Geological report on the Great Davenport Gold Prospect, Kurundi Goldfield. *Bureau of Mineral Resources, Australia, Record* 1965/112 (unpublished).

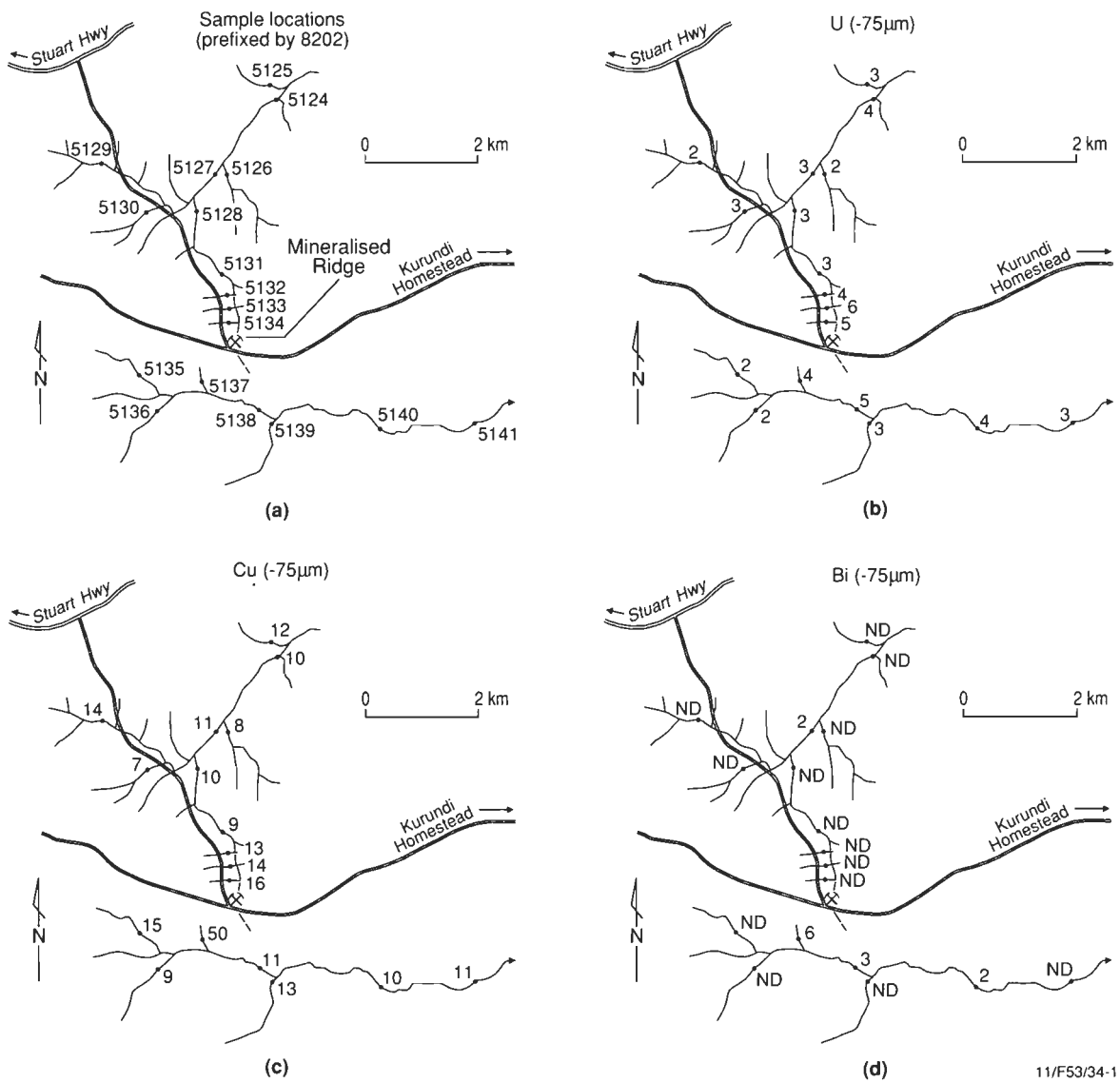

Figure 11. (a) Location of prospect and sample sites in the Munadgee Uranium Prospect area. (b-d) Values for U, Cu and Bi, respectively.

ERRATUM

Figure 6 of

M.J. Jones & E.M. Truswell
Late Carboniferous and Early Permian palynostratigraphy of the Joe Joe Group, southern Galilee Basin, Queensland, and implications for Godwanan stratigraphy

in

BMR Journal, volume 13, No. 2, July 1992, page 156

is incorrect.

Readers wishing to obtain a copy of the correct figure should contact

either Mr. M.J. Jones
172 Park Street
North Fitzroy, VIC 3068

or Dr. E.M. Truswell
Australian Geological Survey Organisation
GPO Box 378
Canberra, ACT 2601

AGSO

AUSTRALIAN GEOLOGICAL SURVEY ORGANISATION

CONTENTS

B93/21039 Cat. No. 93 1524 2